Thermal maturity and history of sediments in the North Alpine Foreland Basin (Switzerland, France)

Roland Schegg

▶ **To cite this version:**

Roland Schegg. Thermal maturity and history of sediments in the North Alpine Foreland Basin (Switzerland, France). Petrography. University of Geneva, 1993. English. NNT : . tel-00923333

HAL Id: tel-00923333

https://theses.hal.science/tel-00923333v1

Submitted on 2 Jan 2014

HAL is a multi-disciplinary open access archive for the deposit and dissemination of scientific research documents, whether they are published or not. The documents may come from teaching and research institutions in France or abroad, or from public or private research centers.

L'archive ouverte pluridisciplinaire **HAL**, est destinée au dépôt et à la diffusion de documents scientifiques de niveau recherche, publiés ou non, émanant des établissements d'enseignement et de recherche français ou étrangers, des laboratoires publics ou privés.

UNIVERSITÉ DE GENÈVE

PUBLICATIONS DU DÉPARTEMENT
DE GÉOLOGIE ET PALÉONTOLOGIE

N° 15
1993

Thermal maturity and history of sediments in the North Alpine Foreland Basin (Switzerland, France)

Maturité et histoire thermique des sédiments de l'avant-pays alpin (Suisse, France)

Roland SCHEGG

ISSN 10 12-2990
Genève 1993

Sections des Sciences de la Terre
13, rue des Maraîchers - CH-1211 Genève 4 - Tél. (022) 702 61 11 - Fax (41-22) 320 57 32

UNIVERSITÉ DE GENÈVE
DÉPARTEMENT DE GÉOLOGIE ET PALÉONTOLOGIE

FACULTÉ DES SCIENCES
Professeur W. Wildi

Thermal maturity and history of sediments in the North Alpine Foreland Basin (Switzerland, France)

THÈSE

présentée à la Faculté des Sciences de l'Université de Genève pour obtenir le grade de Docteur ès Sciences, mention Sciences de la Terre

par

Roland Albert SCHEGG

d'Oberriet (SG)

Thèse No 2612

Genève
1993

UNIVERSITÉ DE GENÈVE

FACULTÉ DES SCIENCES

Doctorat ès sciences
mention sciences de la Terre

Thèse de *Monsieur Roland Albert S C H E G G*

intitulée :

"MATURITE ET HISTOIRE THERMIQUE DES SEDIMENTS DE L'AVANT-PAYS ALPIN (Suisse, France)."

La Faculté des Sciences, sur le préavis de Messieurs W. WILDI, professeur ordinaire et directeur de thèse (Département de géologie et paléontologie), G. GORIN, professeur adjoint (Département de géologie et paléontologie), B. KÜBLER, professeur (Université de Neuchâtel) et L. RYBACH, professeur (ETH Zürich), autorise l'impression de la présente thèse, sans exprimer d'opinion sur les propositions qui y sont énoncées.

Genève, le 7 juillet 1993

Thèse - 2612 -

Le Doyen, Pierre **MOESCHLER**

N.B. - La thèse doit porter la déclaration précédente et remplir les conditions énumérées dans les "Informations relatives à la présentation des thèses de doctorat à l'Université de Genève".

Nombre d'exemplaires à livrer par colis séparé à la Faculté : - 10 -

RESUME

Tout mécanisme de formation d'un bassin sédimentaire porte une signature thermique caractéristique. Inversement, la reconstitution de l'histoire thermique d'un bassin sédimentaire permet d'en tirer des conclusions sur les mécanismes et l'histoire de sa formation. Les méthodes géothermométriques nous permettent d'étudier l'histoire thermique d'un bassin. Les enregistrements réalisés nous renseignent, soit sur les conditions de température (ou conditions T/P) instantanées (températures de fermeture, de cristallisation, etc.), soit sur les effets du couple température-temps (énergie) au cours de la diagenèse (transformation de la matière organique, transformation des minéraux argileux).

Ce mémoire présente les résultats d'une étude réalisée dans l'avant-pays alpin de Suisse et de Haute-Savoie (France). Le bassin molassique s'étend le long du front externe de l'arc alpin sur plus de 800 km, de Chambéry à Vienne. Depuis le front alpin la sédimentation de la Molasse, essentiellement détritique, prograde vers le nord-ouest. Cet élargissement du bassin au cours du temps est matérialisé par la position des biseaux appartenant à des groupes lithostratigraphiques successifs. L'épaisseur des dépôts varie de quelques dizaines de mètres dans la partie distale jurassienne à plus de 4000 m dans la partie proximale subalpine. Sur le plan lithostratigraphique, la Molasse peut être divisée en quatre groupes où les faciès prédominants sont alternativement marins et terrestres: UMM (Molasse marine inférieure, Rupélien-Chattien), USM (Molasse d'eau douce inférieure, Rupélien-Burdigalien?), OMM (Molasse marine supérieure, Burdigalien-Langhien?) et OSM (Molasse d'eau douce supérieure, Langhien-Serravalien). Du nord-ouest au sud-est, le bassin molassique est divisé en trois ensembles tectoniques: i) la Molasse du Jura, ii) la Molasse du Plateau et iii) la Molasse subalpine.

Par le biais d'une meilleure compréhension des processus qui contrôlent le régime paléogéothermique, l'objectif de cette étude est la reconstitution de l'histoire thermique de quelques périmètres du bassin molassique au cours du Tertiaire. La démarche suivie peut être décomposée en trois phases principales:

- *La phase d'échantillonnage*. Afin de rendre les résultats obtenus les plus significatifs possibles, les échantillons ont été prélevés avec une large dispersion géographique. Du sud-ouest au nord-est, cinq régions ont été explorées: Haute-Savoie (Bornes, Plateau de Bornes, Bassin de Bellegarde, Bassin de Rumilly) et bassin genevois, Suisse occidentale (région entre le lac de Neuchâtel et le lac de Genève), région du lac de Thoune, Suisse orientale (région centrée autour du lac de Zürich), Suisse septentrionale (région située dans la prolongation des failles du fossé rhénan vers le sud, dans le Jura tabulaire et le Jura plissé);

- *La phase d'analyse*. Quatre types de méthodes ont été utilisées: étude de la réflectance de la vitrinite, étude diffractométrique des argiles, étude des inclusions fluides et pyrolyse Rock-Eval.

- *La cartographie des résultats et la modélisation de l'histoire thermique*.

Maturation de la matière organique (MO), méthodes d'étude

La MO contenue dans les sédiments se transforme au cours du temps en fonction de la température subie en profondeur. Cette transformation physique et chimique de la MO est considérée comme étant quasiment irréversible. De nombreux paramètres enregistrent le résultat de ce processus. Le taux de matières volatiles, le taux de carbone, le pouvoir calorifique, la réflectance de la vitrinite (R) ou la température maximale de pyrolyse (Tmax).

L'observation microscopique des charbons révèle que ceux-ci sont composés de plusieurs constituants appelés macéraux. Les macéraux sont des débris de plantes houillifiés et des produits de dégradation d'origine végétale. D'après leurs propriétés optiques (PR + morphologie), ils ont été subdivisés en trois groupes : vitrinite, exinite ou liptinite, et inertinite. Le pouvoir réflecteur (PR) est mesuré sur les particules de vitrinite, dont la réflectance évolue d'une manière continue au cours de la houillification. Le pouvoir réflecteur est défini comme le rapport entre l'intensité de la lumière réfléchie par l'échantillon et l'intensité de la lumière

incidente. Afin de mesurer ce rapport, on compare la quantité de lumière réfléchie par une surface identique d'un étalon de référence de PR connu. La réflectance de la vitrinite est exprimée en pour cent de la lumière réfléchie à la lumière incidente.

La pyrolyse Rock-Eval (Espitalié et al. 1985a, 1985b, 1986) effectuée sur de la MO isolée, ou sur des roches riches en MO, fournit différentes informations sur le contenu organique des roches, telles que le potentiel pétrolier des séries rencontrées, la nature des kérogènes, et leur état de maturation. La méthode consiste à chauffer en température programmée (en moyenne 25°C/min), sous atmosphère inerte (hélium) un petit échantillon de roche (100mg environ) afin de déterminer quantitativement et de façon sélective les hydrocarbures libres et les composés hydrocarbonés et oxygénés qui sont expulsés lors du craquage de la MO non extractible de la roche. Les résultats obtenus nous informent sur sept types de paramètres principaux:

- les hydrocarbures libres (S1);
- les composés hydrocarbonés (S2);
- la température maximale de pyrolyse (Tmax);
- les teneurs en CO_2 (S3);
- le carbone total organique (COT)
- les teneurs en COT, permettant de calculer les valeurs des index d'hydrogène (IH) et d'oxygène (IO).

A la suite des travaux de Lopatin (1971) et de Waples (1980), l'analyse de la maturation de la MO (exprimée par la réflectance de la vitrinite) a acquis une signification importante en reconstitutions paléogéothermiques des sédiments enfouis dans les bassins sédimentaires. En partant de l'équation d'Arrhénius, ces auteurs ont montré que la maturation de la MO peut être exprimée par l'intégration du temps et de la température. Cette approche, qui simplifie à l'extrême les conditions réelles, a été critiquée par de nombreux auteurs et, par la suite, plusieurs autres modèles ont été proposés. Actuellement, le modèle qui fait autorité est EASY%Ro de Sweeney & Burnham (1990). Il prend en compte l'énergie nécessaire à la libération de l'eau, des fonctions alcools, des fonctions carboxyles, et des hydrocarbures. Ce modèle permet de calculer la variation de la réflectance de la vitrinite en fonction du temps, d'après l'évolution température-temps d'un horizon stratigraphique. Cette évolution peut être caractérisée par deux paramètres: la variation du gradient géothermique et l'enfouissement. L'analyse de la subsidence repose soit sur des observations de terrain (datations des sédiments, épaisseurs actuelles, érosions, déformations tectoniques et paléobathymétrie), soit sur des hypothèses de contraintes tectono-sédimentaires. Le processus d'itération, fondé sur la comparaison des valeurs mesurées et calculées de réflectance de la vitrinite, permet d'estimer les conditions paléogéothermiques.

La transformation des argiles

De nombreuses transformations minérales sont susceptibles d'enregistrer les effets de la diagenèse. Les associations argileuses et leurs transformations, disparition-néoformation, ont fourni les indicateurs les plus utilisés. La minéralogie des argiles constitue une vaste discipline où les méthodes d'analyse sont dominées par l'étude de la diffraction aux rayons X. En général, deux approches principales sont utilisées pour établir une zonéographie de la diagenèse: la disparition des couches gonflantes et la néoformation de minéraux index. Par exemple, la transformation des smectites (S) en interstratifiées à feuillets de composition illitique (I), alternant avec des feuillets gonflants de type smectite est considérée comme l'une des plus sensible à l'enfouissement. Bien que les différents paramètres contrôlant cette évolution soient encore sujets à discussion, il semble néanmoins acquis que la température y joue le rôle le plus important. Il existe plusieurs méthodes de dosage des couches gonflantes dans les interstratifiés. Une des premières utilisées était la courbe d'étalonnage 10-14Å pour un cristallite infini de Weaver (1956) mais, actuellement, de toutes les méthodes de mesure préconisées dans la littérature, celle de Moore & Reynolds (1989) apparaît la plus judicieuse.

Selon ces auteurs, l'écart entre les raies composites 1(I)-2(S) et 2(I)-3(S) diminue avec l'augmentation des couches gonflantes.

Analyse du pouvoir réflecteur de la vitrinite: résultats

225 échantillons de charbon de l'UMM, USM, OMM et de l'OSM ont été analysés. Leur pouvoir réflecteur moyen (Rr) varie entre 0.21% Rr (échantillon provenant de l'OSM; Suisse orientale) et 1.41% Rr (échantillon de l'USM provenant de la Molasse du Plateau de Bornes; Haute-Savoie, France). La distribution de la réflectance de la vitrinite met en évidence un double contrôle de la maturation de la MO:

- Stratigraphique: Par exemple, les valeurs moyennes varient de 0.38% Rr pour les échantillons de l'OSM (Miocène) à 0.61% Rr pour les échantillons de l'UMM (Oligocène).
- Géographique:

Le Bassin genevois et la Haute-Savoie: les courbes d'isoréflectance montrent une maturation croissante du WNW vers le ESE. Ces isolignes sont obliques aux limites des formations oligocènes, subparallèles au front alpin. Des variations secondaires se superposent à cette tendance générale. Ainsi, à l'est du Salève, dans une zone de direction NE-SW, des valeurs de réflectance atteignant 1.06% Rr ont été observées; au nord d'Annecy, des valeurs supérieures à 1% Rr ont été obtenues localement. Ces variations secondaires semblent s'aligner plus ou moins le long d'accidents tectoniques qui traverse le bassin molassique;

Le Plateau Suisse: on observe une maturation croissante de la Molasse subalpine à l'approche du front alpin. Sur le Plateau, aussi bien d'Ouest en Est que proximalement à distalement, les courbes d'isoréflectance montrent seulement une très légère variation. On observe toutefois quelques anomalies de maturité positives, mais qui semblent être liées à des accidents tectoniques. Par exemple, dans la vallée de la Broye (région de Romont, Suisse occidentale), vallée contrôlée par une importante faille, des valeurs supérieures à 0,5% Rr ont été enregistrées. Des valeurs similaires ont également été constatées au sud du lac de Neuchâtel et le long du lac de Zürich;

La Suisse septentrionale: dans cette région, l'étude des sédiments tertiaires a été complétée d'une analyse de la matière organique dispersée dans des pélites d'âge mésozoïque (Todorov, Schegg & Wildi 1993). Les valeurs observées de réflectance de la vitrinite varient entre 0.24% Rr et 0.54% Rr pour les sédiments du Tertiaire, entre 0.40% Rr et 0.70% Rr pour le Jurassique, et entre 0.49% Rr et 0.80% Rr pour le Trias supérieur. La distribution géographique des valeurs de réflectance indique un état de maturation plus avancé dans la région qui se trouve au sud du fossé rhénan comparé aux régions situées plus à l'est.

Pyrolyse Rock-Eval : résultats

53 échantillons provenant de l'UMM, de l'USM et de l'OMM (Haute-Savoie) ont été analysés. Les résultats Rock-Eval permettent d'attribuer au type III, 50 des échantillons étudiés, et au type II/III, les trois échantillons restants.

La valeur Tmax est considérée comme le principal indicateur de maturation fourni par la pyrolyse. Dans les échantillons étudiés, les valeurs Tmax varient de 380 à 474°C (OMM), de 419 à 571°C (USM) et de 414 à 460°C(UMM). La corrélation Tmax-Rr est assez mauvaise. Ceci est probablement dû à un phénomène d'altération qui semble augmenter les valeurs de OI et Tmax. La carte établie avec les courbes d'isovaleur Tmax ne correspond pas à celle dressée avec les courbe d'isoréflectance.

Les cartes d'isovaleur S2, S3, HI et OI indiquent, par contre, une maturation croissante de l'ouest vers l'est et confirment, ainsi, les résultats de l'analyse du pouvoir réflecteur de la vitrinite.

Analyse des argiles (Haute-Savoie et bassin genevois): résultats

101 échantillons, dont 28 grès et 73 marnes, provenant de l'OMM, de l'USM et de l'UMM ont été analysés par la diffractométrie aux rayons X. La composition minéralogique moyenne (obtenue par dosage semi-quantitatif à partir d'un étalon externe et, ce en tenant compte des coefficients d'absorption massique) est la suivante:

- Marnes: quartz (25.9%), feldspath potassique (2.4%), plagioclase (9.2%), calcite (23.4%), dolomite (4.1%), pyrite (0.3%) et non déterminable (34.7%, correspond à la fraction argileuse);
- Grès: quartz (35.5%), feldspath potassique (11.9%), plagioclase (26.3%), calcite (17.4%), dolomite (1.8%), pyrite (0.1%) et non déterminable (7.0%, correspond à la fraction argileuse).

Dans la fraction <2mm, 6 types de minéraux argileux apparaissent comme les plus fréquents:

- *Le Mica*: Les micas sont ubiquistes dans les échantillons étudiés. La proportion relative des intensités des micas dans la fraction argileuse varie de 27 à 76% (moyenne: 49%) pour les marnes et de 4 à 63% (moyenne: 35%) pour les grès. La représentation ternaire des intensités des pics (001), (002) et (005) indique une tendance phengite des micas;
- *La Chlorite*: La chlorite, comme le mica, est systématiquement présente dans la fraction argileuse. La proportion relative des intensités des chlorites dans la fraction argileuse varie de 4 à 52% (moyenne: 26%) pour les marnes et de 5 à 47% (moyenne: 25%) pour les grès. La chlorite est caractérisée par des pics (001) et (003) faibles et un pic (002) fort. Ceci témoigne de teneurs en Fe ou en métaux lourds élevés;
- *L'interstratifié illite/smectite (I/S)*: Les I/S sont abondants. La proportion relative des I/S dans la fraction argileuse varie de 2 à 60% (moyenne: 20%) pour les marnes et de 0 à 50% (moyenne: 18%) pour les grès;
- *La Kaolinite*: La kaolinite apparaît sporadiquement dans toutes les formations mais, avec une teneur plus élevée pour les échantillons de l'UMM. La proportion relative des intensités des kaolinites dans la fraction argileuse varie de 0 à 60% (moyenne: 5%) pour les marnes et de 0 à 29% (moyenne: 3%) pour les grès;
- *La Corrensite*: La corrensite a été trouvée seulement dans les grès (USM) du Plateau des Bornes, à l'est et à l'ouest du Salève. La proportion relative des intensités des corrensites dans la fraction argileuse varie de 0 à 80% (moyenne: 14%). La corrensite, dont le pic (001) à 28-29Å se déplace à 31-32Å après traitement à l'éthylène-glycol sur les diffractogrammes des préparations séchées à l'air, est composée d'une alternance régulière de couches gonflantes (smectite) et non gonflantes (chlorite). Dans les grès, la corrensite est caractérisée par une série harmonique (00l), dont les pics les plus forts sont les suivants: (001), (002), (004), (006), (009) et (0011);
- *La Serpentine*: La serpentine est observée de façon irrégulière dans les grès de la Haute-Savoie et du bassin genevois et ne montre aucune préférence liée à un niveau stratigraphique. La proportion relative des intensités des serpentines dans la fraction argileuse varie de 0 à 24% (moyenne: 5%). Il est à noter que la corrensite est toujours associée avec la serpentine.

La composition du cortège argileux varie généralement peu avec la position géographique des échantillons. Les associations argileuses, dominées par les micas, les chlorites et les I/S (Haute-Savoie et bassin genevois), nous renseignent probablement plus sur l'origine détritique, ainsi que les sources des sédiments molassiques que sur la transformation diagénétique. Seule, la présence de corrensite dans les grès USM du Plateau des Bornes semble refléter une néoformation diagénétique impliquant une activité élevée du Mg^{2+}, associée, en conditions normales de diagenèse, à une température minimale de 90°C à 100°C (Kübler 1973). Nos observations confirment l'association entre la corrensite et le "matériel basique", maintes fois rapportée dans la littérature.

Dans les échantillons analysés, l'indicateur de diagenèse le plus sensible est le taux de couches gonflantes dans les interstratifiés (I/S). Les cartes illustrant les lignes d'isopourcentage de smectite (S) dans les I/S, montrent clairement une tendance à l'illitisation croissante de l'ouest vers l'est. Cette tendance dans l'évolution thermique avait déjà été mise en évidence par les mesures de réflectance de la vitrinite.

Modélisations thermiques

Selon la répartition des données obtenues, nous avons distingué deux régions dans le bassin molassique et, pour chacune d'elles, nous avons proposé un essai de modélisation thermique adapté.

Suisse septentrionale: Dans cette région, située à l'intersection entre le fossé rhénan et le Jura oriental, les simulations montrent que l'état de maturation de la MO, observé dans les sédiments mésozoïques et cénozoïques, a été atteint seulement au Tertiaire, au cours d'une phase de haute température. Les paléogradients thermiques varient entre 40 et 100°C/km. Les paléotempératures maximales calculées varient entre 53°C et 106°C pour le Jurassique et entre 77°C et 127°C pour les formations du Trias. La phase de haute température postulée pour le Tertiaire pourrait être expliquée par l'existence d'un flux de chaleur par convection, produit par la migration de fluides profonds circulant le long d'accidents tectoniques. Vraisemblablement, pendant les périodes de distension successives du fossé rhénan, au cours de l'intervalle Éocène supérieur - Miocène supérieur.

Bassin molassique s.s.: A des valeurs de réflectance de la vitrinite de 0.3, 0.4, 0.5 et 0.6% correspondent des paléotempératures maximales de l'ordre de 40, 70, 90 et 110°C. Le gradient géothermique actuel relativement élevé au pied du Jura (>35°C/km) se révèle plus faible au niveau du front alpin (<25°C/km). Des valeurs similaires ont été estimées pour les paléogradients tertiaires dans le bassin molassique de Bavière (Teichmüller & Teichmüller 1975, 1986). Si l'on admet un paléogradient géothermique de 25°C/km, l'enfouissement calculé varie entre 1 et 4 km. Il n'y a, jusqu'à présent, aucun modèle géologique valable pouvant expliquer la sédimentation et l'érosion consécutive, d'une couverture molassique si épaisse, surtout dans les parties distales du bassin. L'avantage du modèle ici proposé, intégrant le transport de chaleur par convection, réside dans l'intérêt de pouvoir interpréter l'état de la maturation thermique avec des valeurs d'enfouissement modestes, mais à notre avis, plus réalistes.

Histoire thermique: implications

L'étude de l'évolution de la MO et des minéraux argileux dans les sédiments du bassin molassique nous a permis de mettre en évidence un certains nombre de faits nouveaux:

1.- on constate une augmentation de la maturation thermique:
   - en Haute-Savoie, en allant de l'ouest vers l'est;
   - en Suisse occidentale et orientale, de la Molasse du Plateau vers le front alpin.

2.- il n'existe pas de variation systématique de la maturité de la MO sur le plateau molassique. Seules des anomalies positives, semblant liées à des accidents tectoniques ont été observées.

3.- quantitativement, on note qu'en Suisse septentrionale les paléogradients thermiques varient entre 40 et 100°C/km au Tertiaire. Dans le bassin molassique s.s.: des valeurs de réflectance de la vitrinite de 0.3, 0.4, 0.5 et 0.6%, correspondant à des paléotempératures maximales de l'ordre de 40, 70, 90 et 110°C ont été calculées.

Plusieurs mécanismes influencent la diagenèse. En première approche, il semble que la maturité thermique pourrait être interprétée simplement comme la signature d'un enfouissement primaire des sédiments. Toutefois, certains arguments remettent cette interprétation en question:

- La géométrie générale du bassin molassique suggérerait plutôt une augmentation de la maturation thermique de NW vers le SE, due à une subsidence plus forte vers le front alpin. En conséquence, les courbes d'isoréflectance devraient être parallèles à l'axe du bassin;

- La maturation thermique de l'USM, l'OMM et l'OSM, même pour les parties les plus distales, peut difficilement être interprétée seulement comme conséquence d'une couverture sédimentaire. L'épaisseur maximale des sédiments pouvant surmonter l'USM (c'est à dire OMM et OSM), par exemple, n'atteint que 2 km en Suisse orientale où la série stratigraphique est assez bien conservée;

- Les anomalies positives locales de la réflectance observées sur le plateau molassique, nécessitant des valeurs d'enfouissement local très élevées, ne peuvent être expliquées que par un enfouissement sédimentaire ou tectonique.

Au niveau du front alpin, l'enfouissement nécessaire à la maturation thermique des sédiments peut très bien être associé, au moins en partie, au chevauchement de l'avant-pays par des nappes alpines. C'est ce qui a été probablement le cas pour la Haute-Savoie où l'augmentation de la maturation thermique de l'W vers l'E, oblique par rapport au front alpin et aux limites des formations oligocènes, serait liée à l'empilement croissant des nappes, également de l'W vers l'E. L'idée d'un enfouissement tectonique variant de l'ouest vers l'est a déjà été postulée par plusieurs auteurs pour le domaine des Chaînes subalpines (Kübler et al. 1974, Gorin & Monteil 1990, Moss 1992a, b).

Un autre facteur important contrôlant le champ géothermique est le transport de chaleur par convection. La création d'anomalies thermiques locales, dues à la remontée des eaux "chaudes" dans des zones tectonisées, semble être un mécanisme envisageable pour la formations des anomalies positives locales de la maturité de la MO ou des paléogradients géothermique élevés. Un échauffement transitoire par des fluides "chauds" pourrait aussi expliquer la maturité élevée observée dans les parties distales du bassin, sans faire appel à une couverture sédimentaire importante.

ABSTRACT

In studies of the thermal history of the external part of the alpine ranges, much attention has been given in the past to the Helvetic belt of Switzerland and France. The knowledge concerning paleogeothermal conditions, and the diagenetic evolution of sediments in the Swiss and French Molasse Basin is still rather fragmentary and no detailed basin-wide synthesis has been published yet.

The (paleo)thermal regime of the Molasse basin is probably a highly dynamic system controlled by a large number of interrelated parameters. The aims of the study are, therefore, to contribute to a better understanding of this system. The diagenetic evolution, the paleogeothermal regime and the heat transfer processes in the northern Alpine Foreland Basin (Switzerland, France) are the main topics of this study. Two approaches have been followed:

1) Mapping of indicators of thermal maturity such as vitrinite reflectance, Tmax from Rock-Eval pyrolysis, clay mineral assemblages and the smectite to illite transformation ratio.

2) Basin modelling is used to understand and reconstruct the geological and thermal evolution of the Molasse basin.

The following areas have been studied: i) Haute-Savoie and Geneva basin, ii) Western Switzerland, iii) Lake Thun area, iv) Eastern Switzerland and v) Northern Switzerland.

The main features resulting from vitrinite reflectance analysis in the Molasse Basin can be summarised as follows:

i) Mean average reflectance values increase slowly with age, from 0.38% Rr for samples from the Middle Miocene OSM, to 0.61% Rr for samples from the Oligocene UMM.

ii) In the proximal part of the Molasse Basin, the level of organic maturity in Tertiary sediments increases towards the Alpine front.

iii) The range of vitrinite reflectance values measured in samples from the Plateau Molasse is large (0.21% Rr - 0.64 % Rr). Nevertheless, no pronounced regional trends can be observed. The level of organic maturity of outcrop samples does hardly change from the western part to the eastern part of the basin, although a region of low thermal maturity can be observed east of Lake Zurich (Hörnli gravel fan). The vitrinite reflectance values west or north of Zurich, for example, are much the same as in Western Switzerland. In addition, there is no marked decrease in the maturity level of organic matter from the proximal to the distal parts of the Plateau Molasse.

iv) Isoreflectance contours indicate that variations in thermal maturation of the Plateau Molasse might have a structural control. Areas of increased vitrinite reflectance occur near fault zones or lie parallel to a major topographic structure (Lake Zurich) which may be tectonically controlled.

Rock-Eval pyrolysis results indicate that the organic matter in Tertiary sediments (OMM, USM, UMM) of the Haute-Savoie and Geneva basin is dominated by type III kerogen. Two samples from the UMM showed mixed type II/III kerogen. The thermal maturity of organic matter derived from Rock-Eval Tmax is associated with major uncertainties as indicated for example by the poor correlation between Tmax and Rr. A great part of Tmax data for samples from the OMM and USM have to be considered as unreliable. The maturity trends observed for the vitrinite reflectance could not be confirmed by Tmax data. The isocontour maps for S2, S3, HI and OI indicate distinguished regional W-E trends which may be explained in terms of an increasing level of thermal maturity of organic matter towards the east. Thus confirming vitrinite reflectance results.

The two major features of clay mineral diagenesis of Tertiary formations in the Haute-Savoie and Geneva Basin are the following:

i) The distribution of the percentage of smectite layers in mixed-layer illite/smectite in shales and sandstones reveals a progressive illitisation in a more or less well pronounced W to E direction. This diagenetic trend confirms coalification patterns.

ii) The appearance of corrensite in feldspathic, serpentine-bearing sandstones indicates minimal temperatures of about 90 to 100°C for the frontal part of the Bornes Plateau.

Thermal modelling of the measured maturity data in Northern Switzerland indicates that the present maturation level of the Mesozoic and Cenozoic formations was probably attained during a Tertiary high temperature regime. The computed maximum paleogeothermal gradients in the study area range from 40 to 100°C/km. The calculated maximum palaeotemperatures vary from 53 to 106°C for Jurassic and from 77 to 127°C for Triassic formations. One hypothesis to explain the postulated Tertiary high temperature regime is an enhanced regional heat flow due to convective heat transport. This may be the result of the migration of "hot" fluids from greater depth along faults zones (especially during the extensional period between Late Eocene and Late Miocene).

The main features resulting from thermal modelling in the Molasse Basin can be summarised as follows:

i) Thermal modelling of outcrop samples in the Plateau Molasse requires maximum paleotemperatures of about 40, 70, 90 and 110°C for measured vitrinite reflectance values of 0.3, 0.4, 0.5 and 0.6% respectively.

ii) The Küsnacht drillhole is characterised by a low coalification gradient and a high degree of maturity at shallow depth (0.48% Rr at 350m). When modelling with a classical burial history approach, a considerable amount of erosion (3-4km) is needed to calibrate the calculated data. Alternatively, the high Rr values and the low geothermal gradient could both be explained by a short-time discharge of warm groundwater in this region. The magnitude of erosion (1km) resulting from such a simulation corresponds with values given in the literature (Laubscher 1974, Lemcke 1974, Naef et al. 1985).

The thermal evolution of a foreland basin may be influenced by one or more of the following mechanisms: i) frictional heating next to thrust planes; ii) thermal inversion by emplacement of a thrust sheet with a hotter base; iii) normal burial heating via both tectonic and stratigraphic burial; iv) migration of fluids. The results from this study emphasise the role of the third and forth mechanism.

Generally, the overall level of thermal maturity is controlled by burial heating via stratigraphic and tectonic (at the Alpine front) loading. Conventially, in hypothermal basins, such as the Molasse Basin, the level of thermal maturation is explained often only as a consequence of thick overburden. The results of this study indicate, however, that the observed thermal maturity may be due to a combination of 'not-so-deep' burial and transient heating by warm fluids. In addition, positive palaeogeothermal anomalies along major tectonic fault zones and along major graben structures in the basement (south of the Rhine Graben) indicate that convective heat transport is locally or even regionally a very important heat transport mechanism.

REMERCIEMENTS

Au cours de mes recherches, j'ai bénéficié du soutien, des compétences, de la collaboration et de l'amitié de nombreuses personnes. Je souhaite leur exprimer ici toute ma gratitude.

Walter Wildi a été l'artisan principal de ce projet. Sa rigueur scientifique, sa disponibilité constante et son amitié sans faille m'ont grandement soutenu pendant ces quatre dernières années. Je le remercie vivement pour les longues heures qu'il a consacré à la correction et à la mise en forme des différents manuscrits que je lui ai soumis.

Je tiens également à remercier très chaleureusement les autres membres du jury qui ont accepté de juger cette thèse:

- Georges Gorin a toujours été très attentif au déroulement de mes travaux. Sa vaste connaissance de la matière organique m'a été d'une aide très précieuse;

- Bernard Kübler a, par sa compétence et son esprit critique, considérablement contribué à l'avancement de mes recherches;

- Ladislaus Rybach a manifesté un vif intérêt pour mon sujet de thèse. Je suis très flatté que ce travail puisse bénéficier de son regard d'expert géophysicien, au sens le plus large du terme;

Je tiens aussi à témoigner toute ma reconnaissance à Bertrand Ligouis pour m'avoir initié à la pétrographie de la matière organique.

J'adresse un merci tout particulier à Marc Weidmann pour m'avoir fourni un important examiné dans le cadre de cette étude. En outre, ses nombreuses remarques et critiques scientifiques m'ont été d'une grande utilité.

Je voudrais également associer à mes remerciements tous les collègues et toutes les Institutions qui, par leur précieux concours, ont permis le bon déroulement de mes recherches:

- G. Amberger, J.-P. Berger, T. Bolliger, J. Charollais, J.N. Gabus, T. Gubler, D. Kälin, F. Schlunegger, ainsi que le Musée géologique de Lausanne, pour avoir mis à ma disposition des échantillons et données;

- D. Welte, R. Littke et B. Wygrala pour m'avoir initié à la modélisation thermique;

- M. Burkhard, J.-P. Espitalié, F. Monnier, W. Kalkreuth, E. Kempter, W. Leu, S. Moss, K. Pratt, I. Viczián et M. Wolf pour nos échanges scientifiques fructueux.

- l'Institut Français du Pétrole (IFP) a assuré gracieusement les analyses de Pyrolyse "Rock-Eval". Je suis particulièrement redevable à Monsieur Guy Pichaud pour sa précieuse contribution.

Je remercie vivement le Fonds National Suisse de la Recherche Scientifique (FNSRS, fonds 2.107-0.86, 20-26.218.89 et 21.30.309.90) pour avoir subventionné cette thèse.

Thierry Adatte, George Rumley, Marc Rolli, membres de l'équipe de l'Université de Neuchâtel, ont guidé mes pas à travers les dédales de l'étude des argiles aux rayons X. Qu'ils veuillent bien trouver ici l'expression de ma profonde gratitude.

Les Enseignements du Département de Géologie & Paléontologie de l'Université de Genève ont toujours prêté une oreille attentive à mes interrogations. Je les remercie pour l'intérêt constant qu'ils ont porté à mes recherches et pour la sympathie qu'il m'ont toujours manifestée.

Je tiens aussi à exprimer ma reconnaissance à tous les collaborateurs et assistants techniques de la Section des Sciences de la Terre. Je suis, notamment, grandement redevable à François Gischig, toujours à la recherche du Mieux dans le domaine du polissage des charbons et, à Jacques Metzger, dont les conseils avisés m'ont toujours été d'une grande utilité pour la résolution des problèmes d'ordre graphique.

L'équipe des doctorants et post-doctorants de Genève a su générer une ambiance propice au travail. J'adresse ma profonde gratitude à Thierry Blondel, Quentin Deville, Susanne Feist-Burkhardt, Eric Fookes, Pascal Kindler, Rossana Martini, Véronique Orsat, André Pugin, Daniel Steffen, Mirko Stauffacher, Christian Strohmenger, Günter Trabold, Jesus Angel Uriarte et Alex Waehry.

Bernard Loup a été un partenaire d'une disponibilité totale. Indiana Jones de la géologie, nous avons affronté ensemble mille épreuves: plongée au fond de la lithosphère, traversée de la jungle informatique et, même, le café de 10h!

Merci également à Ivo Todorov, mon partenaire venu du froid, qui m'a montré que la modélisation thermique marche ... même en Bulgarie!

Si le monde des inclusions fluides reste insaisissable, Robert Moritz m'en a néanmoins distillé quelques gouttes. Merci pour son soutien.

Je tiens également à remercier Eric Monteil et Bernard Ujetz pour leur appui précieux dans l'élaboration de certains textes français et anglais.

Enfin, j'exprime à ma famille et à mes amiEs ma plus profonde reconnaissance pour la confiance, la patience et les encouragements qu'ils m'ont accordés pendant mon parcours genevois.

CONTENTS

LIST OF FIGURES

Chapter 1

Chapter 2

Chapter 3

Chapter 4

Chapter 5

Chapter 7

LIST OF TABLES

LIST OF PLATES

LIST OF ANNEXES

Chapter 1: INTRODUCTION

1.1 General outline and aims of the study

1.1.1 Thermal aspects of basin-forming mechanisms

Sedimentary basins may be regarded as a response to persistent (definitive) or transient (recoverable) modifications of the thermo-mechanical structure of the lithosphere (for detailed information, see Beaumont et al. 1982, Karner & Dewey 1986, Beaumont & Tankard 1987, Allen & Allen 1990). The isostatic equilibrium is likely to be disrupted by various changes: change of mass and density, thermal equilibrium profile, state of the intra-plate stress regime. Thus the critical physical parameters are those which describe the mechanical, thermal and rheological conditions :

- mechanics : relative densities of the mantle, crust and sediments; lithospheric and crustal thicknesses; depth of the detachment horizons;
- rheology : elastic thickness, strain rate, viscosity, plasticity, elasticity, etc.
- thermics : heat flux, temperature at the base of the lithosphere, thermal expansion coefficient, conductivity, geothermal gradient, etc.;

Some of these parameters vary as a function of the time elapsed from the last equilibrium situation; the rheological behaviour also depends on the rate of change. Any process able to modify the physical properties of the lithosphere can represent the cause or forming-mechanism of a sedimentary basin. The thermo-mechanical perturbations, which affect the entire lithosphere or distinct layers only, express themselves in the morphology and structure of the basins, in the subsidence history, in the thermal evolution and in the nature and thickness of the sedimentary record.

The thermal regime of sedimentary basins is subjected to thermal boundary conditions. These are the heat input at the base of the system (controlled by heat production, asthenospheric convection, plate tectonics and the thermal behaviour of the lithosphere) and the sediment/water interface or sediment temperature at the top of the system (Welte & Yalçin 1988, Lewis 1990).

The terrestrial heat flow can be described by different components: 1) the heat flow from the upper mantle, 2) the heat generated by the radioactive decay of uranium, thorium, potassium, and other isotopes within the crust and 3) convective heat transport processes in the upper crust and sedimentary basins (Cermák 1989, Cermák & Rybach 1989, Lewis 1990).

A major problem for the reconstruction of thermal processes accompanying basin-forming events is convective heat flow within the upper crust and sedimentary basins. Convective heat flow includes all forms of mass movement : movement of solids, as in the uplift and erosion of mountains or accretionary wedges, and the flow of fluids such as water, magmas or hydrocarbons (Lewis 1990). These processes may mask important, deep-seated thermal phenomena. There is growing evidence in paleogeothermal studies that the paleohydrodynamic regime is a key factor for the paleothermal conditions of sedimentary basins (Lam et al. 1982, Cathles & Smith 1983, Garven & Freeze 1984, Hitchon 1984, Beaumont et al. 1985, Oliver 1986, Bradbury & Woodwell 1987, Beck et al. 1989, Clendenin & Duane 1990, Bredehoeft et al. 1992, and others). Paleogeothermal anomalies may often be caused by uprising deep groundwater or other fluids, including water from the basement along zones of high permeability (Griesser & Rybach 1989, Beck et al. 1989, Nesbitt 1990).

The knowledge of present and past heat flow patterns is, therefore, an important clue for 1) the understanding of the thermal and structural evolution of the lithosphere and, more specifically, of basin-forming mechanisms; 2) the understanding of heat and fluid transfer processes in sedimentary basins.

1.1.2 Previous work on the thermal history and the diagenetic evolution of the northern Alpine Foreland Basin

In thermal history studies of the external part of the alpine ranges, much attention has been given in the past to the Swiss and French Helvetic domain (Frey et al. 1973, Kübler et al. 1974, Sawatzki 1975, Teichmüller & Teichmüller 1978, Kübler et al. 1979, Stalder 1979, Frey et al. 1980, Kisch 1980, Lippmann & Rothfuss 1980, Deconinck & Debrabant 1985, Deconinck & Charollais 1986,

Frey 1986, Giot et al. 1987, Aprahamian 1988, Burkhard 1988, Crumière et al. 1988, Krumm et al. 1988, Mosar 1988, Gorin et al. 1989, Gorin & Monteil 1990, Kuckelkorn et al. 1990, Butler 1991, Moss 1992, Petschick & Ferreiro Mählmann 1992, and others).

The knowledge of paleogeothermal conditions and the diagenetic evolution of sediments in the Swiss and French Molasse Basin are still rather fragmentary (Füchtbauer 1964,1967, Lohr 1967, Lemcke 1972, 1973, Kübler et al. 1979, Rybach & Bodmer 1980, Monnier 1982, Büchi & Bodmer 1983, Kempter 1987, Wolf & Hagemann 1987, Burkhard & Kalkreuth 1989, Keller et al. 1990, Brink et al. 1992, Kälin et al. 1992, Keller 1992) and no detailed basin-wide synthesis has been published yet.

The sedimentary geometry of Tertiary strata, seismic profiles and the subsidence history of the Molasse basin suggest a typical foreland basin structure (Homewood et al. 1986, Pfiffner 1986). Different tectonic processes contributed to the evolution of the Molasse basin: during the Alpine orogeny the area of the Helvetic shelf was affected by processes such as lithospheric deflection in response to thrust loading (craton-ward migration of the foreland basin axis and foreland bulge), the projection of collision-related compressional stresses into the foreland lithosphere (lithospheric buckling, rejuvenation of crustal discontinuities resulting in uplift of basement blocks and basin inversion), as well as by rifting activity and related thermal disturbance of the lithosphere (Ziegler 1992). These tectonic processes must have influenced the thermal boundary conditions (heat flow at the base of the basin, movement of material, e.g. erosion, and of fluids within and into the basin) and the primary (thermal conductivity, heat capacity) and secondary (initial porosity, fracture porosity, porosity-permeability relationship, density) thermo-physical parameters which govern the geothermal regime of the Molasse Basin.

The geothermal regime in peripheral foreland basins is generally characterised as hypothermal, i.e. cooler than normal (Allen & Allen 1990, Robert 1985), since these basins have had no time to re-equilibrate thermally. Thickening of the lithosphere and usually large amounts of "cold", low conductivity, sediments have been deposited within them at high sedimentation rates. The present thermal conditions of the Swiss Molasse basin indicate a low geothermal regime on a basin-wide scale. Geothermal gradients gradually decrease from >35°C/km close to the Rhine Graben in the North to <25°C/km towards the Alps (Rybach 1984). Low paleogeothermal gradients (20-30°C/km), similar to present-day gradients, were calculated for the Tertiary of the Molasse Basin (Wolf 1961, Jacob & Kuckelkorn 1977, Rybach & Bodmer 1980, Rybach 1984, Teichmüller & Teichmüller 1975, 1986). Most authors interpreted the southwards decrease of coalification gradients (0.09 to 0.03 %Rm/km) observed in boreholes of the Bavarian Molasse as caused by a decrease of the geothermal gradient in the same direction (Rybach & Bodmer 1980, Rybach 1984, Teichmüller & Teichmüller 1986). The observed decrease in coalification and geothermal gradients in the northern Alpine Foreland basin have been explained as a result of thickening of the crust towards the Alps.

This simple pattern may, however, be complicated by different, partly interrelated processes:

i) Given the high heat capacity of water, geothermal gradient patterns are necessarily influenced by the hydrodynamic regime of a basin (e.g. Hitchon 1984, and references cited in chapter 1.1.1). Recharge areas (topographic highs) are expected to display low geothermal gradients due to infiltration of cold surface water. Alternatively, regional topographic lows may display high geothermal gradients due to the discharge of warm water from depth and/or due to perturbations of the isotherms as a result of a topographic effect (e.g. river valleys). Therefore, the observed decrease of (paleo)geothermal gradients towards the Alps may be controlled by the (paleo)hydrodynamic regime of the basin.

The present-day heat flow pattern is characterised by several positive anomalies in the eastern part of the basin and by a more or less pronounced decrease in values towards the Alps (Schweizerische Geophysikalische Kommission 1983). Uprising deep groundwater, geographically bound to the Permo-Carboniferous trough, is suggested as a cause of the present-day heat flow anomaly (>150 mW/m^2) in the distal part of the Molasse basin and the Jura ranges in Northern Switzerland (Rybach et al. 1987, Griesser & Rybach 1989). Coupled heat and fluid flow modelling revealed upward flow of water in the crystalline basement from depths of about 6-7km (Griesser & Rybach 1989).

ii) When continental margins in zones of convergence are buried beneath thrust sheets, huge volume of fluids (perhaps one-third to one-half the volume of sediments) expelled from the margin sediments move into the foreland basin (Oliver 1986). These fluids carry heat, minerals and

hydrocarbons and must disturb the geothermal regime of the foreland basin. Oliver (1986) stated that, in the Appalachian trough, gas is more common near the orogen, and oil is more common at a certain distance, possibly as a consequence of the temperature distribution in the fluids as they migrated into the foreland basin. The same observations can be made in the German Molasse Basin, where most oil and gas fields are linked to basin-parallel synthetic and antitethic normal faults (Bachmann & Müller 1991). Generally, gas fields are closer than oil fields to the Alpine front. According to Brink et al. (1992), in the entire Molasse basin, the major part of the hydrocarbons has probably been generated below the Alpine overthrust. Long migration paths would, therefore, be required to reach traps in the northern part of the Molasse basin. These observations indicate: 1) that fluid flow, and hence convective heat flow, may have been an important factor for the paleogeothermal regime in the northern Alpine Foreland Basin and 2) emphasise the role of tectonic structures for the paleohydrodynamic regime.

iii) An important controlling factor on the bulk thermal properties of sedimentary rocks is porosity, due to the differences in the thermal properties of the pore fluids and rock matrix. The specific heat capacity is much higher for water than for rocks (by a factor of about 5 to 1), whereas the thermal conductivity is lower. Therefore, the thermal conductivity of water saturated sediments may increase considerably during compaction. Porosity in the Swiss Molasse basin seems to decrease towards the alpine front due to cementation, increased burial and/or compaction resulting from compressional tectonic stresses in the Alpine foreland (Füchtbauer 1964, Lohr 1967, Lemcke et al. 1968, Büchi & Bodmer 1983, Kälin et al. 1992).

iv) The systematic variation of sediment thickness (increasing towards the Alps) and type of sediments (Molasse formations are coarser grained towards the Alps) could amplify the observed trend of the geothermal gradients. Rybach (1984) noticed that geothermal gradients are inversely proportional to the depth to basement.

1.1.3 Aims of the study

The previous discussion (chapters 1.1.1 and 1.1.2) has shown that the thermal regime in the Molasse basin is probably a highly dynamic system controlled by a large number of interrelated parameters. Therefore, the aims of the study are to contribute to a better understanding of this system. The diagenetic evolution, the paleogeothermal regime and the heat transfer processes in the northern Alpine Foreland Basin are the main topics. Two approaches have been followed in this research:

1) Mapping of indicators of thermal maturity such as vitrinite reflectance, Tmax from Rock-Eval pyrolysis, clay mineral assemblages and the smectite to illite transformation ratio. Maturity maps are a tool for a basin-wide definition of thermal maturity of sediments and for the identification of anomalous zones. Combined with structural data and thermal modelling they allow an interpretation of the paleogeothermal regime and heat transport processes within a foreland basin.

2) Basin modelling is used to understand and reconstruct the geological and thermal evolution of the Molasse basin.

1.2 Geological and stratigraphic framework of the northern Alpine Foreland Basin

1.2.1 Generalities

The study areas (Fig. 1.1) are located in the Swiss and French Molasse Basin, which extends from the Haute-Savoie (France) in the west to the Lienz-Vienna area (Austria) in the east. The Molasse Basin represents a peripheral foreland basin overlying thickened lithosphere (Pfiffner 1986). Like other foreland basins, the Molasse Basin is typically asymmetric. It is filled with Oligocene to Miocene predominantly clastic sediments, which are up to 5000m thick near the Alpine thrust front (Trümpy 1980). The Molasse is underlain by Mesozoic shelf sediments, local Permo-Carboniferous

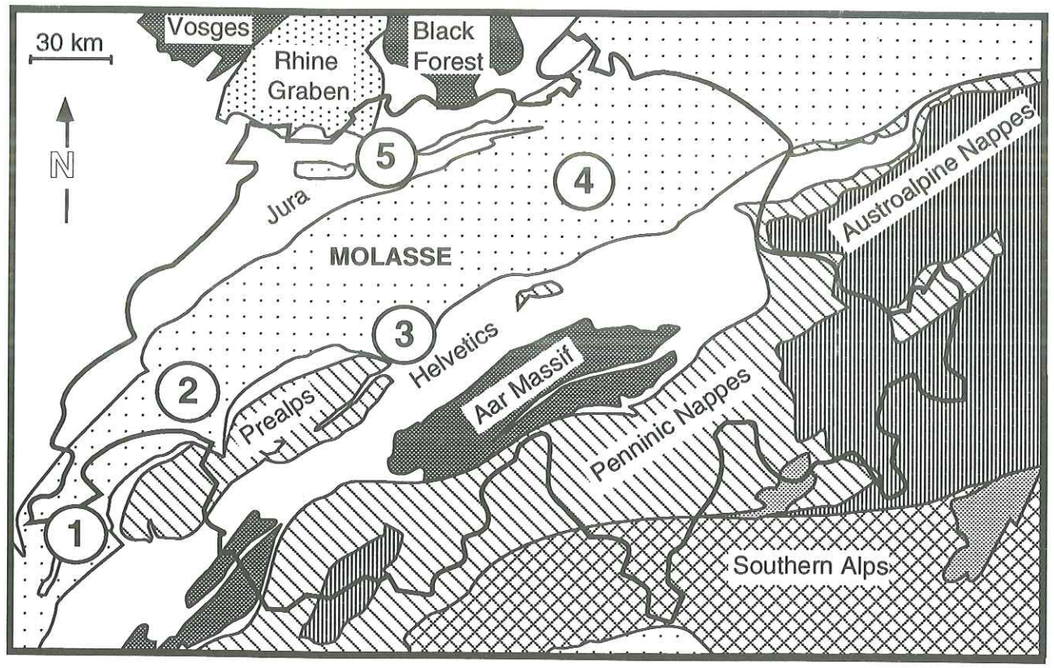

Fig. 1.1: Simplified tectonic map of Switzerland showing the study areas: 1 Haute-Savoie and Geneva Basin, 2 Western Switzerland, 3 Lake Thun area, 4 Eastern Switzerland and 5 Northern Switzerland.

graben sediments and the Variscan basement, the top of which dip southwards underneath the Alpine nappes for at least 50km (Bachmann & Müller 1991). Generally, the thickness of the Mesozoic is lower (<1km) along the axis Black Forest-Aar massif, and increases towards the east and especially towards the Southwest (Trümpy 1980).

The Molasse Basin started to form in Early Oligocene as a narrow orogenic foreland basin filled with marine flysch-like sediments. Depocenters migrated northwards across the foreland in response to the orogenic activity in the adjacent Alps, as shown by the onlap and pinch-out towards the north of successively younger strata.

The Molasse Basin can be divided into two structural units:
(1) The Subalpine Molasse consists of closely imbricated thrust sheets adjacent to the alpine nappes.
(2) The Plateau or Autochthonous Molasse which has been folded into a series of large anticlines and synclines, but remains relatively undisturbed.

Foreland basin deposits are found in a number of structural positions (e.g. Fig. 1.5): (i) within the external zone of the Alps; (ii) in the Subalpine Molasse; iii) in the Plateau Molasse, and (iv) in synclines in the folded and thrusted Jura province (Homewood et al. 1986).

The Molasse sequence comprises two large coarsening and shallowing up cycles separated by the Burdigalian unconformity. It is subdivided into four lithostratigraphic groups (Fig. 1.2):
(1) Lower Marine Molasse (UMM)
(2) Lower Freshwater Molasse (USM)
(3) Upper Marine Molasse (OMM)
(4) Upper Freshwater Molasse (OSM)

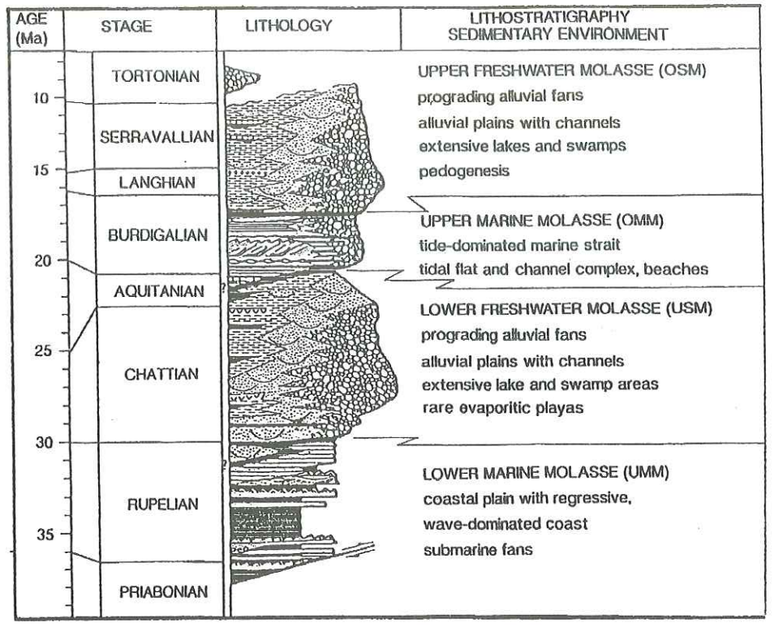

Fig. 1.2: Generalised stratigraphy of the Molasse Basin. Modified after Keller (1989) and Platt (1992).

A more detailed introduction to the geological, stratigraphic and tectonic framework of the Molasse Basin can be found in Lemcke (1974), Laubscher (1974), Trümpy (1980), Matter et al. (1980), Jung (1982), Naef et al. (1985), Homewood et al. (1986, 1989), Mugnier & Menard (1986), Pfiffner (1986), Bachmann et al. (1987), Habicht (1987), Vollmayr & Wendt (1987), Lemcke (1988), Burkhard (1990), Guellec et al. (1990), Bachmann & Müller (1991, 1992), Sinclair et al. (1991), Stäuble & Pfiffner (1991), Berger (1992) and Laubscher (1992), and references therein.

1.2.2 Lower Marine Molasse (UMM, Rupelian-Chattian)

Outcrops of the UMM (s.s.) are found only in the Subalpine Molasse and in the Helvetics (Fig. 1.3). The earliest deposits of the embryonic foreland basin, classically attributed to the Rupelian, are found within and in front of the external fold-thrust nappes of the Helvetic domain (Homewood et al. 1986). The so-called "UMM" deposits of the Jura and the southern Rhine Graben are generally younger (reaching up to Chattian ages) than their southern equivalents (see Berger 1992 for references). The northern limit of the UMM does not lie far north of the present Alpine front along a line Salève-Lausanne-Lucerne-St.Gallen (Trümpy 1980, Gorin et al. 1993). The UMM comprises a thick turbidite sequence at the base followed by storm, wave and tide deposits which are overlain by regressive littoral series indicating a shoreline retreating from the WSW to the ENE, parallel to the basin axis (Diem 1986). In the Subalpine Molasse, the UMM may probably reach thicknesses of over 1000m (Keller 1992).

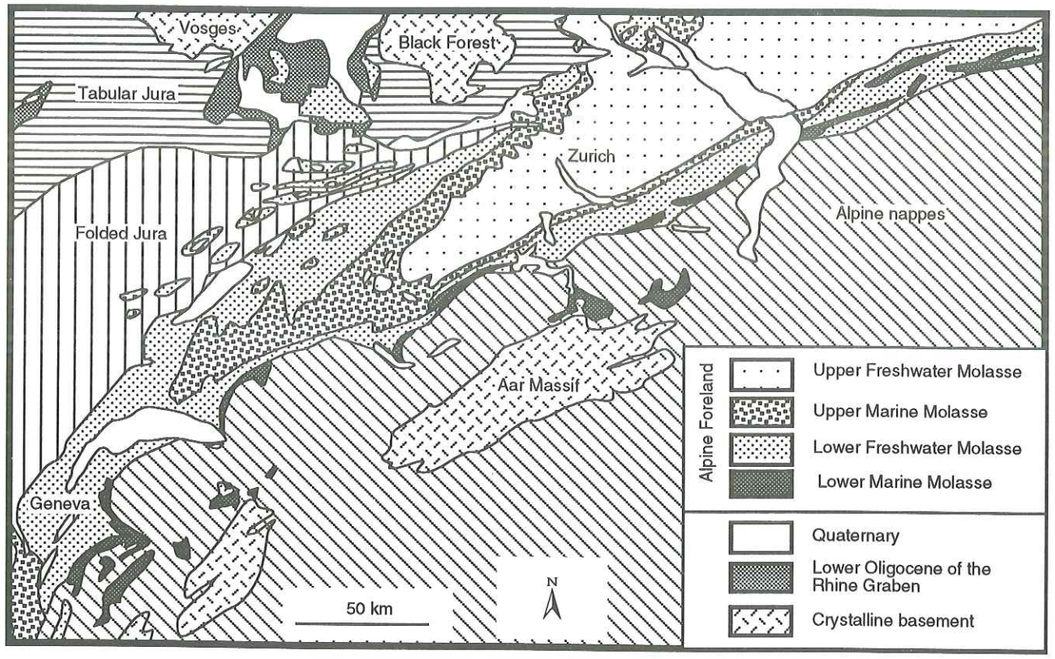

Fig. 1.3: Simplified geological map of the Swiss Molasse Basin (modified after Keller et al. 1990).

The basal turbiditic sediments deposited from the Earliest Oligocene onwards (*Taveyannaz sandstones*, *Val d'Illiez formation*, *Elm formation*), have been called the North Helvetic Flysch (Siegenthaler 1974, Trümpy 1980, Pfiffner 1986). However, Caron et al. (1989) stated that the use of the term Flysch for late orogenic Tertiary deposits on the European foreland in front of the Alps leads to some confusion. According to these authors, Flysch should be restricted to synorogenic, deep marine detrital accumulations of Cretaceous and Paleogene Tethyan basins. Therefore, the North Helvetic Flysch should be included in the stratigraphy of the Molasse sequence (Matter et al. 1980, Diem 1986, Homewood et al. 1986, 1989, Lateltin 1988). Nevertheless, the term Flysch is still a widely used expression for turbiditic deposits of Oligocene age in the Helvetic domain (e.g. Charollais et al. 1988).

More details on the stratigraphy and sedimentology of the UMM can be found in Füchtbauer (1964), Gasser (1966, 1968), Frei (1979), Naef et al. (1985), Diem (1986), Homewood et al. (1986, 1989), Habicht (1987), Lateltin (1988) and Berger (1992).

1.2.3 Lower Freshwater Molasse (USM, Rupelian-Burdigalian?)

At the Rupelian-Chattian boundary the seas retreated from the Molasse depression and the sedimentation was dominated by at least seven gravel fans at the northern margin of the Alps (Büchi & Schlanke 1977). Thick alluvial-fan conglomerates and sandstones were deposited grading northwards into multicoloured sandstones and claystones representing meandering rivers, lakes and floodplain deposits (Bachmann & Müller 1991). Two major types of paleogeographic patterns can be distinguished: a relatively simple pattern of radial drainage in the lower part of the USM ("Chattian") grading in the upper part ("Aquitanian") into a longitudinal system (Trümpy 1980, Homewood et al. 1986). According to Berger (1992), "Chattian" and "Aquitanian" are inaccurate chronostratigraphic terms. A part of the USM is surely of Rupelian age. Therefore, the terms "Chattian" and "Aquitanian" should not be used as local lithostratigraphic units in the Molasse Basin.

In the Subalpine Molasse, the USM reaches its greatest thickness, presumably in the order of 4km. The formation becomes thinner (300m and less) and finer grained towards the Jura, where it is dominated by lacustrine deposits (Trümpy 1980, and others).

Additional information on the USM can be obtained in Trümpy & Bersier (1954), Gasser (1966, 1968), Kissling (1974), Rigassi (1977), Schlanke et al. (1978), Frei (1979), Maurer et al. (1982), Weidmann (1982), Naef et al. (1985), Fasel (1986), Homewood et al. (1986, 1989), Habicht (1987), Nagra (1988), Keller et al. (1990) and Burbank et al. (1992).

1.2.4 Upper Marine Molasse (OMM, Burdigalian-Langhian?)

The base of the OMM (late Aquitanian-Burdigalian) is marked by a time-transgressive surface representing a regional unconformity. The Molasse basin was flooded, initially from the west, and later also from the east, by a shallow tide- and wave-dominated sea, linking the Rhône Basin across the peri-Alpine foredeep with the Vienna Basin and thus with the eastern Paratethys (Homewood et al. 1986). The southern shoreline was indented by two important delta fans (Napf, Hörnli). Outside of the deltas open marine conditions prevailed. Seas were generally shallow and at times brackish. Homewood et al. (1985) suggested meso- to macro-tidal ranges. The younger part of the Upper Marine Molasse ("Helvetian") is characterised by regressive cycles of fan-delta deposits (Homewood et al. 1986).

The major part of the OMM is attributed to the Lower Burdigalian, the "Helvetian" corresponding to the Middle to Late Burdigalian. Only the top of the OMM belongs perhaps to the Langhian (Berger 1992) in the distal area.

Detailed information concerning the OMM can be found in Homewood (1981), Allen et al. (1985), Berger (1985, 1992), Naef et al. (1985), Habicht (1987), Homewood et al. (1986, 1989), Keller (1989, 1992), Schoepfer (1989), Lejay (1991), Schaad et al. (1992) and Allen & Bass (1993).

1.2.5 Upper Freshwater Molasse (OSM, Langhian-Serravallian)

In middle Miocene times, continental sedimentation took over again with large alluvial fans developing at the Alpine thrust front, whereas smaller ones formed at the northern basin margin. Both river systems drained towards an alluvial plain in the Southwest.

Due to the progradation of the fan deltas, the regression marking the onset of the OSM starts earlier in the proximal parts, i.e. the facies limit OMM/OSM is clearly diachronous (Matter & Weidmann 1992). The OSM is dated as Langhian-Serravallian (Berger 1992). The top of the OSM is characterised by an erosional boundary, covered in parts by Pliocene (?) to recent deposits. In the distal parts of the Molasse basin (Jura mountains) OSM sediments are unconformably overlain by Middle to Late Miocene (Berger 1992) conglomerates, sands and gravels (*Graviers du Bois de Raube*, *Hipparionsande*, *Vogesenschüttung*).

The OSM is over 1500 m thick in the central parts of the gravel fans, but only a few hundred meters further north. No OSM deposits have been found in the Plateau Molasse of western Switzerland (Fig. 1.3).

For further reading see Hofmann (1951, 1960), Büchi (1958a, 1958b, 1959), Bürgisser (1980, 1981), Naef et al. (1985), Habicht (1987), Nagra (1988), Homewood et al. (1989), Berger (1992), Bolliger (1992) & Keller (1992).

1.3 Study areas

1.3.1 Haute-Savoie and Geneva Basin

This study area is situated at the western termination of the Molasse basin (Fig.1.1). It includes from northwest to southeast the following tectonic units (Fig.1.4, Fig. 1.5):

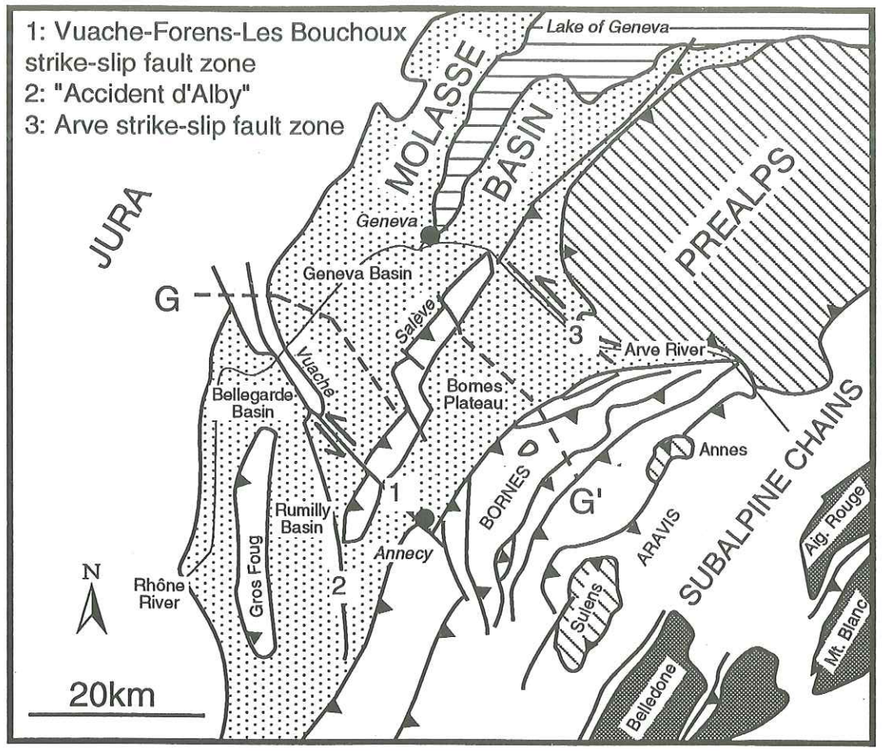

Fig. 1.4: Tectonic map of the Haute-Savoie area and the Geneva Basin (modified after Wildi & Huggenberger 1993). G-G': cross section line of Fig. 1.5.

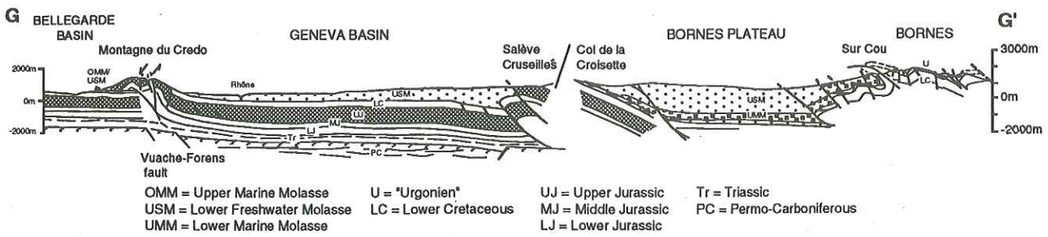

Fig. 1.5: Geological NW-SE profile (G-G' in Fig. 1.4) showing the main tectonic units of the study area.

i) Plateau Molasse: It consists of subhorizontal USM and OMM, which onlaps the Mesozoic and thins out towards the Jura Mountains.

The **Geneva Basin** is situated between the first ridge of the Jura Mountains to the north (called High Chain, Wildi et al. 1991) and the Mount Salève to the south, a thrusted anticline consisting of

Mesozoic sediments. It is limited to the Southwest by a major wrench fault zone (the Vuache-Forens-les Bouchoux tectonic zone, Guyonnet 1988, Wildi et al. 1991), which has given rise to the Mount Vuache. An introduction to the regional geology of the Geneva basin can be found in Douxami (1896), Gignoux & Moret (1939), Rigassi (1957, 1977), Kissling (1974), Charollais et al. (1984), Berger et al. (1987) and Gorin et al. (1993).

Mesozoic sediments in the Geneva Basin form a south-easterly dipping monocline with karstified Urgonian carbonates at the top (Gorin et al. 1993). The coincidence of Permo-Carboniferous structural trends with younger tectonic events suggests that the structural framework of the basin is largely influenced by rejuvenation of these older lineaments (Wildi & Huggenberger 1993, Gorin et al. 1993). NNW-SSE trending wrench fault zones, subparallel to the Vuache fault zone, affect the entire Geneva Basin (Ruchat 1977, Angelillo 1987, Signer 1992, Gorin et al. 1993). According to Gorin et al. (1993), initiation of these marked structural lineaments clearly predates the Late Tertiary phase of Jura folding, because Chattian deposits can be observed to onlap an already existing topography. Towards the front of the Salève thrust, the sediments of the Geneva basin overlie a Permo-Carboniferous half-graben.

Molasse sediments in the Geneva Basin consist only of USM, which can be subdivided into the *Molasse rouge* (also called *Molasse bigarrée* or *Marnes bariolées*) and the *Molasse grise* (also called *Grès et marnes gris à gypse*) ranging in age from late Early Chattian to Early Aquitanian (Rigassi 1957, Kissling 1974, Charollais et al. 1984, Berger et al. 1987). The thickness of USM strata decreases towards the NW, from over 1000m near the Salève to zero (pinch-out) towards the Jura mountains.

The **Bellegarde** and **Rumilly Basins** (Wildi & Huggenberger 1993), separated by the Jura anticline of the Gros Foug, are situated SE of the Vuache-Forens-les Bouchoux wrench fault zone (Fig. 1.4). Their feather-edge western margin is found within the Jura. Their regional geological and stratigraphic framework is described by Douxami (1896), Doncieux (1932), Gignoux & Moret (1939), Michel & Caillon (1957, 1960), Rigassi (1957, 1977), Wagner & Wellhäuser (1966), Donzé & Enay (1972), Jung (1982), Weidmann (1982), Reggiani (1989), Burbank et al. (1992) and Allen & Bass (1993).

Their structural configuration is similar to the one observed in the Geneva Basin (Wildi & Huggenberger 1993). The sedimentary fill consists of USM and OMM. Whereas east of the Rhône river USM deposits rest unconformably on the Lower Cretaceous substratum; west of the Rhône river, OMM lies directly on the Mesozoic limestones. The Molasse clastic wedge thins out towards the west. The USM decreases in thickness from over 1000m near the Alpine front to less than 400m in the Rumilly Basin. The OMM shows the same westward decrease in thickness, with maximum of up to 1950m in the Annecy area (Michel & Caillon 1957).

ii) Subalpine Molasse: It consists of a folded and thrusted complex of UMM and USM which thickens towards the Alpine front. In the study area it is referred to as the **Bornes Plateau** (Gorin et al. 1993), stretching from the Mount Salève to the Alpine front. Molasse deposits in the Bornes Plateau consist of both UMM and USM sediments (Charollais et al. 1988). The UMM comprises the "Subalpine Flysch" and the *Grès de Bonneville* and is dated as Rupelian (Charollais et al. 1984, 1988). The USM of the Bornes Plateau is made up of *Molasse rouge* dated as Rupelian-Chattian, its lower part being clearly older than that of the *Molasse rouge* in the Geneva Basin (Charollais et al. 1981, Berger et al. 1987). Therefore, the Bornes Plateau represents an older basin with a thicker sediment fill than the Geneva Basin (Gorin et al. 1993). The deepest part of the Bornes Plateau, towards the Alpine front (represented here by the Bornes Massif), coincides with an underlying deep Permo-Carboniferous half-graben (Gorin et al. 1993). Faults bounding this half-graben to the south delineate a basement high which underlies the southerly tectonic pinch-out of the Molasse beneath the alpine front (Charollais & Jamet 1990, Huggenberger & Wildi 1991, Gorin et al. 1993).

iii) Bornes Massif (Subalpine Chains): The Bornes Massif forms the frontal mountain range in the central part of the Subalpine Chains (representing the lateral equivalent of the Helvetic zone in Switzerland) between the Arve valley and the Lac d'Annecy. For a review of the Bornes Massif geology see Charollais et al. (1988) and references therein.

The French Subalpine Chains make the foreland fold/thrust belt of the Western Alps. During the alpine orogenic phases, Upper Jurassic, Cretaceous and Tertiary formations have been sheared off from their Jurassic and Triassic substrate, and have been deformed under a moderate overload to form kinks, folds and overthrust, and at greater depth, reverse faults and flat "décollement" contacts (Huggenberger & Wildi 1991). A first deformation phase (mainly Oligocene and early Miocene)

indicates SSE-NNW to SE-NW shortening by folding and thrusting of about 8km, and a second phase (mainly Miocene and Pliocene) is at the origin of 6km of thrusting from ESE or E to WNW or W (Wildi & Huggenberger 1993). Subalpine Chains have been overridden, prior to their formation, by Ultrahelvetic and Penninic nappes. These nappes are represented today in the Subalpine Chains by the Sulens, Annes or Chablais klippen (Moret 1934, Rosset et al. 1976).

In the Subalpine Chains area, foredeep related flexure and sedimentation did not start until the Eocene (Charollais et al. 1988). So far, it has always been assumed that parts of the Subalpine Chains were eroded during the Paleogene prior to flexural subsidence, in places as far down as the Lower Cretaceous. However, new micropaleontological results indicate the presence of limestones of Late Paleocene to Early Eocene age in Ultrahelvetic units (Kindler 1986).

In the Bornes Massif area, foredeep formation coincided in the Middle Eocene with the deposition of the *Formations de l'eocène moyen et supérieur*, including the *Couches des Diablerets* and *Nummulitic limestones* (Charollais et al. 1988). They are overlain by the deeper-water shales and volcanoclastic turbidites of the *Taveyannaz* and *Val d'Illiez formations* (Lateltin 1988) which were deposited in two distinct basins running along the Alpine front during Early to Middle Oligocene (Ujetz & Kindler 1993). Figure 1.6 shows the chrono- and lithostratigraphic relationship of Oligocene deposits in the Helvetic units and Subalpine Molasse in Western Switzerland and Haute-Savoie according to Lateltin (1988). *Taveyannaz* and *Val d'Illiez sandstone formations* stratigraphically overlie the *Schistes à Meletta* and *Marnes à Foraminifères*. The *Taveyannaz sandstones* are overlain by *Wildflysch*, whereas the *Val d'Illiez sandstones* may also be overlain by the littoral deposits of the *Formation de Vaulruz*.

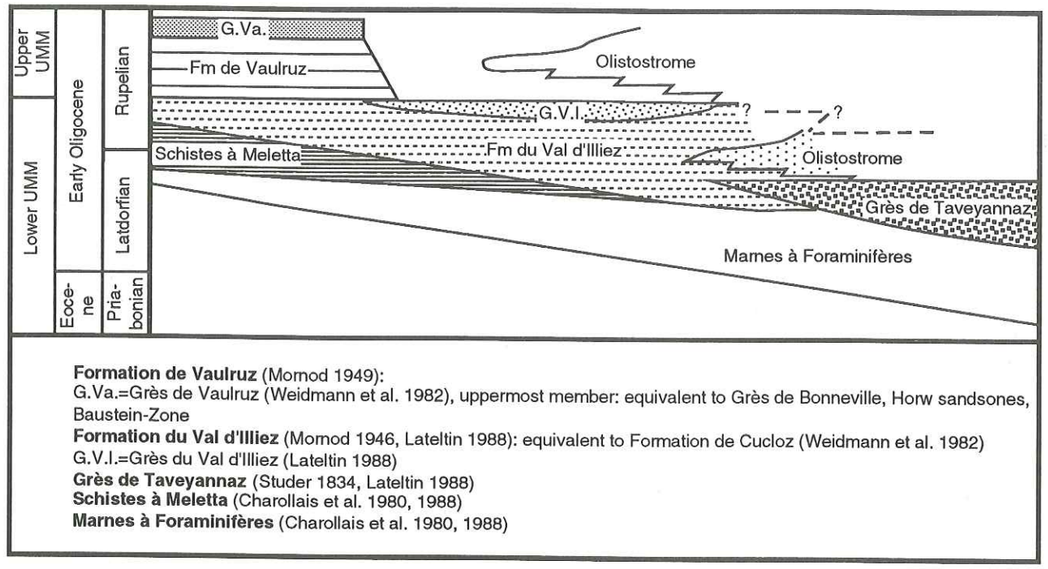

Fig. 1.6: Chrono- and lithostratigraphic relationship of Oligocene deposits in the Helvetic units and Subalpine Molasse in Western Switzerland and Haute-Savoie according to Lateltin (1988).

1.3.2 Western Switzerland

This study area covers the region between the Lake of Neuchâtel in the north and the Lake of Geneva in the south (Fig. 1.7). For an introduction to the regional geology see Mornod (1949), Trümpy & Bersier (1954), Lemcke (1959, 1963), Kissling (1974), Rigassi (1977), Matter et al. (1980), Jung (1982), Weidmann (1982, 1988), Weidmann et al. (1982), Engesser et al. (1984), Berger (1985), Fasel (1986), Jordi (1990) and Gorin et al. (1993).

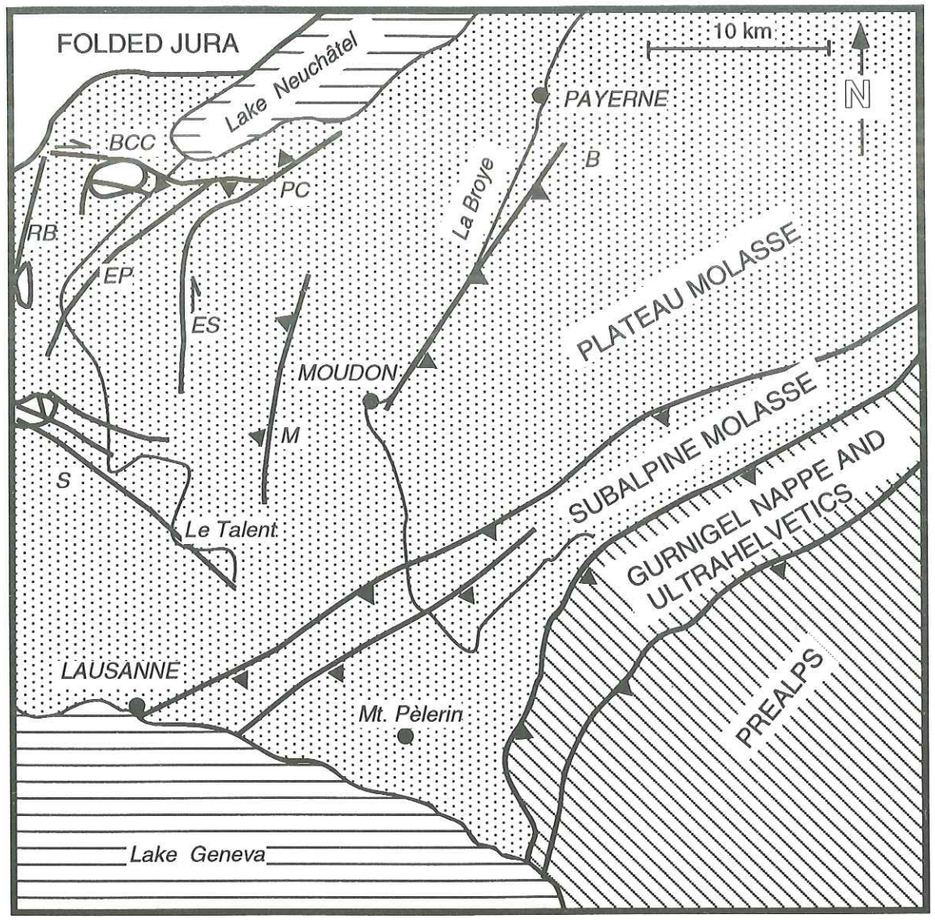

Fig. 1.7: Tectonic map of Western Switzerland. Tectonic structures are modified after Jordi (1990) and Weidmann (in press): BCC=Baulmes-Chamblon-Chevressy thrust, ES=Essertines fault, EP=Ependes fault, M=Mentue thrust, PC=Pomy-Cuarny thrust, RB=Rances-Baulmes fault, S=La Sarraz fault, B=La Broye thrust.

The Molasse Basin extends from the Jura mountains to the NW to the Prealps in the SE (Fig. 1.7); it is subdivided into the following units:

i) Plateau Molasse: The Mesozoic substratum of the Plateau Molasse appears as a monocline dipping south-easterly towards the front of the Subalpine Molasse. Molasse deposits clearly onlap the Mesozoic substratum and thin towards the Jura mountains. The Plateau Molasse consists of subhorizontal USM and OMM deposits which are moderately folded and locally affected by significant wrench fault zones (Jordi 1990, Gorin et al. 1993). These zones predate in some places the deposition of the Chattian USM and probably represent rejuvenated (during the Late Miocene phase of Jura folding and thrusting) Permo-Carboniferous tectonic structures (Burkhard 1990, Gorin et al. 1993). In the study area, the USM is subdivided from base to top into the following formations: *Marnes bariolées s.l.* (equivalent to the *Molasse rouge* of the Geneva Basin), *Calcaires d'eau douce et dolomie*, *Grès et marne gris à gypse* and *Molasse grise de Lausanne,* which range in age from Middle Oligocene to Lower Miocene (Kissling 1974, Jordi 1990).

ii) Subalpine Molasse: The Subalpine Molasse consists of a series of closely imbricated thrust slices adjacent to the Helvetic Zone and tectonically overlain, in part, by the Prealps (Homewood et al. 1986). The contact between the Plateau Molasse and the Subalpine Molasse is marked by a major wrench fault zone affecting the whole Mesozoic and Cenozoic strata and by the pinch-out of UMM

deposits (Gorin et al. 1993). According to these authors, this hinge zone is probably associated with Paleozoic lineaments. The Subalpine Molasse thickens towards the Alpine front where it overlies, like in the Bornes Plateau, a deep-seated Permo-Carboniferous half-graben (Gorin et al. 1993). The lithostratigraphic units encountered are the UMM and the USM. According to Weidmann et al. (1982), the UMM comprises the 3 following formations: i) *Formation de Cucloz* (Early to Middle? Oligocene), ii) *Formation du Wildflysch subalpin* (only close to the alpine front, Middle Oligocene?), and iii) *Formation de Vaulruz* (Middle Oligocene, Rupelian). The *Grès de Vaulruz* is the lateral equivalent of the *Grès de Bonneville* in the Bornes Plateau (Charollais et al. 1988). The USM deposits are represented mainly by the Pèlerin fan system, which is characterised by north-westward facies changes from braided river conglomerates to multistorey, meandering river sand bodies and to lake and floodplain lignites, marls and sands (Fasel 1986, Homewood et al. 1986). According to Fasel (1986), the following units can be distinguished in the Subalpine Freshwater Molasse of Western Switzerland: i) *Molasse rouge* (Middle Oligocene), ii) *Poudingues du Pèlerin* (Middle to Late Oligocene), iii) *Grès de la Cornalle* (Late Oligocene), iv) *Molasse à charbon* (Late Oligocene), and v) *Molasse grise de Lausanne* (Early Miocene).

1.3.3 Lake Thun area

The area is situated in the thrusted Subalpine Molasse Northeast of Lake Thun (Fig. 1.1, Fig. 1.8). It is limited to the SE by the Helvetic Border chain, representing the northernmost Wildhorn nappe, which is thrusted on top of the Subalpine Molasse and Flysch (Scherer 1966, Burkhard 1988, Schlunegger et al. 1993). A triangle zone characterises the transition zone between the Subalpine and the Plateau Molasse (Vollmayr & Wendt 1987). As in the western part of the Molasse Basin, this transition zone seems to be controlled by rejuvenated Permo-Carboniferous lineaments (Vollmayr & Wendt 1987, Gorin et al. 1993). The Subalpine Molasse is folded, thrusted and faulted into a bunch of several thin kilometric slices ("Schuppen") composed of UMM and USM deposits. The following units can be distinguished from SE to NW: i) "Subalpine Flysch", ii) Hilfern-Schuppe, and iii) Blueme-Schuppe (including the Prässere-Schuppe, the Zulg-Hombach-Schuppe and Steffisburg-Schuppe). The lithostratigraphic units encountered are the UMM and USM. The UMM comprises the following formations (see Diem 1986 and Habicht 1987 for a detailed discussion): *Gerstengraben-Formation*, *Horrenbach-Formation* and *Ralligen-Formation*. According to Scherer (1966) and Schlunegger et al. (1993), the USM in the Blueme-Schuppe can be divided, from the base to the top, into the following formations: i) *Homberg beds* (Middle Miocene), ii) *Thun conlomerates* (Middle to Late Oligocene), iii) *Horw marls* (Late Oligocene), and iv) *Gitzischöpf conglomerates* (Late Oligocene).

1.3.4 Eastern Switzerland

The area (Fig. 1.1) covers the area of the Plateau Molasse between the eastern termination of the Jura mountains (Lägern) in the NW and the Subalpine Molasse of Central and Eastern Switzerland in the SE (Fig. 1.9). Detailed studies of the regional geology can be found in Hofmann (1951, 1960), Pavoni (1955, 1956, 1957, 1987), Büchi (1957, 1958a, 1958b, 1959), Lemcke & Wagner (1961), Büchi et al. (1965), Füchtbauer (1967), Hantke et al. (1967), Lemcke et al. (1968), Büchi & Schlanke (1977), Frei (1979), Bürgisser (1980), Hantke (1980), Müller et al. (1984), Naef et al. (1985), Diem (1986), Pfiffner (1986), Sprecher & Müller (1986), Bachmann et al. (1987), Gubler (1987), Habicht (1987), Bolliger et al. (1988), Nagra (1988), Bolliger & Eberhard (1989), Keller (1989), Burkhard (1990), Diebold et al. (1991), Sinclair et al. (1991), Stäuble & Pfiffner (1991), Berger (1992) and Bolliger (1992), and others.

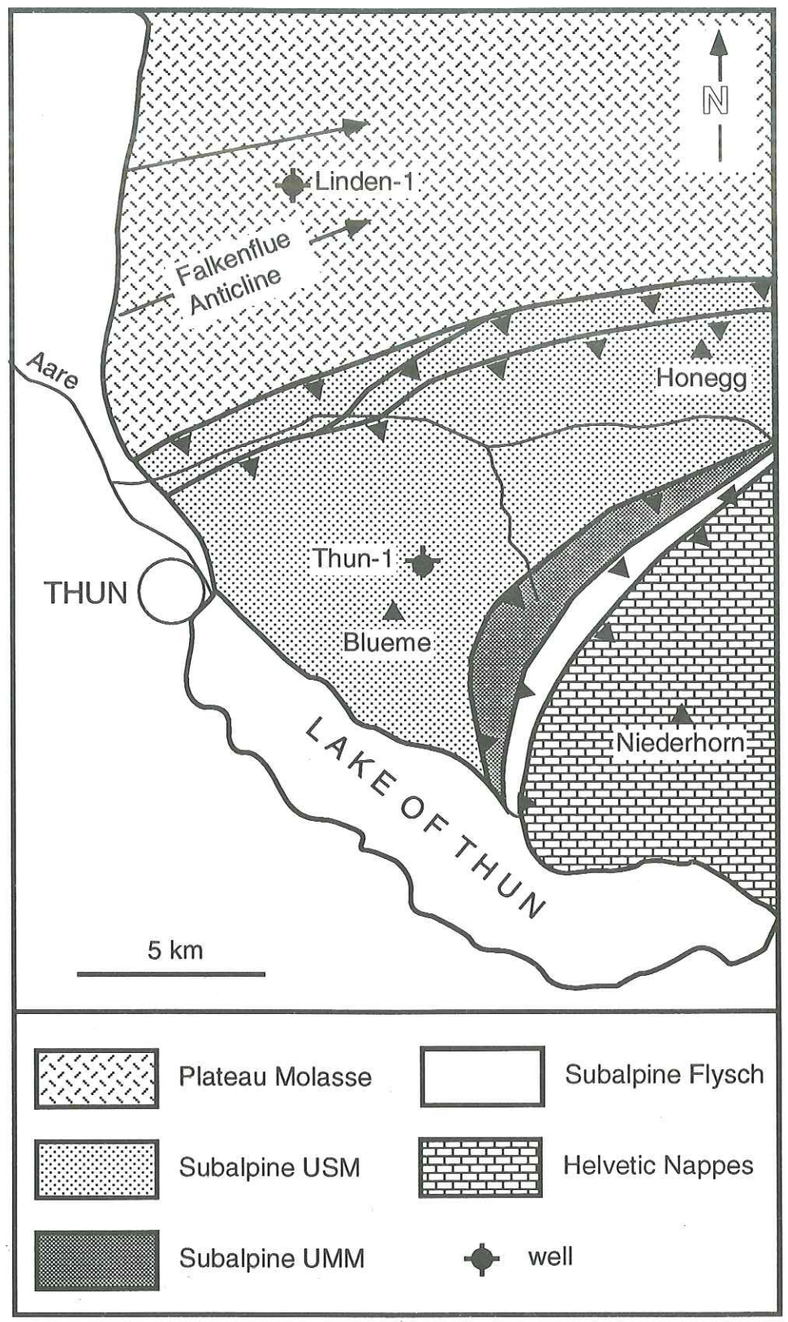

Fig. 1.8: Tectonic map of the Lake Thun region (modified after Schlunegger 1991).

The Molasse sediments in eastern Switzerland overlie an 800 to 1000m thick sequence of Mesozoic sediments (Büchi et al. 1965, Lemcke & Wagner 1961, Lemcke et al. 1968), which rest on the Variscan crystalline basement complex of the European crust. In the distal parts of the Molasse Basin to the north, the basement is cut by the E-W striking late Paleozoic Constance-Frick-Lons le

Saunier trough system (see Debeglia & Gable 1984 and Diebold et al. 1991 for a review). Unlike Western Switzerland, evidence for the occurrence of major Permo-Carboniferous grabens near the Alpine front is still scarce. Marine Mesozoic shelf deposits were deposited during a period of tectonic quiescence and unconformably overlie basement or Late Paleozoic sediments (Diebold et al. 1991). The NW-striking Zurich High is an important basement lineament in this area. It became apparent for the first time during the Late Triassic as illustrated by the thinning of the Keuper and the absence of Rhaetian deposits on its top (Büchi et al. 1965, Bachmann et al. 1987). During the Campanian to mid-Paleocene regional phase of inversion, Mesozoic series over the Zurich High were eroded down to the Oxfordian (Bachmann et al. 1987). According to these authors, this phase of inversion tectonics, affecting large parts of north-eastern Switzerland, is the result of transpressional wrench tectonics.

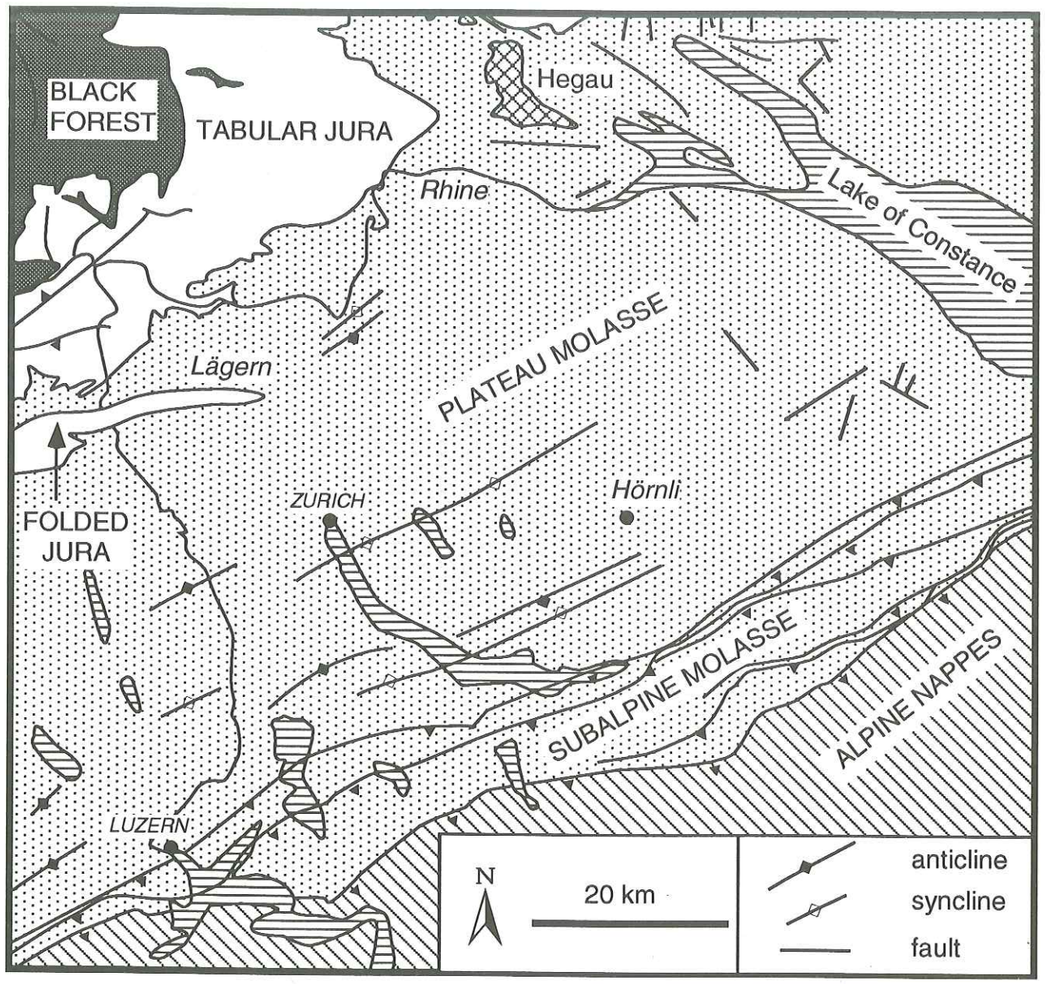

Fig. 1.9: Tectonic map of Eastern Switzerland (modified after Nagra 1988).

The Molasse basin is characterised by a northward thinning of sediments associated with onlap structures (Stäuble & Pfiffner 1991). The Plateau Molasse consists of USM, OMM and OSM. Its structural style is dominated by subhorizontal strata affected by compressional features, such as "ductile" horizontal shortening, minor gentle folds, wrench faults and reverse faults (Breddin 1964, Betz & Wendt 1983, Schrader 1988, Burkhard 1990, Bachmann & Müller 1991, Brink et al. 1992).

This compressional structuration interfered with the effects of the extensional stress regime of the superimposed crustal bending, especially in the distal northern part of the basin (Naef et al. 1985, Diebold et al. 1991, Brink et al. 1992, Laubscher 1992). Both tectonic processes are accompanied by shear force-induced wrench faulting (strike-slip regime). Mesozoic strata underlying the Molasse deposits are generally dipping towards the Alps at low angle. An abrupt change to steeper dips occurs at the transition between Plateau Molasse and Subalpine Molasse. This rupture coincides with the northward pinch-out of the UMM, which overlies a much thinner Mesozoic interval than the USM further north (Stäuble & Pfiffner 1991). The Subalpine Molasse is characterised by intense thrusting of the most internal part and the development of a classical triangle zone, comprising UMM and USM deposits, at the front (Stäuble & Pfiffner 1991).

In Central and Eastern Switzerland, outcrops of the USM are restricted to two narrow zones at the southern and northern border of the Molasse basin (Fig. 1.3). The thickness of USM deposits decreases from 4200m in the south (Frei 1979) to 0m in the north. According to a compilation by Nagra (1988), the following lithostratigraphic units can be distinguished in the USM of Eastern Switzerland: i) *Molasse rouge* (Early Chattian), ii) *Karbonatreiche Molasse* (Early Chattian-Late Chattian), iii) *Granitische Molasse*, including the facies-equivalent *Obere Bunte Molasse* in the upper part (Late Chattian-Aquitanian), and iv) *Oberaquitane Mergelzone* (Late Aquitanian).

Like the USM, the OMM crops out at the southern and northern border of the Molasse Basin (Fig. 1.3). Its thickness decreases from a maximum of 1000m in the south to 0m in the north. Conventionally, deposits of OMM were subdivided in two lithostratigraphic units: "Burdigalian" and "Helvetian" (Büchi & Schlanke 1977, Naef et al. 1985, Habicht 1987). In a recent study, Keller (1989) proposed to distinguish two formations: i) Luzerner Formation (Aquitanian-Burdigalian) and ii) St. Galler Formation (Burdigalian). Dating with Sr-isotopes indicates an age between 18.5 and 17my b.p. for the St. Galler Formation (Keller 1989).

Outcrops of OSM cover a large part of the Plateau in Eastern Switzerland (Fig. 1.3). The OSM is over 1500m thick in the central part of the gravel fans, but thins to a few hundred meters further north. The study area comprises essentially deposits of the alluvial Hörnli fan, the lithostratigraphic subdivisions of which were reviewed by Bolliger (1992). Based on sedimentary facies assemblages, Bürgisser (1980) suggested the following lateral zonation: i) conglomerate facies (proximal fan deposits), ii) conglomerate/siltstone facies (distal fan deposits), and iii) sandstone/siltstone facies (floodplain). In the northern part of the Molasse Basin, the so-called *Glimmersande* were deposited (Hofmann 1960). These micaceous sands, preserved as far west as Bienne, were deposited by the ENE-WSW flowing "Proto-Rhone", coming from the Austrian Alps and the Bohemian massif (Trümpy 1980).

1.3.5 Northern Switzerland

This area is situated at the intersection of the extensional realm of the Rhine Graben and the compressional realm realm of the eastern Jura (Fig. 1.10). Recent detailed reviews of the regional geological framework are given by Trümpy (1980), Müller et al. (1984), Naef et al. (1985), Laubscher (1987, 1992) and Diebold et al. (1991). As this region was studied in collaboration with Dr. I. Todorov (who worked on the thermal maturity of the Mesozoic sediments, see Todorov et al. 1993), only a short introduction on the Cenozoic and Mesozoic structural evolution is given below.

The Triassic-Early Cretaceous subsidence history of Western and Central Europe was dominated by intra-plate tensional stresses (Loup 1992a, 1992b) related to the break-up of Pangea (Ziegler 1987). Western and Central Europe became progressively subjected to regional extension resulting in the development of a complex, multidirectional system of grabens and troughs, many of which are superimposed on Permo-Carboniferous fracture systems (Ziegler 1988).

During Triassic to Middle Jurassic times, the study area was part of the intracontinental German Basin. The so-called "Vindelician High" (extending south-westwards from the Bohemian Massif) separated the German Basin from the broad shelf of the Tethys in the south (Trümpy 1980, Bachmann et al. 1987). This basement high was gradually overstepped from NW to SE by Triassic and Jurassic sediments up to 1000m thick. In the study area, the thickness of Triassic and Jurassic strata is small due to the NW-striking Zurich High which became apparent for the first time during the Late Triassic (Bachmann et al. 1987).

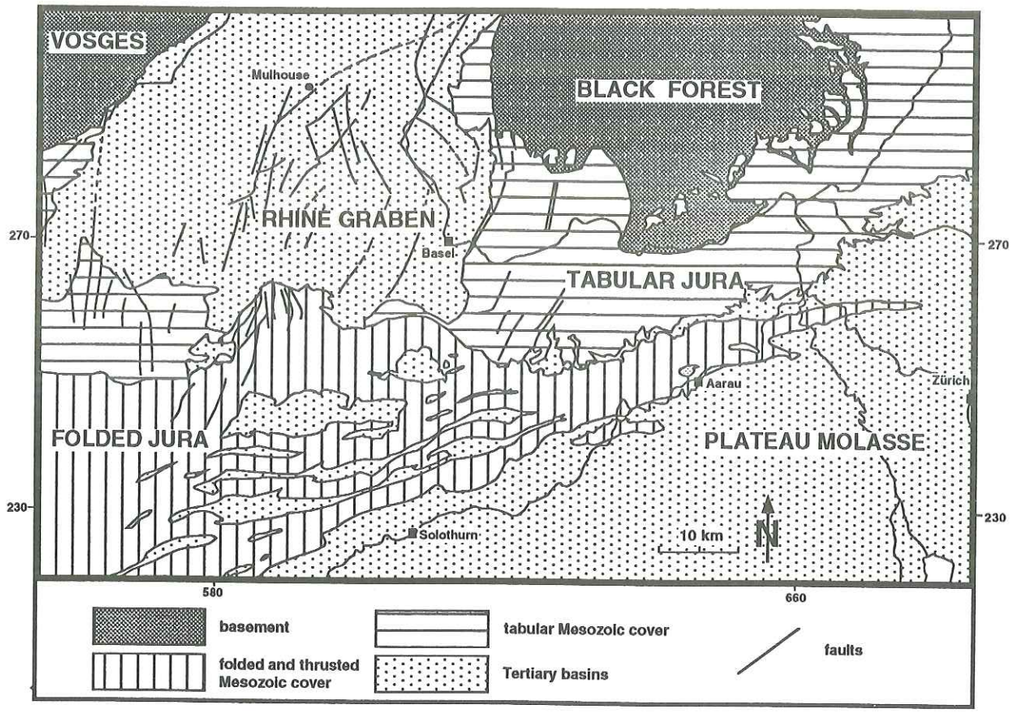

Fig. 1.10: Tectonic map of Northern Switzerland (modified after Todorov et al. 1993).

High subsidence rates during Middle and Late Triassic are observed in the Jura (Wildi et al. 1989). Subsidence rates decrease abruptly during the Early Jurassic and increase again in an irregular pattern in the Middle Jurassic. The Triassic and Middle Jurassic phases are probably due to intracontinental rifting following Late Variscan structures (Wildi et al. 1989).

During the Late Jurassic (Malm) the Vindelician High became fully inundated and was overlaid by up to 600m of limestones and marlstones. Unlike the Triassic to Middle Jurassic series, the Malm thickens towards the SE, thereby emphasising the integration of the future Molasse Basin into the Tethys shelf (Bachmann et al. 1987).

No sediments of Cretaceous age are found in the study area. Tertiary strata lie unconformably on Upper Jurassic sediments. This sedimentary gap is, at least in part, due to the latest Cretaceous-earliest Tertiary inversion tectonics which can be related to stresses that were exerted by the Alpine and Pyrenean orogenic events on the continental forelands of these foldbelts (Ziegler 1987, 1992). The uplift of large areas in the German Molasse Basin resulted in a north-westward truncation of Cretaceous and Upper Jurassic strata (Bachmann & Müller 1991). In the Swiss Molasse basin and the Jura, Cretaceous sediments are only found in the western part of the country (Lemcke 1974, Wildi et al. 1989). It is, however, uncertain to what extent the area coprresponding to the Rhine Graben and the South German Franconian Platform may have been covered by Cretaceous seas (Ziegler 1988). According to Lemcke (1988) this area was a region with little or no sediment accumulation throughout the Cretaceous. There are other observations indicating that Cretaceous strata have never been very thick in this area:

- The thickness of Lower Cretaceous strata (up to Cenomanian) rarely exeeds 100m in field sections located just west of the study area (sections Maiche, Montbéliard or Besançon in Wildi et al. 1989).

- Cretaceous transgressive sediments extended progressively towards the north, where Cretaceous strata become thinner and uncomplete (Trümpy 1980, Bachmann & Müller 1991, their figs. 20.4 & 20.5).

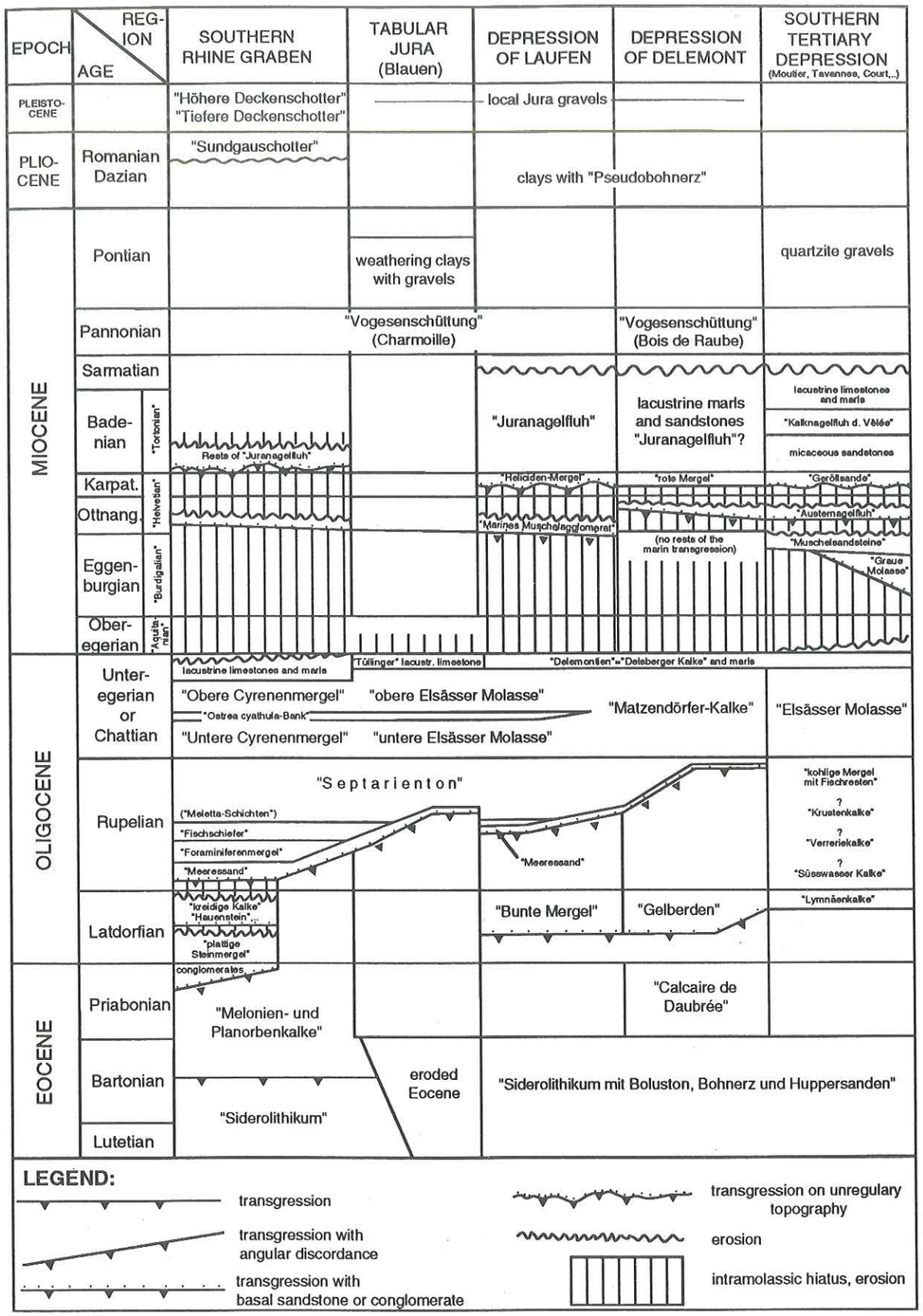

Fig. 1.11: Lithostratigraphic relations of Tertiary sediments between the southern Rheingraben and the Rauracien depression after Naef et al. (1985).

- According to Wildi et al. (1989), the subsidence of the Helvetic passive margin terminated at the end of the Late Jurassic. The Cretaceous subsidence history is probably already controlled by orogenic crustal flexure, with high subsidence rates only in the southernmost parts of the Helvetic realm (sections Aravis, Aermighorn and Alvier in Wildi et al. 1989).

The earliest Tertiary deposits are represented by continental Eocene formations (Naef et al. 1985): *Bohnerz* or *Sidérolithique*, filling karst pockets and caves. A final phase of subsidence in Northern Switzerland started in the Oligocene and ended in the Late Miocene when the Jura started to be folded. This subsidence is mainly controlled by the Rhine Graben rifting (especially for areas in the southern prolongation of the Graben) and by the tectonic loading of the European lithosphere by the Alpine nappes. One of the branches of the Rhine Graben, the "Rauracian depression", runs southwards into the area which was to become the Folded Jura. Oligocene deposits associated with the Rauracian depression are preserved particulary in the synclinal depressions of Laufen, Delémont, Moutier and Tavannes-Court. Figure 1.11 shows the lithostratigraphic relationships of Tertiary sediments between the southern Rheingraben and the Rauracien depression compiled by Naef et al. (1985).

The structural configuration of northern Switzerland is determined by two major basement structures which are (1) the southern termination of the N-S running Cenozoic Rhine Graben, and (2) the eastern part of the E-W striking late Palaeozoic Constance-Frick-Lons le Saunier trough:

(1) The Rhine Graben is a well developed intracontinental rift extending from Mainz in the NNE to Basel in the SSW, separating the elevated Hercynian blocks of the Vosges Massif in the West from the Black Forest Massifin the East (Illies 1974). This rifted area started to subside in the Middle Eocene, with major phases of geothermal flux during Eocene-Oligocene and from the Pliocene to the present (Teichmüller & Teichmüller 1979, see also Robert 1985, p. 191-213). South of Basel, the Graben structure degenerates into a simple flexure at its eastern border. Numerous narrow grabens, normal faults and left-lateral strike-slip faults extend SSW-wards into the epivariscan Mesozoic cover of the Tabular Jura and the folds and thrusts of the Folded Jura (e.g. Laubscher 1982, 1986, 1987, 1992). The main graben structure is in fact a pull apart basin linked to the Bresse Graben further West by a transform fault zone (Lacombe et al. 1990).

(2) This transform fault zone coincides partly with the strike-slip and graben structure of the late Palaeozoic Constance-Frick-Lons le Saunier trough, which is known since a long time in the basement of the western Jura (Debeglia & Gable 1984, cum biblio.), and which has been described in the eastern Jura by Müller et al. (1984), Laubscher (1987) and Diebold et al. (1991). The stratigraphic record and the tectonic structure as deduced from reflection seismics indicate late and post Hercynian subsidence due to strike-slip movements. In Eastern Switzerland, the zone of décollement of the Folded Jura coincides with the southern margin of this trough. Therefore, Laubscher (op. cit.) suggests a remobilisation of this margin during the Tertiary.

Chapter 2: METHODS FOR QUANTIFYING THERMAL DIAGENESIS

2.1 Choice of paleothermometers

There are many methods in the earth sciences to assess the paleogeothermal conditions in sedimentary basins. Both organic and mineral indicators have been used to quantify diagenesis (see reviews in Heroux et al. 1979, Bustin et al. 1985, Robert 1985, Buntebarth & Stegena 1986, Frey 1987, McCulloh & Naeser 1989). Generally, measurable indicators of thermal maturity cannot be directly converted to paleotemperature because they depend on several parameters such as temperature, time, pressure, type of organic matter, rock and mineral composition, eH, pH, and others.

Organic matter (OM) in sediments is very sensitive to heat exposure. The maturation level attained by the OM is almost **irreversible** and depends only on a few factors (Teichmüller & Teichmüller 1986, Tissot et al. 1987). This is why organic diagenesis is so important for reconstructing the thermal history of sedimentary basins. The maturation level of sedimentary OM is usually expressed by the following indicators:

i) optical maturation indices: vitrinite reflectance; thermal alteration index (TAI); spectral fluorescence indicators such as the wavelength of maximum intensity or red/green ratio; see reviews in Correia (1969), Staplin (1969), Ottenjann et al. (1974), Alpern (1976), Stach et al. (1982), Teichmüller & Durand (1983), Tissot & Welte (1984) and Robert (1985).

ii) organic geochemistry parameters of kerogen: caloric value of OM; ash, volatile and moisture contents of coal; fixed carbon of kerogen-containing rocks from proximate analysis, Tmax from Rock-Eval pyrolysis, H/C and O/C ratio from ultimate analysis; electron paramagnetic resonance; stable carbon isotopes; see reviews in Heroux et al. (1979), Durand (1980), Tissot & Welte (1984), Bustin et al. (1985) and Espitalié et al. (1985a, 1985b, 1986).

iii) organic geochemistry parameters of bitumen: extractable organic compounds; biological markers, total extractable organic matter; carbon preference index (CPI); see reviews in Heroux et al. (1979), Durand (1980) and Bustin et al. (1985).

The two methods chosen in this study are vitrinite reflectance and Rock-Eval pyrolysis. Vitrinite reflectance and Tmax from Rock-Eval pyrolysis are the most widely used indicators of thermal maturity in oil and gas exploration (Tissot et al. 1987). Vitrinite reflectance is also regarded as the most reliable and precise method for quantifying organic diagenesis (Bustin et al. 1985). The temperature index obtained from Rock-Eval pyrolysis (Tmax) is another widely used maturation index (Tissot & Welte 1984). In addition, Rock-Eval pyrolysis yields information on the composition of the OM (Espitalié et al. 1985a, 1985b, 1986).

Many maturation indices based on the diagenesis of the mineral fraction have also been proposed. Fluid inclusions trapped in diagenetic overgrowths or pore-filling phases can yield information on minimum burial temperature, fluid pressure and composition (Haszeldine et al. 1984, Buntebarth & Stegena 1986, Mullis 1987a, McCulloh & Naeser 1989, Barker & Goldstein 1990). Fission tracks in apatite or zircon preserve an integrated record of the time spent by a sample below the annealing temperature (e.g. ~120°C for apatite) and can, therefore, be used to decipher the time-temperature history (Naeser 1979, 1981, Gleadow et al. 1983, Green et al. 1989). Other techniques used in paleogeothermal studies are the analysis of the 40Ar/39Ar age spectrum of detrital microcline (Harrison & Bé 1983), oxygen isotopic analysis to neoformed diagenetic silicate minerals in deeply buried shales and sandstones (Savin & Lee 1984), or the study of anchizone minerals and characteristic associations (see review in Kisch 1987).

However, the equilibrium of clay minerals and their mutual transformations (disappearance-neogenesis) probably provided the most used mineral indicators in the past. Clay mineral assemblages in general and the smectite to illite transformation in particular have been used by many investigators as indicators of thermal history (Kübler 1964, 1973, Burst 1969, Foscolos & Stott 1975, Hower et al 1976, Hoffman & Hower 1979, Monnier 1982, Smart & Clayton 1985, Pollastro & Barker 1986, Ramseyer & Boles 1986, Velde et al. 1986, Kisch 1987, Pearson & Small 1988, Weaver 1989, and others).

Clay mineral analysis of shales and sandstones and fluid inclusion analysis of veins are chosen as complementary techniques to the organic diagenesis.

2.2 Solid organic indicators

2.2.1 Maturation of organic matter (OM)

During burial, organic matter in the sediments undergoes an alteration process (Stach et al. 1982, and references therein). For coals, this process corresponds to the progressive transformation of peat into lignite, sub-bituminous coals, bituminous coals, semi-anthracite, anthracite to meta-anthracite (Bustin et al. 1983). The degree of transformation of coal within this sequence is referred to as coal rank. Maturation studies are important in geology because the degree of maturation can be determined not only in coal beds but also in dispersed solid organic matter occurring as a minor constituent in most sedimentary rocks (Teichmüller & Teichmüller 1981).

According to Tissot & Welte (1984), the three main stages of OM evolution in sediments are diagenesis (for a review of terminological problems between organic and inorganic diagenesis see Frey 1987), catagenesis and metagenesis:

i) Diagenesis begins in recently deposited sediments. Microbial activity is one of the main agents of transformation. Chemical rearrangements (polycondensation and insolubilisation) occurring at shallow depth leads to the formation of geopolymers precursing kerogen (kerogen is the fraction of sedimentary OM insoluble in usual organic solvents, Durand 1980). The most important hydrocarbon formed during this early stage is methane. In addition, OM produces CO_2 and H_2O.

ii) Catagenesis results from an increase in temperature and pressure during burial. Thermal degradation of kerogen is responsible for the generation of most hydrocarbons (oil and gas).

iii) Metagenesis is reached only at great depth.

Major chemical changes of kerogen during coalification are i) the elimination of functional groups, ii) the breaking of some carbon-carbon bonds to yield some chain-like material and saturated cycles and iii) increasing aromaticity (Tissot et al. 1987). The alteration of kerogen clearly results in the change of most chemical and physical properties. The maturation indices, based directly or indirectly on such properties, change, therefore, with increasing maturation.

It has long been recognised that temperature is the most important parameter affecting the coalification level of OM (e.g. Karweil 1956). The influence of heating time is still debated. Most of the early studies assumed that the chemical reactions governing organic transformation follow first-order reaction kinetics (Karweil 1956, Lopatin 1971, Connan 1974). The reaction rate is, therefore, related linearly to time and exponentially to temperature. This assumption is crucial for the maturation of organic matter in sediments, because even at very slow rates these reactions can proceed to a very high degree of completion during geological time (Price 1983). A popular and rather simple approach for quantifying organic diagenesis was developed by Lopatin (1971). This method calculates a maturation parameter by integrating the entire time-temperature history of a marker horizon assuming that increasing the temperature by 10 °C doubles the maturation reaction rate. Waples (1980) designed a modified version of Lopatin's method: a calculated maturation parameter TTI (Time Temperature Index) is correlated with the vitrinite reflectance. These basic approaches have been criticised because:

- the effect of heating time on the thermal maturation of sedimentary organic matter seems to be limited (Barker 1983, Price 1983, Barker & Pawlewicz 1986, and references therein). According to Barker (1989), organic matter stabilises with respect to temperature after about 10^6 to 10^7 years in normal burial conditions, 10^4 years in geothermal systems and about 10^{-1} to 10^0 years in contact metamorphism;
- the assumption that the rate of maturation doubles every 10 °C is considered to be inaccurate (Price 1983, Burnham & Sweeney 1989).
- The Lopatin-Waples calculations tend to underestimate thermal maturity at high heating rates (rapid burial) and overestimate it at low heating rates (Wood 1988).

More recently, kinetic models for the simulation of OM maturation, based on viable chemical principles, provide new tools (Braun & Burnham 1987, Quigley et al. 1987, Ungerer & Pelet 1987, Larter 1989, Sweeney 1990, Sweeney & Burnham 1990, Ungerer 1990). Most of these models are still based on the classical formulation of first-order kinetics. However, an important aspect is the consideration of several parallel reactions which accounts for the diversity of composition and distribution of chemical bond types in the original kerogen (Tissot et al. 1987).

2.2.2 Vitrinite reflectance

2.2.2.1 General remarks and definitions

Reflectance of a material is the ratio of reflected light to incident light intensity. The reflectance (R) of solid organic matter is measured on carefully polished sections by means of a photometer mounted on a microscope (detailed descriptions can be found in International Committee for Coal Petrology 1963, 1971 and Stach et al. 1982). The sample is viewed and reflection measurements made under oil immersion (therefore Ro for Roil is often used), using an oil with a known refractive index. When the incident light is perpendicular to the polished section, the reflectance is expressed by the Fresnel-Beers formula:

$$R=[(n-N)2+n2k2] / [(n+N)2+n2k2]$$

where n and k are respectively the refractive and absorption indices of the material and N is the refractive index of the immersion medium, at the wavelength of the incident light. Since N, n and k vary with the wavelength, normalised measurements are made with a monochromatic light at 546 nm. In the case of organic matter, n and k cannot be measured or only with insufficient accuracy (Stach et al. 1982). However, the use of this complex relationship can be avoided by comparing the reflectance of solid organic matter with that of an optical standard of known reflectance.

According to Robert (1985), organic matter can be subdivided into three main groups:

i) The "primary" macerals of coals: They are found in coal seams as well as in "coaly" particles dispersed in sediments. Macerals are classified into three groups (see Stach et al. 1982 for a detailed review of macerals): vitrinite, liptinite, and inertinite either because of similar origin (liptinite) or because of differences in preservation (vitrinite, inertinite).

ii) The "structureless" primary matter: It comprises essentially the fluorescent ground masses or organomineral associations in most oil shales and source rocks. It does not occur frequently in coals.

iii) "Secondary products": Various fixed or mobile components, which originate from the two preceding groups. They include in particular the hydrocarbon compounds.

Vitrinite is the most frequent maceral family of humic coals, and more generally of sedimentary organic matter of terrestrial origin, composed of gels and gelified tissues produced by the decay of ligno-cellulose parts of higher plants (Durand et al. 1986). In the early stage of coalification, there is no vitrinite sensu stricto. The components which will produce vitrinite further on are called huminite. Figure 2.1 shows the classification of the huminite/vitrinite family after Alpern & Teichmüller (1971).

Reflectance may be measured on any of the macerals, but for rank studies huminite/vitrinite is nearly always selected. Vitrinite is preferred because:

- it tends to occur as large homogenous particles (practically, reflectance cannot be safely measured on organic particles or areas less than 5 µm in size, Durand et al. 1986);
- it is the dominant maceral in coals and a common constituent of the organic fraction of many sedimentary rocks;
- its reflectance shows good correlation with other coalification parameter at most rank levels;
- it increases regularly from a minimum of 0.15% to greater than 5.5% at a level equivalent to the lower greenschist metamorphic facies (Bustin et al. 1983).

By convention ulminite B respectively telocollinite are used for maturity determinations (International Committee for Coal Petrology 1963, 1971, McCartney & Teichmüller 1972 and Stach et al. 1982).

LIGNITE-BROWN COAL					BITUMINOUS COAL		
MACERAL GROUP	MACERAL SUBGROUP	MACERAL	MACERAL TYPE	MACERAL VARIETY	MACERAL TYPE	MACERAL	MACERAL GROUP
huminite	humotelinite	textinite	texto-ulminite	A (dark)	telinite 1	telinite	vitrinite
				B (light)			
		eu-ulminite		A (dark)			
				B (light)			
	humodetrinite	attrinite densinite	eu-ulminite	A (dark)	telinite 2	vitrodetrinite	
				B (light)			
	humocollinite	gelinite	detrogelinite telogelinite		desmocollinite		
			levigelinite	eugelinite	telocollinite	collinite	
			porigelinite		gelocollinite		
		corpohuminite	phlobaphinite pseudo-phlobaphinite		corpocollinite		

Fig. 2.1: Correlation of the huminite macerals of brown coals and lignites with the vitrinite macerals of bituminous coals after Alpern & Teichmüller (1971).

Except in extremely high rank coals, vitrinite is uniaxial negative with its optic axis perpendicular to the bedding plane (Bustin et al. 1983). Therefore, when using polarised light a minimum reflectance (Rmin) and a maximum reflectance (Rmax) can be measured; the difference between Rmin and Rmax is termed bireflectance (Davis 1978). There are two major types of reflectance measurements:

i) In low rank organic matter (<1% Rr, Buiskool Toxopeus 1983), the measurement generally used is the mean random reflectance (without any particular orientation of the organic particles) carried out in non-polarised light (Robert 1985). In this study the abbreviation **Rr** is used for this type of measurement.

ii) For high rank organic matter, mean maximum reflectance (Rmax), using polarised light, is preferred (Davis 1978). Mean random reflectance (Rr) is related to the mean maximum reflectance (Rmax) by Rr=1.066*Rmax (Ting 1978).

2.2.2.2 Sampling

225 samples from outcrops, tunnels or mines have been analysed. Most samples have been taken from Tertiary formations (UMM, USM, OMM and OSM) of the northern Alpine Foreland Basin (Fig. 1.1).

Many samples were provided by colleagues working in different parts of the Molasse basin: G. Amberger, J. Charollais, G. Gorin, G. Trabold and W. Wildi in the Geneva Basin and Haute-Savoie; M. Weidmann, J.-P. Berger and J.N. Gabus, as well as the Geological Museum of Lausanne in western Switzerland; F. Schlunegger for the Lake Thun area; T. Bolliger and T. Gubler in eastern Switzerland; D. Kälin and Geological Museum of Lausanne in northern Switzerland.

In order to obtain the most reliable data on thermal maturity, only vitrinite reflectance results of macroscopic coaly fragments (from wood, bark, leaves and smaller plant fragments) and coal seams are included. According to Durand et al. (1986), only series containing a fair amount of organic

matter derived from higher plants can be used with confidence; coals or macroscopic fragments from higher plants are, therefore, safer than dispersed organic matter.

The major problem with organic matter from outcrops is weathering (see review in Davidson 1990). Exposure of coal to the atmosphere or oxygenated waters in the subsurface results in oxidation of the organic and inorganic constituents. In any site, the depth and degree of oxidation will be a function of climate, groundwater conditions, extent of fracturing and of the particle size and composition of the organic matter (Bustin et al. 1983). The same authors reported oxidation depths of up to 10m, locally even deeper.

Petrographic variations in coals attributed to oxidation and weathering include the formation of rims along grain boundaries and microfractures, the formation of micropores and microfissures, increased relief and variation in vitrinite reflectance (Crelling et al. 1979, Marchioni 1983).

The influence of weathering on vitrinite reflectance is debated. Some workers (Benedict & Berry 1964, Kojima & Ogoshi 1973) concluded that vitrinite reflectance variation during laboratory induced oxidation was significant, showing an initial decrease, followed by irregular overall increase. Marchioni (1983) reported that in weathered low rank coal (Rr=0.5%) weathering caused an increase in reflectance. Other workers (Alpern & Maume 1969, Pearson & Kwong 1979, Bustin 1980) have found, however, that naturally weathered outcrop coal had lower reflectance than the fresh equivalents sampled at depth. Chandra (1962) and Ingram & Rimstidt (1984) found no significant difference in Rr due to weathering effects.

Ingram & Rimstidt (1984) point out that weathered samples can give reliable vitrinite mean reflectance value of rank if measurements on vitrinite grains are made away from the weathered features.

2.2.2.3 Sample preparation

The main objective of sample preparation is to produce for microscopic examination a suitable polished surface which should meet the following requirements (Davis 1978):

i) The entire surface should be flat, and with little or no relief between the various coal components or at the edges of coal particles.

ii) It should be free of pits caused by loss of grains.

iii) It should appear substantially free of scratches under the microscope.

Pellets of particulate coal or grain section are the most frequently used specimens for microscopy. The following sample preparation procedure was used:

- Coaly, macroscopically visible fragments are isolated and concentrated by hand-picking.
- The sample is crushed to particle size between 0.4 and 1mm.
- Particles are mixed with a cold mounting epoxy resin (Epofix from Struers) in a plastic mold. The temperature reached during this procedure does not exceed 40°C. If mineral matter is too abundant, the pellet is placed in a ultrasonic cleaner and dried.
- Pellets are ground and polished on a rotating lead disk with different abrasive diamond sprays (6, 3, 1, 0.25 µm).

2.2.2.4 Measuring procedure

A detailed description of the measuring procedure is given by the International Committee for Coal Petrology (1963, 1971) and Stach et al. (1982).

Mean random vitrinite reflectance is determined using a Leitz MPV compact microscope, an immersion objective 50*/0.85 and a sapphire standard (Rr=0.583%). The reflectance of the standard is measured at the beginning and at the end of the procedure in order to check the stability of the measuring equipment. If the difference between these two values is too high (>1% difference, Davis 1978), reflectance determination of the sample are rejected; if not, reflectance values are corrected linearly for this shift. According to Durand et al. (1986), the precision of measurements is very good with modern equipment and the second decimal is considered as significant.

If available, at least 50 telocollinite particles, statistically distributed over the surface of the section, are measured for the reflectance determination of a sample.

2.2.2.5 Presentation of results

For each sample, a mean of the readings is calculated, and generally a standard deviation value given. Data are also presented in the form of frequency histograms, divided into V-steps or 1/2V-steps. V-steps represent a range of 0.1% and 1/2V-steps a range of 0.05% reflectance. In ideal cases, the histograms are single-peaked, but they may be multipeaked and show several groups of values. Coal samples are generally quite suitable for precise reflectance measurements, because they contain an abundance of vitrinite. Multipeaked reflectance histograms are common in samples rich in dispersed organic matter, especially in marine sediments, due to the presence of recycled particles.

2.2.2.6 Isoreflectance maps

Since only outcrop samples were analysed in this study, results are plotted on a map. For a better appreciation of geographical variations in the data, isoreflectance contours were constructed by using a commercial kriging computer program (SURFER).

2.2.2.7 Limitations of the method

Although it is considered by many scientists as the most powerful tool in assessing the thermal maturity of a sample, the vitrinite reflectance technique has several limitations. These can be classified into two major groups: A) artificially induced variations and B) natural variations of vitrinite reflectance.

A) Artificially induced variations

- Quality of the polished surface: Inadequate polishing results into a considerable decrease of mean reflectance, together with an increased standard deviation (Buiskool Toxopeus 1983).
- Caving and mud additives: important for well cutting samples.
- Too few readings: The number of reflectance measurements required for an adequate characterisation of the mean random vitrinite reflectance is a major concern in the petrographic analysis of dispersed organic matter. Barker & Pawlewicz (1992) stated that reflectance values calculated on less than 20 readings of vitrinite are potentially unreliable. However, according to the same authors, it is still a better strategy to concentrate on selecting for analysis a few high-quality vitrinite grains rather than seeking a quantity of inconsistent vitrinite grains in order to make the results more statistically reliable.
- Properly identified vitrinites: Identification of the "good" vitrinite particles is perhaps the major problem for the operator. Generally, in coals, vitrinite reflectance readings are made on wide monomaceralic bands (ulminite B/telocollinite of the International Committee for Coal Petrology 1963, 1971, McCartney & Teichmüller 1972 and Stach et al. 1982, Goodarzi 1987; in part vitrinite A of Brown et al. 1964). The other major component of the vitrinite maceral group is desmocollinite (Stach et al. 1982) or vitrinite B (Brown et al. 1964). However, the distinction between the different kinds of vitrinite is not always straightforward, especially when the preparation is made from powdered samples or dispersed organic matter where the spatial relations between the macerals can no longer be examined (Durand et al. 1986). For instance, the differentiation of pseudovitrinite from telocollinite may be very difficult because the only reliable criterion for the recognition of pseudovitrinite is that of slitted structure (Kaegi 1985). In samples with dispersed organic matter, the recognition of fresh (first-cycle) humodetrinite (vitrodetrinite for higher ranks) and reworked (second-cycle) and generally more mature material is the major problem for rank determinations. Problems of diagnosis may also occur for the distinction between vitrinites and inertinites (particularly between telocollinite and semifusinite) because of the frequent lack of morphological criteria in these two families (Durand et al. 1986).

B) Natural variations of vitrinite reflectance

- Buiskool Toxopeus (1983) has clearly shown the existence of different populations of vitrinite in coals, even in the absence of reworked material. A series of normal, humic coals and coaly shales was found to contain two main groups of vitrinite material: i) vitrinite 1 (including telinite, telocollinite and corpocollinite), which is hydrogen poor, provides higher reflectance and shows no

fluorescence and ii) vitrinite 2 (desmocollinite), which is hydrogen-richer and shows lower reflectance.

- Vitrinite reflectance suppression due to the presence of liptinite: Many investigators (Hutton & Cook 1980, Kalkreuth 1982, Newman & Newman 1982, Goodarzi 1985a, Price & Barker 1985, Durand et al. 1986, Wenger & Baker 1987, Fang & Jianyu 1992) have discussed the phenomenon whereby measured Rr values are lower than expected for a given regional rank. The broad association of liptinite material and vitrinite reflectance suppression is acknowledged by most authors. Some workers believed that bitumens or hydrocarbons diffused into the vitrinite and caused the reflectance suppression (Hutton & Cook 1980, Kalkreuth 1982). Price & Barker (1985) suggested that Rr suppression was due to the incorporation of higher than normal amounts of hydrogen into the vitrinite maceral during diagenesis.

- Variations in the paleoenvironmental conditions during OM deposition: Vitrinite macerals originate primarily from lignin, cellulose and tannins which are transformed, through mouldering and peatification, into humic substances. Since the type and properties of humic acids are influenced by a range of pH conditions and redox potentials relating to different depositional environments, vitrinite macerals also display varying physical and chemical compositions (Murchison et al. 1991). Newman & Newman (1982) believed that vitrinite deposited under anaerobic conditions tends to have a lower reflectance, and that reflectance data from marine and marginal marine sediments should be interpreted with particular caution. According to the same authors, vitrinite in non-marine strata is not completely exempt from reflectance anomalies.

In a recent study, Fang & Jianyu (1992) found that vitrinite macerals with different initial hydrogen contents have different reaction kinetics, with hydrogen-poor, oxygen-rich vitrinite macerals maturing at an enhanced rate compared to vitrinite macerals with higher hydrogen and lower oxygen contents. They showed that even the initial hydrogen content of telocollinite may vary from one coal to another. Therefore, the same reflectance values will not always reflect the same time-temperature history, whereas different reflectance values will not always indicate different organic maturity levels. Fang & Jianyu (1992) concluded that only the reflectance values of equivalent vitrinites (those similar to the telocollinites in "normal coals" in initial composition and kinetics) are comparable in determining basin-by-basin thermal histories.

Differences in the parent vegetation may also result in different vitrinites. Sittler (1979) found vitrinite reflectance values in Upper Cretaceous and Tertiary coals derived from resinous trees lower than in Paleozoic coals, for the same maturation stage.

- Dependence of vitrinite reflectance on the lithology: The influence of different overlying or enclosing lithologies on vitrinite reflectance has been debated since a long time (Sofiyev et al. 1962, Damberger 1968, Teichmüller & Teichmüller 1968, Jones et al. 1972, Bostick & Foster 1975, Rhoades et al. 1975, Pearson Murchison 1989, Murchison et al. 1991). Jones et al. (1972) reported mean vitrinite reflectances from seams overlain by sandstones as being lower than those from seams overlain by argillaceous rocks. Bostick & Foster (1975) concluded that vitrinites from sandstones generally had lower reflectances than those associated with argillaceous rocks. Recent studies confirmed these observations (Pearson & Murchison 1989, Murchison et al. 1991). There is so far no agreement among scientists to explain the reflectance suppression under or in sandstones. Good heat conduction within sandstones (Damberger 1968), confinement of volatiles within mud and shalestones and their much easier escape from sandstones (Jones et al. 1972), different microbiological activity in the sedimentary environments (Fermont 1988, Murchison et al. 1991), or oxidation during or after diagenesis were invoked to explain the influence of lithology on vitrinite reflectance.

- Influence of pressure on coalification: The opinion that static pressure delays chemical coalification has been confirmed again recently by carbonisation experiments under various pressures (Horváth 1983, Goodarzi 1985b). On the other hand, tectonic stresses may influence the Rmax values and the anisotropy of vitrinites. By inducing parallel ordering of aromatic lamellae, pressure enhances the "physio-structural" coalification, especially at high rank stages (Stach et al. 1982).

- Alteration: This problem is treated in chapter 2.2.2.2.

2.2.3 Rock-Eval pyrolysis

2.2.3.1 General remarks

Rock-Eval pyrolysis is used to determine the petroleum potential and thermal maturity of rocks. It provides a rapid evaluation of the type of solid organic matter (kerogen = fraction of the organic matter which is insoluble in the usual organic solvents, Durand 1980) contained in rock sample. Three main types of kerogen are recognised. They are characterised by their respective evolution (coalification) path in the van Krevelen (H/C versus O/C) diagram (Tissot & Welte 1984):

- Type I kerogen, derived from algal lipids or from organic matter enriched in lipids by microbial activity, shows a high initial H/C ratio and a high potential for oil and gas generation.
- Type II kerogen, related usually to marine organic matter deposited in a reducing environment, shows important, but lower than Type-I, H/C ratios.
- Type III kerogen, derived from terrestrial higher plants, shows low H/C ratios and O/C ratios comparatively higher than in the two other types. The chemical evolution of coal during maturation is similar to that of Type-III kerogen.

Pyrolysis involves heating of a sample at a pre-selected rate in an inert atmosphere and monitoring the type and amount of gases produced. The analysis simulates maturation of organic matter by progressively heating rock samples to temperature up to 600°C. This heating distils the free organic compounds, then cracks pyrolytic products from the kerogen. A detailed introduction to the Rock-Eval pyrolysis technique and applications can be found in Espitalié et al. (1985a, 1985b, 1986).

2.2.3.2 Sampling

53 outcrops samples in the Geneva Basin and Haute-Savoie (Fig. 1.4) have been chosen for Rock-Eval analysis. Most samples (52) consist of "clean" coaly fragments, which were concentrated by hand-picking from the original rock samples). One sample is an organic-rich marl (RS54). With the exception of the marl sample, the vitrinite reflectance of all samples has been measured. For a discussion of weathering problems see chapter 2.2.2.2.

2.2.3.3 Instrumentation and operating conditions

Samples were analysed at the IFP (Institut Français du Pétrole) in Paris by Guy Pichaud. The equipment used was a *Rock-Eval II*. Samples were desiccated and ground prior to analysis. A known quantity of the sample (for coals ≈10mg) is heated at 250°C for 3 minutes in the oven. The products are swept by an inert gas (helium) to a flame ionisation detector. The free hydrocarbons in the rock are vaporised and recorded as an initial peak **S1**. Then the sample is heated to 600°C at 25°C increase per minute. The remaining organic matter is thermally cracked releasing hydrocarbons which produce a second peak **S2**. Maximum production of these hydrocarbons (top of peak) occurs at a temperature called **Tmax**. At the same time, the CO_2 produced up to 390°C is measured by a thermal conductivity detector and recorded as a third peak **S3**. The temperature range from 250°C to 390°C was chosen because, in this temperature window, CO_2 is produced from organic matter with little interference of minerals (carbonates, bicarbonates). The total organic carbon (**TOC**) of the sample is obtained by summing the carbon in the pyrolysate with that obtained by oxidising the residual organic matter at the final temperature of 600°C (peak **S4**).

2.2.3.4 Rock-Eval parameters

Measured primary parameters:

- S1: This parameter quantifies the free hydrocarbons (HC) present in the sample and is expressed in mg HC per gram of sample. It represents the fraction of the original genetic potential which has been effectively transformed into hydrocarbons and depends on the level of maturation and on migration phenomena (Espitalié et al. 1985b).
- S2 represents the residual petroleum potential which has not yet been used to generate hydrocarbons. S2 varies with TOC, type of organic matter and maturation level, and is expressed in mg HC per gram of sample (Espitalié et al. 1985b).

- S3: This parameter is a measure of the oxygen content in the kerogen and is expressed in mg CO_2 per gram of sample. Like S2, S3 varies with TOC, type of organic matter and maturation level (Espitalié et al. 1985b).
- Tmax: The temperature index, Tmax (°C), has become a widely used maturation index, as it increases with the maturation of organic matter (Tissot & Welte 1984). Tmax varies with the type of organic matter, with Tmax sensitivity being the best for determining the degree of maturation of OM Type III (Espitalié 1986). For Type II and Type III OM oil formation starts at Tmax=430-435°C (0.4-0.5%Rr and 0.5-0.6%Rr respectively), whereas gas formation starts at Tmax of about 450°C (~1%Rr) for Type II and at about 465°C (~1.3%Rr) for Type III organic matter (Espitalié et al. 1985b).
- TOC: It is a measure of the quantity of organic carbon in a sample and is expressed in weight %. It can be used for source rock characterisation (Espitalié et al. 1986).

Calculated parameters:

- The hydrogen index (**HI**) is defined as HI=S2 / TOC (mg HC/g TOC).
- The oxygen index (**OI**) is defined as OI=S3 / TOC (mg CO_2/g TOC).

Kerogen type can be characterised by OI and HI, as the latter correlate respectively with the atomic O/C and H/C ratios (Katz 1983, Espitalié et al. 1986). A modified van Krevelen diagram, in which the hydrogen and oxygen indices are substituted for the atomic H/C and O/C ratios, provide a measure of kerogen type (Espitalié et al. 1985b, 1986).

Another useful diagram is the Tmax vs. HI crossplot, which helps to characterise the type of organic matter and its level of maturation (Espitalié et al. 1985b, 1986).

- The production index (**PI**) is defined as PI=S1 / (S1+S2). In absence of migration, PI is an evaluation of the transformation ratio which is defined as the ratio of the petroleum actually formed by the kerogen to the genetic potential, i.e., to the total amount that the kerogen is capable to generate (Tissot & Welte 1984). The continuous increase of this ratio as a function of depth makes it a valuable index of maturation (Tissot & Welte 1984). The beginning of the oil window ranges between PI values of 0.05 and 0.1, the maximum oil formation being generally attained between 0.3-0.4 PI (Espitalié et al. 1986).

The validity of these parameters is subjected to the following constraints (Espitalié et al. 1986):

- TOC< 0.3%: all parameters unreliable
- TOC<0.5%: OI unreliable
- S1 and S2< 0.2 mg HC per gram of sample: PI and Tmax unreliable. Peters (1986) rejected PI and Tmax only when S2<0.2 mg HC per gram of sample.

The different measured and calculated parameters were mapped and isovalue contours were calculated by kriging.

2.2.3.5 Problems and limitations in evaluating Rock-Eval pyrolysis results

- Coal samples: Coals of higher plant origin do not generally respond to pyrolysis in the same way as dispersed Type III organic matter (Peters 1986). Therefore, HI vs. OI plots may misrepresent the type of organic matter. For reasons not fully understood, some coals known from elemental analysis and microscopy to be Type III plot between Type II and Type III kerogens on HI vs. OI diagrams (Peters 1986). Typically, coals show HI values between 50 to 250 mg HC/g TOC (Espitalié et al. 1986).
- Alteration: All types of organic matter are exposed to oxidation during transport, deposition, and diagenesis. Oxidation tends to remove hydrogen and add oxygen to the kerogen (Durand & Monin 1980), and thus decreases the HI and increases the OI (Espitalié et al. 1986). Oxidised kerogens usually show high Tmax values or lack an S2 peak (Peters 1986).
- Migration of oil: Heavy ends of migrated oil and indigenous bitumen can affect the S2 and Tmax of the kerogen (Peters 1986). The S2 peak is made only of hydrocarbons coming from kerogen cracking and from the volatilisation of heavy hydrocarbons, which, usually, represent only a few percents of S2. Tmax may, however, be more or less strongly lowered due to the pyrolysis of migrated resins or asphaltenes (Espitalié 1986). Migrated oil is a likely explanation in cases of immature rocks with high PI values (Espitalié et al. 1986). Natural contamination is most severe where oil has migrated into coarse-grained or fractured organic lean rocks.

- Influence of the mineral matrix: For argillaceous rocks containing less than 0.5 wt.% TOC, HI values are likely to be too low and Tmax too high because of adsorption of pyrolitic organic compounds into the mineral matrix (Peters 1986). Espitalié (1986) stated that the heaviest hydrocarbon compounds, making up peaks S2 and S1, are the most easily retained in mineral matrices and "cooked" during heating. According to this author, this retention will have two main effects: i) a decrease of S1 and S2 and ii) an increase of Tmax, but without going above an increase of 5 to 6°C for Type II and 10 to 12°C for Type III (coal).
- Problems associated with Tmax: Variations of Tmax are due to different reasons: i) variations of Tmax with operating conditions such as rate of heating, weight sample or grain size (Espitalié 1986), ii) heavy oil accumulations (see above), iii) mineral matrix effects (see above) and type of organic matter (Espitalié 1986). Important quantities of recycled (higher rank) organic matter in a low maturity sample can shift the Tmax by up to 20°C (Peters 1986). Tmax values for samples with S2 peaks less than 0.2 mg HC/g TOC are often inaccurate and should be rejected (Peters 1986).

2.3 Mineral indicators

2.3.1 Clay mineral analysis

2.3.1.1 General remarks

Numerous studies of clay mineralogy in sedimentary rocks have demonstrated specific depth-dependant diagenetic changes (see reviews by Weaver 1979, Hower 1981, Kisch 1983 and Kübler 1984). Though much of the literature pertained to shales (e.g. Millot 1963, 1970, Dunoyer de Segonzac 1970, Velde 1979, Singer & Müller 1983, Weaver 1989) there is an ever growing literature on clay mineral diagenesis in sandstones (e.g. Wilson & Pittman 1977, Hoffman & Hower 1979, Pittman 1979, McDonald & Surdam 1984, Bjorlykke et al. 1989). X-Ray diffraction (XRD) has been the essential tool used in clay mineral studies of sedimentary rocks.

In physico-chemical terms, diagenesis can be regarded as the process of equilibration of mineral (mostly detrital) phases with aquatic environments of differing salinities, under conditions of increasing temperature and pressure (Singer & Müller 1983). According to Friedman & Sanders (1978), diagenesis involves, among other things: i) compaction, ii) addition of new material, iii) removal of material, iv) transformation of material by change of mineral phase, and v) replacement of one mineral phase by another.

The diagenetic clay mineral assemblage in sandstones is considerably more diverse than that of shales. This diversity is undoubtedly caused by the high permeability of sandstones in contrast to the low permeability of shales (Hoffman & Hower 1979). In shales, the pore-water chemistry appears to be controlled largely by the chemistry of the solids. However, the most critical factor in the diagenesis of sandstones is the nature of porewater flow and the degree of mass transfer taking place as a result of this (Bjorlykke et al. 1989).

2.3.1.2 Shale diagenesis

Hoffman & Hower (1979) stated that the generally reliable mineralogical criteria indicating increasing diagenesis in shales include: A) conversion of smectite to illite through a mixed-layer series, B) appearance of chlorite and C) disappearance of potassium feldspar by decomposition:

A) The smectite to illite transformation

The transformation of smectite to illite is probably the volumetrically most important clay mineral reaction in sedimentary rocks (Pytte & Reynolds 1989). Weaver (1956), Burst (1959) and Powers (1959) were the first to discuss this conversion. More recent studies include those by Perry & Hower (1970), Reynolds & Hower (1970), Hower et al. (1976), Boles & Franks (1979), Hoffman & Hower (1979), Johns & Kurzweil (1979), Srodon (1980, 1984), Rettke (1981), Monnier (1982), Pollastro (1985), Smart & Clayton (1985), Ahn & Peacor (1986), Bell (1986), Bethke & Altaner (1986), Chang et al. (1986), Keller et al. (1986), Pollastro & Barker (1986), Ramseyer & Boles (1986), Velde et al. (1986), Pearson & Small (1988), Glasmann et al. (1989), Inoue et al. (1989), Pytte & Reynolds (1989), Elliott et al. (1991), Lanson & Champion (1991), McCarty & Thompson

(1991), Buatier et al. (1992), Bühmann (1992), Lanson & Velde (1992) and Velde & Vasseur (1992).

It is generally accepted that the percentage of smectite layers in illite/smectite (%S in I/S) invariably decreases with increasing temperature. Potentially, therefore, the mineral is a sensitive indicator of thermal transformation. In addition to the grade-dependent proportion of smectite layers, illite/smectites exhibit a sequence of interlayering schemes that begins with random interstratification (Reichweite R=0, Brindley & Brown 1980), proceeds to short range ordering (R=1) and then to long range ordering (R=3) of the illite and smectite layers (Hoffman & Hower 1979). Virtually all mixed-layers containing 40 to 100% smectite layers are randomly interstratified; at less than 40% smectite layers, ordered interstratification is the general rule (Reynolds & Hower 1970). The illitisation of smectite is of discontinuous nature.

The exact mechanism by which smectite reacts to form illite is imperfectly understood. For a further discussion of this question see Dunoyer de Segonzac (1970), Hower et al. (1976), Boles & Franks (1979), Hoffman & Hower (1979), Bell (1986), Bethke & Altaner (1986), Ramseyer & Boles (1986), Elliott et al. (1991), Lanson & Champion (1991) and Awwiller (1993). The chemical changes involved in this reaction are the input of Al and K, and the release of Si, Mg and Fe (Eslinger & Pevear 1988). In a detailed mineralogical and chemical study, Hower et al. (1976) concluded that the decomposition of the K-feldspar, and perhaps of detrital potassium micas, provided the necessary K and Al for the smectite to be converted to illite. They proposed the following reaction:

smectite + K-feldspar (+mica?) = illite + quartz + chlorite.

In contrast, Boles & Franks (1979) proposed that the reaction involves a selective decomposition of the smectite layers in the I/S itself, a conservation of Al, and a concentration of potassium already present in the I/S clay.

The primary controls on the smectite-to-illite reaction in shales are temperature, time, and rock and fluid chemistry:

i) Temperature and time: It appears that the measurable mineralogical changes, correlated with temperature, occur over the continuum between room temperature (soils) and perhaps 300°C (Srodon & Eberl 1984). In a diagenetic environment, however, the illitisation reaction becomes detectable only at temperatures significantly higher than surface temperatures (Srodon & Eberl 1984). Pytte & Reynolds (1989) found an inverse correlation between temperature and time for a fixed composition of I/S and underlined the overwhelming importance of temperature. They concluded that the smectite-to-illite is mainly controlled by kinetic factors and proposed a sixth-order kinetic expression to describe the extent of the I/S reaction . Similar reaction kinetic approaches have been used by other workers (Eberl & Hower 1976, Bethke & Altaner 1986, Elliott et al. 1991). In contrast to the above, Weaver (1979) has compiled evidence from I/S extending over an age range of 325 my which shows that temperature, but not time, is the major control on % smectite in I/S.

ii) Rock and fluid chemistry: Temperature and time can only be important factors if the ions necessary for the reaction are present. Little is known of the composition of shale pore waters, but due to the low permeability of shales, pore waters must be strongly influenced by mineral dissolution and precipitation reactions within the shale itself (Eslinger & Pevear 1988). An important factor is the availability of K for the illitisation of smectite, which seems to be derived usually from detrital K-feldspars, mica or the smectite itself (Hower et al. 1976, Boles & Franks 1979). Strong inhibiting effects on the illitisation of smectite due to the release of Ca (e.g. during the albitisation of plagioclase) and Mg have been demonstrated experimentally by Blank & Seifert (1976) and Roberson & Lahann (1981). There is growing evidence that compositional varieties of smectite react differently to temperature increase during burial (e.g. Boles & Franks 1979).

B) Appearance of chlorite and kaolinite disappearance

Authigenic or neoformed chlorite is a relatively common constituent of sandstones and to a lesser extent of limestones; in shales however, due to the presence of detrital chlorite, it is difficult to determine how much diagenetic chlorite is present (Weaver 1989). It can be formed as a by-product of the smectite to illite reaction. This transformation usually goes through an intermediate stage of chlorite/smectite mixed layers, which often shows ordered layering (Dunoyer de Segonzac 1970, Kisch 1987).

Corrensite is defined as a 1:1 regularly interstratified trioctahedral chlorite/trioctahedral smectite or trioctahedral chlorite/trioctahedral vermiculite mineral (Lippmann 1954, Bailey 1982). In diagenesis, corrensite often occurs in intermediate stages when smectite converts to an equilibrium mineral assemblage of illite and chlorite (Dunoyer de Segonzac 1970, April 1981). Usually, there are four

facies associated with corrensite: i) evaporites, ii) carbonates, iii) volcanic and volcano-detrital facies, and iv) greywackes (Kübler 1973). The main requirement for the formation of chlorite/smectite mixed-layer minerals seems to be the availability of abundant Mg; Mg-rich varieties can form in hypersaline fluids without the need for elevated temperatures (Weaver 1989). According to Kübler (1973), corrensite appears under normal diagenetic conditions at temperatures of about 90 to 100°C and at 200°C in the low pressure hydrotherms.

Hower's et al. (1976) data from Oligocene-Miocene sediments of the Gulf Coast (USA) indicate that chlorite first occurs at a depth of about 2.5km or 70°C and increases in abundance between 2.5 and 4.3km, whereas the kaolinite content abruptly decreases below 3.4km. Similar observations were reported by other workers (Füchtbauer & Goldschmidt 1963, Dunoyer de Segonzac 1969, Scotchman 1987, Weaver 1989). These mineralogical changes and the systematic illitisation of smectite suggest that both smectite and kaolinite are involved in the formation of chlorite. As for the illitisation of smectite, the replacement of kaolinite by illite and/or chlorite is strongly dependent on the concentration of cations such as K, and Mg and Fe, respectively (Kisch 1987). In a review, Weaver (1989) concluded that kaolinite may be destroyed or modified at temperatures possibly as low as 70°C or may persist to 375° C, though 200°C is a more reasonable maximum for shales in which kaolinite is not the predominant physil.

C) Disappearance of potassium feldspar

Generally, shale diagenesis is considered to be an isochemical process with respect to the whole-rock chemistry (e.g. Hower et al. 1976, Pollastro 1985, Pearson & Small 1988). However, there are major changes in mineralogy and transfer between the coarse- and fine-size fractions. With increasing depth, in the coarse fraction of the shale, K-feldspar is either dissolved or albitised and the potassium is transferred to the fine fraction (Hower et al. 1976). These authors reported a major decrease in amount of K-feldspar between 2.5 and 3.7km, a depth below which this mineral is absent.

Other researchers suggested that reactants and products move readily between interbedded sandstones and shales (e.g. Boles & Franks 1979). Data published by Awwiller (1993) indicate that potassium is likely transferred into shales during smectite illitisation via fluids derived from interbedded sandstones.

D) Illite crystallinity

Weaver (1960) observed that illite peaks vary considerably in shape and width. He proposed the "sharpness ratio" to quantify this phenomenon and found that peak sharpness increased with increasing diagenetic and metamorphic grades. A more convenient parameter for the quantitative evaluation of peak sharpness is Kübler's (1964, 1968) "illite crystallinity index" (**IC**). It is defined as the width at the half height of the first diffraction peak of the mica group, measured in mm or degrees 2θ. IC is considered as useful parameter of incipient metamorphism in shales, marls, limestones and dolomites. It has been calibrated with mineralogical associations and compared with the potential oil window and vitrinite reflectance data (Kübler 1968, Héroux et al. 1979). Major problems in the use of this parameter are related to the sensitivity of IC to an increase of Mg or Na activities versus K and to the widening of the 001 peak due to the neoformation of clay minerals (Kübler 1990).

2.3.1.3 Sandstone diagenesis

The main processes during sandstone diagenesis are compaction, dissolution or recrystallisation of grains and precipitation of cement (Pettijohn et al. 1987). The volumetrically important common cements are silica, carbonates, sulphates and clays. The clay minerals found in sandstones include kaolinite, smectite, illite, chlorite, and mixed-layer clays as interstratified illite/smectite and chlorite/smectite (Bjorlykke et al. 1989).

Three types of clay minerals can be distinguished:

i) Neoformed or authigenic clay minerals: It is now well established that many, perhaps most, of the clay minerals in sandstones were formed during burial by fluids migrating through permeable sandstones (see review in Weaver 1989, Small et al. 1992a,b). Authigenic clays occur as pore linings, pore fillings, pseudomorphous replacements and fracture fillings (Wilson & Pittman 1977). According to these authors, an authigenic origin can be established on the basis of clay composition, structure, morphology and distribution, and sandstone textural properties. Their most reliable criteria are a) delicacy of clay morphology, which precludes sedimentary transport, b) occurrence of the clay as pore linings, and c) composition radically different from associated allogenic clays. A number of

factors influence the type of clay mineral that will grow in a sandstone: pore water chemistry, temperature, pressure, detrital mineralogy, organic content and composition, and tectonics (Weaver 1989).

ii) Allogenic clay minerals: Sandstones also contain allogenic clays which originate from terrigenous material (e.g. shale clasts) or are introduced subsequently to deposition as a result of bioturbation or infiltration (Wilson & Pittman 1977).

iii) Transformed clay minerals: Transformed clay minerals are those that form from the alteration of a pre-existing mineral. Examples of transformations are biotite to kaolinite, feldspar to kaolinite, kaolinite to illite, smectite to illite or ferromagnesium minerals to corrensite (Kübler 1973, Hoffman & Hower 1979, Eslinger & Pevear 1989).

Clay mineral trends during sandstone diagenesis are similar to those found in shales (see chapter 2.3.1.2 and Kisch 1983). The main differences are due to variations in starting materials and rock permeability (Eslinger & Pevear 1988). The clay mineral detritus in shales is a function of the mineralogy in the source terrain and of depositional conditions. The clay-sized clay mineral detritus in sandstones is, by definition, minimal. The detritus that has a clay mineralogy is mostly that found in lithic fragments, individual micas or chlorite in volcanic clasts (Eslinger & Pevear 1988). In contrast to the repetitive nature of mineral assemblage in shales, the mineral assemblage in sandstones is dependent on the pore water composition; therefore, absence of a given mineral does not indicate that the sandstone has not been subjected to the metamorphic grade that would produce that mineral (Hoffman & Hower 1979).

2.3.1.4 Sampling and sample preparation

101 outcrop samples from Molasse and Flysch sediments in the Haute-Savoie and Geneva areas (Fig. 1.4) have been analysed by X-ray diffraction (XRD). 28 samples consist of sandstones and 73 samples consist of siltstones, marls, shales or schists. The samples were prepared by the clay mineral laboratory of the Geological Institute in Neuchâtel. Two sample preparation methods have been applied:

Randomly oriented powders of the bulk sample are used for characterisation of the whole-rock mineralogy. The sample is first ground to a particle size of about 1 to 5 mm, dried at a temperature of 110° C, and then ground again to a homogenous powder with particle sizes < 40µm. 800 mg of this powder are pressed (20 bars) in a powder holder covered with a blotting-paper.

Oriented carbonate-free clay aggregates of the 2-16 µm and <2 µm fraction are used in XRD analysis for a first evaluation of the part of detritic minerals (generally phyllosilicates and granular minerals) and that of diagenetic minerals (generally clay minerals) in the small size fraction of a rock. However, this approach has to be applied with care, because, for example, diagenetic kaolinite or chlorite may have sizes exceeding 20 µm (Kübler 1987). Samples were prepared according to the standardised method described by Kübler (1987):

i) Small fractions extraction

A. Consolidated rocks: 10-100 g of sample are cleaned from alteration planes, then washed and dried, and finally ground. The ground of non carbonated rocks is poured into a tube which is filled with demineralised water up to a third of its volume, and then rotated during 12 hours in a rotary (30 rotations per minute). Carbonated rocks are decarbonated using a non complexing, non oxidising acid (hydrochloric acid). Whether the suspension comes from mixing or from decarbonatisation, it needs several washings with demineralised water using a centrifugation technique.

B. Loose rocks: Grinding is unnecessary. Mixing and rinsing are enough. It is however useful to wash immediately with demineralised water, with a pH maintained at 7.5.

ii) Fraction separation

The fraction separation is done with the centrifuge. Separation is based on the law of Stokes in which G, the gravity acceleration, is accelerated through rotation.

iii) Preparation of oriented plates

Normal glass plates are rinsed in alcohol and dried. Then 1 to 2 cc of suspension are sampled with a pipette and carefully poured onto the plate so that the suspension is distributed homogeneously on the whole plate. The preparation is then left to dry.

2.3.1.5 X-ray diffraction analysis

XRD analysis were performed by T. Adatte and G. Rumley (Institut de Géologie de Neuchâtel) using a SCINTAG XRD 2000 with the following characteristics:

Energy: 45 kV, 40 mA
Radiation: CuKα, λ=1.54060 Å
Spectral detector: Germanium crystal: PSI 1 Peltier cooled from Kevex
Continuous scan: 1°/min
Normal slits: 0.5 / 03
Chopper increment: 0.03° 2θ
Kα2–stripping active
Fast Fourier Noise Filter active
Background correction automatic
Noise treshhold=1.5 (whole-rock specimen) and 1.7 (oriented plates)
ESD (estimated standard deviation) multiplier=4.0
Sample spin: rotating sample plate, average diameter 15 mm (whole-rock)
and 25 mm (oriented plates)

XRD analysis of oriented clay specimens were made after air drying at room temperature and glycolation for 24 hr. Whole-rock random powder patterns were recorded from 1° to 65° 2θ, and oriented clay specimen from 1° to 50° 2θ.

2.3.1.6 Interpretation of X-ray powder diffraction results

The method for the semi-quantitative analysis of the bulk rock mineralogy (obtained by XRD patterns of random oriented powder samples) is using external standards. Generally, X-ray intensities reflected by components (e.g. minerals) in mixtures are related to proportions of the components and it is reasonable to expect that quantitative analysis can be made on this basis (Brindley 1980). According to this author, the proportion w_p of a component P in a mixture can be determined from the intensity I_p of a suitable X-ray reflection, if a pure sample of P, having the same diffraction characteristics as P in the mixture, is obtained. If $I°p$ is the intensity from the pure material (external standard), then the following relation can be obtained:

$$I_p = I°_p * (\mu_p/\mu)\, w_p$$

where μ_p is the mass attenuation coefficient of the pure material and μ is the average mass attenuation coefficient of the sample (matrix=clay minerals and minerals).

In this study, a computer program developed by Rolli (1992), which is based on previous works by Ferrero (1966), Persoz (1969) and Kübler (1983), was used. This program allows to quantify the abundance (**Cm**) of 13 minerals common in sedimentary rocks and uses the following X-ray reflections:

Gypsum (020)	11.59 (°2θ CuKα)
Phyllosilicate (hkl)	19.90 (°2θ CuKα)
Goethite (130)	21.22 (°2θ CuKα)
Anhydrite (002/020)	25.44 (°2θ CuKα)
Aragonite (111)	26.22 (°2θ CuKα)
Quartz (101)	26.65 (°2θ CuKα)
K-Feldspars (002)	27.51 (°2θ CuKα)
Na-Feldspars (002)	27.89 (°2θ CuKα)
Calcite (104)	29.41 (°2θ CuKα)
Ankerite (104)	30.80 (°2θ CuKα)
Dolomite (104)	30.94 (°2θ CuKα)
Halite (200)	31.69 (°2θ CuKα)
Magnesite (104)	32.63 (°2θ CuKα)
Hematite (104)	33.15 (°2θ CuKα)
Pyrite (200)	56.29 (°2θ CuKα)

The measure ID (non-identified components) is defined by the program as ID=100%-$\sum$Cm and represents, usually, the clay mineral fraction of the sample. The major problem encountered is over-estimation (e.g. $\sum$Cm>100%). According to Rolli (1992), this can be due to a preferential orientation

of the crystallites (especially for the calcite), to a higher mass attenuation coefficient of the non-quantified matrix (e.g. ID) or to a calibration problem.

2.3.1.7 Fine-fraction mineralogy (size-fraction <2 μm and 2-16 μm)

A) Clay minerals

Qualitative identification: X-ray identification of clay minerals is based essentially on recognition of structural characteristics, the most important one being layer spacing. Oriented samples of most clay minerals show almost exclusively the 00L diffractions from which the layer spacings are obtained by the means of the Bragg law. Clay minerals diffraction patterns are characterised by the peak's position, intensity, shape and breadth (Moore & Reynolds 1989). Detailed identification procedures are given by Brindley & Brown (1980), as well as by Moore & Reynolds (1989), and the following discussion is mainly derived from these authors.

Generally, four basic groups of clay minerals can be distinguished (Eslinger & Pevear 1988): i) those with a first order basal reflection near 7 Å (1:1 minerals, e.g. kaolinite or serpentinite), those with a first order basal reflection near 10Å (non-swelling 2:1 minerals, e.g. mica), iii) those with a first order basal reflection near 14 Å (swelling 2:1 minerals, e.g. smectite, and non-swelling chlorite), and iv) sepiolite and palygorskite.

In the following, a short introduction to the main characteristics of clay minerals identified (see chapter 5) in this study will be given:

Kaolinite and serpentinite:

Kaolinite is a dioctahedral 1:1 clay mineral with the general formula $Al_2Si_2O_5(OH)_4$. Serpentinite is a trioctahedral 1:1 clay mineral with the general formula $Mg_3Si_2O_5(OH)_4$. All kaolinites and serpentinites give basal reflections at approximately 7.2 Å (001) and 3.6 Å (002). Commonly, serpentinites have basal spacings slightly larger than kaolinites: the (002) reflection for antigorite is at 3.63 Å, whereas that for kaolinite is at 3.57 Å. A major problem for the identification of kaolinite is the fact that even-order chlorite peaks superimpose or nearly superimpose on the members of the kaolinite 00L series. However, most kaolinites have the 002 peak at 24.9 ° 2θ, and a common type of chlorite has its 004 reflection at 25.1 ° 2θ. As the lines are sharp, usually, a partial resolution can be seen. In other cases only heat or chemical treating allows to identify mixtures of kaolinite and chlorite (see Moore & Reynolds 1989 for a discussion).

Chlorite and chlorite/smectite, including corrensite:

Chlorites are 2:1 layer silicates with interlayers of octahedral hydroxide. They can be either di- or trioctahedral, but they are usually trioctahedral. The main cations in the 2:1 octahedral sheet and octahedral interlayer sheet are Mg and Fe^{2+}. Al and Fe^{3+} substitute for the divalent cations and produce a positive charge. Chlorites are characterised by a sharp, integral sequence of OOL lines based on a repeat of d(001)=14.2 Å. The second order peak is at about 7.10 Å, the third order peak at about 4.74 Å, the fourth order peak at about 3.54Å and the fifth order peak at about 2.84 Å. The relative intensities of these peaks vary with heavy element content (Fe primarily), the 1st and 3rd order reflections decreasing with respect to the 2nd and 4th order reflections as the Fe content is increased. Mg-rich chlorites are characterised by the first four 00l peaks having rather similar intensities (Weaver 1989). Ternary intensity diagrams (001-002-003 and 002-003-004) allow to visualise the described relationships of peak intensities and are used to estimate the heavy metal content.

Chlorite forms two-component interstratified minerals with all the other common phyllosilicate layer types. Composition and ordering possibilities for a given mixed-layer chlorite species are more restricted than those displayed by other minerals, such as illite/smectite (Reynolds 1988). According to this author, almost all reported mixed-layer chlorite minerals can be classified into two types, i) nearest ordered types (R=1) containing equal proportions of the two components, and ii) randomly interstratified (R=0) minerals whose composition lies near one end of the range or the other. Definitive identifications of mixed-layered chlorite minerals depend on good diffraction patterns (at least 4 or 5 peaks) of the 00l series of reflections. However, these 00L peaks may often not be identified. This is due to several reasons: i) peak interferences from discrete chlorite, kaolinite and illite, ii) low intensities of higher angle peaks, iii) low quantities of C/S in the clay mineral aggregate

or iv) bad preferred orientation of the clay aggregate. Interference problems can be dealt with by a deconvolution procedure, which is included as standard program in the SCINTAG XRD 2000 system.

Randomly interstratified chlorite minerals are less frequently reported than ordered varieties and are often more poorly defined (Reynolds 1988). According to this author, the most useful reflections for estimating composition in these minerals are the 002/002 and 004/005 peaks. However, in this study, only the high-intensity 001/001 peak (between 14-15 Å in air-dried samples and 14-17 Å in glycolated samples) could be identified with some certainty using deconvolution techniques. Therefore, only the occurrence of randomly stratified C/S is reported in this study.

The dominant type of observed ordered mixed-layer chlorite mineral is the 1:1 trioctahedral corrensite, originally defined by Lippmann (1956). The diffraction patterns of corrensites are characterised by an integral sequence of OOL lines based on d(001)=31.1 Å for low-charge corrensite and todusite (dioctahedral corrensite), and d(001)=28.5 Å for the high-charge variety (Reynolds 1988). The high-charge corrensite can be distinguished from the others by its peak position and a relatively strong 003 reflection.

Mica:

All phyllosilicates showing a rational series of basal reflections with d(001)=10 Å are designed as mica. This group of minerals includes trioctahedral 2:1 layer silicates such as phlogopite or biotite and dioctahedral 2:1 layer silicates such as muscovite, phengite or illite. Illite is referred to by many authors as a substantially not expanding, dioctahedral, aluminous, potassium mica-like mineral which occurs in the clay-size fraction of sedimentary rocks (see Srodon & Eberl 1984 and Weaver 1989 for a review). Micaceous materials analysed by XRD in the clay mineral fraction of sedimentary rocks fall in three categories: i) pure illite, ii) highly illitic I/S, and iii) detrital micas (e.g. phengite). Ternary intensity diagrams (001-002-005) of the basal reflections allow to define fields related to a specific chemical composition (Rey & Kübler 1983).

Illite/smectite:

Mixed-layer illite/smectite (I/S) are characterised by broad, non-integral, and asymmetrical 00L peaks. The peak positions of mixed-layer clays can be considered to be the weighted means of the peaks of each component. The recognition of mixed-layer illite/smectite is complicated, especially in 5-9° 2θ range, by the presence of other discrete minerals such as mica, chlorite or chlorite/smectite. In these cases, deconvolution procedures helped to decipher the mixed-layer peaks. Identifiable I/S peaks in this study are i) the 001/001 (10-15 Å for air-dried and 10-17 Å for glycolated samples), ii) the 001/002 (8.5-9.8 Å for glycolated samples), and ii) the 002/003 (5.6-5.1 Å for glycolated samples).

Different approaches have been proposed for estimating the percentage of smectite layers in mixed-layer illite/smectite (e.g. Weaver 1956, Reynolds & Hower 1970, Weir et al. 1975, Johns & Kurzweil 1979, Srodon 1980, 1984, Moore & Reynolds 1989). These methods are based on i) comparisons between measured and calculated XRD patterns, ii) on peak positions or iii) on angular distances between high angle reflections. The major problem in this study was the occurrence of only 3 basal peaks: 001/001 (nearly always recognised), 001/002 (sometimes) and 002/003 (sometimes). Therefore, different estimations methods are used:

i) Weaver (1956): This author published a diagram indicating the migration of the 001/001 peak of I/S as a function of the expanded 17 Å-layers. Although this migration curve can lead to "serious errors of interpretation" (Reynolds & Hower 1970), it is a way to handle the observed diffraction patterns in a somewhat quantitative way, especially in cases where higher angle reflectances are missing.

ii) Moore & Reynolds (1989): The method proposed by these authors takes into account the angular difference Δ1 between the 001/002 and the 002/003 peak and relates it to the composition of the I/S. The authors state that this approach has different advantages:

- It is relatively insensitive to goniometer zero-alignment problems and specimen displacement errors.
- The sensitivity of the composition estimate is enhanced because the two peaks involved in the measurement move in opposite directions to the composition changes.

According to these authors, the proportion of smectite can also be estimated by using only the 001/002 or 002/003 peak.

iii) Vuitel (1987) in a review, which was based essentially on previous studies by Reynolds & Hower (1970), Brindley & Brown (1980) and Srodon (1980, 1984), proposed a slightly different relation between %S in I/S and Δ1 (angular difference between 001/002 and 002/003). In addition he established a diagram which relates the %S in I/S to Δ1 and Δ2 (angular difference between 001/001 and 001/002).

B) Semiquantitative estimation of the amount of phyllosilicate

The intensities of selected XRD peaks were measured for a semiquantitative estimate of the proportion of clay minerals present in the <2μm fraction. This method gives the relative proportion of the clay minerals normalised to 100%. The relative percentage of a mineral is calculated in the following way:

$$\% \text{ rel. Min1.} = \text{Intensity (Min1)} / \sum \text{Intensity(Min}_i\text{)}$$

The intensity of the following peaks are used in this study:

- 001/001 of I/S
- 002 of corrensite
- 001 of mica
- 001 of serpentine
- 002 of chlorite
- 001 of kaolinite

As the even-order chlorite peaks superimpose or nearly superimpose on the members of the kaolinite 00L series, the relative proportion of each mineral in this peak is calculated using the 004 peak of chlorite (chlo) and the 002 peak of kaolinite (kao) which, usually, can be distinguished easily:

$$X(kao)=\text{Intensity(kao002)} / [\text{Intensity(kao002)}+\text{Intensity(chlor)}]$$
$$\text{Intensity(kao001)}=X*\text{Intensity(kao001chlor002)}$$

Absolute intensity values for each clay mineral are indicated for a better appreciation of the "real" quantity present in each sample.

The abundance of each clay mineral was mapped and isoreflectance contours were calculated by kriging.

C) Associated minerals

Absolute intensities for the following minerals in the <2 μm and the 2-16 μm fraction are indicated in this study:

- Quartz: 100 peak at 4.26 Å (35% intensity)
- K-feldspar: peaks 220, 002, 040 at about 3.25 Å
- Plagioclase: peaks 002, 040, 220 at about 3.19 Å

2.3.2 Fluid inclusion analysis

2.3.2.1 General remarks

According to Roedder (1984), the fluid inclusions are formed by crystal growth when advancing faces, edges and corners of the growing crystal are disturbed (primary inclusions), by fracturing and healing of crystals during mechanical disturbances or by overgrowth of a crystal (secondary and pseudosecondary inclusions). Several fluid inclusion generations within a crystal record the evolution of fluid composition in time. This technique may, therefore, yield direct information on the temperature and pressure evolution of a rock sample, as well as on the composition of the paleofluids. For a review of analysis techniques and interpretation of results see Hollister & Crawford (1981), Roedder (1984), Shepherd et al. (1985), Mullis (1987a), Burrus (1989) and Barker & Goldstein (1990).

2.3.2.2 Sampling

Samples were taken from two coarse crystalline calcite veins at the eastern end of the Salève mountain (Fig. 1.4) which crosscut the bedding of the Urgonian limestones (early Cretaceous) at a high angle.

These subvertical veins are parallel with the NNW-SSE trending wrench fault zones which affect the entire region (see chapter 1.3.1), and may be related to the final phase of the alpine orogeny which lead to the formation of the Jura Mountains and the uplift of the Molasse basin. Therefore, evaluated trapping conditions reflect probably post-Molasse-depositional temperatures.

2.3.2.3 Analytical method

Fluid inclusions were studied by microthermometry, i.e., temperatures of phase transitions were determined on a microscope equipped with a heating and cooling stage. Double-polished sections (~80mm) and calcite cleavage sections were prepared. Microthermometric runs were performed on a Leitz Laborlux microscope equipped with a Leitz L32-UT50 and a Nikon ELWD C40X long focus objectives, and a Fluid Inc. "Reynolds"-USGS-design gas-flow heating/freezing stage (Woods et al. 1981, Roedder 1984). Synthetic fluid inclusions (Sterner & Bodnar 1984) were used to calibrate the system at temperatures of -56.6°C, 0.0°C and 374.1°C. Precision and accuracy are between ±0.2°C between -70°C and 40°C and ±1°C above 40°C.

2.3.2.4 Problems in interpretation of results

There are five basic assumptions to fluid inclusion studies (Roedder & Bodnar 1980): i) The inclusion traps a one-phase fluid. ii) The volume of the inclusion does not change after trapping. iii) The composition of the trapped fluid does not change. iv) The effects of pressure are known. v) The time and mechanism of trapping are known. Violation of one or more of these assumptions may lead to unreliable interpretations and are often related to one of the following processes: stretching, leaking or necking-down (Roedder 1981, Bodnar & Bethke 1984, Meunier 1989, Burrus 1989). Stretching is a permanent deformation of the host crystal. If the host stretches to the extent that the internal pressure equals external pressure, then the inclusion will be reequilibrated to the new pressure and temperature conditions. The pressure difference also may cause the inclusion to decrepitate, fracturing the host mineral and, therefore, material can be lost (leaking) or gained by the inclusion.
Because calcite is a relatively soft and cleavable mineral, it tends to reequilibrate when heated to temperatures higher than those of initial entrapment (Goldstein 1986, Prezbindowski & Larese 1987). In the case of calcite cements in sedimentary rocks, the resulting fluid inclusion population could contain a nearly complete record of burial fluids in which a particular rock has been bathed (Goldstein 1986). Fluid inclusions trapped in calcite may yield homogenisation temperatures approaching maximum temperatures of a system.
During annealing and recrystallisation of relatively large inclusions and fractures, progressively smaller inclusions form in an attempt to reduce the amount of surface energy (Mullis 1987a). This process is called necking-down. As long as the trapped fluid remains homogenous, necking-down does not influence the composition or density of the system. However, if phase changes occurred prior to completion of necking-down, the new inclusions may show important differences in composition and density from the precursor inclusion. Careful textural observations help to recognise such features.
In the case of aqueous inclusions with no dissolved gases, the main parameters obtained during microthermometric analysis are the melting temperature of ice (Tm ice) and the homogenisation temperature (Th). Because the melting temperature of ice in saline solutions is related to its salt content, freezing temperatures can be used to estimate the salinity of aqueous solutions. For pure aqueous NaCl solutions, the measured Tm can be converted directly to weight% using melting data established by Potter et al. (1978). If the volume and composition of an aqueous inclusion have remained constant since its formation, the homogenisation temperature is a minimum estimate of trapping temperature. To obtain the real trapping temperature, the pressure of formation has to be considered. If composition and density of a given fluid inclusion are known and if the experimental P-V-T-X properties of the involved fluid are available, the isochores of that fluid may be calculated (Roedder 1984). Since entrapment must lie somewhere along the evaluated isochore at some temperature greater than the homogenisation temperature, the actual trapping temperature must be evaluated along the isochore by an independent geobarometer (Mullis 1987a). The paleopressure can be estimated from the sedimentary history.

Chapter 3: VITRINITE REFLECTANCE RESULTS

A part of the results presented in this chapter has already been published (Schegg 1992a, Schegg 1992b, Schegg & Moritz 1993, Todorov et al. 1993).

3.1 The microscopically recognisable constituents of the organic matter

No detailed maceral analysis was performed. But amounts of each main maceral type (vitrinite, liptinite, inertinite) have been estimated during vitrinite reflectance measurements. Results are shown in table A1.

Maceral of the huminite/vitrinite group (plate 1) make up the bulk of the organic material. The total huminite/vitrinite contents range generally from 80 to 100 vol% (mineral-matter free). Some samples from coal seams may show lower contents. Within the huminite/vitrinite group, main components were eu-ulminite and gelinite, respectively desmocollinite and telocollinite. The macroscopic coaly particles are nearly exclusively made of homogenous telocollinites. Samples from coal seams show a wider spectra of maceral varieties: telinite, vitrodetrinite, desmocollinite, telocollinite, corpocollinite.

Liptinite content in the studied samples is low to moderate (0-10 vol%). Predominant liptinite macerals are sporinite, cutinite and colloresinite (plate 1). Colloresinite occurs often as cell fillings in telinite or as a band in a vitrinite matrix and is characterised by a reflectance closer to vitrinite than to liptinite.

Macerals of the inertinite group form up to 20 vol%. Significant contributions come from inertodetrinite, semifusinite and fusinite (plate 1), other inertinite macerals like sclerotinite occur only in traces. In some samples, material of a transitional nature between vitrinite and inertinite has been found.

The most common mineral component in the samples is pyrite. It occurs generally as fine concretion (often in a framboidal form) and as pyritised cell structure.

3.2 Alteration of the organic matter

Alteration problems have been discussed in chapter 2.2.2.2. As most samples have been taken from outcrops, they are invariably oxidised to some degree. Oxidation of the studied samples could be identified by a number of petrographic characteristics: micropores, microfissures or oxidation rims on the macerals, brownish tint throughout the entire coal particle, high relief around particle borders. Highly weathered samples are characterised by the physical breakdown of coal to fine particles. However, even in highly weathered samples a complete range of fresh to oxidised particles has been found. Therefore, reflectance measurements can also be performed in these samples with some caution.

In order to assess qualitatively the degree of oxidation, an oxidation scale going from 0 to 4 has been established (see plate 2 and 3):

0 : fresh
1 : slightly altered: first microfractures
2: moderately altered: micropores and microfractures, sometimes brownish tint
3: strongly altered: breakdown of the coal macerals to fine particles with high relief
4: completely altered: unrecognisable macerals, often highly pyritised

Results of this classification are shown in table A1. 42% of the samples showed no microscopic evidence of oxidation: 32% of the samples have been judged to be slightly , 16% moderately, 8% highly and 2% completely oxidised.

3.3 Vitrinite reflectance results

Vitrinite reflectance results are presented in table A1 and vitrinite histograms are shown in annex 1. The analysis of 4 shale samples (RS324, Weid105, Weid106, Weid130) containing dispersed organic matter shows high reflectance values (1.07-1.22% Rr) and a large scatter of measurements. These observations indicate reworking of organic matter which was already coalified. This type of material was therefore not used for the interpretation of the results. Totally altered samples (alteration class 4, table A1) are not used either.

The reflectance values of the studied samples vary stratigraphically and geographically in systematic ways.

3.3.1 Stratigraphic variations

Reflectance values range from 0.21% Rr in a sample from the OSM of the Hörnli gravel fan in Eastern Switzerland, to 1.41% Rr in a sample from the USM of the Bornes Plateau in Haute-Savoie. The distribution of vitrinite reflectance values in the studied sedimentary formations clearly reveals that there is a stratigraphic control on maturation (Fig. 3.1). Generally, mean average reflectance values increase slowly with age, from 0.38% Rr for samples from the Middle Miocene OSM, to 0.61% Rr for samples from the Oligocene UMM. The range of values can, however, be quite large. Samples from the USM display values ranging from 0.30 to 1.41% Rr.

3.3.2 Geographical variations

Figure 3.1 shows that thermal maturity of the samples varies also geographically. Mean average values for samples from the Subalpine Molasse are for example slightly higher than those from Plateau Molasse. To represent this geographical variation, reflectance values were mapped and isoreflectance contours were calculated. The limited and uneven distribution of samples does not enable a unique interpretation. Nevertheless, the chosen representation shows the general trends and some interesting anomalies. In order to account for the problem of alteration of samples (see discussions in chapter 3.2 and 2.2.2.2) two types of maps were constructed: 1) maps, where all samples are represented and 2) maps, where only fresh or slightly altered samples are represented.

Results from the five study areas are presented below.

3.3.2.1 Haute-Savoie and Geneva Basin

Results are shown in figures 3.2 and 3.3. Isoreflectance contours display a clear regional W-E trend indicating an increase in maturation towards the Alps. The isoreflectance lines seem to run slightly oblique to today's Alpine front. Some analysed Eocene samples from "Les Carroz" (not represented on the map in figs. 3.2 and 3.3) situated in the "Massif de Platé", about 10km east of the Bornes Plateau, show very high reflectance values (up to 1.61% Rr). Local variations are superimposed on this general W-E trend. An area oriented NE-SW, south-west of the Prealps, displays high reflectance values of up to 1.06% Rr. Major tectonic structures, the "Arve" strike-slip fault and the thrust front of the Subalpine Molasse, are located close to this zone. Other points of locally high reflectance values (1.41% Rr and 1.25% Rr, Fig. 3.2 and 3.3) have been measured in an area 10km north of Annecy. The maximum value of 1.41% Rr was measured at a branch coal. This branch is probably part of the woody material which was often washed into the sedimentary environment of these clastic rocks. That is why it is difficult to explain this outstanding value just as a consequence of reworked high rank coal. It is interesting to note that this sample was found close to the "Cruseilles" strike-slip fault (situated at the western end of the "Salève" mountain). There is only a small difference between the isoreflectance map including all measured samples and the one including only unaltered or slightly altered samples. Nevertheless, some high values could be due to an alteration effect.

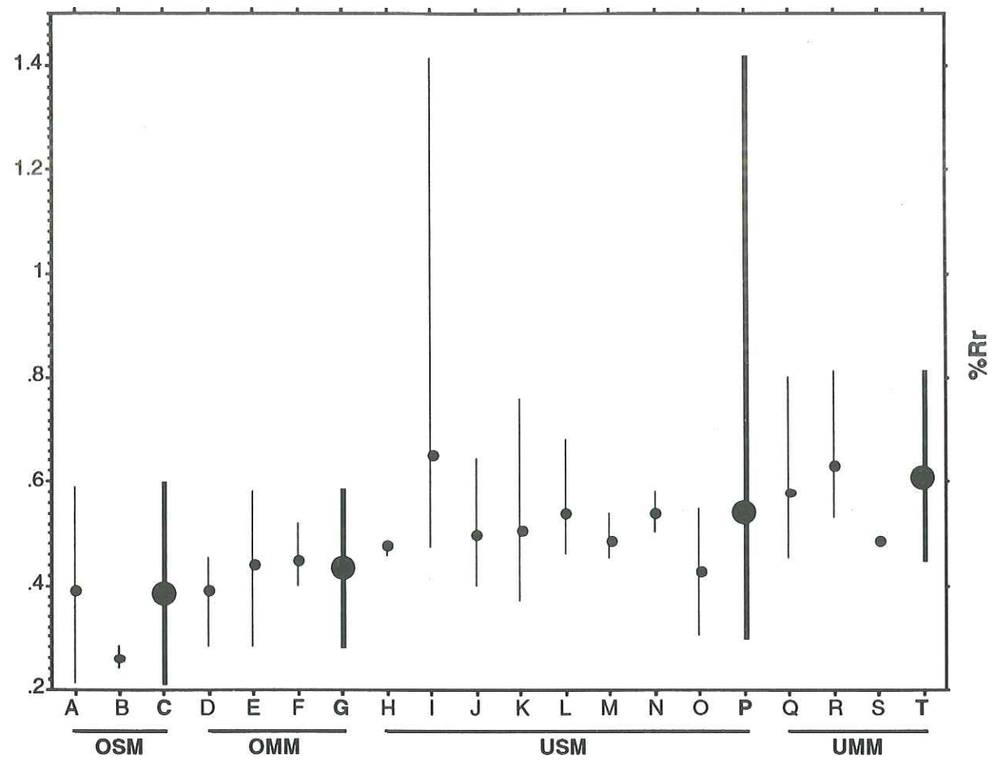

OSM
A: Eastern Switzerland, Plateau Molasse, Rr_{mean}=0.39, s=0.1, range=0.21-0.59, n=21
B: Northern Switzerland, Jura, Rr_{mean}=0.26, s=0.03, range=0.24-0.28, n=2
C: all samples, Rr_{mean}=0.38, s=0.1, range=0.21-0.59, n=23
OMM
D: Haute-Savoie, Plateau Molasse, Rr_{mean}=0.39, s=0.05, range=0.28-0.45, n=12
E: Western Switzerland, Plateau Molasse, Rr_{mean}=0.44, s=0.06, range=0.28-0.58, n=59
F: Eastern Switzerland, Plateau Molasse, =0.45, s=0.04, range=0.4-0.52, n=7
G: all samples, Rr_{mean}=0.43, s=0.06, range=0.28-0.58, n=78
USM
H: Haute-Savoie, Plateau Molasse, Rr_{mean}=0.48, s=0.01, range=0.47-0.48, n=3
I: Haute-Savoie, Subalpine Molasse, Rr_{mean}=0.65, s=0.26, range=0.47-1.41, n=21
J: Western Switzerland, Plateau Molasse, Rr_{mean}=0.5, s=0.05, range=0.4-0.64, n=25
K: Western Switzerland, Subalpine Molasse, Rr_{mean}=0.51, s=0.1, range=0.37-0.76, n=15
L: Lake Thun area, Subalpine Molasse, Rr_{mean}=0.54, s=0.08, range=0.46-0.68, n=10
M: Eastern Switzerland, Plateau Molasse, Rr_{mean}=0.49, s=0.05, range=0.45-0.54, n=3
N: Eastern Switzerland, Subalpine Molasse, Rr_{mean}=0.54, s=0.04, range=0.5-0.58, n=3
O: Northern Switzerland, Jura, Rr_{mean}=0.43, s=0.1, range=0.3-0.55, n=5
P: all samples, Rr_{mean}=0.54, s=0.16, range=0.3-1.41, n=85
UMM
Q: Haute-Savoie, Subalpine Molasse, Rr_{mean}=0.58, s=0.11, range=0.45-0.8, n=7
R: Haute-Savoie, Subalpine Chains, Rr_{mean}=0.63, s=0.08, range=0.53-0.81, n=18
S: Northern Switzerland, Jura, Rr=0.49, n=1
T: all samples, Rr_{mea}=0.61, s=0.09, range=0.45-0.81, n=26

Fig. 3.1: Range and mean average values of vitrinite reflectance in the lithostratigraphic units of the Molasse Basin for different geographical and tectonic settings. Rr_{mean}=mean average vitrinite reflectance value; s=standard deviation, n=number of samples.

Fig. 3.2: Simplified tectonic map of the Haute-Savoie and Geneva Basin areas with A) mean vitrinite reflectance values from surface samples and B) isoreflectance lines. All measured samples included. The two outstanding values (marked by stars) were not used for the calculation of isoreflectance lines.

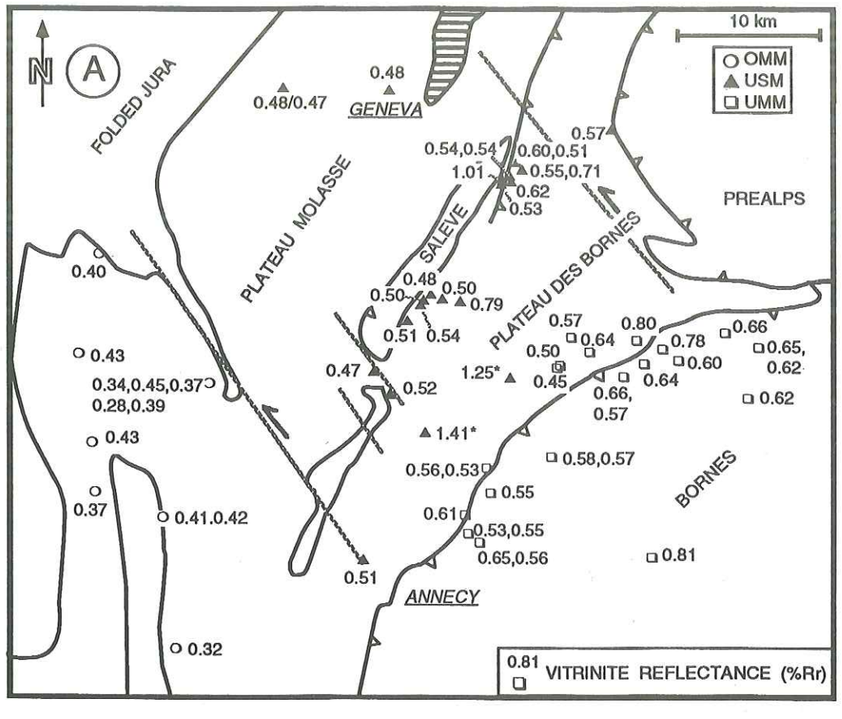

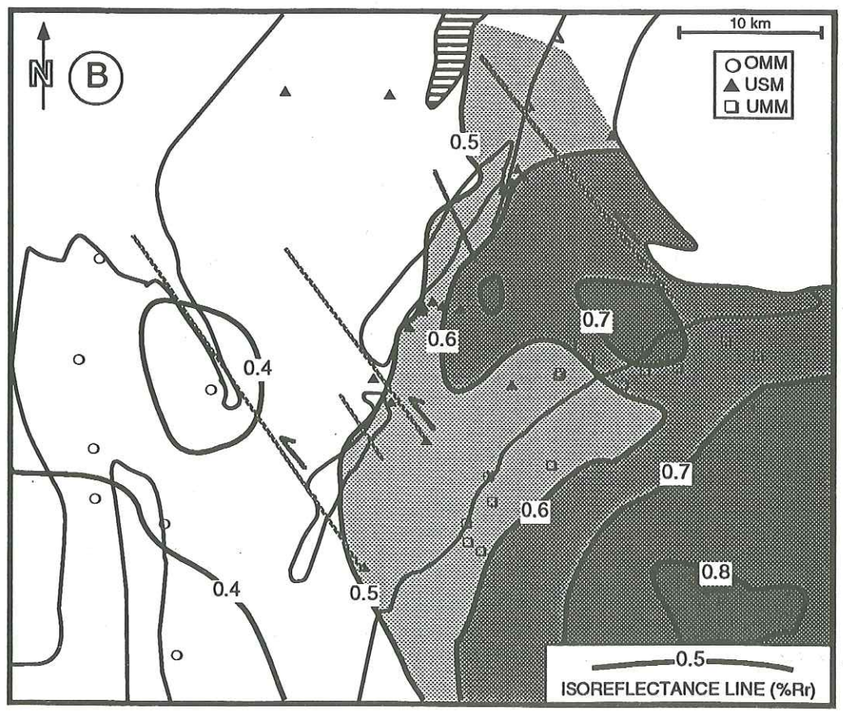

Fig. 3.3: Simplified tectonic map of the Haute-Savoie and Geneva Basin areas with A) mean vitrinite reflectance values from surface samples and B) isoreflectance lines. Only fresh or slightly altered samples included. The outstanding value (marked by a star) was not used for the calculation of isoreflectance lines.

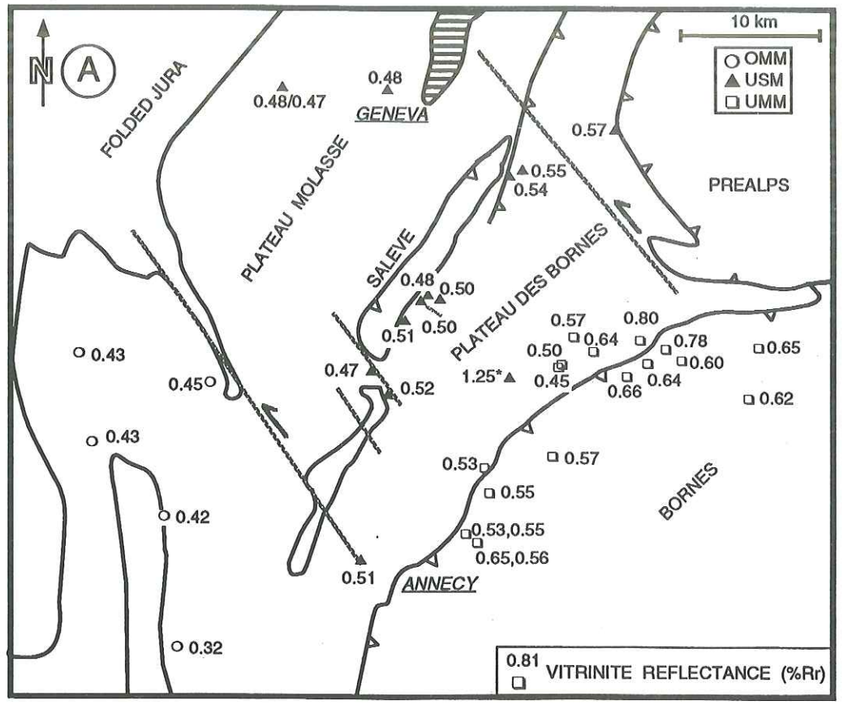

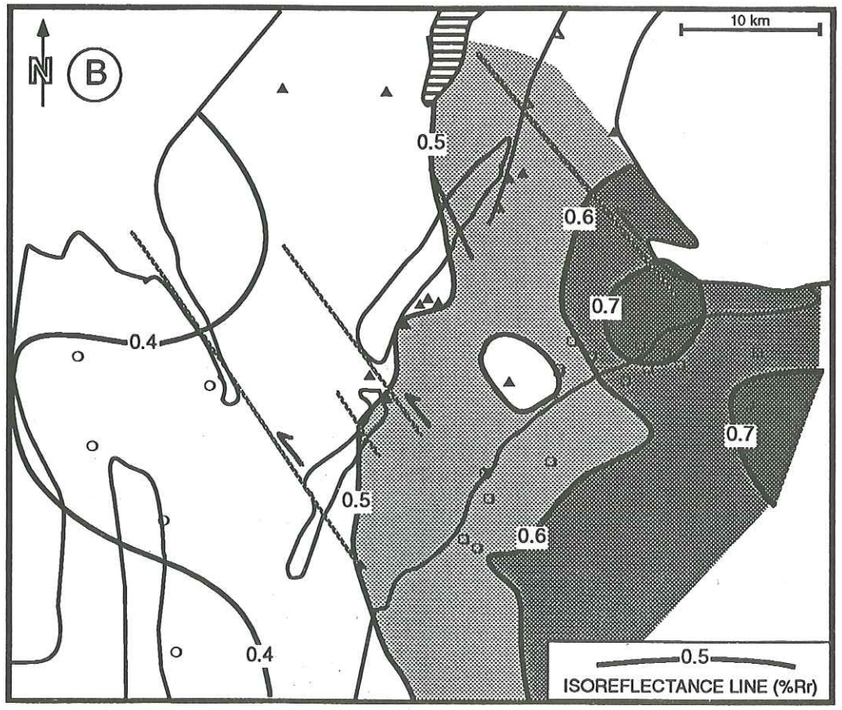

3.3.2.2 Western Switzerland

Results are shown in figures 3.4 and 3.5. The isoreflectance lines in the southern part of this area indicate an increase in OM maturation towards the Alps. This trend predominantly occurs in the Subalpine Molasse north of Lake Geneva. In the Plateau Molasse variations in vitrinite reflectance are rather sporadic. The most striking features are two limited regions with relatively high maturation levels (Rr>0.5%). One of those zones is situated just south of Lake Neuchâtel. The three analysed samples (Rr up to 0.64%) in this region are lying close to the Pomy-Cuarny thrust (PC in fig. 3.4B); they come from the USM and show moderate alteration. Hence, this anomaly is not displayed in figure 3.5. Another area of increased thermal maturity is situated about 10 km south-east of Lake Neuchâtel, in the Broye valley, where values of up to 0.58% Rr were measured. Almost all samples within this zone come from the OMM and are generally well preserved. Again a thrust (La Broye, B in fig. 3.4 and 3.5) is located close to this zone.

3.3.2.3 Lake Thun area

Results are shown in figures 3.6 and 3.7. All samples have been taken in the Subalpine USM and display vitrinite reflectance values ranging from 0.48% Rr to 0.68% Rr. There is neither a clear regional trend (Fig. 3.6), nor a marked stratigraphic trend (i.e. no clear increase of % Rr with depth, Fig. 3.7).

3.3.2.4 Eastern Switzerland

Results are shown in figure 3.8. Despite a limited number of samples in this area, some general trends are clearly observed. Isoreflectance lines show a general increase in thermal maturation towards the Alpine front. This pattern is disturbed by an area of increased vitrinite reflectance running parallel to Lake Zurich which is believed to be tectonically controlled (Hantke 1967). Samples taken from OSM sediments east of Lake Zurich (e.g. Hörnli gravel fan) are thermally less mature than those taken west of Lake Zurich. Samples from the distal part of the Plateau Molasse (between the eastern termination of the folded Jura and Zurich) display surprisingly high maturity values (0.40-0.52% Rr).

3.3.2.5 Northern Switzerland

Tertiary: Results are shown in figure 3.9. Vitrinite reflectance values for Miocene sediments range between 0.24% Rr for a sample of the Vogesenschotter and 0.28% Rr for a sample of the OSM. The Rr values for the Oligocene samples vary from 0.30% Rr to 0.55% Rr. Samples in the western part of the study area are immature (0.24-0.28% Rr). Further east, in a region situated in the southern prolongation of the eastern Rhine Graben border, vitrinite reflectance increases to values of up to 0.55% Rr. A consecutive decrease in the maturity of the Tertiary sediments towards the eastern termination of the Folded Jura seems to be indicated by an immature sample from the Lower Freshwater Molasse (RS223, 0.30% Rr).

In the following, a short summary of results from Mesozoic sediments in Northern Switzerland (table A3) will be given. A detailed discussion of results can be found in Todorov et al. (1993):

Middle and Upper Jurassic: Vitrinite reflectance values range from 0.40% Rr for a sample of the Hauptrogenstein to 0.69% Rr for a sample of the Opalinus Ton. The geographical distribution of vitrinite reflectance data indicates an increase of maturity from SE to NW.

Lower Jurassic: The mean vitrinite reflectance varies between 0.44% Rr (Jurensis Mergel) and 0.70% Rr (Insektenmergel). Geographically, Rr values indicate an increase in maturity of Liassic sediments from SE to NW, towards the Rhine Graben.

Fig. 3.4: Simplified tectonic map of Western Switzerland with A) mean vitrinite reflectance values from surface and near surface samples and B) isoreflectance lines. All measured samples included. Tectonic structures modified after Jordi (1990) and Weidmann (in press): BCC=Baulmes-Chamblon-Chevressy thrust, ES=Essertines fault, EP=Ependes fault, M=Mentue thrust, PC=Pomy-Cuarny thrust, RB=Rances-Baulmes fault, S=La Sarraz fault, B=La Broye thrust.

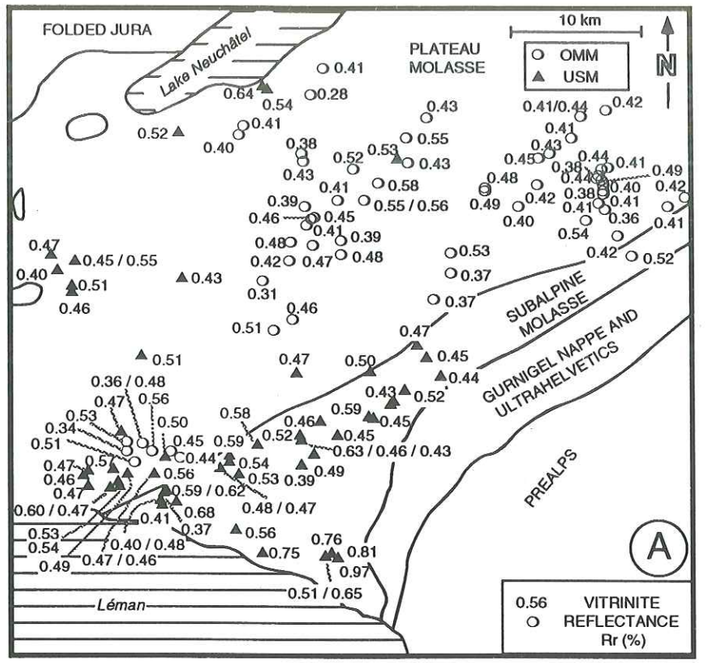

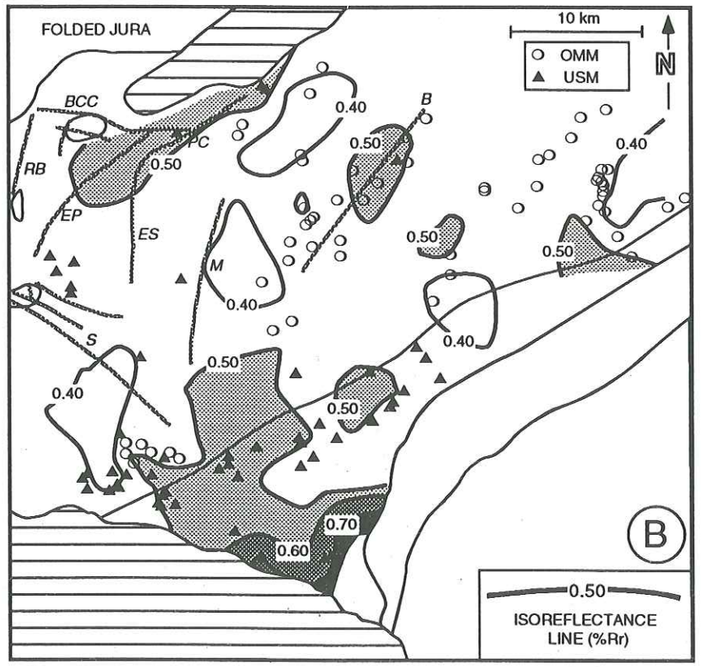

Fig. 3.5: Simplified tectonic map of Western Switzerland with A) mean vitrinite reflectance values from surface and near surface samples and B) isoreflectance lines. Only fresh or slightly altered samples included. Tectonic structures modified after Jordi (1990) and Weidmann (in press): BCC=Baulmes-Chamblon-Chevressy thrust, ES=Essertines fault, EP=Ependes fault, M=Mentue thrust, PC=Pomy-Cuarny thrust, RB=Rances-Baulmes fault, S=La Sarraz fault, B=La Broye thrust.

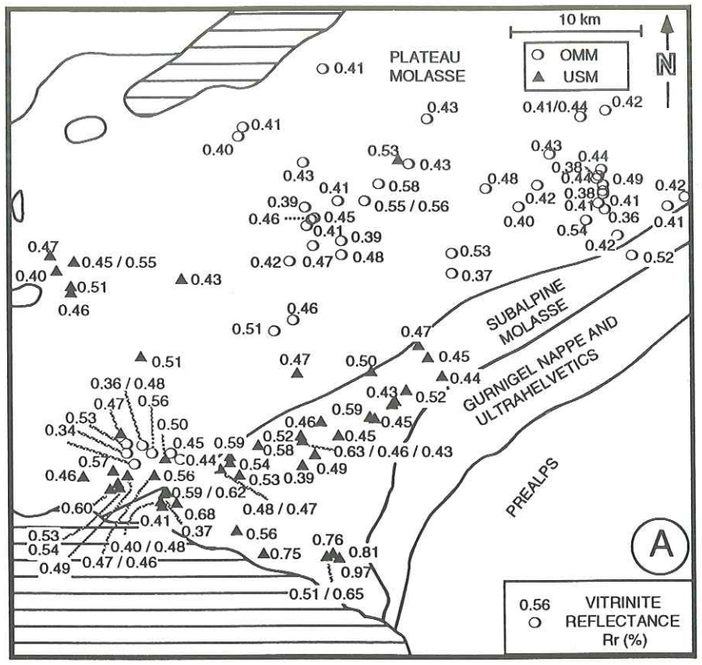

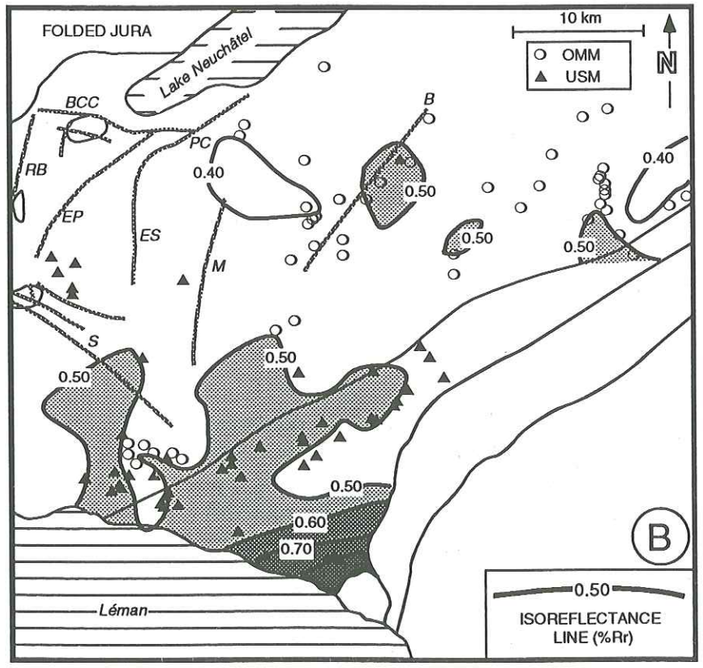

Fig. 3.6: Tectonic map of the Lake Thun region (modified after Schlunegger 1991) with mean vitrinite reflectance values of surface samples. The sample marked with a star is moderately altered.

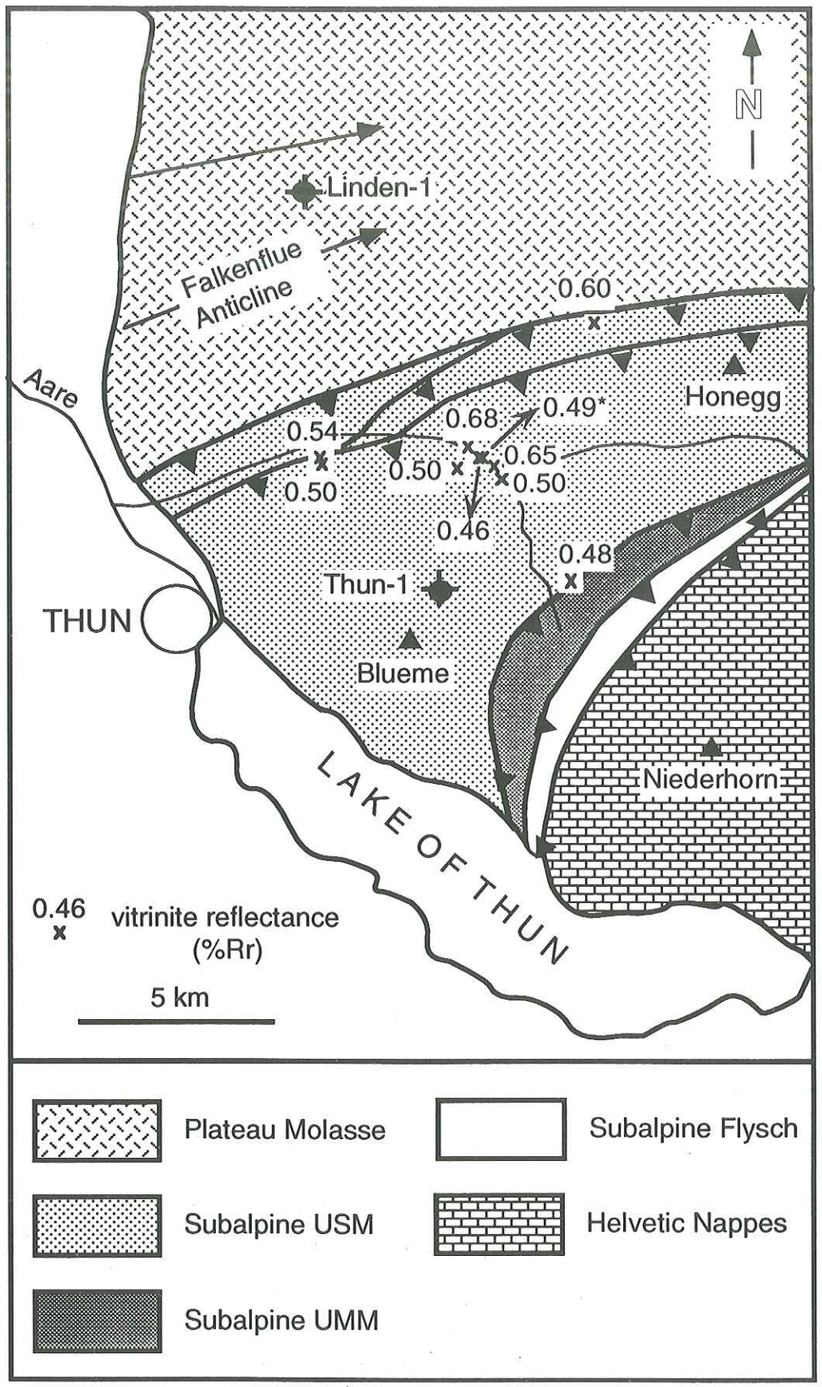

Fig. 3.7: Synthetic lithostratigraphic profile ("Prässerebach" section, modified after Schlunegger 1991) of the Subalpine Molasse in the Lake Thun area with sample location and vitrinite reflectance values. The sample marked with a star is moderately altered.

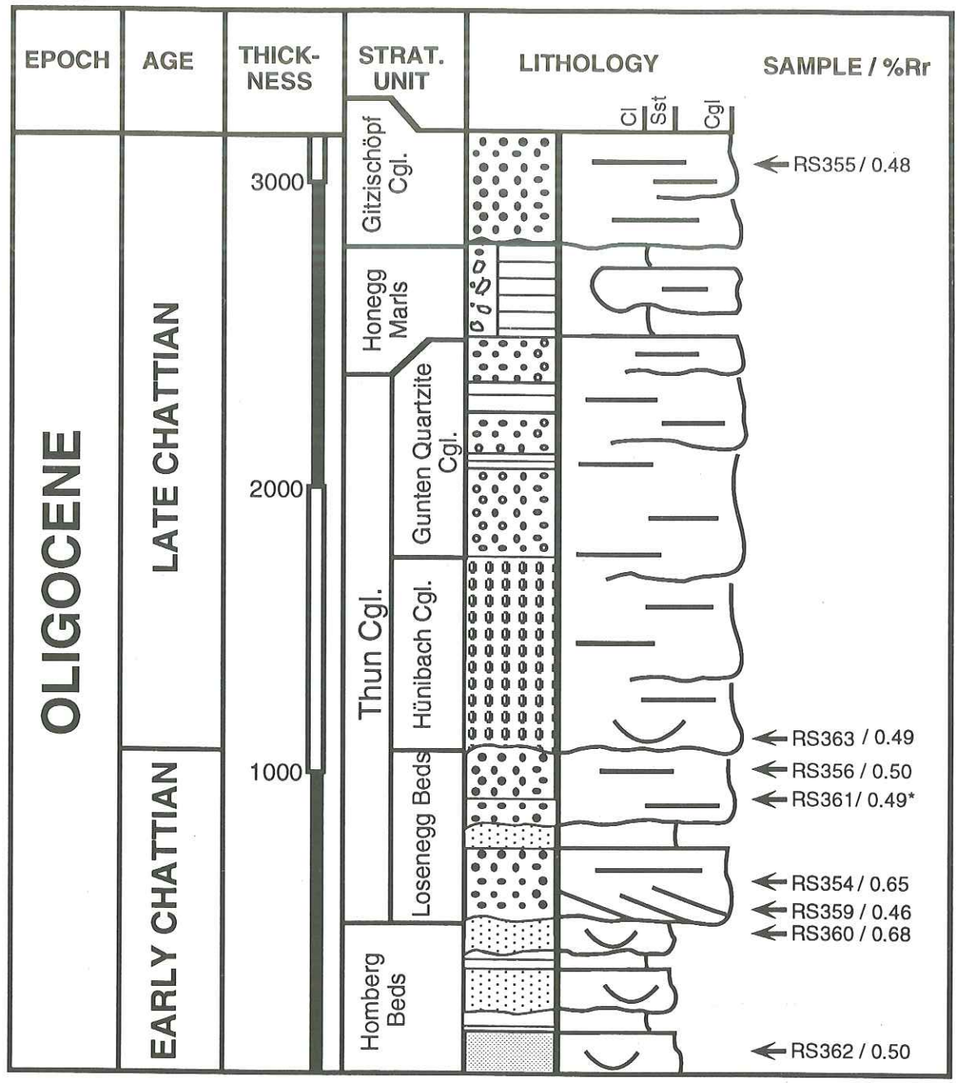

Middle and Upper Triassic: The measured Rr values range between 0.49% Rr (Rhät) and 0.80% Rr (Rhät).

According to Wolf & Hagemann (1987, their table 4) the increase of vitrinite reflectance with depth for the Mesozoic section in the NAGRA wells Schafisheim, Weiach and Riniken is 0.65, 0.37 and 0.96 % Rr/km respectively. The reconstruction of 5 complete stratigraphic profiles based on information from outcrops, shallow boreholes and literature (more details in chapter 7.3.1) allowed to obtain roughly estimated reflectance gradients of Mesozoic and Tertiary sediments in the south of the Rhine Graben. The following values were calculated: Delémont 0.3% Rr/km, Muttenz 0.8% Rr/km, Trimbach 0.5% Rr/km, Passwang 0.5% Rr/km and Staffelegg 0.7% Rr/km.

Fig. 3.8: Simplified tectonic map of Eastern Switzerland with A) mean vitrinite reflectance values from surface or near surface samples (all measured samples included), B) isoreflectance lines (all measured samples included), C) mean vitrinite reflectance values from surface or near surface samples (only fresh or slightly altered samples inluded) and D) isoreflectance lines (only fresh or slightly altered samples inluded).

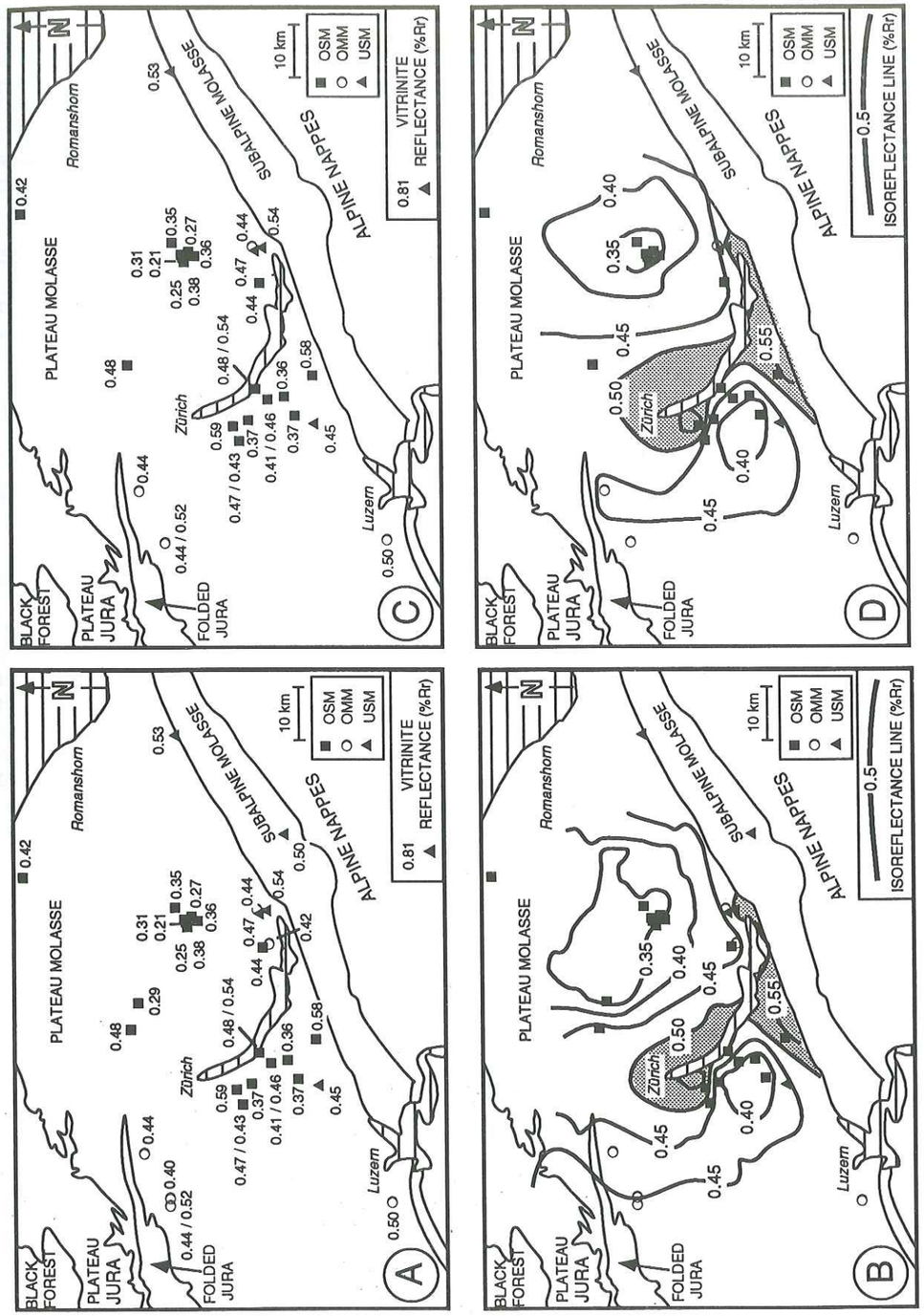

Fig. 3.9: Tectonic map of Northern Switzerland (modified after Todorov et al. 1993) with mean vitrinite reflectance values from surface samples. The samples marked with a star are moderately altered.

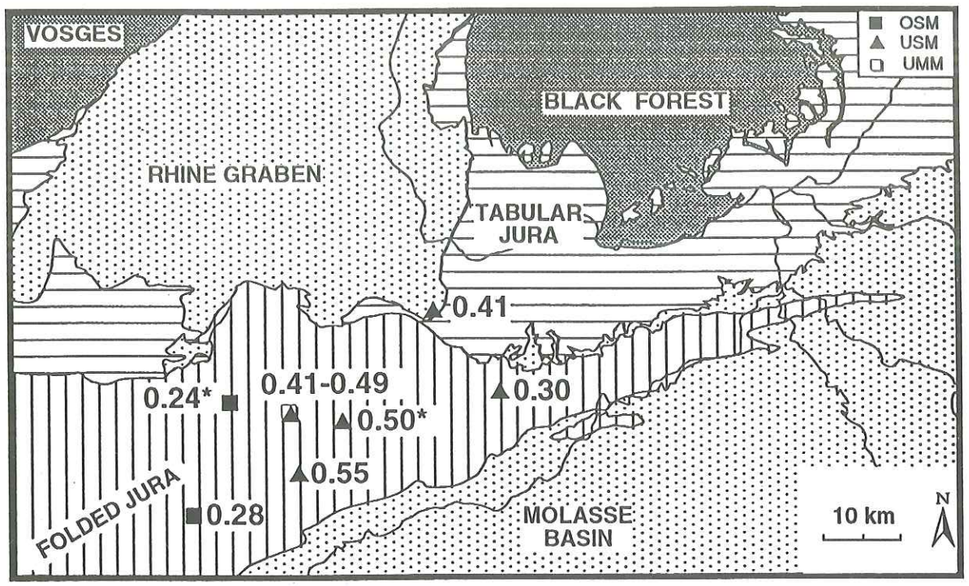

3.5 Comparison with previous studies in the Swiss and French part of the Molasse Basin

3.5.1 Haute-Savoie and Geneva Basin

Data measured in this region agree broadly with those reported by Kübler et al. (1979), Gorin et al. (1989), Gorin & Monteil (1990), Moss (1992). These previous studies have concentrated essentially on the Subalpine Chains, and only little data (5 Rr values) have been published for the Molasse Basin (s.s.). It should be noted that Kübler et al. (1979) reported lower maturity values for the Plateau Molasse (0.29% Rr for one sample taken from the OMM) and for the Bornes Plateau (average value of 0.48% Rr for 4 samples). The studies of Gorin & Monteil (1990) and Moss (1992) confirm the maturation trend observed in this study. Moss (1992) showed that the west to east increase in the level of Rr can be observed for both Tertiary and Mesozoic sediments.

3.5.2 Western Switzerland

The only study on maturation of organic matter in this region is that by Kübler et al. (1979), with values generally lower than those in our study. A comparison of vitrinite reflectance measurements performed on samples taken from the same material (Geological Museum in Lausanne) or from the same location shows that the values of Kübler et al. (1979) are in average 0.09% Rr lower than those obtained in this study (see table 2). There may be two main reasons for this discrepancy:
i) Operator induced variations of vitrinite reflectance values can be quite high, especially in the case of dispersed organic matter (Dembicki 1984). Coals and phytoclasts, on the other hand, are regarded as rather unproblematic materials for vitrinite reflectance measurements. In order to check the reliability of our own vitrinite reflectance measurements, ten samples were sent to the Geological Survey of Canada in Calgary (Dr. W. Kalkreuth). Results are shown in table A2. Differences between the analyses are small. The mean average vitrinite reflectance difference is 0.03% Rr. These results indicate that operator induced variations of Rr values are unlikely.
ii) The most important step in sample preparation is polishing. Inadequate polishing results in a considerable decrease of mean vitrinite reflectance (Buiskool Toxopeus 1983).

3.5.3 Lake Thun area

The data of this study correspond well with two vitrinite reflectance values (0.60 and 0.63% Rr) published by Burkhard & Kalkreuth (1989).

3.5.4 Eastern Switzerland

No vitrinite reflectance value from outcrop samples has been published yet. The coalification profile of the Küsnacht 1 well (Rybach & Bodmer 1980) gives some indications. The shallowest analysed sample at a depth of about 350m has a vitrinite reflectance of 0.48% Rr. Given the low coalification gradient of 0.08% Rr/km, a surface value of about 0.45% Rr can be extrapolated. This is in good agreement with data from this study.

3.5.5 Northern Switzerland

No data on vitrinite reflectance values of organic matter in Tertiary sediments of Northern Switzerland have been published.

3.6 Discussion of vitrinite reflectance results

Results from Northern Switzerland are not included in the following, but will be discussed in detail in chapter 7.3.1 together with results from thermal modelling.

The main observations resulting from vitrinite reflectance analysis in the Molasse Basin can be summarised as follows:

i) Mean average reflectance values increase slowly with age, from 0.38% Rr for samples from the Middle Miocene OSM, to 0.61% Rr for samples from the Oligocene UMM.

ii) In the proximal part of the Molasse Basin, the level of organic maturity in Tertiary sediments increases towards the Alpine front.

iii) The range of vitrinite reflectance values measured in samples from the Plateau Molasse is large (0.21% Rr - 0.64 % Rr). Nevertheless, no pronounced regional trends can be observed. The level of organic maturity of outcrop samples does hardly change from the western to the eastern part of the basin, although a region of low thermal maturity can be observed east of Lake Zurich (Hörnli gravel fan). The vitrinite reflectance values west or north of Zurich, for example, are much the same as in Western Switzerland. In addition, there is no marked decrease in the maturity level of organic matter from the proximal to the distal parts of the Plateau Molasse.

iv) Isoreflectance contours indicate that variations in thermal maturation of the Plateau Molasse might have a structural control. Areas of increased vitrinite reflectance occur near fault zones or lie parallel to a major topographic structure (Lake Zurich) which may be tectonically controlled (Hantke 1967, p.12).

The increase of thermal maturity towards the Alps is probably a consequence of increasing burial depth towards the orogenic belt. Lateral variations of vitrinite reflectance in the Plateau Molasse might have different causes:

i) Alteration: Comparison of isoreflectance maps including all measured samples with those including only unaltered or slightly altered show only slight differences. The main features can be observed in both representations. Given the uncertainties concerning the influence of weathering on vitrinite

reflectance (increase, decrease or no effect?, amplitude?, see chapter 2.2.2.2 for discussion), it is difficult to objectively take into consideration this parameter.

ii) Natural variation of vitrinite reflectance: As discussed in chapter 2.2.2.7 variations 1) in the paleoenvironmental conditions during deposition of the organic matter, 2) of the maceral composition in coal and sedimentary organic matter, 3) in the initial hydrogen content of the vitrinite or 4) of the lithology can influence vitrinite reflectance values. However, the studied samples show little variation in maceral composition. With the exception of some coal samples, the overwhelming majority of samples has a nearly monomaceralic composition (vitrinite). Hydrogen-rich macerals (liptinite) are a minor constituent of the samples and an influence of maceral composition on vitrinite reflectance can, therefore, be ruled out. The anomalies are observed over small areas and studied sediments were formed in the same depositional system. Therefore, little variation in the source and composition of the organic matter is expected.

iii) Topography: The limited topographic relief differences (less than 300m) indicate that the anomalies are not due to erosion exposing more mature rocks. In addition, samples have not been taken from the valley floors but from the flanks. Given the extremely low coalification gradients (<0.1% Rr/km) in the Molasse Basin (see Robert 1985 for a review), local erosion amounts of over 1000m would be required to explain these anomalies. This seems to be very unlikely.

iv) Stratigraphy: A stratigraphic control is unlikely for most observed vitrinite anomalies, because increased vitrinite reflectance values are generally observed within the same sedimentary formation.

v) Geothermal field: As discussed in chapter 2.2.1, vitrinite reflectance responds primarily to increasing burial temperature, and thus can be correlated to its maximum burial temperature. Therefore, the local increases of vitrinite reflectance may be related to variations in the paleogeothermal field. Because increased vitrinite reflectance values are generally situated along fault or thrust zones, a plausible hypothesis to explain the increased thermal maturity of organic matter is a local to regional high paleoheat flow due to ascending warm fluids channelled by tectonic structures. The role of fluid flow through fractures or thrusts has been treated by many authors and is often associated with metamorphism, with the accumulation of hydrocarbons, with the deposition of ores, and with the transfer of heat (Meier et al. 1979, Hoffers 1981, Cathles & Smith 1983, Hitchon 1984, Sibson 1987, 1990, Sibson et al. 1988, Vrolijk et al. 1988, Del Rey & Hamza 1989, Drury 1989, Griesser & Rybach 1989, Mathieu & Velde 1989, Bethke & Marshak 1990, Clendenin & Duane 1990, Nesbitt 1990, Roberts 1990, 1991, Butler 1991, Bredehoeft et al. 1992, Zhang & Davis 1993, and others).

The level of OM maturity in outcrop samples from the Molasse Basin in Switzerland and France is higher than expected from erosion estimates indicating a decollement induced uplift of the Molasse basin which increases from several hundred meters in the north and east to over 2000m in the south-west (Laubscher 1974, Lemcke 1974, Monnier 1982, Schaer 1992). To the east, in the Bavarian Molasse, similar values of vitrinite reflectance are reached only at great depths, because the increase of coalification with depth is extremely low in the Molasse Basin (Teichmüller & Teichmüller 1975, Jacob & Kuckelkorn 1977, Jacob et al. 1982, Rybach 1984). In the Anzing 3 well, situated in the eastern part of the Bavarian Plateau Molasse, a vitrinite reflectance value of 0.51% Rr is reached only at a depth of 2600m. In the Miesbach 1 well, situated in the Subalpine Molasse, vitrinite reflectance values greater than 0.5% Rr are only found at depths greater than 4000m (Jacob & Kuckelkorn 1977).

Vitrinite reflectance results may be easily interpreted in the context of a hypothermal foreland basin, if the results of a recent study (Kälin et al. 1992) on rock density and compaction in the Plateau Molasse (indicating eroded overburden thicknesses of up to 4km) were confirmed. However, there is no geological evidence for large amounts of burial and consecutive uplift/erosion during the Neogene (Laubscher 1987, 1974; Naef et al. 1985), especially in distal parts of the Molasse basin. Furthermore, no viable tectonic concept explains the accumulation and subsequent removal of an additional 4km of sediments during the Middle Miocene on the Plateau Molasse.

If the level of maturation is influenced only by the overburden-thicknesses, a decrease in the level of maturity of organic matter from the west to the east should be observed, since erosion has cut

much deeper into the Western Molasse basin than in the east. In addition, a decrease in maturity from proximal to distal parts of the Plateau Molasse should be observed, since sediment thicknesses decrease generally towards the outer part of the Molasse Basin. This is not the case in the areas we studied. Vitrinite reflectance values west or north of Zurich are the same as in Western Switzerland. This observation supports the hypothesis that the thermal regime of the Molasse basin is largely influenced by other factors than the overburden thicknesses. Convective heat transport could explain in part the observed high coalification level of surface samples. For a detailed discussion of this point see chapter 1.1.2 and chapter 7 (thermal modelling).

Chapter 4: ROCK-EVAL PYROLYSIS RESULTS FROM THE HAUTE-SAVOIE AND GENEVA BASIN

4.1 Geochemical characterisation of organic matter

Results of Rock-Eval pyrolysis are summarised in table B1. The raw data have been evaluated using the following boundary conditions (see chapter 2.2.3.4 and table B1):

A: S2>0.2 mg HC/r rock and TOC>0.5% (Peters 1986).
B: S1>0.2 mg HC/g rock, S2>0.2 mg HC/r rock and TOC>0.5% (Espitalié et al. 1986)

4.1.1 OMM

TOC contents range from 5.6 to 59.95. Samples from the OMM are characterised by low S1 and S2 values and high S3 values. The resulting hydrogen indices are low (average value of A: 29 mg HC/TOC and B: 34 mg HC/TOC). The oxygen indices show a wide range of values (63 - 211 mg CO_2/TOC). OMM samples are characterised by high OI values. The HI-OI diagram (Fig. 4.1 A,B) indicates type III kerogen.

Discussion : In samples from the OMM very little "free" hydrocarbons are present. The formation of hydrocarbons in coals becomes substantial only at the beginning of the oil window (especially above Rr>0.7%, Teichmüller & Durand 1983). The observed S1 values are, therefore, in agreement with the low level of thermal maturity (Rr: 0.32-0.45%) measured for samples from the OMM. An additional factor may be a depletion in S1 values due to weathering (Peters 1986). The S2 peak is thought to be a measure of the hydrocarbon generation potential of a sample. Given the high vitrinite content of the samples (table A1), the observed low S2 and HI values can be easily interpreted in terms of maceral composition. The oxygen content expressed by S3 or OI is high and quite variable and can only partly be explained by natural variation of the organic matter. The most likely additional factor is alteration which may considerably increase the oxygen content (Espitalié et al. 1986).

4.1.2 USM

TOC contents range from 0.3 to 87.8% with an average of 40.6%. The majority of samples is depleted in S1; 16 out of 25 samples have S1 values of less than 0.2 mg HC/g rock. The other samples, with the exception of sample RS88 (S1=35.54 mg HC/g rock) show generally low S1 values (0.28-2.23.mg HC/g rock). S2 and HI are extremely variable. S2 range from 0.26 to 280.45 mg HC/g rock and HI range from 4 to 409 mg HC/TOC. S3 and OI vary from 0.46 to 48.74 Mg CO_2/g rock and from 1 to 269 mg CO_2/TOC respectively. The HI-OI diagram (Fig. 4.1 C,D) indicates type III kerogen.

Discussion : Thermal maturity of organic matter, indicated by vitrinite reflectance data (table B1) puts the USM into the lower part of the catagenesis. The very low S1 values of samples from the USM must, therefore, be attributed to a depletion in S1 due to weathering. The generally low S2 and HI values may be interpreted in terms of maceral composition which is dominated by vitrinite. The very high generation capacity of sample Weid93 (S2=280.45 mg HC/g rock, HI=409 mg HC/TOC) is probably due a rather high liptinite content (see table A1). A part of the samples, depleted in S2, is also characterised by high oxygen indices (>100 mg CO_2/TOC). This observation may be a further argument that samples with very low S2 (<0.2 mg HC/g rock) are affected by weathering, although different oxidation conditions at deposition cannot be excluded.

Fig. 4.1: HI versus OI diagram for Tertiary samples of the Haute-Savoie and Geneva Basin indicating type III kerogen.

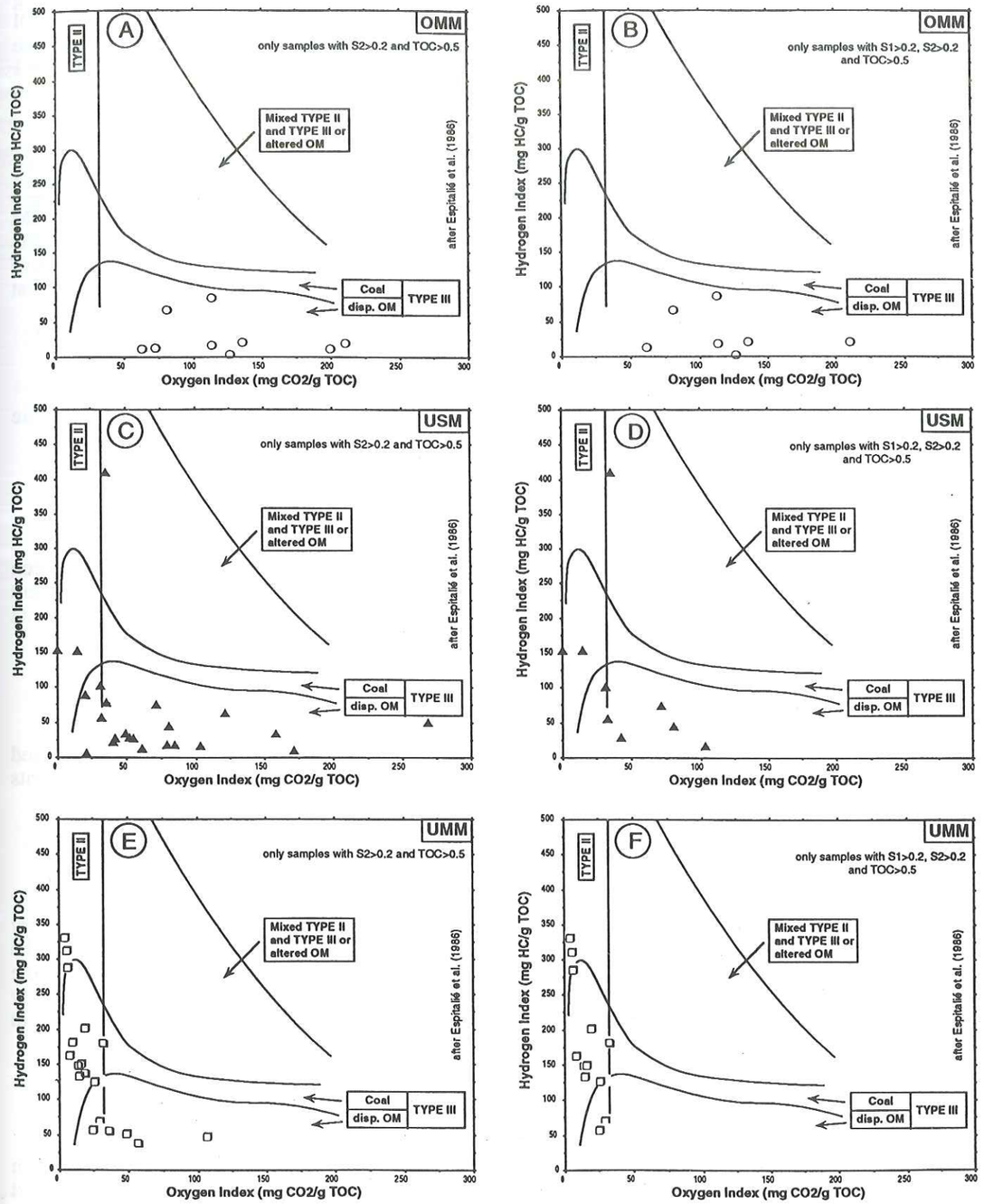

4.1.3 UMM

TOC contents range from 1 to 78.7% with an average of 42.5%. Compared to the results from the OMM and USM, S1, S2 and HI values are relatively high, varying from 0.02 to 30.30 mg HC/g rock , from 0.57 to 261.05 mg HC/g rock and from 41 to 332 mg HC/TOC respectively. S3 and OI values are low. The maximal S3 value is at only 22.16 mg CO_2/g rock. With the exception of one sample (RS120), oxygen indices are always less than 57 mg CO_2/TOC. The HI-OI diagram (Fig. 4.1 E,F) indicates that most samples are of type III kerogen. Two samples (RS186, RS191) seem to consist of type II kerogen.

Discussion : Relatively high free hydrocarbon content and generation capacity can be explained by the level of thermal maturity of the organic matter (more mature than in the OMM and USM) and by a higher initial hydrogen content of the organic matter (->see generally higher liptinite content of UMM samples in table A1). These results are confirmed by a study of the Oligocene Meletta shales in the Bornes Massif (Gorin et al. 1989). These authors concluded that the organic matter of this shale is of mixed type II/III and was formed in dysaerobic, confined marine conditions. They reported also that a part of the amorphous organic matter is hydrogen-rich.

4.1.4 Eocene formation

Only one sample was analysed. The TOC content is 7.5%. All measured values (S1, S2, S3) are low. These results are easily explained by the high level of maturation (Rr=1.53%) of the sample.

4.2 Geographical variation of Rock-Eval parameters

In order to represent the geographical variation of Rock-Eval results, different parameters have been plotted and isovalues calculated. Two types of isovalue maps have been constructed: i) maps, where data have been evaluated using the boundary conditions of Peters (1986) and ii) maps, where data have been evaluated using the boundary conditions of Espitalié et al. (1986).

4.2.1 TOC (Fig. 4.2 A, Fig. 4.3 A)

Isocontour maps of TOC show no clear regional trend. This is expected because the analysed samples are of heterogeneous nature (marl, phytoclast-rich sandstone, hand-picked coaly fragments with various amounts of mineral matter).

4.2.2 S1 (Fig. 4.2 B, Fig. 4.3 B)

Apart from the S1 anomaly at the western end of the Salève mountain, which is due to the very high value of sample Weid93 (see chapter 4.1.2), substantial values can only be observed in the Subalpine Chains. The isovalue maps indicate a eastward increase for samples of the UMM in the Bornes Massif. Given the irregular distribution of the TOC contents, the increase in thermal maturity to the east (see chapter 3.3.2.1) is the most likely explanation for the increase of free hydrocarbons in the samples.

4.2.3 S2 (Fig. 4.2 C, Fig. 4.3 C)

Isocontour maps show that samples from the Plateau Molasse have generally lower S2 values when compared to samples from the Subalpine Molasse and Subalpine Chains. A general west to east increase, with maximum values at the eastern end of the Salève and in the eastern part of the Bornes, can be observed. According to Espitalié et al. (1985b), during thermal maturation S2 respectively HI values reach their maximum at the beginning of the oil window (0.5-0.7% Rr for type III kerogen). Vitrinite reflectance results indicate that the Subalpine Molasse and the Subalpine Chains have attained

Fig. 4.2: Geographical variation of Rock-Eval pyrolysis parameters (A: TOC, B: S1, C: S2, D: S3, E: HI, F: OI) from Tertiary samples of the Haute-Savoie and Geneva Basin. Samples evaluated using the boundary conditions of Peters (1986): S2>0.2 mg HC/r rock and TOC>0.5%.

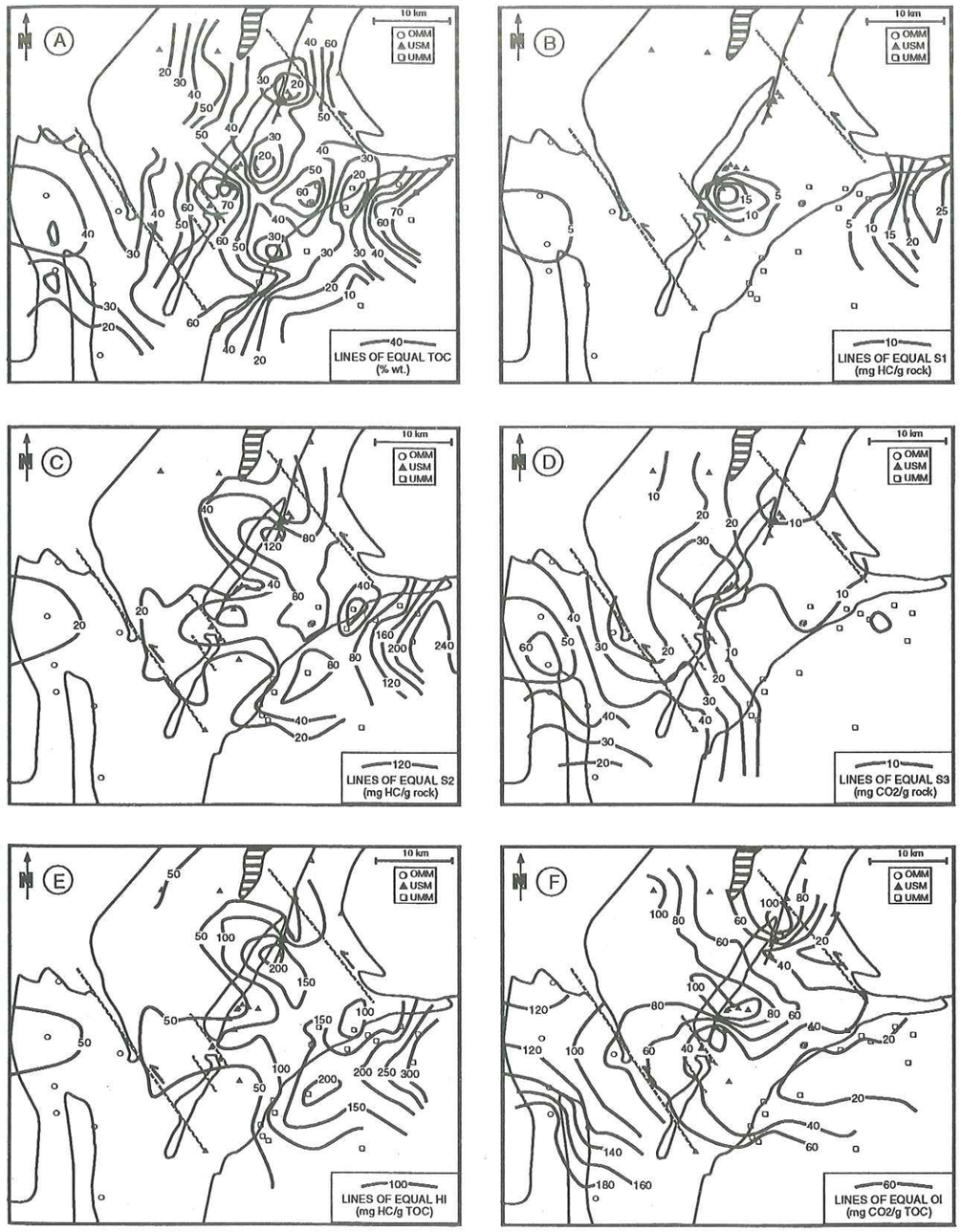

Fig. 4.3: Geographical variation of Rock-Eval pyrolysis parameters (A: TOC, B: S1, C: S2, D: S3, E: HI, F: OI) from Tertiary samples of the Haute-Savoie and Geneva Basin. Samples evaluated using the boundary conditions of Espitalié et al. (1986): S1>0.2 mg HC/g rock, S2>0.2 mg HC/r rock and TOC>0.5%.

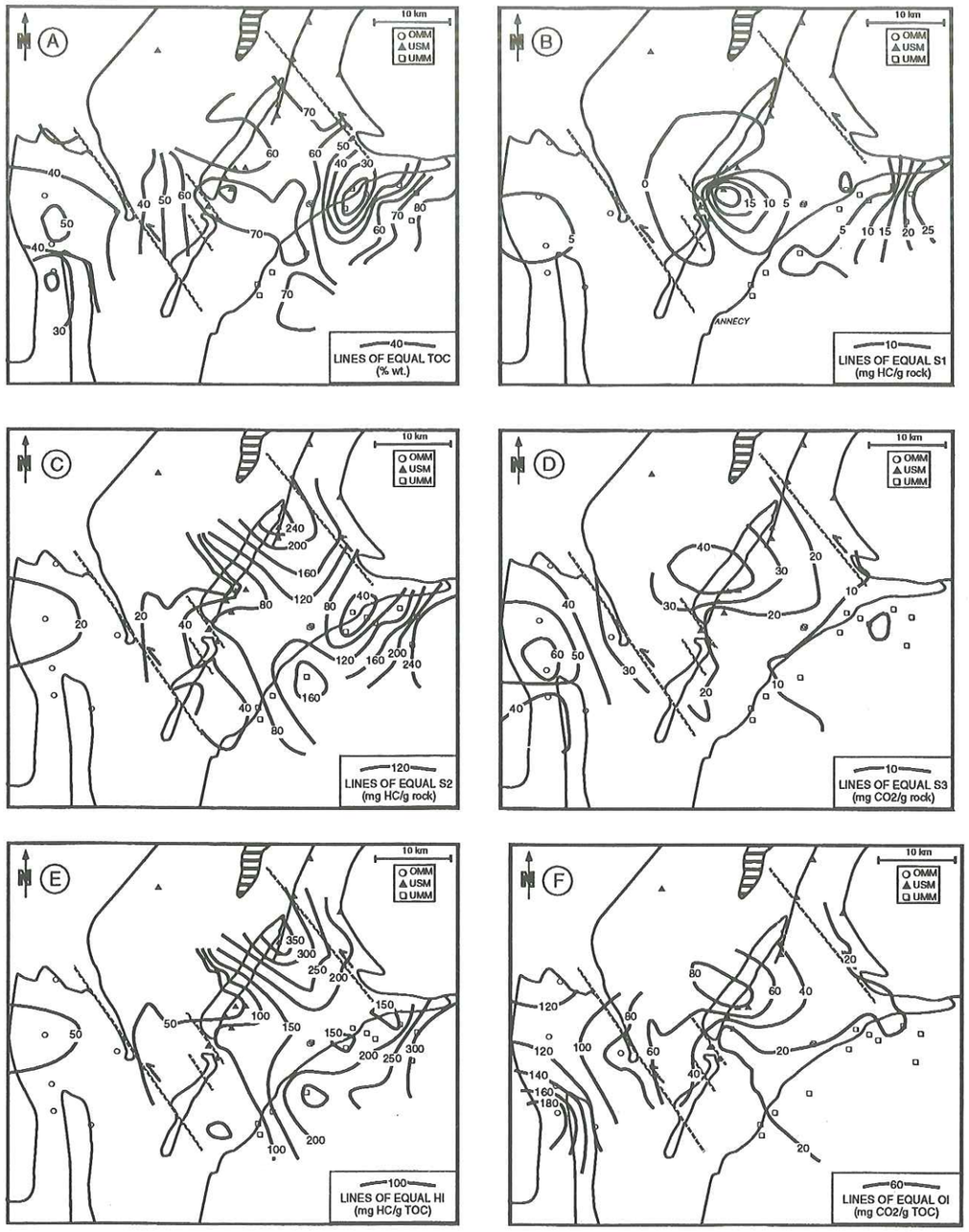

the oil window, the observed trend of S2 values may, therefore, be related to the thermal maturity of the samples. This trend could, however, be amplified by an increase of the initial hydrogen content of the organic matter in the same direction (see chapter 4.1.3).

4.2.4 S3 (Fig. 4.2 D, Fig. 4.3 D)

Isocontour maps show a regional trend indicating decreasing values towards the Alpine front. Maximum values are observed for samples from the OMM situated in the eastern part of the study area. The decrease of S3 towards the east is in agreement with the general geochemical trends during maturation which predict a strong initial decrease of oxygen for type III kerogen. Nevertheless, a part of this increase has probably to be attributed to alteration.

4.2.5 HI (Fig. 4.2 E, Fig. 4.3 E)

Isocontour maps show a clear regional trend indicating an eastward increase in HI. Maxima are found at the eastern end of the Salève and in the eastern part of the Subalpine Chains. Contour maps of HI values confirm the interpretation of chapter 4.2.3. It should be noted that the maximum at the eastern end of the Salève corresponds well with vitrinite reflectance data (see chapter 3.3.2.1) indicating a maturity anomaly in this region.

4.2.6 OI (Fig. 4.2 F, Fig. 4.3 F)

Isocontour maps show a pronounced trend of increasing OI values towards the west. This observation is in line with the one for isocontour maps of S3. The contour maps for OI confirm, therefore, the interpretation of chapter 4.2.4.

4.3 Maturation level of the organic matter

4.3.1 Tmax

4.3.1.1 OMM

Tmax values for OMM samples range from 380 to 474°C (table B1). Vitrinite reflectance data (table A1) range from 0.32 to 0.45% Rr. The HI versus Tmax diagram is generally used to estimate roughly the thermal maturity. Our plot (Fig. 4.4 A,B) indicates that a large part of the samples is within the oil window. Vitrinite reflectance data (Fig. 4.4 A,B) do not agree with this interpretation. The Tmax versus OI diagram (Fig. 4.4 C) shows that a part of the samples, with increased Tmax values, fall outside the evolutionary pathway for humic coals. Results from natural and artificial oxidation (Landais et al. 1984) indicate an increase in Tmax values with increasing alteration. Therefore, an oxidation phenomena might be one cause for the abnormal Tmax distribution. There is, however, no positive correlation between OI and Tmax. Additional mechanisms which may increase the thermostability of carbon structures have to be imagined. Landais et al. (1984) showed for example that during an oxidation phenomena thermally stable cation/organic matter bonds are formed. An increase in Tmax due to surface alteration must, therefore, not necessarily be related to an increase in the oxygen content of the organic matter. It is interesting to note that vitrinite reflectance values seem to be much less sensitive to oxidation phenomena than Tmax.

4.3.1.2 USM

Tmax values for the USM vary between 419 and 571°C (table 1). The HI versus Tmax diagram (Fig. 4.4 D,E) indicates a wide range (immature to overmature) of organic maturity levels. Vitrinite reflectance data range from 0.47 to 1.41% Rr with an average value of 0.6% Rr (table A1) and put the USM into the lower part of the catagenesis. Minimal values of Tmax are in accordance with this

Fig. 4.4: HI versus Tmax and OI versus Tmax diagrams for samples from the OMM (A, B, C), USM (D, E, F) and UMM (G, H, I) in the Haute-Savoie and Geneva Basin.

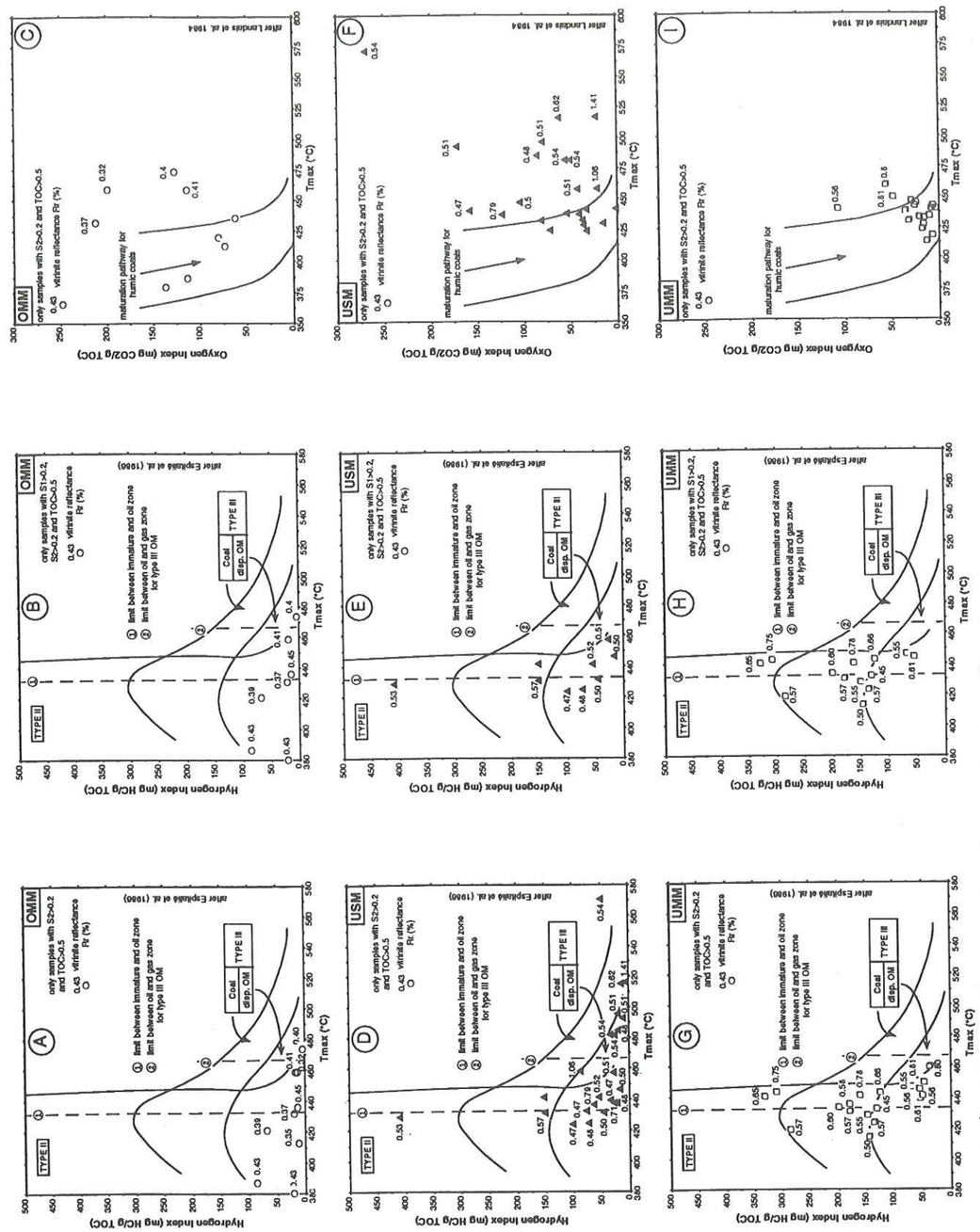

Fig. 4.5: Simplified tectonic maps of the Haute-Savoie and the Geneva Basin with Tmax values from Rock-Eval pyrolysis (A, C) and calculated isocontour lines (B, D).

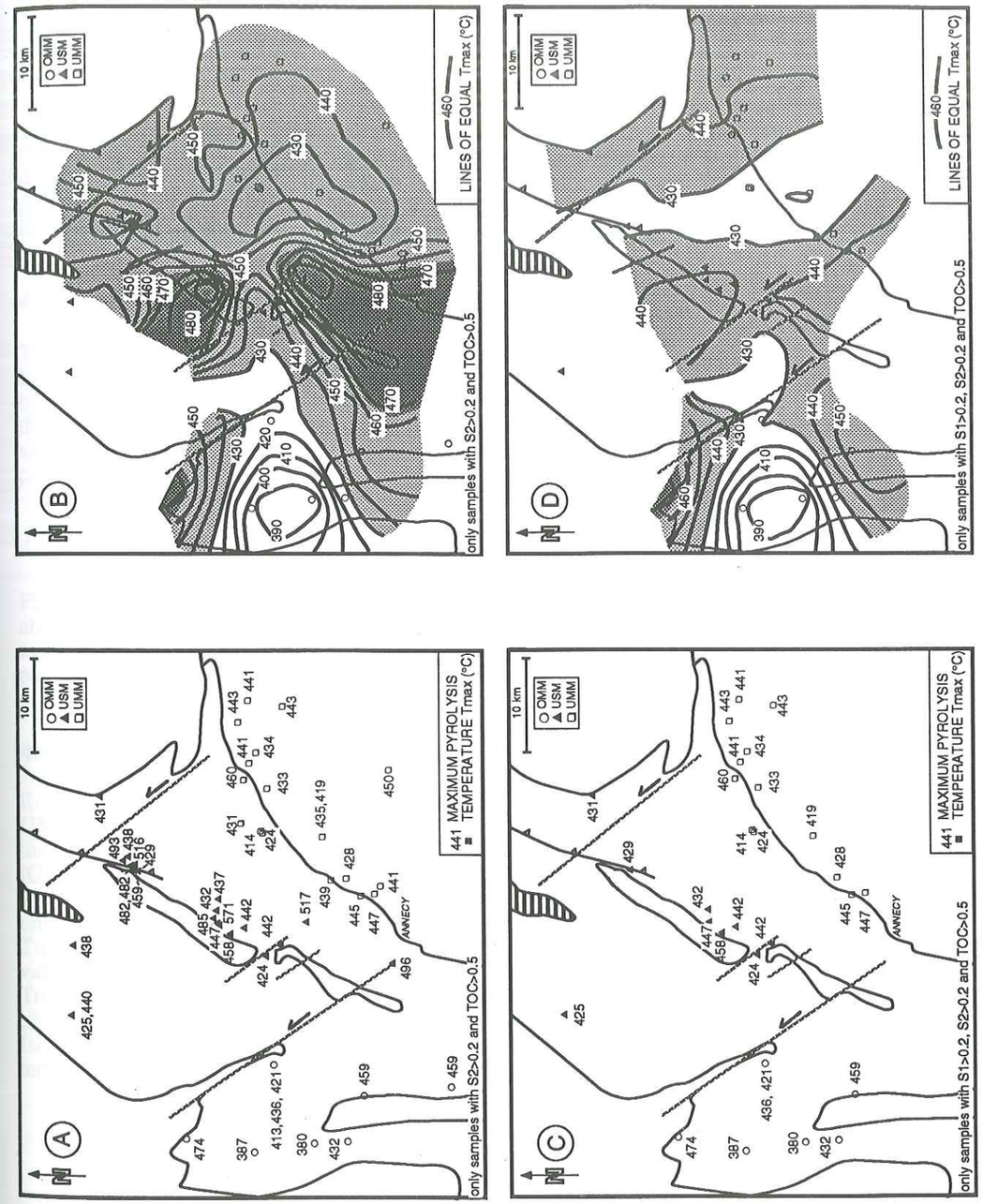

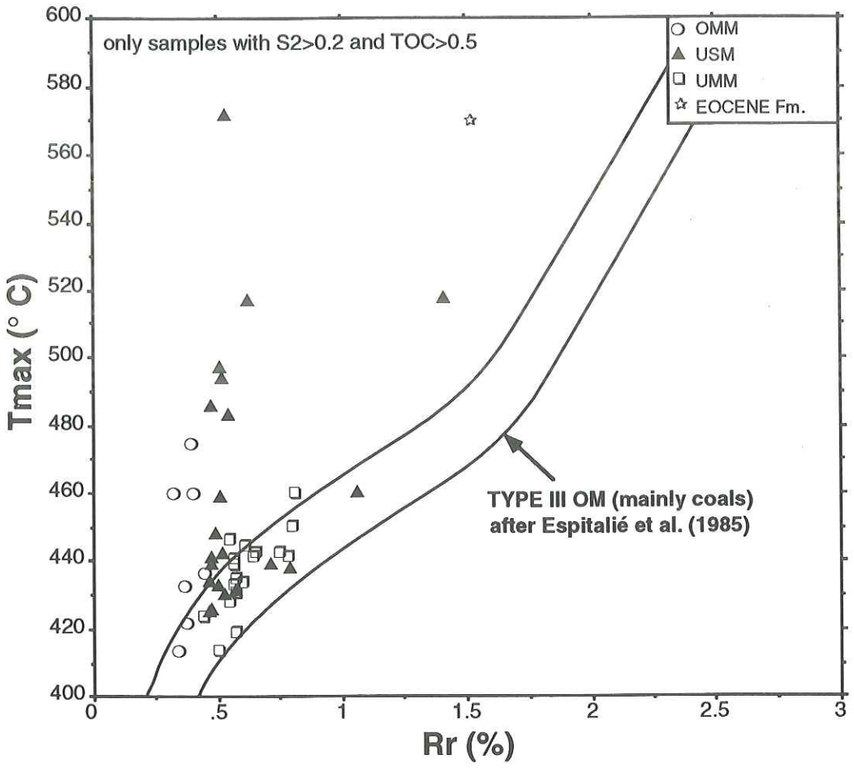

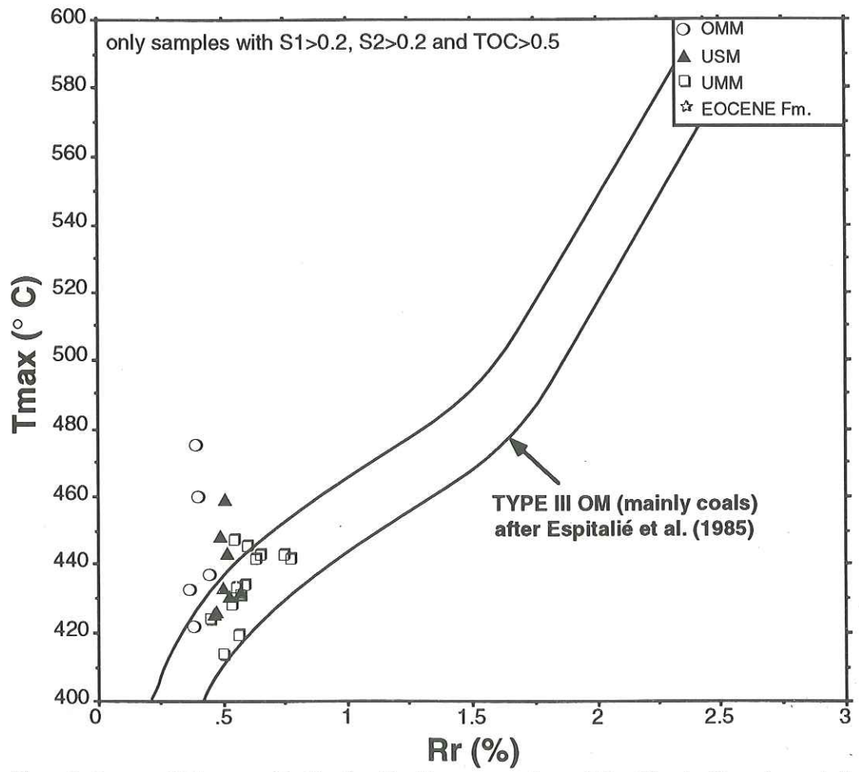

Fig. 4.6: Correlations of Tmax with Rr for Tertiary samples of the Haute-Savoie and the Geneva Basin.

interpretation. The abnormal Tmax distribution may again (as in the case of the OMM, see chapter 4.3.1.1) be attributed to an oxidation phenomena (Fig. 4.4 F). Vitrinite reflectance values do not seem to be influenced by these phenomena. The sample with the highest Tmax (571° C) has a vitrinite reflectance value of only 0.54% Rr.

4.3.2.3 UMM

Tmax values for UMM samples range from 414 to 460°C (table B1). The HI versus Tmax diagram (Fig. 4.4 G,H) puts these samples into the lower oil window. Vitrinite reflectance results (0.45-0.81% Rr) are in good agreement with the Tmax data. Only 3 samples plot outside the maturation pathway for humic coals in the OI versus Tmax diagram (Fig. 4.4 I) indicating , therefore, a limited influence of alteration for these samples.

4.3.2.4 Geographical variation

Tmax values have been mapped (Fig. 4.5 A,C) and isocontours calculated (Fig. 4.5 B,D). Isocontour maps show no clear regional trend. These maps are characterised more by anomalies than by regional trends. Major parts of the area seem to be in the oil window (Tmax>430° C), especially to the east. It has to be noted that these maps can hardly be compared to the isoreflectance maps of the same region (Fig. 3.2 and 3.3). The natural variation of Tmax (type of organic matter) and alteration problems can explain this misfit.

4.3.2.5 Correlation of Tmax with Rr

Figure 4.6 shows a correlation of Tmax values with vitrinite reflectance values. A lot of samples plot above the correlation trend for coal established by Espitalié et al. (1985b), especially when using the evaluation conditions of Peters (1986). As discussed in the previous chapters, an oxidation phenomena is the most likely explanation for the increase in Tmax.

4.4 Conclusions

Rock-Eval pyrolysis results indicate that the organic matter in Tertiary sediments (OMM, USM, UMM) of the Haute-Savoie and Geneva basin is dominated by type III kerogen. Two samples from the UMM showed mixed type II/III kerogen. Similar results have been obtained in previous studies (Gorin et al. 1989, Gorin & Monteil 1990).

The thermal maturity of organic matter derived from Rock-Eval Tmax is associated with major uncertainties as indicated for example by the poor correlation between Tmax and Rr. A large part of Tmax data from the OMM and USM have to be considered as unreliable. Apart from these unreliable values, Tmax measurements can be regarded as roughly coherent with vitrinite reflectance results. Tmax data from the UMM are in accordance with vitrinite reflectance results. The maturity trends observed for the vitrinite reflectance could not be confirmed by Tmax data.

Isocontour maps for S2, S3, HI and OI indicate regional W-E trends which may be explained in terms of an increasing level of thermal maturity of organic matter towards the east.

Chapter 5: CLAY MINERAL DIAGENESIS

A part of the results presented in this chapter has already been published (Schegg 1992a, Schegg & Moritz 1993).

5.1 Bulk-rock mineralogy

As pointed out by Monnier (1982), the average composition of the Molasse deposits based on X-ray diffraction of 2088 samples from 18 wells in Switzerland corresponds to a feldspathic sandstone with a calcareous argillaceous cement. This author calculated the following average bulk-rock mineralogy: quartz (27.3±7.2%), K-feldspar (4.5±3.2%), plagioclase (14.8±8.0%), calcite (20.0±7.1%) and dolomite (6.2±5.6%).

5.1.1 Bulk-rock mineralogy of shale samples

Results of bulk-rock mineralogy of shale samples are summarised in table C1 (A). The average composition based on 73 shale samples is as follows:

quartz	25.9±9.2%
K-feldspar	2.4±3.0%
plagioclase	9.2±6.3%
calcite	23.4±15.8%
dolomite	4.1±7.2%
pyrite	0.3±0.7%
ID (attributed to the clay minerals)	34.7±15.0%

Isocontour maps for each mineral in shale samples from the Haute-Savoie and Geneva Basin indicate a generally rather homogeneous distribution (Fig. 5.1). Neither quartz (Fig. 5.1 A), K-feldspar (Fig. 5.1 B) and plagioclase (Fig. 5.1 C), nor the non-identified components which represent usually the clay mineral fraction of the samples (Fig. 5.1 F) show a clear regional trend. Calcite (Fig. 5.1 D) seems to be more abundant in samples from the Subalpine Chains than in the Molasse Basin s.s.. With the exception of two samples from the Plateau Molasse, the dolomite (Fig. 5.1 E) content is low and evenly distributed. The calculated silicate index (Fig. 5.1 G) and carbonate index (Fig. 5.1 H) reflect well the previous observations. Bulk-rock mineralogy of shale samples does not seem to be strongly influenced by stratigraphy.

5.1.2 Bulk-rock mineralogy of sandstone samples

Results of bulk-rock mineralogy of sandstone samples are summarised in table C1 (B). The average composition based on 28 sandstone samples is as follows:

quartz	35.5±5.6%
K-feldspar	11.9±7.8%
plagioclase	26.3±9.9%
calcite	17.4±12.5%
dolomite	1.8±2.0%
pyrite	0.1±0.3%
ID (attributed to the clay minerals)	7.0±7.0

The distribution of each mineral in samples from the Haute-Savoie and Geneva Basin indicate only small geographical variations (Fig. 5.2). Contents of K-feldspar (Fig. 5.2 B) and

Fig. 5.1: Bulk rock mineralogy: isocontour maps of main components and calculated parameters of shale samples. ID = non-identified component (represents usually the clay mineral fraction of the samples), index S = silicate index (quartz/quartz+feldspars, Zimmermann et al. 1976), index C = carbonate index (dolomite/dolomite+calcite, Zimmermann et al. 1976). Note that the size of sample symbols is proportional to the quantity of the represented mineral.

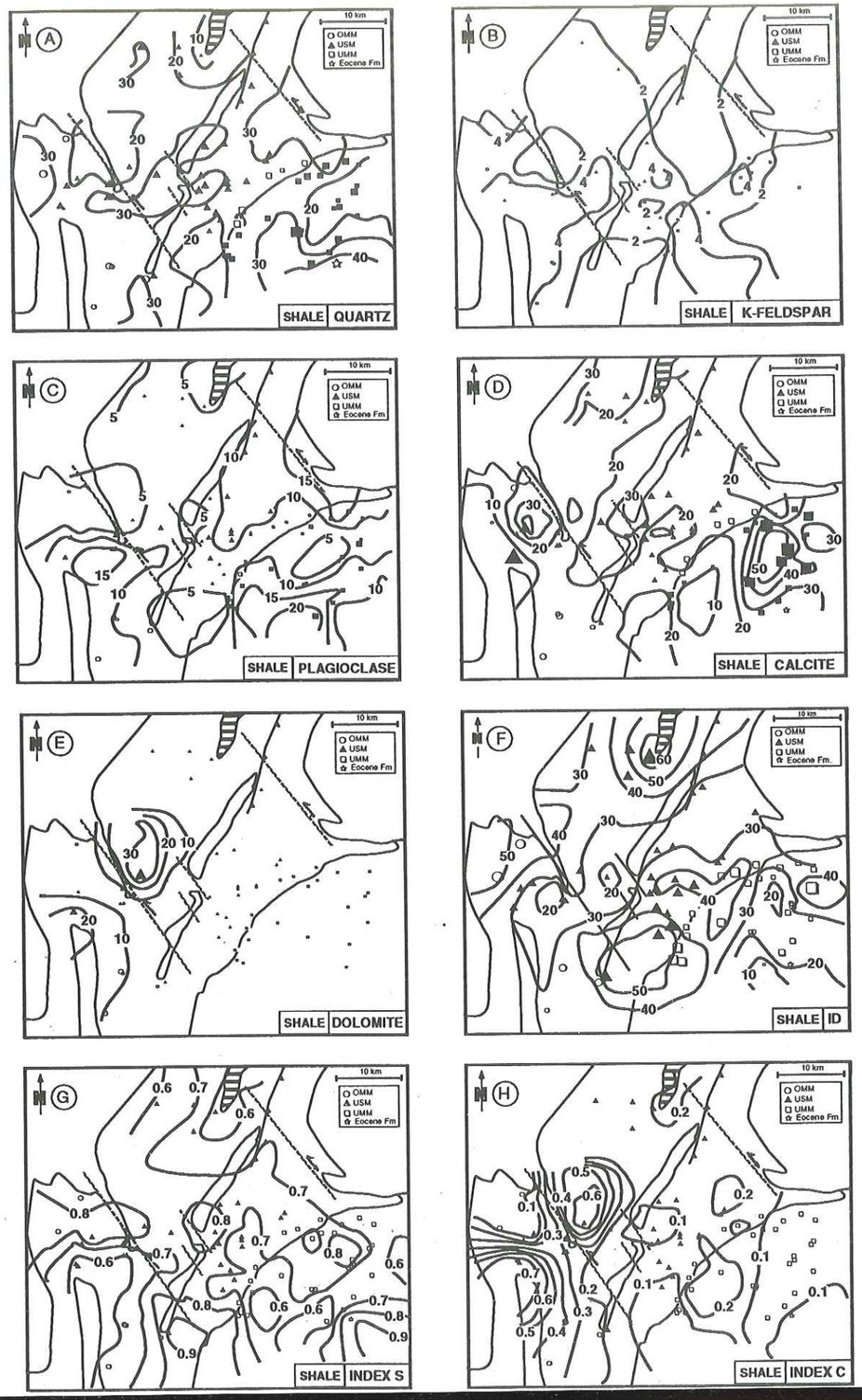

Fig. 5.2: Bulk rock mineralogy: isocontour maps of main components and calculated parameters of sandstone samples. ID = non-identified component (represents usually the clay mineral fraction of the samples), index S = silicate index (quartz/quartz+feldspars, Zimmermann et al. 1976), index C = carbonate index (dolomite/dolomite+calcite, Zimmermann et al. 1976). Note that the size of sample symbols is proportional to the quantity of the represented mineral.

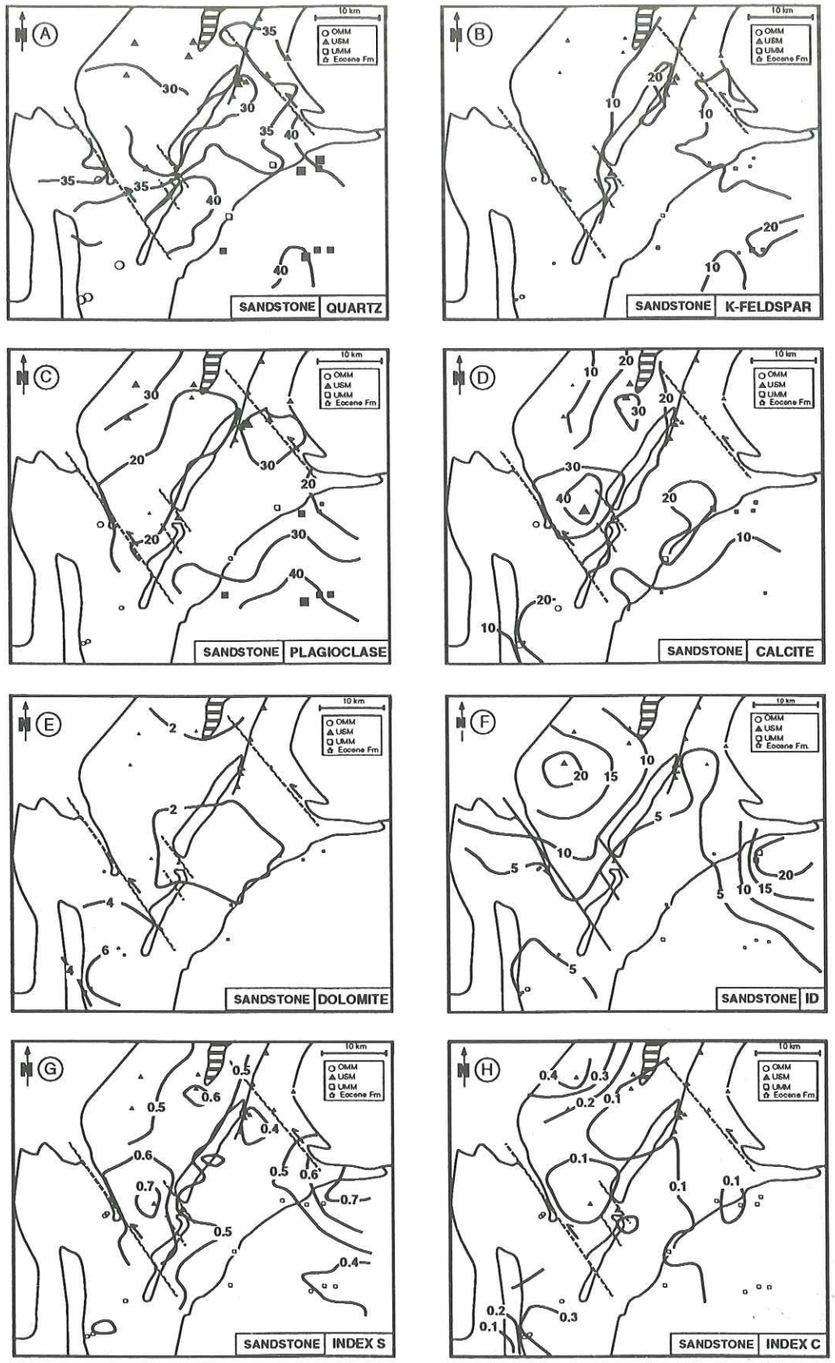

plagioclase (Fig. 5.2 C) are much higher than those in shale samples, whereas the calcite content is generally lower. There seems to be no major stratigraphic control on bulk-rock mineralogy.

5.2 Mineralogy of the fine-fraction (<2µm, 2-16µm)

The relative proportion of phyllosilicates in the <2µm fraction of shale and sandstone samples is summarised in table C2. Absolute intensities (in CPM = counts per minute) of main peaks of phyllosilicates in the <2µm fraction are represented in table C3 and absolute intensities of associated minerals (quartz, K-feldspar, plagioclase) in the <2µm and the 2-16µm fraction in table C4.

5.2.1 Shale samples

The fine fraction of shale samples comprises dominantly mica, chlorite, mixed-layer illite/smectite with variable amounts of kaolinite. Main associated minerals in the fine fraction are quartz, K-feldspar and plagioclase which are present in almost all studied samples (table C4).

5.2.1.1. Mica

Discrete micas are always present. The relative proportion of mica in the <2µm fraction ranges from 27 to 76% with an average of 49% (table C2 A). Micas are usually characterised by well individualised reflections (see annex 2 and table C3). Ternary intensity diagrams of the harmonic series (001) of micas can be used to define fields relating to a specific chemical composition (Rey & Kübler 1983). Micas of the <2µm fraction (Fig. 5.3 A) and the 2-16µm fraction (Fig. 5.3 B) plot in a field comprised between phengitic and illite.

The cristallinity index (IC) has been measured in all samples (table C5 A). IC data for shale samples show a wide variation of values ranging from 0.15 to 1.22° 2θ. The low mean average value of 0.33° 2θ indicates anchimetamorphic conditions. These observations suggest that samples are still in a field where this index reflects the detrital origin, the inheritance of mica cristallinity and the first effects of diagenesis. The assigned diagenesis zones 2 and 3 (Kübler et al. 1979) correspond well to the measured maturity level of the organic matter.

5.2.1.2 Chlorite

Chlorite is ubiquitous. The relative proportion of chlorite in the <2µm fraction ranges from 4 to 52% with an average of 26% (table C2 A). It can be easily identified by its generally well individualised base reflections (annex 2 and table C3). As stated by Moore & Reynolds (1989), increasing Fe or other heavy metal concentrations causes a weakening of the (001), (003) and (005) reflections relative to the (002) and (004) reflections. Triangle plots (001-002-003 and 002-003-004) of both the <2µm fraction (Fig. 5.4 A,C) and the 2-16µm fraction (Fig. 5.4 B,D) indicate that chlorites in the shale samples are Fe- or heavy metal rich.

Fig. 5.3: Ternary intensity (001-002-005) diagrams of the harmonic series of micas. A: Ternary plots for sandstone and shale samples of the <2µm fraction, B: Ternary plots for sandstone and shale samples of the 2-16µm fraction, C: Triangle of reference which defines fields relating to a specific chemical composition.

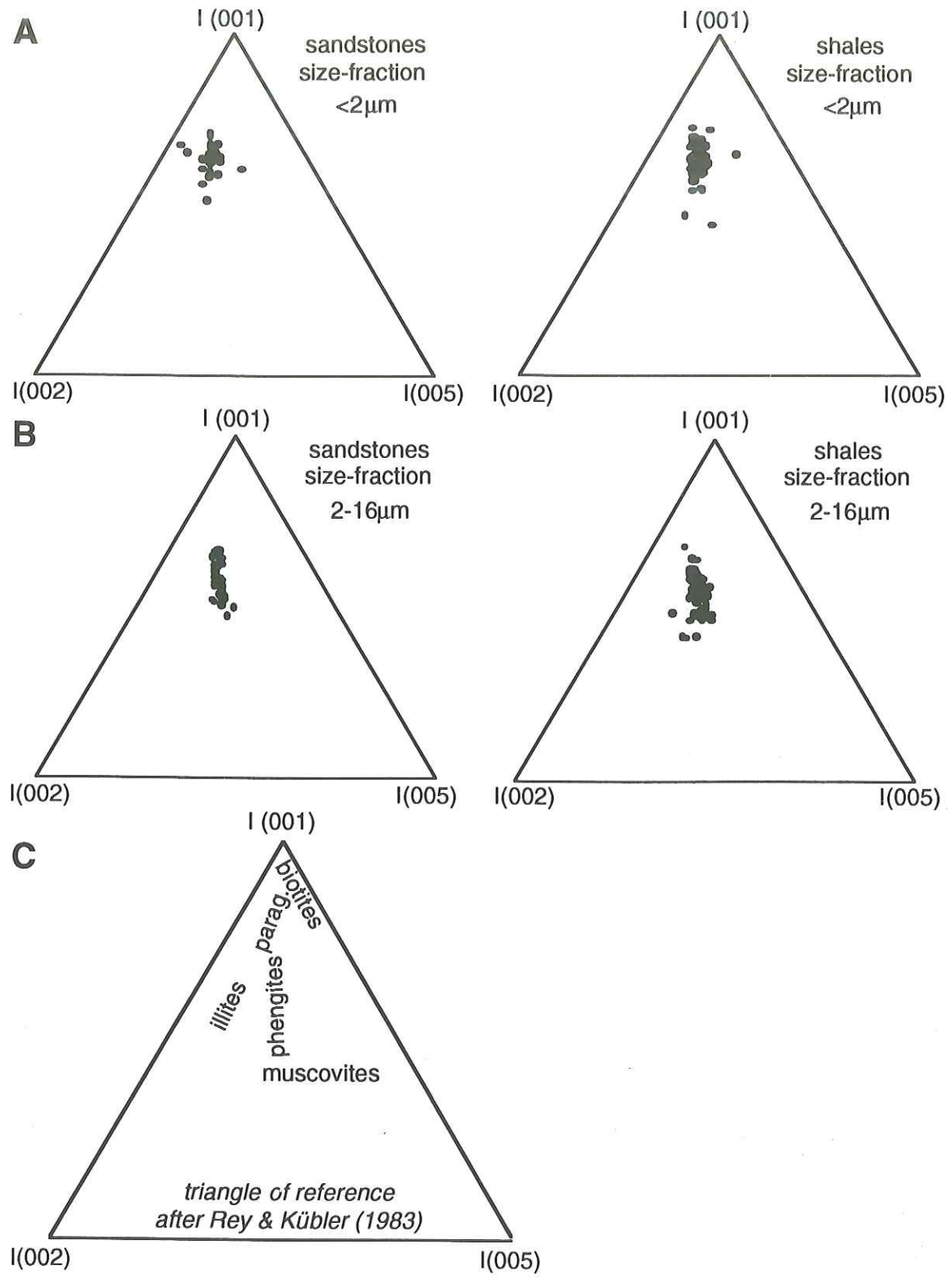

Fig. 5.4: Ternary intensity diagrams of the harmonic series (00l) of chlorite. A: Ternary (001-002-003) plots for sandstone and shale samples of the <2µm fraction, B: Ternary (001-002-003) plots for sandstone and shale samples of the 2-16µm fraction, C: Ternary (002-003-004) plots for sandstone and shale samples of the <2µm fraction, D: Ternary (002-003-004) plots for sandstone and shale samples of the 2-16µm fraction.

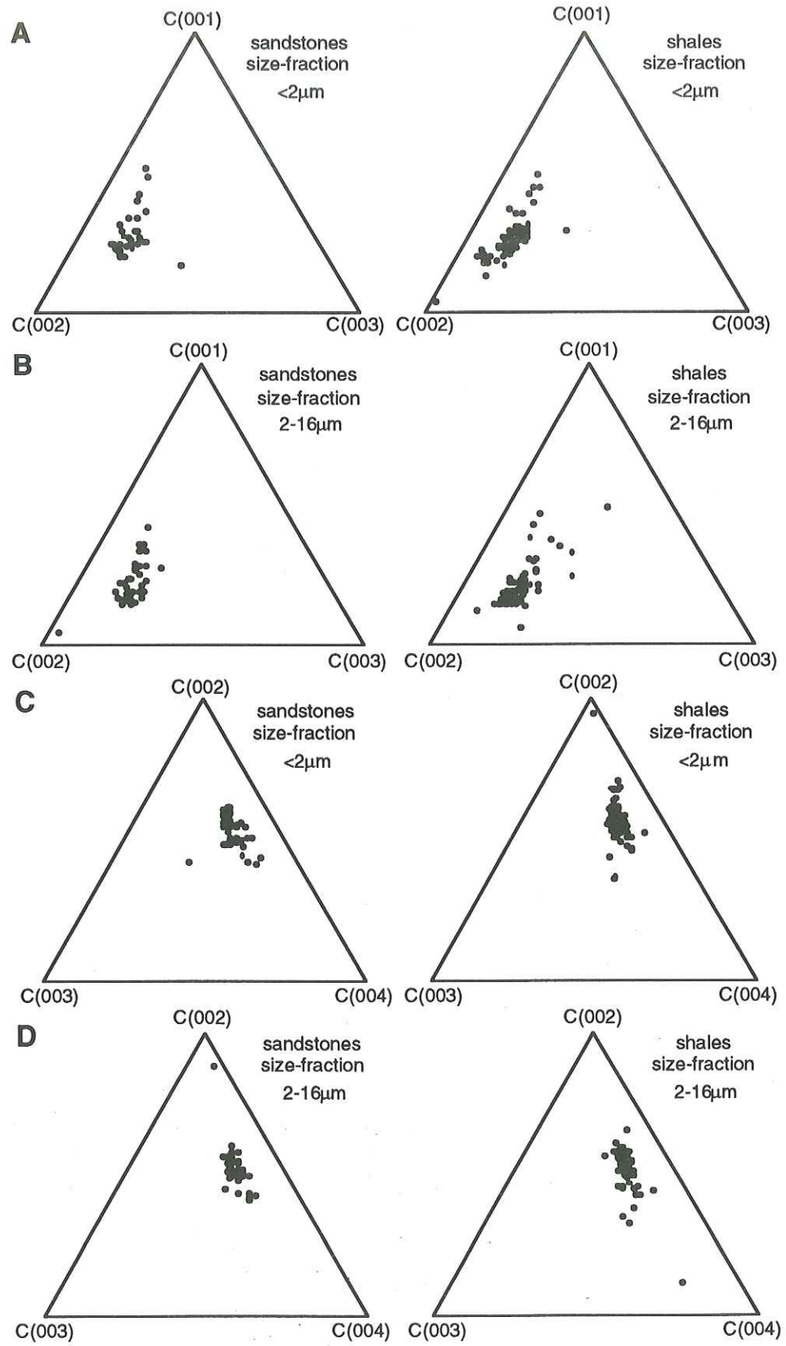

5.2.1.3 Mixed-layer illite/smectite (I/S)

I/S are a rather abundant component of the fine fraction. The relative proportion of I/S in the <2µm fraction ranges from 2 to 60% with an average of 20% (table C2 A). I/S are characterised by a strong and broad reflection of the air dried samples at 10-15° 2θ, which shows a shift to lower angles after saturation with ethylene glycol (annex 2). A deconvolution procedure revealed that there is probably a mixture of different mixed-layer clay minerals (see for example Lanson & Champion 1991 and Lanson & Velde 1992) with, however, a significant content of I/S. A more precise identification of the I/S was hindered by the masking effect of discrete micas and chlorites. Therefore, often only the (001)/(001) peak of I/S could be observed. The only signs of I/S at higher angles in these cases are some broadened or asymmetric peaks of illite or chlorite due to interference effects. Higher angle peaks (001/002 and 002/003) have been observed in 21 samples (see examples in annex 2 and table C5 A). Composition of I/S is discussed in chapter 5.4.

5.2.1.4 Kaolinite

The occurrence of kaolinite in the fine fraction is rather sporadic. The relative proportion of kaolinite in the <2µm fraction ranges from 0 to 43% with an average of 5% (table C2 A). Kaolinite has been observed in all stratigraphic units, but it is most abundant in samples from the UMM. The mineral is identified through its (001) and (002) reflections (annex 3, RS133). These findings are in agreement with earlier studies (e.g. Kübler 1970). Kaolinite is present in the Bavarian part of the Molasse Basin (Füchtbauer 1964) and the High Rhine and the Rhodanian Basins (Sittler 1965). According to Monnier (1982), it was never encountered in the Swiss part of the Molasse Basin. However, some additional analyses of sandstone and shale samples from the USM and OSM of Eastern Switzerland reveal the presence of kaolinite (annex 4).

5.2.2 Sandstone samples

The fine fraction of sandstone samples comprises dominantly mica, chlorite, mixed-layer illite/smectite with variable amounts of kaolinite, corrensite and serpentine. Main associated minerals in the fine fraction are quartz, K-feldspar and plagioclase, which are present in almost all studied samples (table C4).

5.2.2.1 Mica

Discrete mica is generally the most abundant component. The relative proportion of mica in the <2µm fraction ranges from 4 to 63% with an average of 35%. Micas are characterised by a harmonic series of well individualised basal reflections (see annex 3). Micas of the <2µm fraction (Fig. 5.3 A) and the 2-16µm fraction (Fig. 5.3 B) plot in fields which indicate tendencies phengite-illite.

IC data show a small variation of values ranging from 0.12 to 0.34° 2θ with a mean average value of 0.23° 2θ. These results indicate anchimetamorphic conditions. The clear discrepancy between coalification data (chapter 3), indicating low-temperature conditions, and IC data, indicating anchimetamorphic grade (see table 3 in Kübler et al. 1979), can be explained by a detrital origin for the illite.

5.2.2.2 Chlorite

Chlorite is ubiquitous. The relative proportion of chlorite in the <2µm fraction of sandstone samples ranges from 5 to 47% with an average of 25% (table C2 B). It can be easily identified by its generally well individualised base reflections (annex 3 and table C3). Triangle plots (001-002-003 and 002-003-004) of both the <2µm fraction (Fig. 5.4 A,C) and the 2-16µm fraction (Fig. 5.4 B,D) indicate that chlorites in the sandstone samples are Fe- or heavy-metal rich. It is interesting to note that there is no significant difference with the results from the shale samples.

5.2.2.3 Mixed-layer illite/smectite (I/S)

I/S is generally a major component of the fine fraction of sandstone samples, except in samples where corrensite has been found (table C2 B). The relative proportion of mixed-layer illite/smectite in the <2µm fraction of sandstone samples ranges from 0 to 50% with an average of 18% (table C2 B). I/S in sandstone samples show the same characteristics as those in shale samples (see chapter 5.2.1.3 and annex 3). Higher angle peaks (001/002 and 002/003) have been observed in 11 samples (table C5 B) and composition of I/S is discussed in chapter 5.4.

5.2.2.4 Kaolinite

As in shale samples, the occurrence of kaolinite in the fine fraction is rather sporadic. The relative proportion of kaolinite in the <2µm fraction ranges from 0 to 29% with an average of 3% (table C2 B). Kaolinite has been observed in all stratigraphic units, but it is most abundant in samples from the UMM.

5.2.2.5 Corrensite

The occurrence of corrensite is rather sporadic and restricted to samples from the USM of the Bornes Plateau (table C2 B). The relative proportion of corrensite in the <2µm fraction of sandstone samples ranges from 0 to 80% with an average of 14% (table C2 B). The most diagnostic criteria for corrensite were the superlattice peak at 28-29Å, which shifts to 30-31Å (annex 3, table C6) when treated with ethylene glycol and the appearance, after glycol solvation, of the (004) reflection at about 7.8Å (Moore & Reynolds 1989, Weaver 1989).

Most glycolated patterns show strong basal reflections at n=1, 2, 4, 6, 9 and 11 (table C6). Rather regular integral d-values (table C6), sharp superlattice reflections (annex 3, sample RS232), and the position of the (004) reflection of glycolated corrensite near 7.8Å and the (009) reflection of glycolated corrensite near 3.45Å (annex 3, RS232) suggest an almost perfect 1:1 ratio of chlorite to smectite layers (Morrison & Parry 1986). According to Reynolds (1988), reflections produce rational diffraction patterns based on d(001)=31.1Å for low charge (trioctahedral) corrensite and todusite (dioctahedral chlorite/smectite), and d(001)=28.5Å for the high charge corrensite. Todusite produces a pattern very similar to corrensite, except that the relative intensities differ (Reynolds 1988). The intensity of the (004) peak is higher than the (006) peak for low charge corrensite and lower for todusite. Our observations (annex 3 and table C6) suggest a low charge (trioctahedral) corrensite. Note, however, that a low-Fe corrensite and a high Fe-todusite could produce similar diffraction patterns (Reynolds 1988).

5.2.2.6 Serpentine

The occurrence of serpentine is sporadic and not restricted to any stratigraphic formation (table C2 B). The relative proportion of serpentine in the <2µm fraction of sandstone samples ranges from 0 to 24% with an average of 5% (table C2 B). Serpentine can be identified by the (001) peak at about 7.25-7.35Å and the (002) peak at about 3.61-3.66Å (annex 3, sample RS232). it should be noted that the occurrence of corrensite is generally associated with the occurrence of serpentine.

5.3 Geographic variations of minerals in the fine fraction

5.3.1 Shale samples

Geographic variations of mineral contents in shale samples are summarised in a series of isocontour maps: figure 5.5 shows the variation of the relative proportion of phyllosilicates in the <2µm fraction, figure 5.6 shows the variation of absolute intensities of phyllosilicates in the <2µm fraction, figure 5.7 shows the variation of absolute intensities of associated minerals in the <2µm fraction and figure 5.8 shows the variation of absolute intensities of associated minerals in the 2-16µm fraction.

There are no major variations in the relative proportion of mica (Fig. 5.5 A), chlorite (Fig. 5.5 B) and I/S (Fig. 5.5 C) in the clay mineral fraction. Kaolinite is essentially restricted to samples from UMM in the Subalpine Chains (Fig. 5.5 D). The clay mineral assemblages seems, therefore, to be rather constant throughout the study region. Isocontour maps of absolute intensity for mica (Fig. 5.6 A), chlorite (Fig. 5.6 B), I/S (Fig. 5.6 C) and kaolinite (Fig. 5.6 D) indicate generally lower values for samples close to the Alpine front and those from the Subalpine Chains.

Absolute intensities of associated minerals show an interesting feature. Intensities of K-feldspar in the <2µm fraction are quite low (<2000 CPM) for UMM samples from the Subalpine Chains and for samples located close to the Alpine front (Fig. 5.7 F) when compared with values from the Plateau Molasse or the Subalpine Molasse. A similar observation can be made for the 2-16µm fraction (Fig. 5.8 F). Intensities are, however, higher than in the <2µm fraction. Plagioclase (Fig. 5.7 E, Fig. 5.8 E) and quartz (Fig. 5.7 D, Fig. 5.8 D) in both size fractions show no geographic significant trends.

5.3.2 Sandstone samples

Geographic variations of mineral contents in sandstone samples are summarised in a series of isocontour maps: figure 5.7 shows the variation of absolute intensities of associated minerals in the <2µm fraction; figure 5.8 shows the variation of absolute intensities of associated minerals in the 2-16µm fraction; figure 5.9 shows the variation of the relative proportion of phyllosilicates in the <2µm fraction and figure 5.10 shows the variation of absolute intensities of phyllosilicates in the <2µm fraction.

The relative proportions of mica (Fig. 5.9 A), chlorite (Fig. 5.9 B) and I/S (Fig. 5.9 C) in the <2µm fraction are generally rather important. Their amount is, however, considerably reduced at the eastern and western part of the Salève mountain. This is due the occurrence of corrensite (Fig. 5.9 E) and serpentine (Fig. 5.9 F). It is interesting to note that the appearance of corrensite seems to be closely associated with the occurrence of serpentine. The proportion of I/S shows a decrease towards the Alps. Kaolinite occurs sporadically in all studied formations (Fig. 5.9 D). Isocontour maps of absolute intensities for mica (Fig. 5.10 A), chlorite (Fig. 5.10 B) and I/S (Fig. 5.10 C) indicate generally lower values for samples close to the Alpine front and those from the Subalpine Chains.

Fig. 5.5: Isocontour maps of the relative proportion (in %) of phyllosilicates in the <2µm fraction of shale samples. Note that the size of sample symbols is proportional to the quantity of the represented mineral.

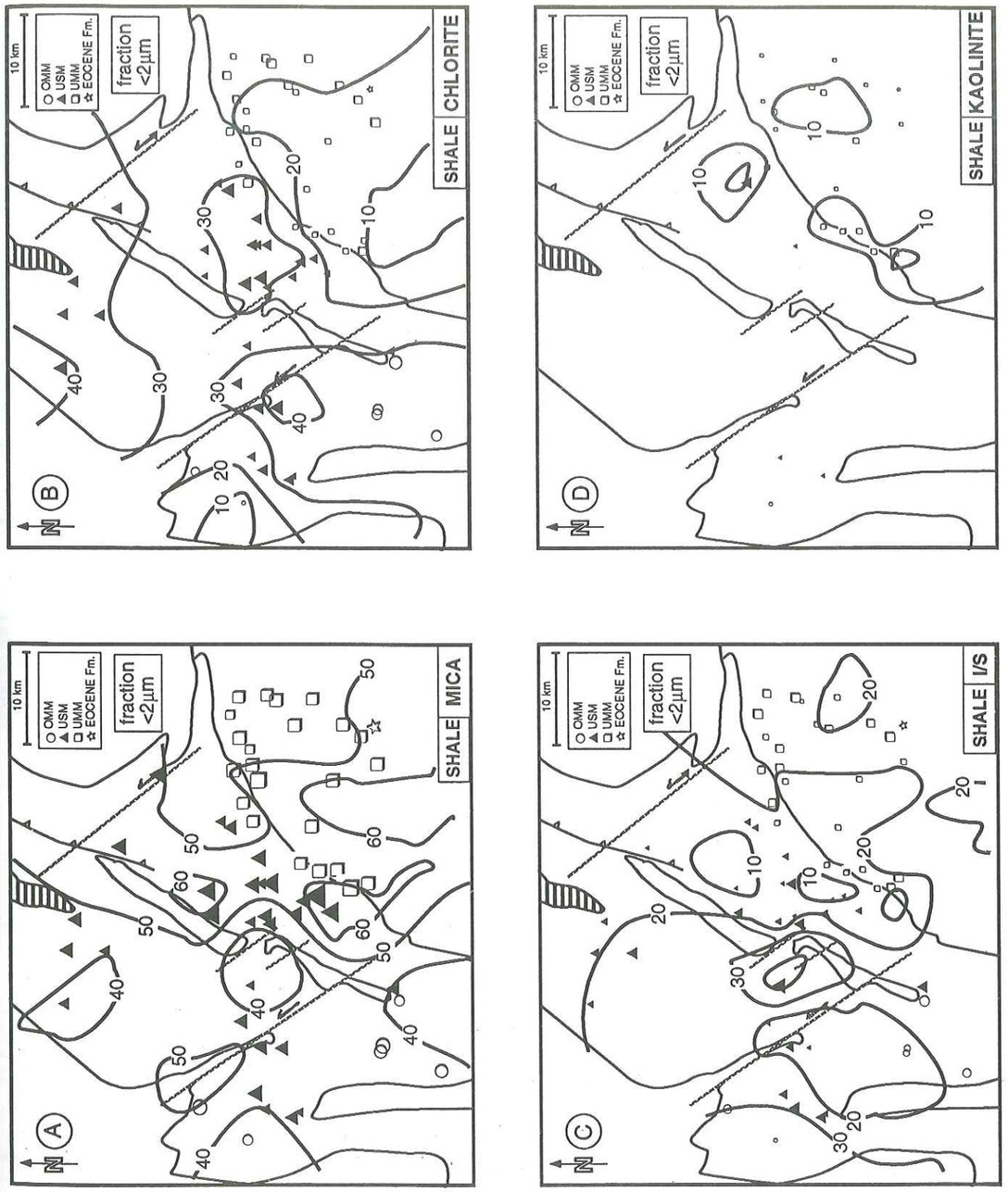

Fig. 5.6: Isocontour maps of the absolute intensities (in CPM = counts per minute) of phyllosilicates in the <2µm fraction of shale samples.

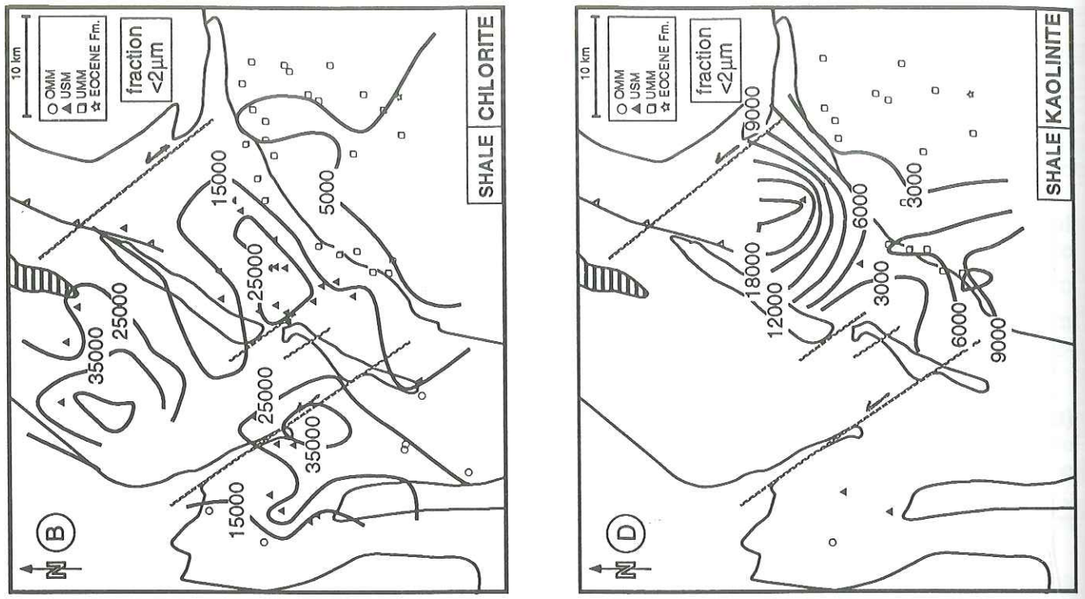

Fig. 5.7: Isocontour maps of the absolute intensities (in CPM = counts per minute) of associated minerals in the <2µm fraction of sandstone (A-C) and shale samples (D-F).

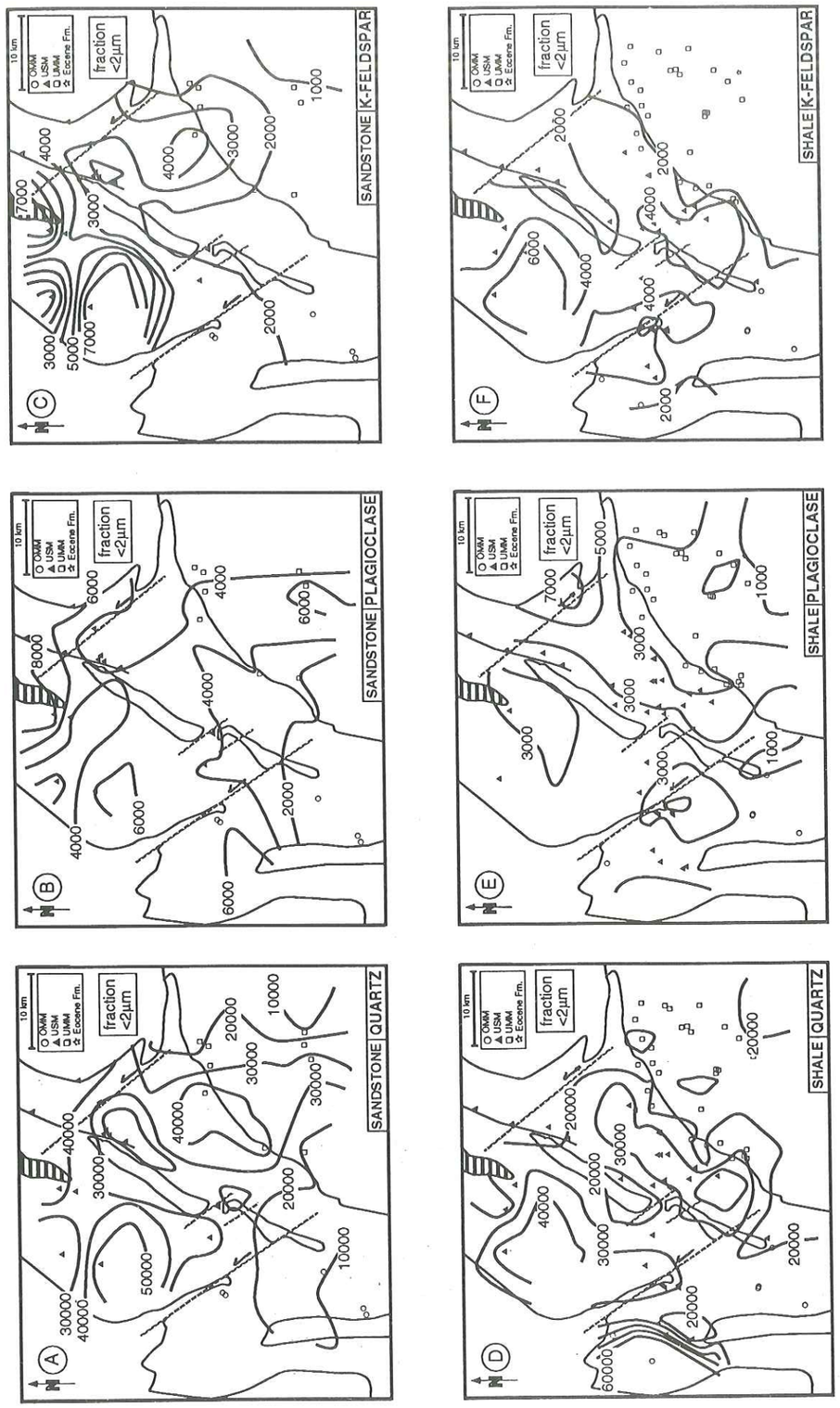

Fig. 5.8: Isocontour maps of the absolute intensities (in CPM = counts per minute) of associated minerals in the 2-16µm fraction of sandstone (A-C) and shale samples (D-F).

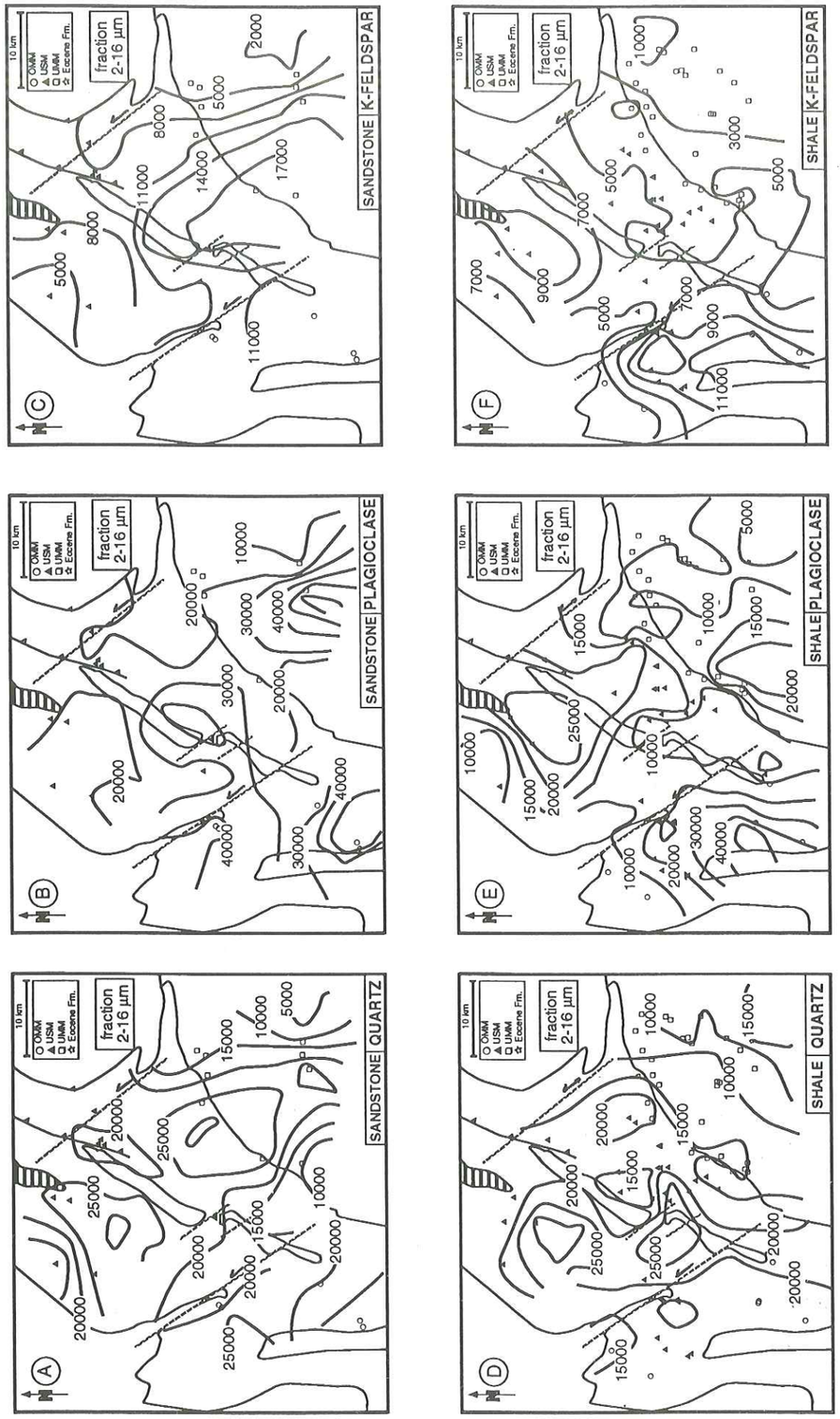

Fig. 5.9: Isocontour maps of the relative proportion (in %) of phyllosilicates in the <2µm fraction of sandstone samples. Note that the size of sample symbols is proportional to the quantity of the represented mineral.

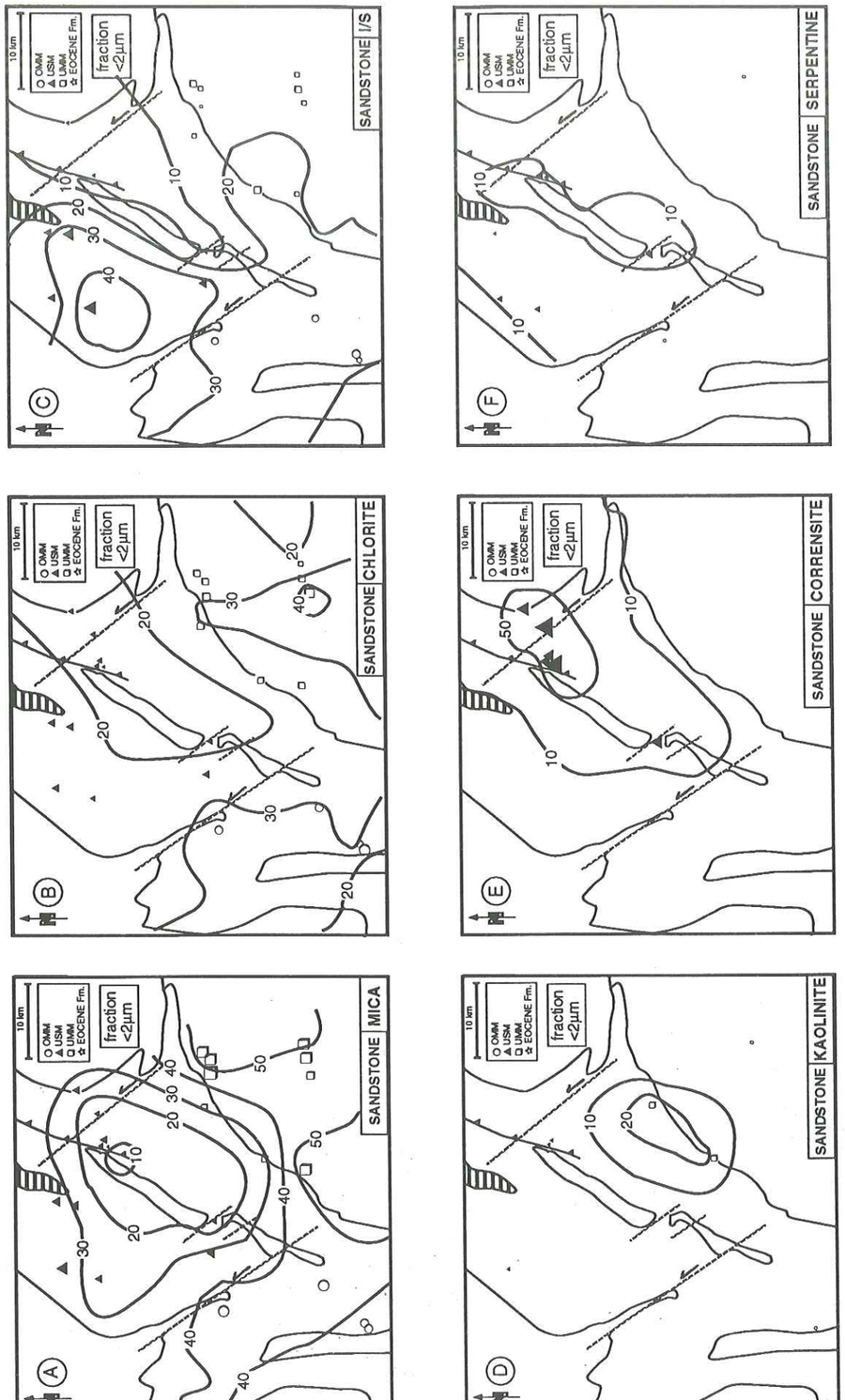

Fig. 5.10: Isocontour maps of the absolute intensities (in CPM = counts per minute) of phyllosilicates in the <2µm fraction of sandstone samples.

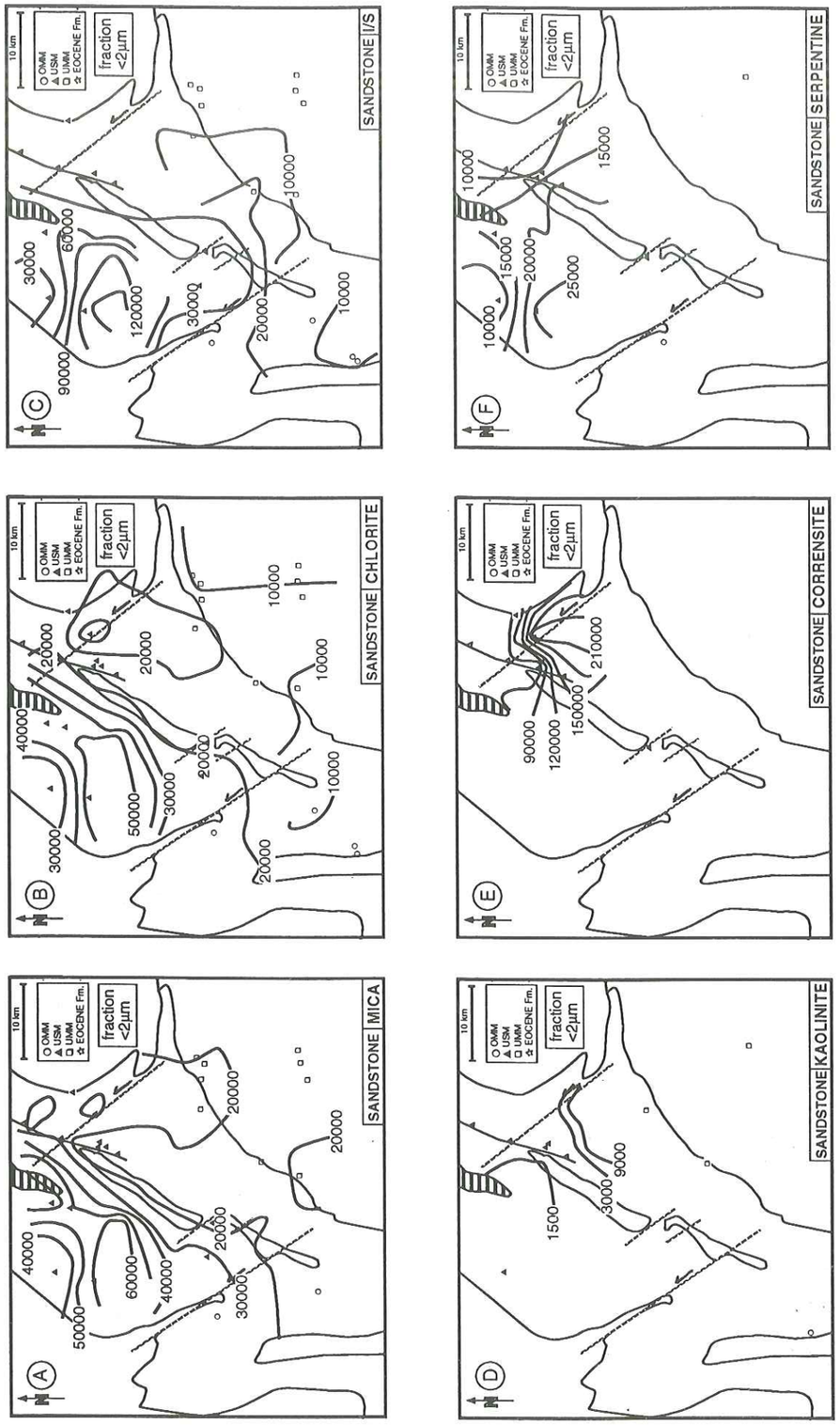

Intensities of K-feldspar in the <2µm fraction are low for samples from the Subalpine Molasse and the Subalpine Massif (Fig. 5.7 C). The 2-16µm fraction (Fig. 5.8 F) shows a more or less well pronounced W-E trend of decreasing K-feldspar intensities. Plagioclase (Fig. 5.7 E, Fig. 5.8 E) and quartz (Fig. 5.7 D, Fig. 5.8 D) in both size fractions show no significant trends.

5.4 Variation of smectite layers in mixed-layer illite/smectite (I/S)

Results of estimations of %S in I/S are summarised in table C5 and in a series of isocontour maps representing the geographical variation of the percentage of smectite layers in I/S using different estimation methods (Figs. 5.11, 5.12, 5.13 and 5.14). [The different estimations methods have already been discussed in chapter 2.1.3.7.]

5.4.1 Shale samples

The isocontour maps (Fig. 5.11, 5.12) show a clear geographic trend. There is a marked decrease in the percentage of smectite layers from the Plateau Molasse towards the Subalpine Chains. A WNW-ESE trend is well outlined in figures 5.11 D (estimation method of Weaver 1956) and 5.11 F (estimation method of Moore & Reynolds 1989 based on position of the 002/003 peak). Other isocontour maps (Fig. 5.11 E, Fig. 5.12 D, E, F) are more difficult to interpret. This is probably due to the limited number (->scarcity of high angle reflections) and the irregular distribution of data points.

5.4.2 Sandstone samples

Despite a limited number of data points, all isocontour maps for sandstone samples (Fig. 5.13 and 5.14) show a clear regional trend of decreasing percentage of smectite layers in I/S from the West to the East. The diagenetic trends for both lithologies (sandstones and shales) seems to be rather similar. Both show the progressive illitisation of I/S towards the Alpine front, in a more or less well outlined West to East direction.

5.5 Correlation between vitrinite reflectance (%Rr) and percentage smectite (%S) layers in mixed-layer illite/smectite (I/S)

The similarity of isoreflectance maps (see chapter 3) and isocontour maps representing the %S in I/S is striking. A relation between these two thermal indicators seems therefore very likely. As vitrinite reflectance data together with I/S composition are only available for 8 samples, a direct correlation between %Rr and %S in I/S cannot be established. Therefore, an alternative approach has been chosen to correlate both data sets. Isocontour maps have been calculated by kriging. These calculations were performed with the same parameters, the resulting grids (25*25) are, therefore, identical. In order to increase the reliability of this approach, grid points in regions where sampling density is too low have been discarded. The correlation between organic and clay mineral diagenesis is based on the comparison between %Rr and %S values in the remaining 300 grid points. This approach cannot result in a reliable and precise relationship, but it allows to compare these two diagenesis indicators in a somewhat statistical manner. The %Rr data set is represented in figure 3.2. The I/S composition data set comprises results from sandstone and shale samples.

Figure 5.15 a shows a correlation where the %S in I/S has been estimated by the method of Weaver (1956) and figure 5.15 B shows a correlation where the %S in I/S has been estimated by the method

Fig. 5.11: Tectonic maps representing the %S in I/S (A-C) and corresponding isocontour maps (D-F) of shale samples. The different methods (see chapter 2.3.1.7) to estimate the I/S composition are based on: IS1 = position of the 001/001 peak (Weaver 1956), IS2 = position of the 001/002 peak (Moore & Reynolds 1989), IS3 = position of the 002/003 peak (Moore & Reynolds 1989).

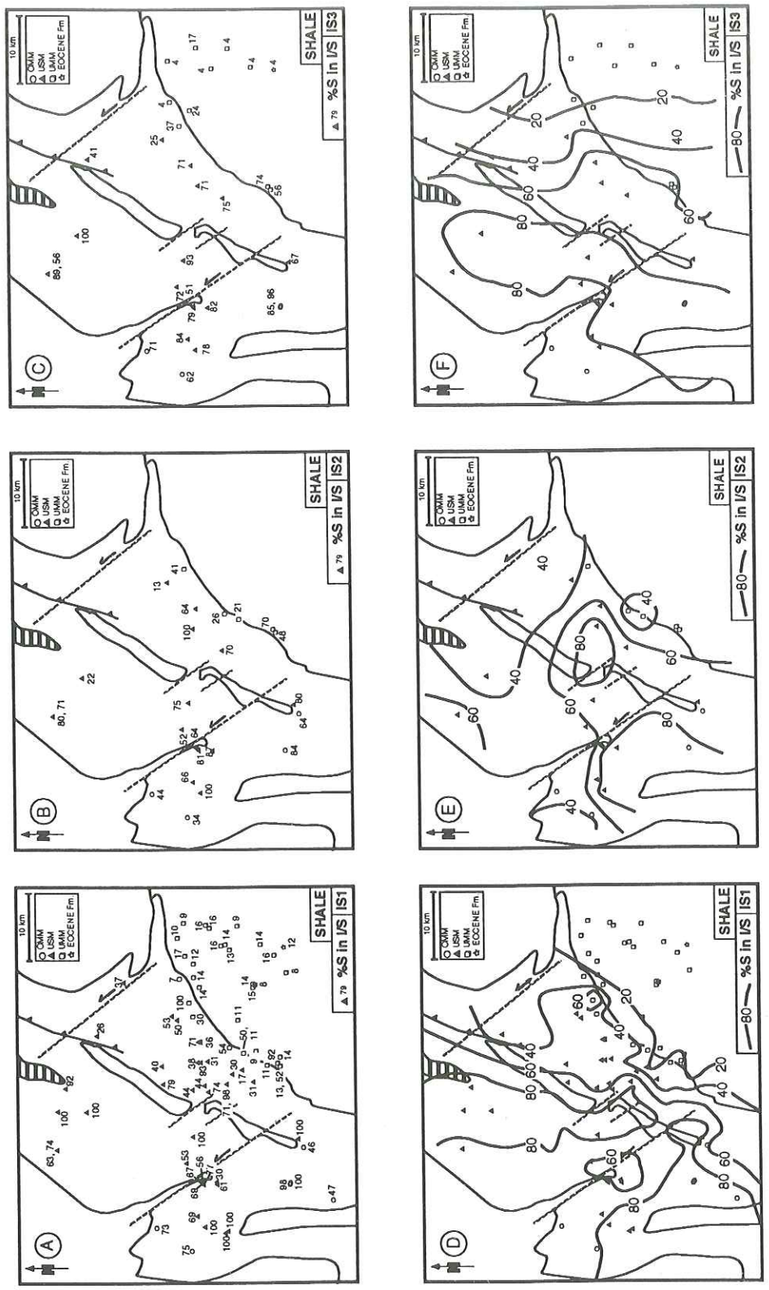

Fig. 5.12: Tectonic maps representing the %S in I/S (A-C) and corresponding isocontour maps (D-F) of shale samples. The different methods (see chapter 2.3.1.7) to estimate the I/S composition are based on: Δ1a = angular difference of the 001/002 and the 002/003 (Moore & Reynolds 1989), Δ1b = angular difference of the 001/002 and the 002/003 (Vuitel 1987), Δ1/Δ2 = angular differences Δ1 (001/002 and 002/003) and Δ2 (001/001 and 002/003) (Vuitel 1987).

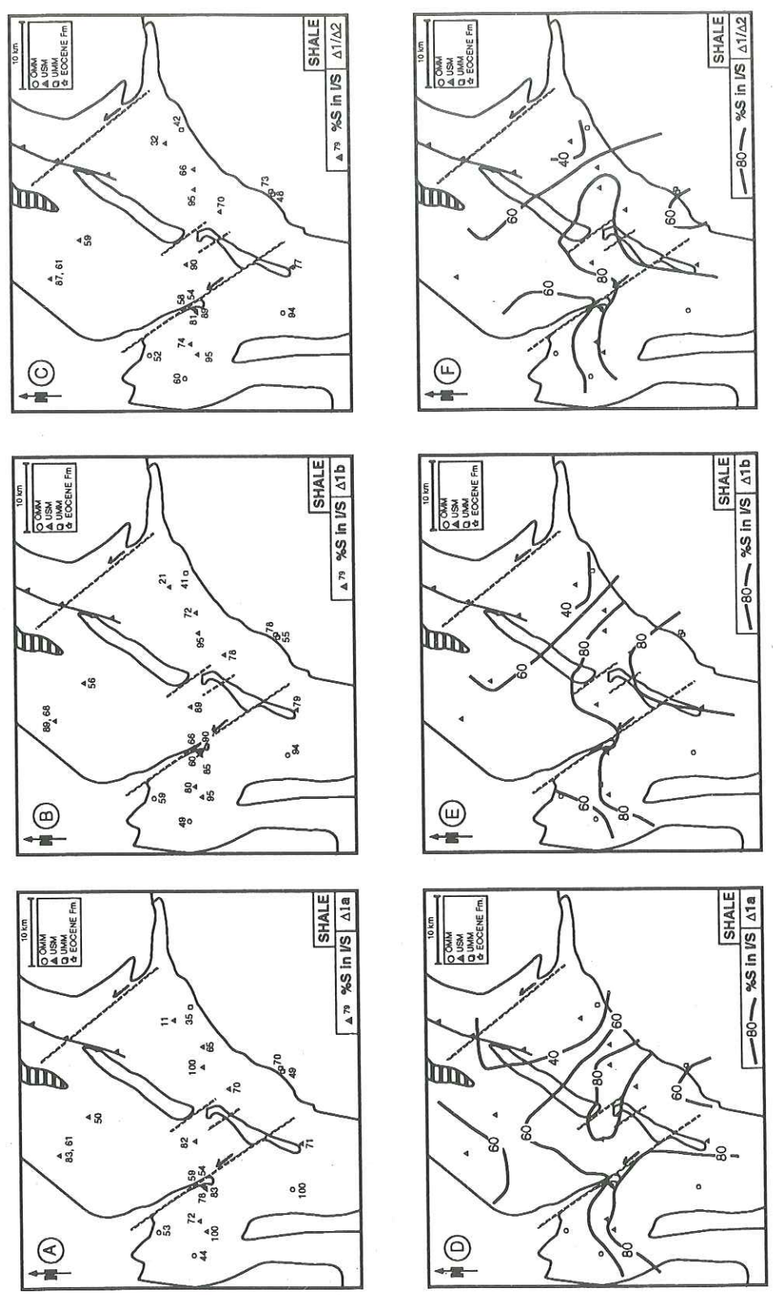

Fig. 5.13: Tectonic maps representing the %S in I/S (A-C) and corresponding isocontour maps (D-F) of sandstone samples. The different methods (see chapter 2.3.1.7) to estimate the I/S composition are based on: IS1 = position of the 001/001 peak (Weaver 1956), IS2 = position of the 001/002 peak (Moore & Reynolds 1989), IS3 = position of the 002/003 peak (Moore & Reynolds 1989).

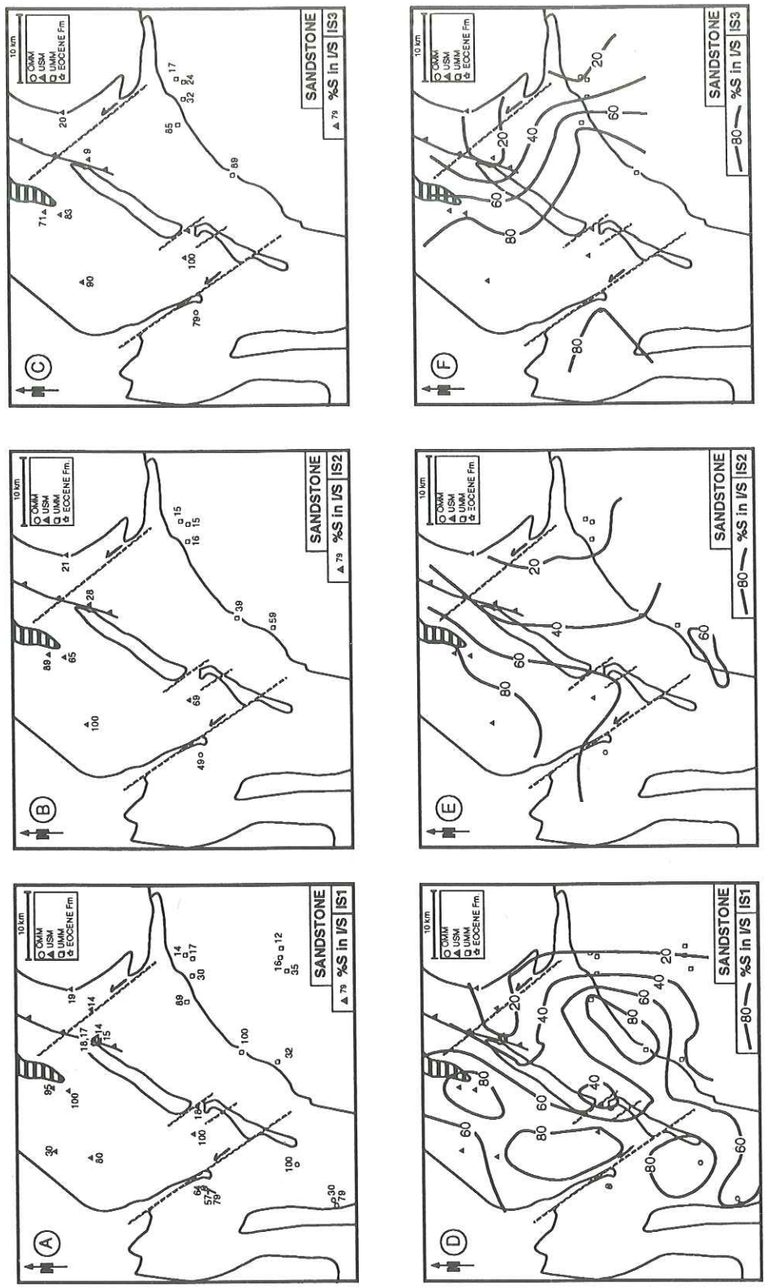

Fig. 5.14: Tectonic maps representing the %S in I/S (A-C) and corresponding isocontour maps (D-F) of sandstone samples. The different methods (see chapter 2.3.1.7) to estimate the I/S composition are based on: Δ1a = angular difference of the 001/002 and the 002/003 (Moore & Reynolds 1989), Δ1b = angular difference of the 001/002 and the 002/003 (Vuitel 1987), Δ1/Δ2 = angular differences Δ1 (001/002 and 002/003) and Δ2 (001/001 and 002/003) (Vuitel 1987).

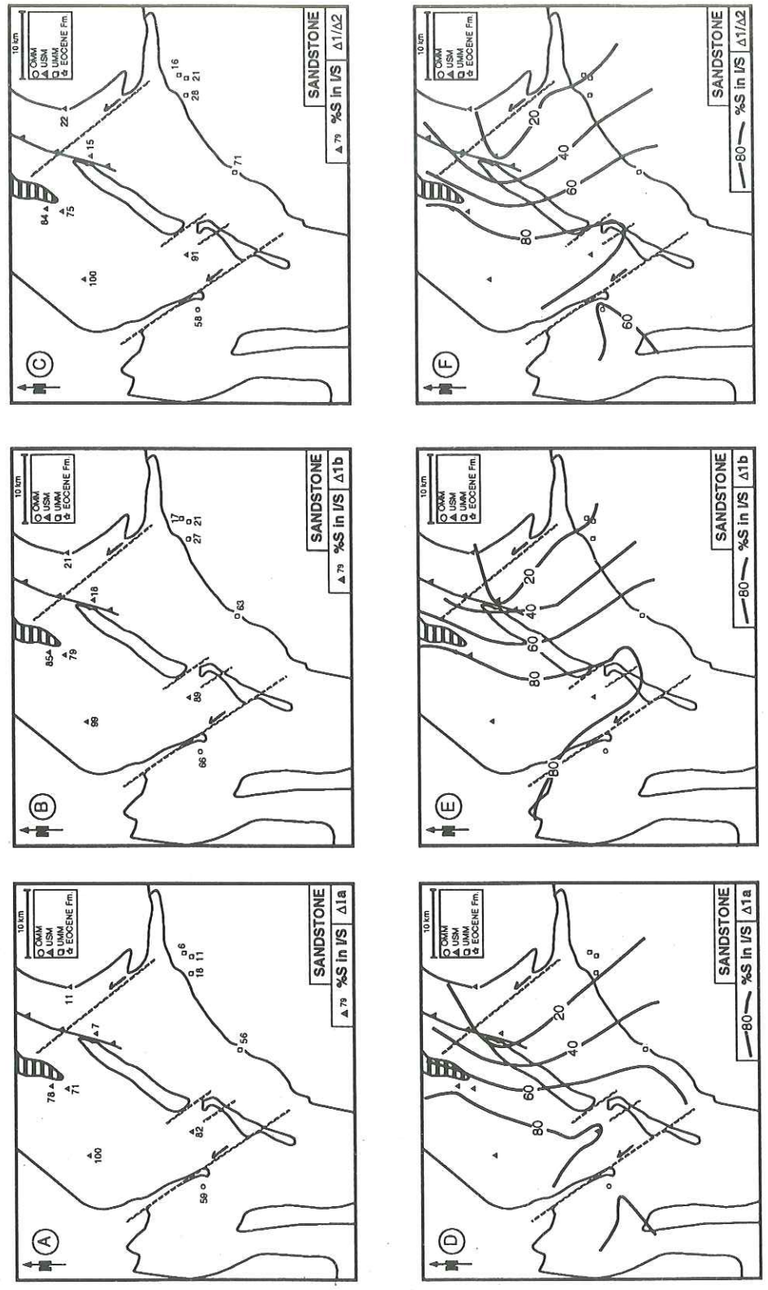

Fig. 5.15: Correlation between %Rr and %S in I/S.

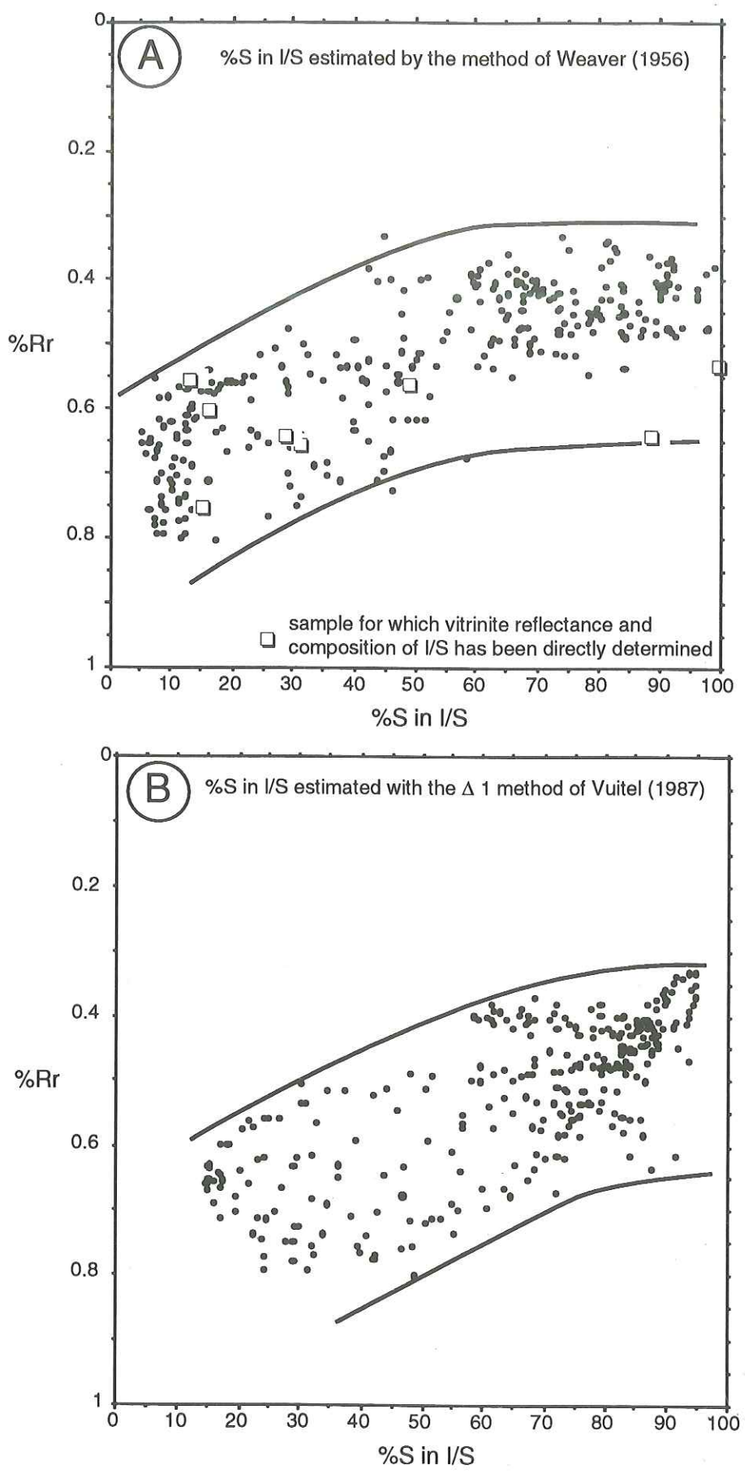

of Vuitel (1987). As expected, there is large scatter of data. Nevertheless it is interesting to note that the decrease of %S in I/S (down to smectite values <20%) seems to occur over a relatively short %Rr-interval (between ~0.3 and ~0.8 %Rr). Our plots are in line with observations from other Tertiary basins which indicate that at the beginning of diagenesis, a rapid decrease in smectite layers in I/S together with a slow increase in thermal maturity of organic matter (see for example Kübler 1984 or Francu et al. 1990).

5.6 Discussion of clay mineral diagenesis

Summary of main results:

i) Bulk-rock mineralogy is rather stable throughout the study area and is dominated by quartz, calcite, plagioclase, K-feldspar, dolomite and various phyllosilicates. Sandstone samples show much higher plagioclase and K-feldspar contents than shale samples. There is no major stratigraphic control on bulk-rock mineralogy.

ii) The fine fraction of shale samples comprises dominantly mica, chlorite, mixed-layer illite/smectite with variable amounts of kaolinite.

iii) The fine fraction of sandstone samples comprises dominantly mica, chlorite, mixed-layer illite/smectite with variable amounts of kaolinite, corrensite and serpentine.

iv) Main associated minerals in the fine fraction are quartz, K-feldspar and plagioclase.

v) There are no major geographical variations in the relative proportion of phyllosilicates in the fine fraction of shale samples. Mineral assemblages seems to be rather uniform.

vi) The most striking feature of the clay mineralogy of sandstone samples is the occurrence of corrensite.

vii) Absolute intensities of K-feldspar in the fine fraction of sandstone and shale samples seems to be reduced in the eastern part of the study area (Subalpine Chains).

viii) There is a marked (~W-E) decrease in the percentage of smectite layers from the Plateau Molasse towards the Subalpine Chains.

ix) The decrease of %S in I/S (down to smectite values <20%) seems to occur over a relatively short %Rr-interval (between ~0.3 and ~0.8 %Rr).

The most prominent changes in the clay mineralogy of sedimentary rocks upon burial diagenesis are the progressive disappearance of smectite and kaolinite, and the emergence of illite and chlorite as the major phyllosilicates at the onset of anchimetamorphism (Burst 1959, Weaver 1959, Kisch 1987).

The results from this study show no evidence for the neoformation of illite and chlorite. This is probably due to the presence of large amounts of detrital phyllosilicates which tends to mask any diagenetic evolution. Arguments for a detrital origin of most phyllosilicates are the following:

- The Molasse deposits consist of a succession of rather immature clastic sediments derived from the erosion of the Alpine orogenic belt. The sediments originate from sedimentary and crystalline rocks. Weathering of these rocks has probably given way to the production of most common clay minerals.

- The relative contents of illite, chlorite and I/S are generally rather constant throughout the study area. There are no geographic trends which could be related to a diagenetic phenomena. The occurrence of abundant chlorite and illite in thermally immature sediments in the western part of the study area shows that the clay mineral distribution is largely controlled by the detrital input from the Alps.

- Illite cristallinity data (chapter 5.2.1.1) in both studied size fractions (<2µm and 2-16µm) indicate anchimetamorphic conditions and suggest a detrital origin of the micas.

- There are no major differences in the chemical composition of micas and chlorites in both size fractions (Fig. 5.3 and 5.4).

- In the Haute-Savoie and Geneva Basin, kaolinite has been observed in all stratigraphic units, but it is most abundant in samples from the UMM. There are also indications for the presence of kaolinite in samples from the USM and OSM of Eastern Switzerland (annex 4). Different explanations for the presence of kaolinite may be mentioned:

i) Kaolinite mainly forms in surficial environments through pedogenetic processes (Chamley 1989). Though kaolinite is considered to be characteristic of the humid tropics, it forms readily in the humid temperate regions (Weaver 1989).

ii) Kaolinites could be of detrital origin.

iii) Kaolinite may also develop during early diagenesis due to the circulation of acid solutions (Dunoyer de Segonzac 1969). Indications for neoformation of kaolinite in the Molasse Basin were reported by Füchtbauer (1964) and Monnier (1979). Füchtbauer (1964) observed authigenic kaolinite cements in sandstones of the Bausteinschichten in Bavaria.

None of these possibilities can be completely excluded. Further detailed diagenesis studies may help to resolve this problem.

Chamley (1989) stated that clay minerals such as illite, chlorite or kaolinite are not very sensitive to slight or moderate depths of burial. Clay diagenetic modifications affecting sediments buried less than 2 km are, therefore, usually much less important than the modification induced by changes in tectonic activity, climate, paleocirculation or detrital sources. The generally small mineralogical changes within the fine fraction of the samples from the Molasse Basin can be interpreted in terms of the level of diagenesis. Vitrinite reflectance data (chapter 3) indicate a generally low level of thermal maturity. Given additionally the low level of precision in the estimation of the proportion of phyllosilicates, it is not surprising to find rather stable clay mineral assemblages which reflect still the depositional mineralogy. These observations do not suggest that there is no transition of smectites or smectite-rich I/S to chlorites or illites, especially in the Subalpine Chains. However neoformation of chlorites or illites in slightly buried sediments appears to account for only a very small part of the total clay, which is generally not recognisable by most chemical and mineralogical techniques (Chamley 1989).

There is, however, evidence from clay mineral studies in the Subalpine Chains that the transition of smectite to chlorites (limestones) or to illites (clayey sediments) accounts for geographical variations of clay mineral assemblages in Mesozoic formations (Deconinck & Debrabant 1985, Deconinck & Charollais 1986, Chaplet 1992, Moss 1992a). Deconinck & Debrabant (1985) stated that clay mineral assemblages of Upper Cretaceous limestones in the Bauges (south-west part of the Subalpine Chains) have a detrital origin and are rich in smectite, whereas in the Bornes the assemblages are dominated by diagenetic chlorite and illite. Moss (1992a) came to similar results in a study of Early Cretaceous mudrocks. He concluded that the north-eastern part of the Subalpine Chains, where samples are composed solely of illite and chlorite, has experienced greater burial temperature than the south-western part.

The most important diagenetic process in shale and sandstone samples of the Haute-Savoie and Geneva Basin is the progressive decrease of the percentage of smectite layers in mixed-layers illite/smectite (I/S). I/S compositions in sandstones and shales show a ~W-E decrease in smectite layers. These results are in line with previous clay mineral studies from the Subalpine Chains (Deconinck & Debrabant 1985, Deconinck & Charollais 1986, Chaplet 1992, Moss 1992a). This diagenetic trend is also in accordance with vitrinite reflectance data from Tertiary (chapter 3) and Mesozoic (Moss 1992b) sediments demonstrating both across and along strike variations within the Molasse Basin and the French Subalpine Chains.

It is generally agreed that in mud-shales, but not necessarily in sandstones, diagenetic I/S and illite formed from a smectite precursor (Weaver 1989). In addition to forming from volcanic glass, smectite seems to precipitate directly in pore spaces of sandstone and apparently forms in weathering environments (alteration of feldspar, micas, FeMg silicates) characterised by very slow movement of water either in swampy lowlands or in arid to semiarid regions (Berner 1971). Given the high

amounts of feldspars in clastic Molasse sediments, smectite in continental deposits of the Molasse Basin may have a pedogenetic origin. Generally, smectite is believed to be of detritic origin (see also discussion above).

The reconstruction of paleotemperatures based on I/S composition is rather delicate. As discussed in chapter 2.3.1.2, the smectite to illite reaction depends on various factors.

An important factor is the availability of K for illitisation of smectite. It is generally assumed that the K and Al needed for the reaction derive from coarser, non-sheet silicate constituents, such as K-feldspar or mica (e.g. Hower et al. 1976). The result from this study indicate that K-feldspars and micas are ubiquitous. Potassium should, therefore, not be a limiting factor for the illitisation reaction in the study area. K-feldspar distribution in the fine fraction of shale and sandstone samples shows a marked decrease in regions of high diagenetic level. This observation could indicate a progressive dissolution of K-feldspar and a transfer of K to the fine fraction due to progressive illitisation of smectite.

Weaver (1989) compiled temperature data for the conversion of smectite to I/S in the Gulf Coast region. He reported that the first occurrence of authigenic illite layers range from 55°C to 100°C and the top of the 4:1 zone (20%S in I/S) ranges from about 100°C to 160°C. Srodon & Eberl (1984) compiled data from the North Sea, the Gulf Coast and the Douala basin (their curve for Central Poland is not reliable, oral communication of Srodon in Weaver 1989). Their graph (their fig. 21) indicates the following temperature ranges for a fixed I/S composition: 80%S in I/S->50-80°C, 60%S in I/S->60-90°C, 40%S in I/S->80-110°C and 20%S in I/S->120-200°C. Actually, considering the amount of variation due to different measuring methods and different geochemical conditions during burial, temperature data of these different basins cluster fairly well. Let us apply these paleotemperature estimations to the study area, with an assumed paleogeothermal gradient of 25°/km (Rybach 1984) and a mean annual surface temperature of 15°C (Hochuli 1978). The following approximated burial depths may then be calculated:

80%S in I/S: 1.5-2.5km
60%S in I/S: 2-3km
40%S in I/S: 2.5-4km
20%S in I/S: 4-7.5km

Implications of these results will be discussed further in chapter 8.

An important feature of the clay mineral diagenesis in sandstone samples is the appearance of corrensite. Corrensite and mixed-layer chlorite/smectite may be formed authigenically in sandstones (Weaver 1989), but may also be explained as an intermediate stage of transformation from smectite into chlorite (Kisch 1987). The occurrence of corrensite in the western part of the Molasse Basin has already been described by Monnier (1979, 1982). He stated that, in the Swiss Molasse Basin, the transformation of smectite to a 2:1 mixed-layer silicate occurs simultaneously with the transformation of smectite to a regular interstratified smectite/chlorite. In well Sorens 1 (Western Switzerland) clearly recognisable corrensite occurs at a depth of about 2900m and in well Savigny 1 at a depth of 1900m (Monnier 1979). The main requirements for the formation of corrensite seems to be temperature and the availability of abundant Mg. A likely Mg source in these sandstone samples may be serpentine which is always associated with the appearance of corrensite. According to Kübler (1973), corrensite appears under normal diagenetic conditions at temperatures of about 90 to 100°C. This temperature estimation agrees rather well with that from I/S, at least for the corrensite occurrence at the eastern end of the Salève mountain. The occurrence of corrensite in a sandstone sample at the western end of the Salève is in contradiction to I/S data indicating a low level of diagenesis (80%S in I/S) in this area.

According to the general schemes of Kübler et al. (1979), corrensite appears in diagenesis zone 2 at an equivalent coal rank of 0.5-0.6% Rr. The corrensite occurrences in the Haute-Savoie are in line with vitrinite reflectance data (see chapter 3.3.2.1). Vitrinite reflectance values are around 0.5% Rr at the western end of the Salève Mountain and between 0.5-0.6% Rr at the eastern end.

5.7 Conclusions

The two major features of clay mineral diagenesis in Tertiary formations of the Haute-Savoie and Geneva Basin are the following:

i) The distribution of the percentage of smectite layers in mixed-layer illite/smectite in shales and sandstones reveals a progressive illitisation in a more or less W to E direction. This diagenetic trend confirms coalification patterns.

ii) The appearance of corrensite in feldspathic, serpentine-bearing sandstones indicates minimal temperatures of about 90 to 100°C for the frontal part of the Bornes Plateau.

Chapter 6: FLUID INCLUSIONS

Data presented in this section come from one sample site, therefore results should be considered as preliminary.

Fluid inclusions from a calcite vein of the "Monnetier"-fault at the north-eastern end of the Salève mountain were used to evaluate fluid trapping conditions in a region of increased vitrinite reflectance. Samples have been taken from an outcrop situated along the road Mornex-Monnetier (coordinates: 506000/112550, altitude: 620m). The Salève is a thrusted anticline consisting of Jurassic and Cretaceous sediments (Guellec et al. 1990) which has been sheared off during the final phase of the Alpine orogeny (Jura folding, late Miocene and Pliocene). The sampled calcite veins are located in Early Cretaceous Urgonian limestones, which underlie Oligocene Molasse sediments in the Haute-Savoie. These veins are part of a NW-SE running "Arve" strike-slip fault system. This strike-slip fault was mainly active during and after the final phase of alpine orogeny. Therefore, evaluated trapping conditions reflect post-Molasse-depositional temperatures.

Fluid inclusions yield bulk homogenisation temperatures between 62.6°C and 73.8°C (mean average = 69°C). Last melting of ice occurs at -0.2°C and -0.3°C, thus indicating low salinities of about 1 weight% NaCl equivalent for the trapped fluid.

When assuming the type of pressure conditions (lithostatic or hydrostatic) and the maximum thickness of overlaying sediments at the time of trapping, one can estimate the pressure on the fluid at the time of entrapment. If the composition and density of the fluid is known, this pressure value allows to correct measured homogenisation temperature and obtain the true temperature of entrapment (Potter 1977).

Because it was not possible to define whether fluid inclusions have been trapped under lithostatic or hydrostatic pressure conditions, both possibilities have been included in the calculations. Estimations of overburden thickness are associated with major uncertainties. In Eastern Switzerland, where the Molasse sequence is more or less entirely preserved, maximum thicknesses of the formations overlaying the USM reach up to 2km. This is in good agreement with estimated overburden in the western Molasse Basin (Lemcke 1974). Results from clay mineral diagenesis (chapter 5.6) indicate, however, an overburden thickness of at least 3-4km at the eastern end of the Salève. The following schema shows estimated trapping temperature and resulting paleogeothermal gradients for the time of entrapment using different assumptions concerning pressure conditions and overburden thicknesses:

Measured homogenisation temperature Th=69°C		*P* (MPa)	*ΔT* (°C)	*Tmax* (°C)	*dT/dz* (°C/km)
lithostatic pressure conditions					
average rock density 2.7g/cm3					
overburden thickness	1km	27	32	101	86
	2km	53	52	121	53
	3km	80	73	142	42
	4km	106	93	162	37
hydrostatic pressure conditions					
fluid density 1g/cm3					
overburden thickness	1km	10	18	87	72
	2km	20	26	95	40
	3km	30	34	103	29
	4km	40	42	111	24

P = pressure on the fluid at the time of entrapment
ΔT = temperature correction for fluid inclusion homogenisation temperature (Th) based on volumetric properties of the system NaCl-H2O (Potter 1977), corrections for a 1wt % NaCl equivalent solution.
Tmax = maximum trapping temperature
dT/dz = calculated paleogeothermal gradient at the time of entrapment assuming a mean annual surface temperature of 15°C

Temperature estimates from fluid inclusion data seem to be consistent with those from clay mineral analysis which indicate temperature of at least 90°C in the eastern part of the study area. The paleogeothermal gradients are, however, higher than expected for the Molasse basin (Teichmüller & Teichmüller 1986), except in the case of hydrostatic pressure condition with high overburden thicknesses. Such high gradients could be related to variations in the geothermal field. A plausible hypothesis for an increased heat flow is that warm, probably dilute, fluids were channelled along tectonic lineaments during the late evolution of the Molasse basin. Finally, it must be noted that our fluid inclusion data agree well with previous studies by Mullis (1987b) suggesting the migration along tectonic structures of low-salinity fluids, possibly of meteoric origin, to great depths into sedimentary rocks during the Tertiary in Northern Switzerland.

Chapter 7: THERMAL MODELLING

Part of the results presented in this chapter has already been published (Schegg 1992a, Schegg 1992b, Todorov et al. 1993).

7.1 Modelling tools

One of the aims of numerical modelling of sedimentary basins is to try to determine an accurate temperature history by integrating factors which control temperatures and by enabling a calibration with thermal indicators.

Sophisticated basin models consist generally of three parts:

1) a geohistory model which reconstructs the burial history, basement subsidence, vertical fluid flow and the changes of pressure, porosity, permeability and fluid flow rate with time and depth;

2) a thermal history model which, based on the burial history and a geochemical model of kerogen maturation, reconstructs heat flow history, paleotemperatures and thermal maturity of organic matter;

3) a hydrocarbon generation model including time and depth of peak generation of oil and gas (Wei et al. 1990).

Numerous recent publications dealing with sedimentary basins in very different tectonic or geodynamic settings have confirmed the possibility of reconstructing the paleogeothermal history using the techniques exposed above (see references in Buntebarth & Stegena 1986, Tissot et al. 1987, Welte & Yalçin 1988, McCulloh & Naeser 1989, Wei et al. 1990, Waples et al. 1992a, 1992b, and others).

A model is only as good as its calibration. Calibration, i.e. obtaining an optimum fit between measured and modelled parameters, is the key to effective modelling. While vitrinite reflectance values are the basis for most paleogeothermal calibrations, a large number of parameters can be used as calibrants (e.g. measured porosity, sedimentation rates, pressure gradients, Rock-Eval Tmax,...).

Theoretical aspects of OM maturation, and especially the evolution of vitrinite reflectance as a function of temperature and time, have been discussed in chapter 2.2.1. The EASY%Ro-model of Sweeney and Burnham (1990) was used in this study. This model uses an Arrhenius first-order parallel reaction approach with a distribution of activation energy. It enables the calculation of the vitrinite maturation history (%Rr versus time) for a given temperature history (temperature versus time) and applies to values of mean random vitrinite reflectance from 0.3 to 4.5% Rr.

The keystone in thermal modelling is the construction of burial curves, for which uncertainties on the amount and timing of erosion are a major problem. This is especially crucial when only calibration data from outcrop samples are available. In such cases modelling has to be performed entirely with assumptions on missing sections.

The techniques of subsidence analysis have been described by Sleep (1971), Watts & Ryan (1976), Steckler & Watts (1978) and Van Hinte (1978). The subsidence history of the Jura, Swiss Plateau and Helvetic paleogeographic domains have been discussed by Lemcke (1974), Funk (1985), Naef et al. (1985), Wildi et al. (1989), and Loup (1992a, 1992b). Subsidence curves in this study have been constructed with BACKSTRIP89 (developed at the *Département de Géologie et Paléontologie* in Geneva, for a description see Loup 1992a). This basin analysis program takes into account parameters such as sediments thickness (present day thickness, compaction, erosion and deformation), age of sediments, depositional depth and eustatic sea-level variations. For thermal modelling, however, only simple burial diagrams (without eustatic and bathymetric corrections) have been used.

7.2 Modelling strategy

An iteration process is used to reconstruct the thermal history. The combination of the structural history (burial vs. time) and of a first simplified thermal history (geothermal gradient vs. time) results into a temperature history. By mathematical modelling (e.g. EASY%Ro-model of Sweeney & Burnham 1990), the evolution of kerogen and related maturity indices can be obtained. The comparison of forward modelled and measured maturity indices allows to adjust progressively the parameters which determine the thermal history.
There is growing evidence that the paleogeothermal regime of sedimentary basins is influenced by the paleogeohydrological conditions (Beck et al. 1989; Oliver 1986, see also chapter 1.1.2). The thermal regime of a sedimentary basin may be influenced by factors such as the hydraulic conductivity, density and viscosity of water, basin geometry, topography, water-table configuration, thermal conductivity, geothermal heat flow, and climate (Garven & Freeze 1984). Many of these parameters change in time and space and obviously heat flow values and/or geothermal gradients will be directly affected by these variations.
Two different approaches are chosen in this study. 1) The "burial history approach" assumes that the temperature history of a formation mainly depends on the burial depth. The thermal conditions are governed by constant geothermal gradients and heat flow values. There is an increase in temperature during burial and a decrease during erosion. 2) The "geohydrological approach" is based on a modified burial history. This approach assumes varying geothermal gradients (both in time and depth) due to changing paleogeohydrological conditions. Rapid changes in temperature for short periods could be expected with an influx of hot (or cold) water.

7.3 "Burial history approach"

7.3.1 Northern Switzerland

A detailed discussion of the methods and results in this region has already been given in Todorov et al. (1993). Therefore, only a shortened version will be presented hereafter.

7.3.1.1 Constraints for thermal modelling

The approach for modelling the thermal maturation of Mesozoic and Cenozoic rocks in the study area is similar to that described by Todorov et al. (1992):

i) Construction of burial history diagrams

The Mesozoic and Tertiary burial histories of 8 sites (see table D1 and Fig. 7.1 for location) in Northern Switzerland have been constructed based on information from outcrop or borehole data. A major problem for the construction of burial curves in Northern Switzerland is the sedimentary gap between Upper Jurassic and Tertiary sediments. Cretaceous strata have probably never been very thick in this area (Trümpy 1980, Lemcke 1988, Wildi et al. 1989, Bachmann & Müller 1991 and discussion in chapter 1.3.5). A thickness of 100m of Early Cretaceous deposits was assumed. There are also large uncertainties about the amount of erosion in late Neogene times (see Laubscher 1974, Lemcke 1974, Naef et al. 1985, Brink et al 1992, Kälin et al. 1992, Schegg 1992b). Our Neogene burial histories are mainly based on observed and regionally extrapolated sediment thicknesses in the distal part of the Molasse Basin (Liniger 1925, Suter 1978, Müller et al. 1984, Naef et al. 1985, Matter et al. 1987, 1988a, 1988b, Nagra 1988, Keller et al. 1990, Diebold et al. 1991).

ii) Construction of a time-temperature history

The burial diagrams combined with an initial set of paleogeothermal gradients and mean annual surface temperatures enables the calculation of a time-temperature history for each formation. Generally, several thermal histories may result in the same maturation profile. Therefore it is essential to begin with an evaluation of the tectonic history (see also chapter 1.3.5) of the study area in order to guess its thermal implications. A "normal" paleogeothermal gradient of 30°C/km was assumed for the Triassic, Jurassic and Lower Cretaceous. Volcanic activity preceding the Eocene rifting process of the Rhine Graben demonstrates that mantle upwelling evolved since mid-Cretaceous times (Illies 1977).

A gradient of 50°C/km was assumed for this pre-rifting period. Major tectonic events in the study area (Rhine Graben rifting and Jura folding) took place between Late Eocene and late Middle Miocene (Laubscher 1982). The thermal history of the Rhine Graben is characterised by a major phase of geothermal flux in the Eocene, preceding the main rifting process which started in Middle Miocene times (Teichmüller & Teichmüller 1979). A high paleogeothermal regime in the southern part of the Rhine Graben realm during Neogene times is indicated by increased volcanic activity (Kaiserstuhl, Hegau). For thermal modelling, paleogeothermal gradients higher than those in the pre-rifting period have been assumed in the study area between Late Eocene and Late Miocene. Gradients at the end of the Cenozoic are supposed to be close to the present ones.

The mean annual temperature at the sediment/air or at the sediment/water interface was estimated at 15°C during the Mesozoic and Tertiary. Palynological investigations (Hochuli 1978) suggest, for example, temperatures of 15-18°C for the North Alpine Foreland during the Oligocene. Present day values are set at 10°C.

iii) Simulation of the vitrinite reflectance evolution

The time-temperature histories of different formations of a stratigraphic section are then introduced into the EASY%Ro model of Sweeney & Burnham (1990) in order to calculate its maturation profile.

iv) Calibration of modelling results

Comparison between modelled and measured vitrinite reflectance enables the optimisation of the paleogeothermal model: the thermal constraints (in our case the geothermal gradient during the Tertiary) are changed until there is a best fit between modelled and measured values.

This approach will not result in a unique solution, because several thermal histories may lead to the same maturation profile. Moreover, admitting uncertainties of the input parameters, it is obvious that our calculations cannot be more than a first approximation, which has to be calibrated with other methods.

Fig. 7.1: Tectonic map of Northern Switzerland with location of modelling sites and calculated paleogeothermal gradients during Late Paleogene and Early Neogene.

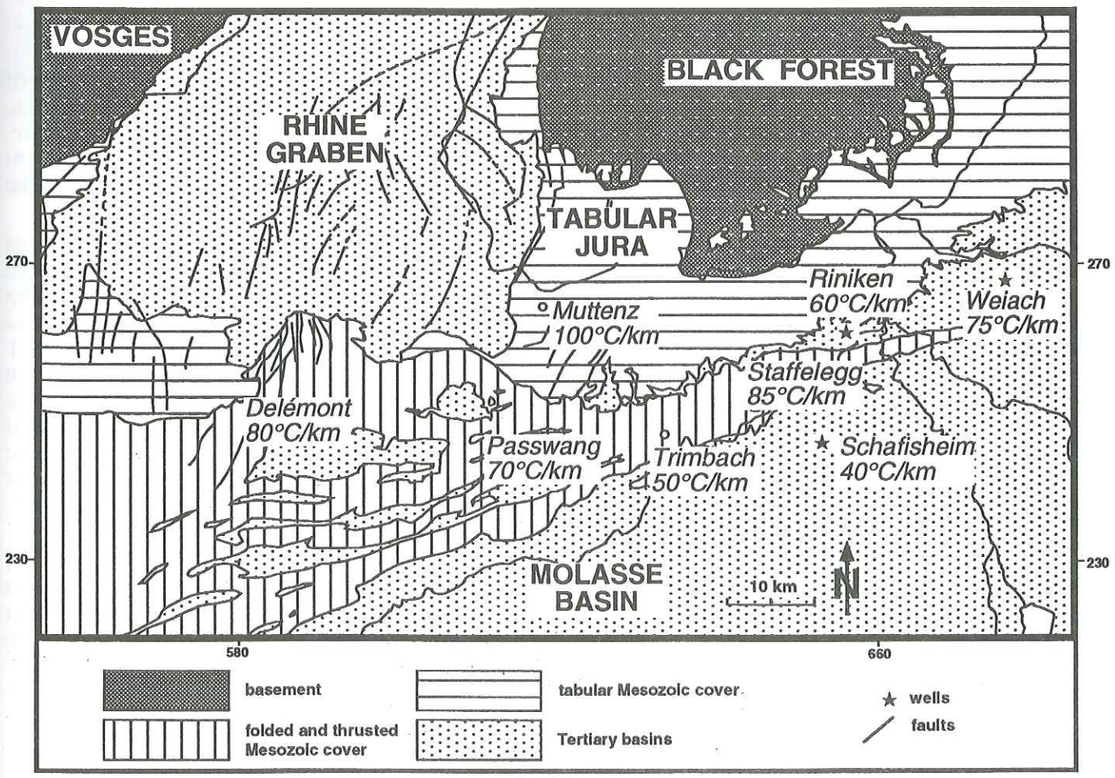

7.3.1.2 Results

The thermal histories of 8 sections comprising Cenozoic and Mesozoic sediments have been modelled (see results summarised in table D1 and figure 7.1). The vitrinite reflectance evolution of five formations for the section Muttenz and the correlation between measured and calculated values are shown in figure 7.2. Maturation histories for the oldest formations of the 8 studied profiles are represented in figure 7.3.

As burial diagrams indicate, maximum palaeodepth were attained during the Late Miocene (Fig. 7.3). For the oldest modelled formations of each profile, these depths range between 860m (Staffelegg, Insektenmergel) and 1990m (Schafisheim, Orbicularis Mergel).

The calculated maximum palaeotemperatures for the different formations are as follows: Middle Triassic formations (77-127°C), Upper Triassic formations (88-119°C), Lower Jurassic formations (65-106°C), Middle Jurassic formations (53-104°C), Upper Jurassic formations (72°C) and Tertiary formations (26-70°C). With the exception of the Schafisheim (40°C/km) and Trimbach (50°C/km) sections, the corresponding paleogeothermal gradients during Late Eocene to late Middle Miocene are very high (60-100°C/km).

Sections (Fig. 7.1) which are near the Rhine Graben (Muttenz, Delémont and Passwang) or which are oriented along the axes of the Permo-Carboniferous trough (Staffelegg, Riniken and Weiach) display high paleogeothermal gradients during Late Eocene to late Middle Miocene (60-100°C/km), whereas sections, situated closer to the Molasse basin (s.s.), show lower gradients (Trimbach and Schafisheim, 50 and 40°C/km respectively).

Our results indicate that, due to a high paleogeothermal regime and an important burial depth, maturation of Mesozoic and Cenozoic sediments was completed only by the end of late Middle Miocene (Fig. 7.2 and 7.3). According to our model the diagenesis level of the rocks rapidly increased during Late Oligocene to Late Miocene times. This hypothesis is also supported by the fact that the thermal maturity of Mesozoic sediments does not increase, even when modelling with a Mesozoic paleogeothermal gradient which is much higher than the assumed value of 30°C/km.

7.3.2 Molasse Basin (s.l.)

As it was practically impossible to construct maturation profiles covering the whole stratigraphy of the Molasse Basin, an different approach from that used in Northern Switzerland has been chosen. Calibration data come only from outcrop samples. Burial history curves of these sample sites are, therefore, based entirely on assumptions of maximum overburden thicknesses and subsequent erosion. There are major uncertainties about the erosion estimates in the Molasse Basin (Lemcke 1974, Laubscher 1974, Monnier 1982, Kälin et al. 1992).

Therefore, the approach chosen for thermal modelling uses hypothetical subsidence curves simulating the burial and erosion history of the eroded section. Subsidence history curves from forelands are typified by i) the sudden onset of rapid and often considerable subsidence coinciding with foredeep formation, ii) a segmented profile, reflecting discontinuous loading and iii) high rates of flexural uplift ('re-bound') with the removal of the original load (Allen & Homewood 1986). Tertiary subsidence curves of the North Alpine Foreland Basin in Switzerland and France have been published by Lemcke (1974), Naef et al. (1985), Homewood et al. (1986) and Moss (1992b). The burial/uplift curves are generally presented as V-shaped. Moss (1992b) stated that given the length of time between onset of foredeep sedimentation and uplift, the slowness of Alpine convergence and the inertia of heating and cooling rocks, broader burial curves are more realistic. According to this author it is possible that periods of residence time at maximum burial depth are likely to be in the region of 5-6 my.

Schematic time-temperature curves for two time horizons corresponding to the base of the USM (30 my) and the OMM (20 my) have been constructed, assuming that the temperature of a formation is mainly depending on the burial depth. Therefore, maximum burial temperatures are reached at maximum burial depths. In order to constrain the thermal history, the following assumptions are made:

Fig. 7.2: Thermal modelling of the Muttenz section: Rr values calculated by the EASY%Ro model for different formations are indicated during burial history [burial depth (m) versus age before present (my bp)]. For the present (0 my bp) the calculated and the measured values are shown. Vitrinite reflectance values in brackets should be treated with care as the standard deviations are too high (>0.1). Variations of the geothermal gradients (dT/dz) are shown in the heading of each burial history diagram. The diagram in the lower right corner shows the correlation of measured and calculated Rr values. Modified after Todorov et al. (1993).

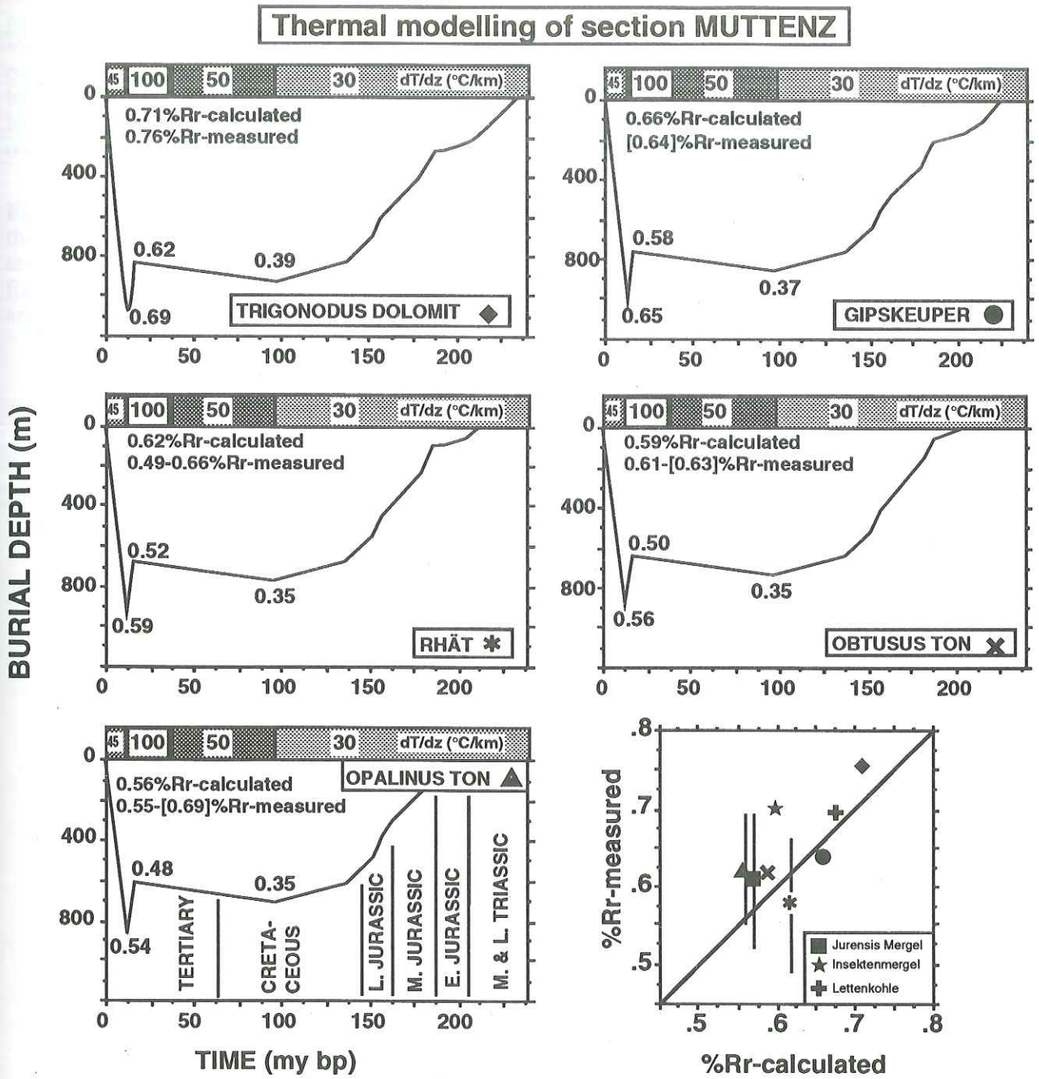

- The mean annual surface temperature is estimated at 20°C during the Oligocene and Miocene. This is a conservative value because palynological investigations (Hochuli 1978) suggest temperatures of 15-18°C during the Oligocene. Present day values are at 10°C.

- Maximum paleodepths were reached towards the end of the Middle Miocene (12my). This period is marked by the end of Molasse sedimentation and the start of uplift and erosion (Lemcke 1974, Naef et al. 1985, Mugnier & Menard 1986, Pfiffner 1986). The start of the uplift history is set at 12 my, although thrusting and uplift in more internal parts of the basin (Subalpine Molasse) probably took place earlier (Burkhard & Kalkreuth 1989).

Fig. 7.3: Thermal modelling of the oldest sampled sedimentary formation in 8 stratigraphic sections (see Fig. 7.2 for explanation of the diagram). Measured Rr values marked with a star are from Wolf & Hagemann (1987); vitrinite reflectance values marked by (f) are based on spectral fluorescence measurements. Vitrinite reflectance values in brackets should be treated with care as the standard deviations are too high (>0.1). Modified after Todorov et al. (1993).

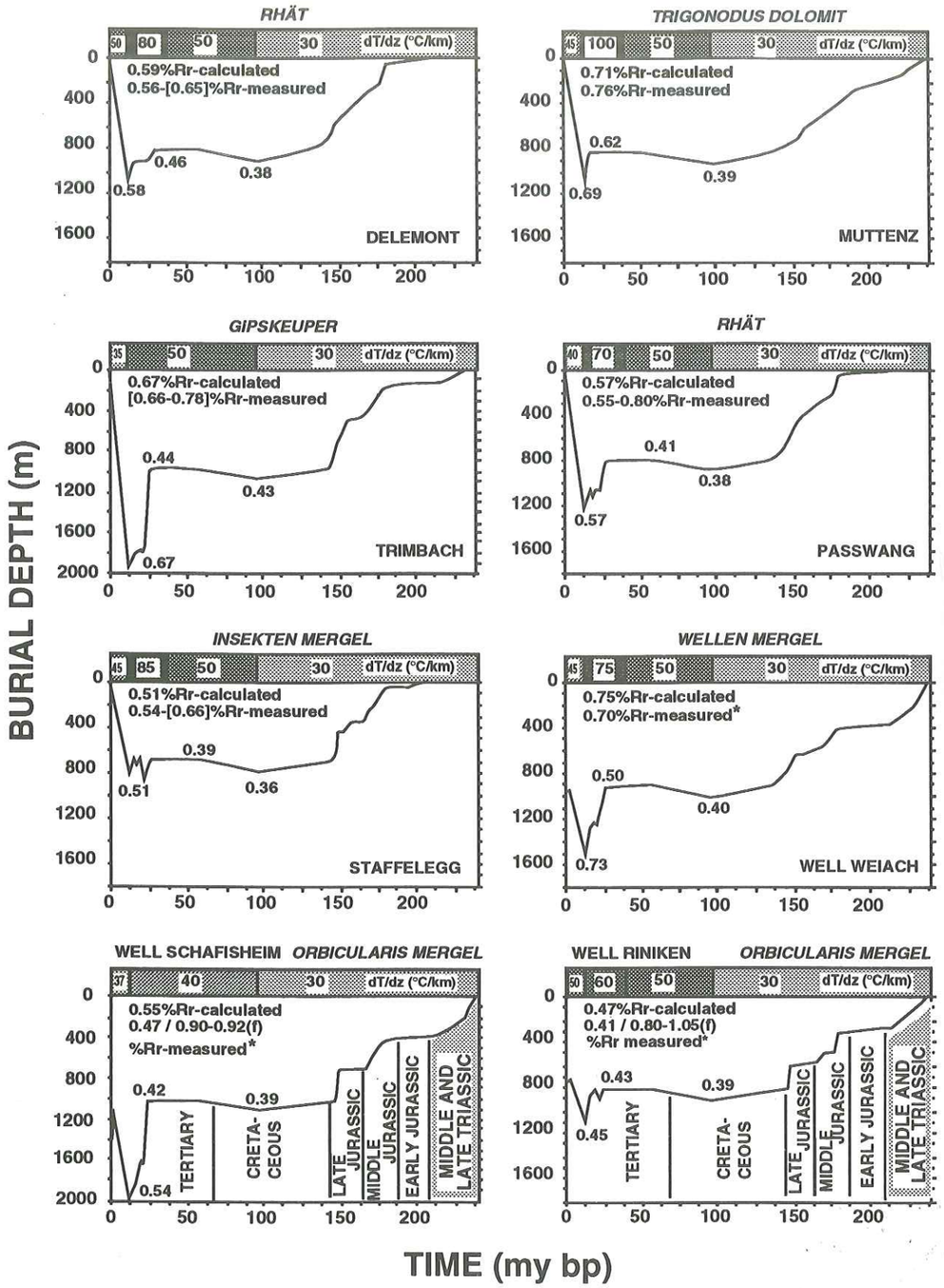

Two types of temperature histories with maximum paleotemperature, varying from 40°C to 160°C, are used to model final (present day) maturation values for each time horizon: i) V-shaped curves (Fig. 7.4) and ii) modified V-shaped curve characterised by a broader base (Fig. 7.5).

Figure 7.4 shows a diagram of calculated vitrinite reflectance values (%Rr) versus maximum paleotemperature (Tmax). The plot clearly indicates that time "plays" only a minor role. Measured vitrinite reflectance values of outcrop samples in the Plateau Molasse range from 0.2 to 0.6% Rr. Thermal modelling shows that paleotemperatures of 40, 70, 90 and 110°C for measured vitrinite reflectance values of 0.3, 0.4, 0.5 and 0.6% Rr respectively are required. With an assumed average paleogeothermal gradient of 25°C/km paleodepths of up to 4 km would be required to explain these vitrinite reflectance values from surface samples. This is much more than expected from the overlaying stratigraphic column, almost entirely preserved in the eastern part of the Swiss Molasse basin. The thickness of sediments, overlying analysed outcrop samples (e.g. OMM and OSM), may have extended to 2 km in the most proximal part of the basin. In the distal parts, however, this overburden thickness decreases to some hundred meters (Matter et al. 1980).

Fig. 7.4: Thermal modelling with the EASY%Ro model of Sweeney & Burnham (1990) enables the calculation of mean vitrinite reflectance values (Rr) for a given stratigraphic level if the time-temperature history is known. The final Rr-values of two different time horizons (20my and 30my) for changing (maximum temperature Tmax varying from 40 to 150°C) V-shaped temperature histories are plotted on a Rr versus Tmax diagram. Modified after Schegg (1992b).

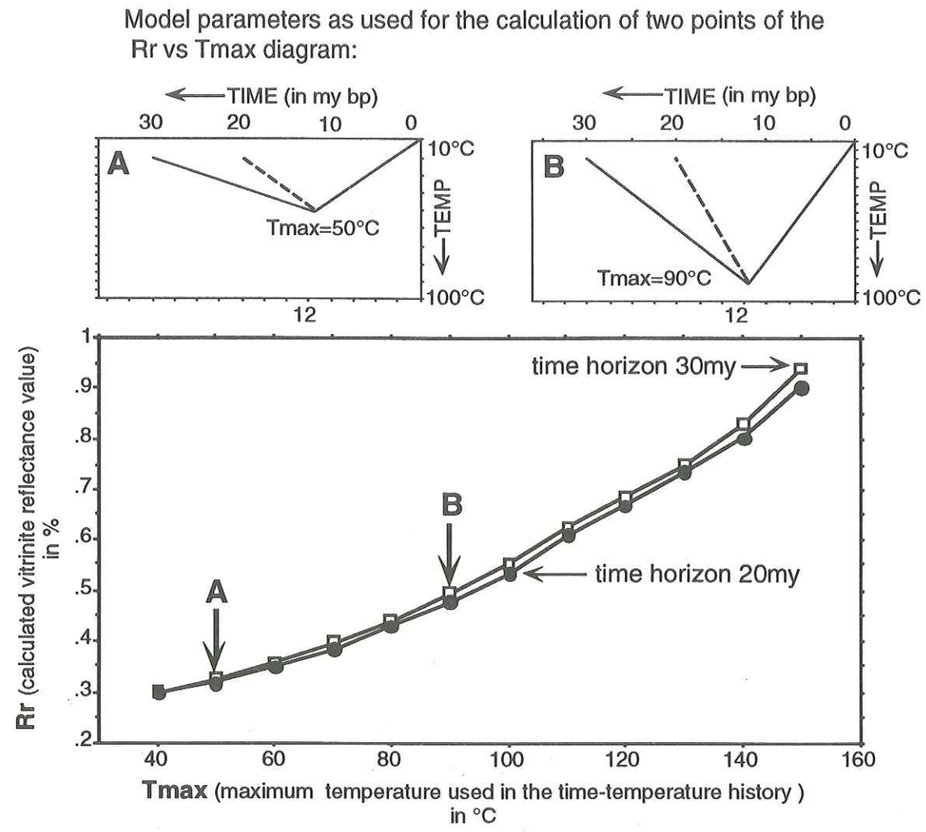

The zone of increased thermal maturity in the La Broye valley (chapter 3.3.2.2) shows vitrinite reflectance values of 0.52-0.58%. This is an increase of over 0.1% Rr when compared to the average values from the surrounding area. In terms of maximum paleotemperatures, an increase of about 30°C is suggested by these calculations.

Figure 7.5 shows a comparison between thermal modelling results of V-shaped and modified V-shaped temperature histories for the 30my time horizon. Differences between these models are generally small (only 5° C for a Rr-value of 0.5%). These results indicate also that attained maximum paleotemperature controls the maturity of the organic matter.

Fig. 7.5: Thermal modelling with the EASY%Ro model of Sweeney & Burnham (1990) enables the calculation of mean vitrinite reflectance values (Rr) for a given stratigraphic level if the time-temperature history is known. The final Rr-values of the 30my time horizon for two types of temperature histories (V-shaped and modified V-shaped) are plotted on a Rr versus Tmax (= maximum burial temperature) diagram.

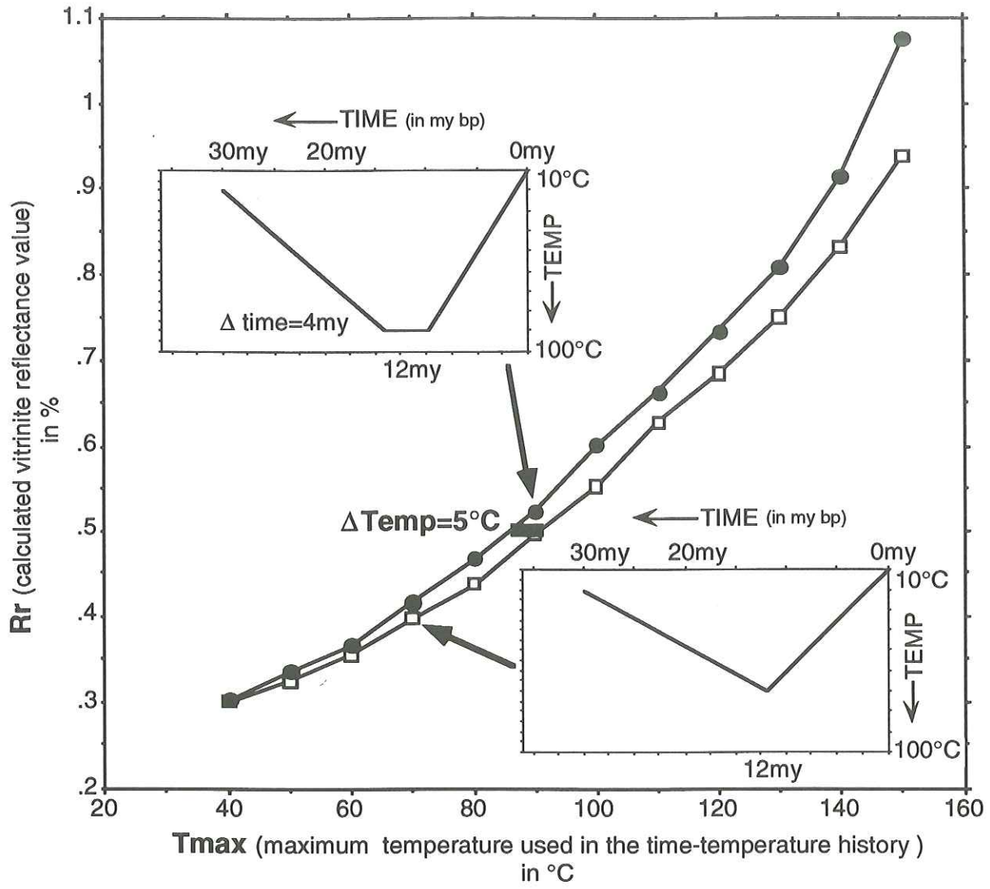

7.4 "Geohydrological approach"

This is a conceptual approach, which uses a speculative model. However, its aim is to show that the observed coalification pattern could be modelled without requiring much erosion in a generally low-temperature regime. The latter is typical for the Molasse Basin.

Since only outcrop samples are analysed in this study, modelling results for each surface point have to be calibrated with only one measured vitrinite reflectance value. Therefore, published vitrinite reflectance data from the Küsnacht drillhole are used (Rybach & Bodmer 1980) to calibrate the geohydrological approach. As in other wells of the Molasse basin (Teichmüller & Teichmüller 1986), there is a low coalification gradient (0.08% Rm/km) indicating a low paleogeothermal gradient.

For the construction of the burial history curves, the amount of eroded section has been set to a value of 1km. This is higher than estimates for this region (Laubscher 1974, Lemcke 1974, Naef et al. 1985), but lower than estimates of the burial history approach or of a recent study on rock density and compaction in the Swiss Molasse basin (Kälin et al. 1992). The latter study indicated values of about 4km.

The present day geothermal gradient pattern of the Swiss Molasse basin (Rybach et al. 1987; Vollmayr 1983) is characterised by a rapid increase of temperature near the surface (30-60°C/km, <500m). One plausible explanation for this high near-surface gradient is convective heat transport by groundwater (Rybach & Bodmer 1980). Although there are no indications so far, it is possible that the thermal gradient and depth of this zone may have changed in time and space. If this is the case, this may be the result of a change in the fluid flow pattern in the Molasse basin due to:

- variations of the topography.
- fluids tectonically expelled from the orogenic belt.
- climatic variations influencing the infiltration rate of recharge areas (Balderer 1990).
- a variation of the groundwater interface (surface separating low mineralised groundwater of Na-HCO_3-type above and strongly mineralised groundwater of Na-Cl-type below) observed within the deeper and central part of the Molasse basin (Balderer 1990).

Figure 7.6 presents the input parameters and resulting temperature as well as maturity values of a successful simulation. The main assumptions are a deepening of the base and an increase of the near surface gradient at the time of maximum burial. This variation (probably due to increased convective heat transport) could be caused in part by the high relief of the Alps during the Early and Middle Miocene (Pfiffner 1986). The combination of the burial history (Fig. 7.6 D) and the variation of the mentioned thermal parameters (Fig. 7.6 A-C) enables the calculation of the temperature history (Fig. 7.6 E) for certain time horizons. Using the EASY%Ro-model, these temperature histories can be "transformed" into maturity histories (Fig. 7.6 F). The comparison between the modelled and measured coalification profile of the Küsnacht drillhole (Fig. 7.6 G) indicates a "good fit".

7.6 Discussion of thermal modelling results

7.6.1 Northern Switzerland

The information resulting from the present investigations (vitrinite reflectance->chapter 3.3.2.5 and thermal modelling) in the south of the Rhine Graben and the Eastern Jura can be summarised as follows:

i) Vitrinite reflectance values of Tertiary samples display a large range of values (0.24-0.54%Rr). The degree of diagenesis varies geographically. Relatively high vitrinite reflectance values are observed in the southern prolongation of the eastern Rhine Graben border.

ii) The measured vitrinite reflectance of Mesozoic sediments varies between 0.40 and 0.80%Rr. Vitrinite reflectance values of Jurassic sediments increases slightly from south-west to north-east, whereas Triassic samples show no geographical variation.

iii) Measured and estimated coalification gradients are high (0.3-0.96%Rr/km).

iv) Thermal modelling results indicate that the final (present-day) maturation level of the Mesozoic and Tertiary sediments was completed during Late Oligocene to Late Miocene. The inferred paleogeothermal gradients during this period are high (40-100°C/km).

Thermal modelling has shown that very high paleogeothermal gradients during the Tertiary are necessary to explain the maturation level of Mesozoic and Tertiary sediments. There are, however, other indications for a Tertiary high geothermal regime in or near the study area:

Fig. 7.6: Thermal modelling in the Küsnacht well with the EASY%Ro model (Sweeney & Burnham 1990) and a conceptual model which takes into account hypothetical effects of convective heat transport ("geohydrological approach"). The variation of different input parameters (A-D) enables the calculation of time-temperature histories (E). Using the EASY%Ro model these temperature histories can be "transformed" into maturity histories (F). (G) shows the comparison between modelled and measured coalification profile.

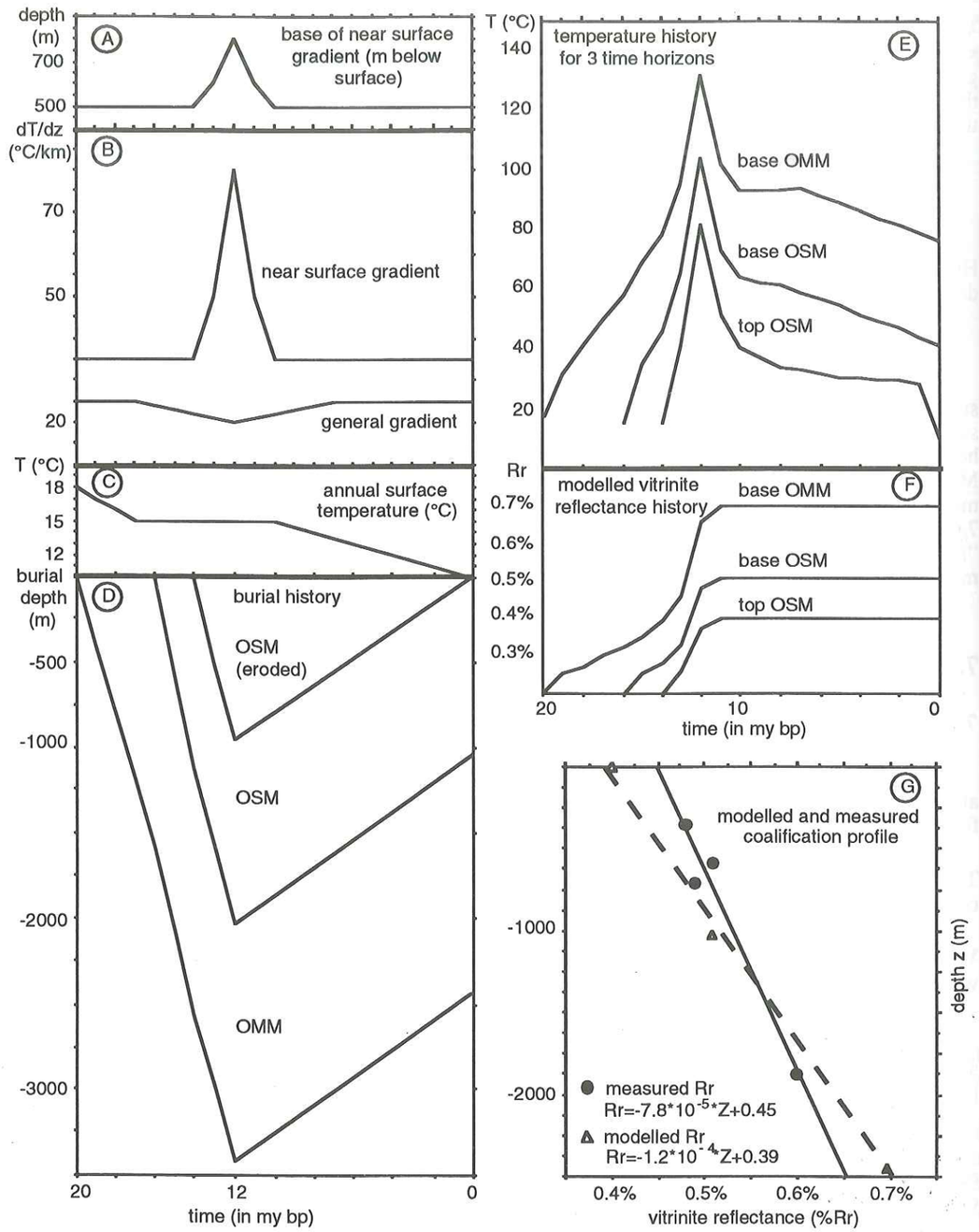

- Coalification gradients, similar to those observed in the study area, are reported from the Rhine Graben by Teichmüller (1979). According to this author, coalification gradients and present day geothermal gradients in deep wells of the Upper Rhine Graben are quite high, ranging between 0.29 to 1.14 %Rr/km and between 47.6 to 76.9°C/km respectively. Generally, it is assumed that the higher the coalification gradient, the higher the paleogeothermal gradient (Bustin et al. 1985). The observed coalification gradients in the Rhine Graben and in the study area are one order of magnitude higher than those of the Molasse basin, where the inferred Tertiary geothermal gradients vary between 20 and 30°C/km (Rybach 1984, Teichmüller & Teichmüller 1986). For these reasons paleogeothermal gradients in Northern Switzerland should be much higher than those of the Molasse basin. For the Rhine Graben, paleogeothermal gradients of up to 80°C/km during the main rifting phases were proposed (Buntebarth 1979, Teichmüller & Teichmüller 1979). These values are close to those obtained by thermal modelling in this study.

- A Tertiary high-temperature regime in Northern Switzerland is also indicated by a fluid inclusion study of Mullis (1987b).

The inferred Tertiary high temperature regime in the study area could be due to an increased heat flow associated with the Rhine Graben rifting and the "constructive interference" of the Rhine Graben with the Alpine forebulge during post-Early Miocene times (Laubscher 1992). The Upper Rhine Graben is characterised by high present-day heat flow densities, going up to values of 160 mW/m^2 (Cermák 1979). A mean value of 112±34 mW/m^2 was reported by Morgan (1982). Doebl et al. (1974) and Buntebarth (1979) found that the Rhine Graben was already an area of high heat flow during the peak volcanic activity and early rift genesis in the Lower Tertiary. Generally, it seems that regions with high surface heat flow values are characterised by a weakened (e.g. thinned) continental crust (Cermák 1979). Indeed, the present-day heat flow anomaly in the Rhine Graben corresponds well with the mantle bulge underneath the rift (Illies 1975). According to this author the crust -mantle boundary is located at a depth of only 24 km below the Kaiserstuhl area. But the anomalous heat flow is not limited to the Rhine Graben structure itself; increased geothermal activity may be traced far to the NNE into the Braunschweig-Altmark region (Bram 1979).

A prolongation of the Rhine Graben geothermal anomaly into the study area is supported by the survey of heat flow densities (Bodmer 1982, Bodmer & Rybach 1984) and geothermal gradients (Rybach et al. 1987). The relatively high regional heat flow values may be partly explained by the reduced crustal thickness in the study area ranging from about 27km in the northern part to about 33km in the southern part (Illies 1975, Deichmann 1990). But, as stated by Person & Garven (1992), the estimates of lithosphere thinning in the Rhine Graben (s.s.) are too small to account for the observed present-day thermal anomalies. An additional heat transport by convection along fault zones is, therefore, probable (Meier et al. 1979). There is growing evidence that the paleogeothermal regime of sedimentary basins depends often directly upon the palaeogeohydrological conditions (Oliver 1986, Beck et al. 1989, Person & Graven 1992, Schegg 1992a, 1992b). Geothermal anomalies are often caused by uprising deep groundwater or other fluids, including water from the basement along highly permeable zones (Hitchon 1984, Nesbitt 1990).

The geothermal regime in Northern Switzerland is characterised by a strong positive heat flow anomaly (>150mW/m^2) in the lower Aare valley which is associated directly with the southern margin of the Permo-Carboniferous trough underlying the main Jura overthrust (Griesser & Rybach 1989). These authors favour uprising deep groundwater as the mechanism creating the observed anomaly. Their results reveal the draining effect of the Permo-Carboniferous trough and indicate that vertical permeability is present in the vicinity of the trough even at depths of several kilometres. Previous diagenesis studies in the same region interpreted the presence of salt-poor fluids in the Triassic rocks as a result of enhanced groundwater activity already during the Tertiary (Mullis 1987b , Ramseyer 1987).

The thermal maturity of Mesozoic and Cenozoic sediments may, therefore, be due to an enhanced convective heat supply in the study area between late Eocene and late Miocene. It is obvious that the distribution and the depth-range of deep faults, linear fractures and graben structures have strongly controlled the paleogeothermal pattern. In the study area, the high density of faults active in Tertiary times supports this hypothesis. Numerous narrow grabens, normal faults and left-lateral strike-slip faults extend SSW-wards from the Rhine Graben into the Epivariscan Mesozoic cover of the Tabular Jura and into the folds and thrusts of the Folded Jura (e.g. Laubscher 1982, 1986, 1987). According to the same author (1987), even Palaeozoic fault zones were reactivated during Late Eocene and Early

Miocene. The maturity pattern of Tertiary sediments (high vitrinite reflectance values in the prolongation of the eastern Rhine Graben border where tectonic fault activity is maximal, see figure 3.16) may be a further argument in favour of an enhanced regional heat flow due to convective heat transport along highly fractured zones.

7.6.2 Molasse Basin (s.l.)

The main features resulting from thermal modelling in the Molasse Basin can be summarised as follows:

i) Thermal modelling of outcrop samples in the Plateau Molasse requires maximum paleotemperatures of about 40, 70, 90 and 110°C for measured vitrinite reflectance values of 0.3, 0.4, 0.5 and 0.6% respectively.

ii) The Küsnacht drillhole (Rybach & Bodmer 1980) is characterised by a low coalification gradient and a high degree of maturity at shallow depth (0.48% Rr at 350m). When modelling with a classical burial history approach, a considerable amount of erosion (3-4km) is needed to calibrate the calculated data. Alternatively, the high Rr values and the low coalification gradient could both be explained by a short-time discharge of warm groundwater in this region. The magnitude of erosion (1km) resulting from such a simulation corresponds with values given in the literature (Laubscher 1974, Lemcke 1974, Naef et al. 1985).

Maturation patterns at the surface of the Swiss Molasse basin (chapter 3) are mainly determined by the individual thermal history of each sample site. Many, partly interrelated, parameters have an influence: sedimentary and/or tectonic overburden, local uplift/erosion, heat flow at the base of the Molasse basin, convective heat transport (fluids expelled from the orogenic belt, rising deep groundwater in fracture zones, gravity-driven fluid flow), long term changes in surface temperature, sedimentation rate, topography and the geometry of the formations.

Conventionally, maximum burial depth is regarded as the most important factor for coalification in hypothermal basins. Thermal modelling indicates maximum paleotemperatures of up to 110°C for surface samples in the Plateau Molasse.

These temperatures may be easily interpreted in the context of a low geothermal regime, if the results of the burial history approach or the results of a recent study (Kälin et al. 1992) on rock density and compaction in the Plateau Molasse (indicating eroded overburden thicknesses of up to 4km) were confirmed. This seems, however, unlikely (see discussion chapter 3.6).

Convective heat transport may partially explain the inferred paleotemperatures and the observed coalification pattern. There are some indications for this interpretation:

i) The present day heat flow anomaly in Northern Switzerland, explained by uprising deep groundwater (Rybach et al. 1987), shows that convective heat transport is important for the present geothermal regime.

ii) Within the present day heat flow pattern of the Swiss Molasse basin, geothermal anomalies can be found.

iii) Second order variations in the coalification pattern of the investigated areas can not be explained only as the result of locally very high overburden-thicknesses and high uplift/erosion values. These small scale anomalies, which may be structurally controlled, probably resulted from the regional discharge of warm fluids.

Similar phenomena have been postulated elsewhere: Clendenin & Duane (1990) confirmed a tectonic link between the Appalachian-Ouachita orogeny and the Mississippi Valley-type Pb-Zn deposits of its foreland basin. Seismic pumping and distal fluid focusing along faults appeared to be a plausible mechanism to move hot reactive fluids to the sites of ore deposition. Thermal anomalies could also be explained by a gravity-driven fluid flow (Hitchon 1984) which is controlled by high permeable fault zones or rising deep ground water in fracture zones.

iv) Thermal modelling, assuming some hypothetical effects of convective heat transport, can successfully simulate low-gradient coalification profiles with a low overburden-thickness.

v) A hydrothermal influence is also proposed for an important maturation anomaly (Rr of up to 1.3% at a depth of only 3100m) in the Miesbach 1 well in Bavaria (Jacob & Kuckelkorn 1977).

The influence of the paleogeohydrological system on the paleogeothermal regime of the Molasse basin has been underestimated in the past. Nevertheless, burial depth is also a very important parameter to interpret coalification patterns. The increase of thermal maturity towards the Alps is probably a consequence of increasing burial depth towards the orogenic belt.

Chapter 8: SYNTHESIS OF RESULTS AND CONCLUSIONS

8.1 Synthesis of results

8.1.1 Organic diagenesis

The main observations based on organic diagenesis can be summarised as follows:

i) There is a stratigraphic control on maturation of organic matter. Mean average vitrinite reflectance values of surface samples increase slowly with age: from 0.38% Rr for samples from the Middle Miocene OSM to 0.61% Rr for samples from the Oligocene UMM.

ii) In the proximal part of the Molasse Basin, the level of organic maturity in Tertiary sediments increases towards the Alpine front.

iii) The range of vitrinite reflectance values measured in samples from the Plateau Molasse is large (0.21% Rr - 0.64 % Rr). Nevertheless, no pronounced regional trends can be observed. The organic maturity level of outcrop samples does hardly change from the western part to the eastern part of the basin. In addition, there is no marked decrease in the maturity level of organic matter from the proximal to distal parts of the Plateau Molasse.

iv) Isoreflectance contours indicate that variations in thermal maturation of the Plateau Molasse might have a structural control. Areas of increased vitrinite reflectance occur near fault zones (Arve strike-slip, Pomy-Cuarny thrust, la Broye thrust) or lie parallel to a major topographic structure (Lake Zurich), which may be tectonically controlled.

v) Rock-Eval pyrolysis results indicate that the organic matter in Tertiary sediments (OMM, USM, UMM) of the Haute-Savoie and Geneva basin is dominated by type III kerogen. Two samples from the UMM showed mixed type II/III kerogen.

vi) The thermal maturity of organic matter derived from Rock-Eval Tmax is associated with major uncertainties as indicated by the poor correlation between Tmax and Rr. The maturity trends observed for the vitrinite reflectance could not be confirmed by Tmax data. The isocontour maps for S2, S3, HI and OI indicate regional W-E trends which might be explained in terms of an increasing level of thermal maturity of organic matter towards the east. Thus confirming vitrinite reflectance results.

vii) Thermal modelling has shown that very high Tertiary paleogeothermal gradients (40-100°C/km) are necessary to explain the maturation level of Mesozoic and Tertiary sediments in Northern Switzerland, a region which is situated at the intersection of the extensional realm of the Rhine Graben and the compressional realm of the eastern Jura.

viii) Thermal modelling of outcrop samples in the Plateau Molasse requires maximum paleotemperatures of about 40, 70, 90 and 110°C for measured vitrinite reflectance values of 0.3, 0.4, 0.5 and 0.6% respectively. These temperatures could be explained in the framework of a hypothermal foreland basin, if eroded overburden thicknesses of up to 4km are assumed. However, there is no geological evidence for the deposition and subsequent erosion during the Neogene, especially in the distal parts of the Molasse Basin.

ix) Thermal modelling, taking into account convective heat transport, could explain in part the inferred paleotemperatures and the observed coalification patterns. The Küsnacht drillhole (Rybach & Bodmer 1980) is characterised by a low coalification gradient and by a vitrinite reflectance value of 0.48% at a depth of 350m. When modelling with a classical burial history approach, a considerable amount of erosion (3-4km) is needed to calibrate the measured data. Alternatively, the relatively high Rr values at shallow depth and the low coalification gradient could both be explained by a short-time discharge of warm groundwater in this region.

8.1.2 Mineral diagenesis

The major features of mineral diagenesis in Tertiary formations of the Haute-Savoie and Geneva Basin are the following:

i) Bulk-rock mineralogy of Molasse deposits is rather stable throughout the study area and is dominated by quartz, calcite, plagioclase, K-feldspar, dolomite and various phyllosilicates.

ii) The fine fraction of shale samples comprises dominantly mica, chlorite, mixed-layer illite/smectite with variable amounts of kaolinite.

iii) The fine fraction of sandstone samples comprises dominantly mica, chlorite, mixed-layer illite/smectite with variable amounts of kaolinite, corrensite and serpentine.

iv) There are no major geographical variations in the relative proportion of phyllosilicates in the fine fraction of shale samples. Mineral assemblages seem to be rather uniform.

v) The most striking feature of the clay mineralogy of sandstone samples is the occurrence of corrensite. The appearance of corrensite in feldspathic, serpentine-bearing sandstones indicates minimal temperatures of about 90 to 100°C for the frontal part of the Bornes Plateau.

vi) The most important diagenetic process in shale and sandstone samples of the Haute-Savoie and Geneva Basin is the progressive decrease of the percentage of smectite layers in mixed-layers illite/smectite (I/S). I/S compositions in sandstones and shales show an eastward decrease in smectite layers.

vii) Temperature estimate from fluid inclusion data seem to be consistent with those from clay mineral analysis which indicate temperatures of at least 90°C east of the Salève. The paleogeothermal gradients are, however, higher than expected for the Molasse basin (Teichmüller & Teichmüller 1986), except in the cases of hydrostatic pressure condition and high overburden thicknesses.

8.1.3 Comparison between organic and mineral diagenesis in the Haute-Savoie and Geneva Basin

In the Haute-Savoie and Geneva Basin, the similarity of isoreflectance maps (chapter 3) and isocontour maps representing the %S in I/S (chapter 5) is striking. A relation between these two thermal indicators seems therefore very likely. The correlation between %Rr and %S in I/S (Fig. 5.15) indicates that the decrease of %S in I/S (down to smectite values <20%) occurs over a relatively short %Rr-interval (between ~0.3 and ~0.8 %Rr).

Estimated paleotemperatures for the OMM in the western part of the study area (Bellegarde and Rumilly Basin) are about 70°C when using thermal modelling results of vitrinite reflectance data and between 50-80°C when using I/S composition data.

For the Bornes Plateau, vitrinite reflectance data indicate a temperature range between 90 and 110°C. This is in agreement with the appearance of corrensite in sandstone samples at the front of Bornes Plateau indicating temperatures of at least 90°C. I/S composition data suggest temperatures between 50 and 80°C for the western part of Bornes Plateau and temperatures probably greater than 120°C for the eastern part of the Bornes Plateau. Pressure-corrected trapping temperatures of fluid inclusions in a calcite vein at the eastern end of the Salève mountain range from 101 to 162°C (lithostatic pressure conditions) and from 87 to 112°C (hydrostatic pressure conditions) for overburden thicknesses varying from 1 to 4km respectively.

8.2 Implications for the thermal history of the Molasse Basin

The thermal evolution of a foreland basin may be influenced by one or more of the following mechanisms (Moss 1992b):

i) frictional heating next to thrust planes;

ii) thermal inversion by emplacement of a thrust sheet with a hotter base;

iii) normal burial heating via both tectonic and sedimentary burial;

iv) migration of fluids

Our results emphasise the role of the last two mechanism.

8.2.1 Frictional heating

Frictional heating along thrust planes might have played a role in the Subalpine Molasse or the Subalpine Chains. However, according to Bustin (1983), measurement of the levels of organic maturation below and within shear zones of thrust faults in the Rocky Mountains has revealed no general thermal metamorphism that can be attributed to faulting, with the exception of very narrow films immediately adjacent to, or within the shear zone. The major factor against frictional heating being important on anything larger than a local scale, is that the high fluid content expected with the emplacement of thrust sheets would quickly dissipate any frictionally-produced higher temperatures (Moss 1992b). Such a mechanism has not been revealed by our data.

8.2.2 Thermal inversion by emplacement of a thrust sheet

The temperature effects of overthrusting may be important in the most internal parts of the Molasse Basin (Subalpine Molasse and Subalpine Chains). Many studies dealing with thermal perturbation due to overthrusting processes assume instantaneous thrust sheet emplacement and the development of a sawtooth-shaped temperature profile within the overthrusted sequence immediately after emplacement (e.g. Oxburgh & Turcotte 1974, Angevine & Turcotte 1983). Equilibrium times of many tens of million years for sheets in the range of several kilometres thickness are suggested by these authors. However, these models oversimplify the problem, for example by neglecting the physical and thermal characteristics of lithologies or by using instantaneous thrust sheet emplacement rates.

Wygrala et al. (1990) developed a 2-D model of overthrusting in order to investigate the sensitivity of the thermal effects to various parameters during the actual overthrusting process. Their results indicate that sawtooth-shaped temperature profiles cannot develop under realistic geological conditions due to equilibrium processes during overthrusting. Temperature inversions can only develop with rapid overthrusting rates, i.e. in excess of ca. 4-5cm/year.

However, overthrusting rates in the foreland fold/thrust belt of the Swiss Alps are much lower. Pfiffner (1986) restored a cross-section in eastern Switzerland and suggests average thrust-advance rates of 3mm/yr for the UMM and 2mm/yr from the USM on to the OSM. Data from western Switzerland indicate an approximate rate of thrust tip propagation of about 7mm/yr for the Oligocene and Miocene. In a study on vertical versus horizontal motions in the Alpine orogenic wedge, Sinclair & Allen (1992) proposed advance rates of the Alpine thrust wedge during the mid-Oligocene of about 2mm/yr.

8.2.3 Normal burial heating via both tectonic and sedimentary burial

In the Molasse Basin, one of the main factors controlling the paleotemperature regime, and hence the thermal maturity of sediments, is burial via sedimentary and tectonic loading. Vitrinite reflectance data indicate that there is a stratigraphic control on maturation of organic matter. Mean average vitrinite reflectance values increase slowly with age. This shows the influence of stratigraphic burial. Subsurface vitrinite reflectance data are needed to assess whether the increase of thermal maturity in the Subalpine Molasse towards the Alps is a consequence of increased sedimentary burial towards the orogen (pre-thrusting coalification) or of tectonic burial (syn- or post-thrusting coalification). The level of organic maturity in the Subalpine Molasse of Germany is believed to be of pre-thrusting origin (Jacob & Kuckelkorn 1977, Jacob et al. 1982).

There are, however, observations in the Haute-Savoie and Geneva Basin which indicate that tectonic burial may have played an important role. Results from vitrinite reflectance and clay mineral analysis indicates an increase of thermal maturity of Molasse sediments in an eastward direction. Isomaturity contours run slightly oblique to the Alpine front. Variation in maximum burial temperatures seem, therefore, to be more marked along strike of the Alpine front than across. The level of organic maturity of Mesozoic and Tertiary horizons in the Subalpine Chains shows a similar trend, indicating greater burial temperatures in the north-eastern (Bornes, Aravis, Haut-Giffre) than the south-western (Vercors, Chartreuse) part (Moss 1992a,b). According to the same author, there are two possible causes of the along strike variation in burial temperature: i) increasing sedimentary burial in the north-eastern part of the Subalpine Chains due to the increased thickness of foredeep sediments or ii) increased burial via emplacement of allochthonus thrust sheets. He considered that the main cause was the emplacement of the Prealpine thrust sheets in the NE in the upper Oligocene.

The overall geometry of the Molasse basin tends to suggest a NW to SE increase in maturity. Normally, locations close to the orogen subsided more rapidly and for a longer period than those close to the feather-edge of the basin. In the Haute-Savoie, recent investigations by Huggenberger & Wildi (1991) and Wildi & Huggenberger (1993) showed a close relationship between the tectonic history of the Subalpine Chains (characterised by changing directions of tectonic transport during deformation) and the evolution of the adjacent foreland basin. According to these authors, a first deformation phase of the Subalpine Chains (mainly Oligocene and Early Miocene) resulted into a SSE-NNW to SE-NW shortening of about 8km by folding and thrusting, whereas a second phase produced 6km of thrusting from the ESE or E to WNW or W (mainly Miocene and Pliocene).

Northward migration of depocenters in the Molasse Basin of the Haute-Savoie during the Oligocene can be associated with the first deformation phase. The change of transport direction of Alpine nappes in early Miocene times from ~NW to ~W resulted in a major switch of the overall subsidence and overburden pattern. No outcrops of OMM have been found east of a line which corresponds approximately to the Vuache wrench fault. This may be due to the postulated early inversion of the Tertiary basins in the Bornes Plateau and the Bornes domains (Huggenberger & Wildi 1991). In the Voiron-Chambéry-Annecy region (Rhône-Alp), up to 1150m of Miocene marine sediments are preserved (Allen & Bass 1993). According to these authors, the early Burdigalian seaway was established by the flooding from the south of a number of narrow N-S or NNE-SSW oriented continental basins. Subsequently, these basins were filled by the progradation of deposits from the Alpine front into the seaway. The westward progradation and the generally W-E increase in thickness of OMM deposits (Michel & Caillon 1957) may be associated with the flexural subsidence related to the westward advance of the Alpine orogenic wedge.

The estimated burial-depths for the USM in the eastern part of the Bornes Plateau (at least 3-4km) can hardly be explained as a consequence of sedimentary covering. In Eastern Switzerland where the Molasse sequence is more or less entirely preserved, maximum thicknesses of up to 2km are measured for the formations overlaying the USM. This is in good agreement with the estimated missing sections of the western Molasse Basin (Lemcke 1974). Moreover, given the possibility of an early inversion of the Bornes Plateau and the Bornes Massif, we considered here that the main cause of increased burial temperature in this part of the Haute-Savoie was the emplacement of Alpine nappes (Helvetic, Ultrahelvetic, Penninic) onto the foreland. The importance of Penninic thrust sheets in increasing the overburden and thermal maturity in the north-east part of the Subalpine Chains has already been noted by Sawatzki (1975), Kübler et al. (1974), Gorin & Monteil (1990) and Moss (1992a,b). These authors estimated overburden thicknesses between 3 and 6km for this area. For the Prealps, which lie further to the east, a maximum overburden of up to 10km was postulated by Mosar (1988).

8.2.4 Migration of fluids

Both theoretical models and geological studies (Hitchon 1984, Majorowicz et al. 1984, Oliver 1986, Bethke & Marshak 1990, Deming et al. 1990, Deming & Nunn 1991, Deming et al. 1992, and others) have shown the relationship of fluid migration to temperatures and heat flow in foreland areas. In a sedimentary basin, fluid flow can be driven by several mechanisms (Bethke 1989): i) gradient of hydraulic potential imposed by topographic variations of the water table, buoyancy associated with fluid density contrasts due to temperature (thermal convection) or composition

(thermo-haline convection) and iii) expulsion of free or bound water during compaction and diagenetic processes. Quantitative modelling indicates that the topographic relief of a tectonic belt provides the dominant driving force for migration in a foreland basin (Bethke & Marshak 1990). Ground waters recharging in the uplifted areas move to depth and migrate along deep aquifers at velocities which may reach meters to tens of meters per year (Bethke et al. 1988). Migrating ground waters transport heat that is conducted from the lower crust and redistribute it towards discharge areas. Recharge areas (topographic highs) are expected to display low geothermal gradients and regional topographic lows may display high geothermal gradients (Hitchon 1984).

In the Molasse Basin, present-day geothermal gradients decrease from >35°C/km in the N to <25°C/km towards the Alps (Rybach 1984). Teichmüller & Teichmüller (1986) showed, based on coalification gradients from boreholes, that the paleogeothermal gradients in the Molasse Basin decrease towards the Alps. The observed decrease in coalification and geothermal gradients in the northern Alpine foreland basin has usually been explained as a result of thickening of the crust towards the Alps. Alternatively, this pattern may also be explained as a result of the (paleo)hydrodynamic regime. Our results could not demonstrate the existence of a basin-wide hydrological system, but emphasised i) the role of fluids in creating local thermal anomalies which seem to be controlled by tectonic structures (see discussions in chapter 3.6 and 7.6.1) and ii) the role of transient heating by warm fluids on maturation of organic matter (see discussions in chapter 7.4 and 7.5).

8.3 Conclusions

Mapping of indicators of thermal maturity in the Molasse Basin (Switzerland, France) allowed to define the level and the geographical variation of organic matter and mineral diagenesis on a basin-wide scale. Results indicate that the paleogeothermal regime of the Molasse Basin is controlled by several interrelated mechanisms. Generally, the overall level of thermal maturity is controlled by burial heating via sedimentary and tectonic (at the Alpine front) loading. Conventially, in hypothermal basins, such as the Molasse Basin, the level of thermal maturation is explained often only as a consequence of thick overburden. The results of this study indicate, however, that the observed thermal maturity may be due to a combination of 'not-so-deep' burial and transient heating by warm fluids. In addition, positive palaeogeothermal anomalies along major tectonic fault zones and along major graben structures in the basement (south of the Rhine Graben) indicate that convective heat transport is locally or even regionally a very important heat transport mechanism.

REFERENCES

AHN, J.H. & PEACOR, D.R. 1986: Transmission and analytical electron microscopy of the smectite to illite transition. Clays and Clay Min. 34, 165-179.

ALLEN, P.A. & ALLEN, J.R. 1990: Basin analysis: principles and applications. Blackwell Scientific Publication, London.

ALLEN, P.A. & BASS, J.P. 1993: Sedimentology of the Upper Marine Molasse of the Rhône-Alp region, Eastern France: implications for basin evolution. Eclogae geol. Helv. 86, 121-172.

ALLEN, P.A., MANGE-RAJETZKY, M., MATTER, A. & HOMEWOOD, P. 1985: Dynamic palaeogeography of the open Burdigalian seaway, Swiss Molasse basin. Eclogae geol. Helv. 78, 351-382.

ALPERN, B. 1976: Fluorescence et réflectance de la matière organique dispersée et évolution des sédiments. Bull. Centre Rech. Pau-SNPA 10, 201-220.

ALPERN, B. & MAUME, F. 1969: Étude pétrographique de l'oxydation naturelle et artificielle des houilles. Rev. Ind. Miner. 51, 979-997.

ALPERN, B. & TEICHMÜLLER, M. 1971: Classification et corrélation des constituants de la vitrinite (houilles) et de l'huminite (lignites). C.R. Ac. Sci. Paris D272, 775-778.

ANGELILLO, T. 1987: Les marnes et grès gris à gypse ("Molasse Grise") du Bassin genevois. Diplôme, Dép. de Géolgie et Paléontologie, Université de Genève, Suisse (unpubl.).

ANGEVINE, C.L. & Turcotte, D.L. 1983: Oil generation in overthrust belts. Bull. amer. Assoc. Petroleum Geol. 67, 235-241.

APRAHAMIAN, J. 1988: Cartographie du métamorphisme faible à très faible dans les Alpes françaises externes par l'utilisation de la cristallinité de l'illite. Geodinamica Acta 2, 25-32.

APRIL, R.H. 1981: Trioctahedral smectite and interstratified chlorite/smectite in Jurassic strata of the Connecticut Valley. Clays and Clay Min. 29, 31-39.

AWWILLER, D.N. 1993: Illite/smectite formation and potassium mass transfer during burial diagenesis of mudrocks: a study from the Texas Gulf Coast Paleocene-Eocene. J. sediment. Petrol. 63, 501-512.

BACHMANN, G.H., MÜLLER, M. & WEGGEN, K. 1987: Evolution of the Molasse Basin (Germany, Switzerland). Tectonophysics 137, 77-92.

BACHMANN, G.H. & MÜLLER, M. 1991: The Molasse basin, Germany: evolution of a classic petroliferous foreland basin. In: Spencer, A.M. (Ed.): Generation, Accumulation and Production of Europe's Hydrocarbons. Special Publication of the European Association of Petroleum Geoscientists No.1, Oxford University Press, Oxford, 263-276.

BACHMANN, G.H. & MÜLLER, M. 1992: Sedimentary and structural evolution of the German Molasse Basin. Eclogae geol. Helv. 85, 519-530.

BAILEY, S.W. 1982: Nomenclature for regular interstratifications. Clay Minerals 17, 243-248.

BALDERER, W. 1990: Past and future evolution of flow systems as reponse to changing climatic conditions and anthropogenic influences. Memoires of the 22nd Congress of IAH, Vol. XXII, Lausanne, 1990 , 741-750.

BARKER, C.E. 1983: Influence of time on metamorphism of sedimentary organic matter in liquid-dominated geothermal systems, western North America. Geology 11, 384-388.

— 1989: Temperature and Time in the Thermal Maturation of Sedimentary Organic Matter. In:Naeser, N.D. & McCulloh, T.H. (Eds.): Thermal History of Sedimentary Basins: Methods and Case Histories. Springer-Verlag, New-York, Berlin, London, Paris, Tokyo, 73-98.

BARKER, C.E. & GOLDSTEIN, R.H. 1990: Fluid-inclusion technique for determining maximum temperature in calcite and its comparison to the vitrinite reflectance geothermometer. Geology 18, 1003-1006.

BARKER, C.E. & PAWLEWICZ, M.J. 1986: The correlation of vitrinite reflectance with maximum temperature in humic organic matter. In: Buntebarth, G. & Stegena, L. (Eds.): Lecture Notes in Earth Sciences 5: Paleogeothermics., Springer-Verlag, Berlin, Heidelberg, New-York, London, Paris, Tokyo , 79-93.

BARKER, C.E. & PAWLEWICZ, M.J. 1992: An estimate of the minimum number of mesurements needed to constrain the mean random vitrinite reflectance of disseminated organic matter. Abstr. Ninth Annual Meeting of the Society for Organic Petrology, University Park, Pennsylvania 1992 , 10-11.

BEAUMONT, C., BOUTILIER, R., MACKENZIE, A.S. & RULLKÖTTER, J. 1985: Isomerization and aromatization of hydrocarbons and the paleothermometry and burial history of Alberta foreland basin. Bull. amer. Assoc. Petroleum Geol. 69, 546-566.

BEAUMONT, C., KEEN, C.E. & BOUTILIER, R. 1982: On the evolution of rifted continental margins: comparison of models and observations for the Nova Scotian margin. Geophys. J. royal astr. Soc. 70, 667-715.

BEAUMONT, C. & TANKARD, A.J. 1987: Sedimentary basins and basin-forming mechanisms. Can. Soc. Petroleum Geol. Mem. 12.

BECK, A.E, GARVEN, G. & STEGENA, L. 1989: Hydrogeological Regimes and Their Subsurface Thermal Effects. Geophysical Monograph 47, IUGG Vol.2, Washington.

BELL, T.E. 1986: Microstructure in mixed-layer illite/smectite and its relationship to the reaction of smectite to illite. Clays and Clay Min. 34, 146-154.

BENEDICT, L.G. & BERRY, W.F. 1964: Recognition and measurement of coal oxidation. Coal Group, Geol. Soc. America, Miami, Bituminous Coal Research Rept., Monroeville Pa.

BERGER, J.-P. 1985: La transgression de la Molasse marine supérieure (OMM) en Suisse occidentale. Münchn. Geowiss. Abh., Reihe A, Geol. Paläont. 5.
— 1992: Correlative chart of the European Oligocene and Miocene: Application to the Swiss Molasse Basin. Eclogae geol. Helv. 85, 573-609.
BERGER, J.-P., CHAROLLAIS, J. & HUGUENEY, M. 1987: Nouvelles données biostratigraphiques sur la Molasse rouge du bassin genevois. Arch. Sci. Genève 40, 77-95.
BERNER, R.A. 1971: Principles of chemical sedimentation. McGraw-Hill, New York.
BETHKE, C.M. & ALTANER, S.P. 1986: Layer-by-layer mechanism of smectite illitization and application to a new rate law. Clays and Clay Min. 34, 136-145.
BETHKE, C.M., HARRISON, W.J., UPSON, C. & ALTANER, S.P. 1988: Supercomputer analysis of sedimentary basins. Science 239, 261-267.
BETHKE, C.M. & MARSHAK, S. 1990: Brine migrations across North America- The plate tectonics of groundwater. Ann. Rev. Earth planet. Sci. 18, 287-315.
BETHKE, E. 1989: Modeling subsurface flow in sedimentary basins. Geol. Rdsch. 78, 129-154.
BETZ, D. & WENDT, A. 1983: Neuere Ergebnisse der Aufschluss- und Gewinnungstätigkeit auf Erdöl und Erdgas in Süddeutschland. Bull. Ver. schweiz. Petroleum-Geol. u. -Ing. 49/117, 9-36.
BJORLYKKE, K., RAMM, M. & SAIGAL, G.C. 1989: Sandstone diagenesis and porosity modification during basin evolution. Geol. Rdsch. 78, 243-268.
BLANK, P. & SEIFERT, W. 1976: Zur Untersuchung diagenetischer Tonmineralbildungen und deren experimentelle Modellierung. Z. angew. Geol. 22, 560-564.
BODMER, P. 1982: Geothermische Karte der Schweiz: Wärmestromdichte. Comm. suisse de géophysique, Wabern.
Bodmer, P. & Rybach, L. 1984: Geothermal map of Switzerland (Heat flow density). Matér. Géol. Suisse, Sér. géophys. 22, Berne.
BODNAR, R.J. & BETHKE, P.M. 1984: Systematics of stretching of fluid inclusions I: fluorite and sphalerite at 1 atmosphere confining pressure. Economic Geol. 79, 141-161.
BOLES, J.R. & FRANKS, S.G. 1979: Clay diagenesis in Wilcox sandstones of southwest Texas: implications of smectite diagenesis on sandstone cementation. J. sedim. Petrol. 49, 55-70.
BOLLIGER, T. 1992: Kleinsäugerstratigraphie in der lithologischen Abfolge der miocänen Hörnlischüttung (Ostschweiz) von MN3 bis MN7. Eclogae geol. Helv. 85, 961-1000.
BOLLIGER, T. & EBERHARD, M. 1989: Neue Floren- und Faunenfunde aus der Oberen Süsswassermolasse des Hörnligebietes (Ostschweiz). Vjschr. natf. Ges. Zürich 134, 109-138.
BOLLIGER, T., GATTI, H. & HANTKE, R. 1988: Zur Geologie und Paläontologie des Zürcher Oberlandes. Vjschr. natf. Ges. Zürich 133, 1-24.
BOSTICK, N.H. & FOSTER, J.N. 1975: Comparison of vitrinite reflectance in coal seams and in kerogen of sandstones, shales, and limestones in the same part of a sedimentary section. In: Alpern, B. (Ed.): Pétrographie de la matière organique des sédiments, relations avec la paléotempérature et le potentiel pétrolier. Colloque Internationale, C.N.R.S., Paris , 13-25.
BRADBURY, H.J. & WOODWELL, G.R. 1987: Ancient fluid flow within foreland terrains. In: Goff, J.C. & Williams, B.P. (Eds.): Fluid Flow in Sedimentary Basins and Aquifers. Geol. Soc. Spec. Publ. 34, 87-102.
BRAM, K. 1979: Heat flow measurements in the Federal Republic of Germany. In: Cermák, V. & Rybach, L. (Eds.): Terrestrial heat flow in Europe. Springer Verlag, Heidelberg-Berlin-New York , 191-196.
BRAUN, R.L. & BURNHAM, A.K. 1987: Analysis of chemical reaction kinetics using a distribution of activation energies and simpler models. Energy and Fuels 1, 153-161.
BREDDIN, H. 1964: Die tektonische Deformation der Fossilien und Gesteine in der Molasse von St. Gallen (Schweiz). Geol. Mitt. 4, 1-114.
BREDEHOEFT, J.D., BELITZ, K. & SHARP-HANSEN, S. 1992: The hydrodynamics of the Big Horn basin: A study of the role of faults. Bull. amer. Assoc. Petroleum Geol. 76, 530-546.
BRINDLEY, G.W. 1980: Quantitative X-ray mineral analysis of clay. In: Brindley, G.W. & Brown, G. (Eds.): Crystal Structures of Clay Minerals and Their X-ray Identification. Mineralogical Society Monograph No. 5, London, 411-438.
BRINDLEY, G.W. & BROWN, G. 1980: Crystal Structures of Clay Minerals and Their X-ray Identification. Mineralogical Society Monograph No. 5, London.
BRINK, H.-J., BURRI, P., LUNDE, A. & WINHARD, H. 1992: Hydrocarbon habitat and potential of Swiss and German Molasse Basin: A comparison. Eclogae geol. Helv. 85, 715-732.
BROWN, H.R., COOK, A.C. & TAYLOR, G.H. 1964: Variations in the properties of vitrinite in isometmorphic coal. Fuel 43, 111-124.
BUATIER, M.D., PEACOR, D.R. & O'NEIL, J.R. 1992: Smectite-illite transition in Barbados accretionary wedge sediments: TEM and AEM evidence for dissolution/crystallization at low temperature. Clays and Clay Min. 40, 65-80.
BÜCHI, U.P. 1957: Zur Gliederung der OSM zwischen Bodensee und Reuss. Bull. Ver. schweiz. Petroleum-Geol. u. -Ing. 24/66, 35-42.
— 1958a: Geologie der Oberen Süsswassermolasse (OSM) zwischen Reuss und Glatt. Bull. Ver. schweiz. Petroleum-Geol. u. -Ing. 25/2, 5-24.

— 1958b: Zur Geologie der Oberen Süsswassermolasse OSM zwischen Töss- und Glattal. Eclogae geol. Helv. 51, 73-105.
— 1959: Zur Stratigraphie der Oberen Süsswassermolasse (OSM) der Ostschweiz. Eclogae geol. Helv. 52, 449-460.
BÜCHI, U.P. & BODMER, P. 1983: Der Tiefenverlauf der seismischen Geschwindigkeiten in den Molassesedimenten des schweizerischen Mittellandes. Bull. Ver. schweiz. Petroleum-Geol. u. -Ing. 49/116, 3-13.
BÜCHI, U.P., LEMCKE, K., WIENER, G. & ZIMDARS, J. 1965: Geologische Ergebnisse der Erdölexploration auf das Mesozoikum im Untergrund des schweizerischen Molassebeckens. Bull. Ver. schweiz. Petroleum-Geol. u. -Ing. 32/82, 7-38.
BÜCHI, U.P. & SCHLANKE, S. 1977: Zur Paläographie der Schweizerischen Molasse. Erdöl-Erdgas-Zeitschrift 93, 57-69.
BÜHMANN, C. 1992: Smectite-to-illite conversion in a geothermally and lithologically complex Permian sedimentary sequence. Clays and Clay Min. 40, 53-64.
BUISKOOL TOXOPEUS, J.M.A. 1983: Selection Criteria for the Use of Vitrinite Reflectance as a Maturity Tool. In: Brooks, J. (Ed.): Petroleum Geochemistry and Exploration of Europe. Geol. Soc. Spec. Publ. 12, Blackwell Scientific Publications, London , 295-307.
BUNTEBARTH, G. 1979: Eine empirische Methode zur Berechnung von paläogeothermischen Gradienten aus dem Inkohlungsgrad organischer Einlagerungen in Sedimentgesteinen mit Anwendung auf den mittleren Oberrheingraben. Fotschr. Geol. Rheinld. u. Westf. 27, 97-108.
BUNTEBARTH, G. & STEGENA, L. 1986: Methods in Paleogeothermics. In: Buntebarth, G. & Stegena, L. (Eds.): Lecture Notes in Earth Sciences 5: Paleogeothermics. Springer-Verlag, Berlin, Heidelberg, New-York, London, Paris, Tokyo, 5-39.
BURBANK, D.W., ENGESSER, B., MATTER, A., WEIDMANN, M. 1992: Magnetostratigraphic chronology, mammalian faunas, and stratigraphic evolution of the Lower Freshwater Molasse, Haute-Savoie, France. Eclogae geol. Helv. 85, 399-431.
BÜRGISSER, H.M. 1980: Zur mittel-miozänen Sedimentation im nordalpinen Molassebecken: Das "Appenzellergranit"-Leitniveau des Hörnli-Schuttfächers (Obere Süsswassermolasse, Nordschweiz). Mitt. geol. Inst. ETH u. Univ. Zürich (N.F.) 232.
BÜRGISSER, H.M. 1981: Fazies und Paläohydrologie der Oberen Süsswassermolasse im Hörnli-Fächer (Nordostschweiz). Eclogae geol. Helv. 74, 19-28.
BURKHARD, M. 1988: L'Helvétique de la bordure occidentale du massif de l'Aar (évolution tectonique et métamorphique). Eclogae geol. Helv. 81, 63-114.
— 1990: Aspects of the large-scale Miocene deformation in the most external part of the Swiss Alps (Subalpine Molasse to Jura fold belt). Eclogae geol. Helv. 83, 559-583.
BURKHARD, M. & KALKREUTH, W. 1989: Coalification in the northern Wildhorn nappe and adjacent units, western Switzerland. Implications for tectonic burial histories. Int. J. Coal Geol. 11, 47-64.
BURNHAM, A.K. & SWEENEY, J.J. 1989: A chemical kinetic model of vitrinite maturation and reflectance. Geochimica et Cosmochimica Acta 53, 2649-2657.
BURRUS, R.C. 1989: Paleotemperatures from fluid inclusions: advances in theory and technique. In: Naeser, N.D. & McCulloh (Eds.): Thermal history of sedimentary basins. Methods and case histories. Springer-Verlag, New York, 119-131.
BURST, J.F. 1959: Postdiagenetic clay mineral environmental relationships in the Gulf Coast Eocene. Clays and Clay Min. 6, 327-341.
— 1969: Diagenesis of Gulf Coast Clayey Sediments and Its Possible Relation to Petroleum Migration. Bull. amer. Assoc. Petroleum Geol. 53, 73-93.
BUSTIN, R.M. 1980: Oxidation characteristics of some sheared coal seams of the Mist Mountain Formation, southeastern Canadian Cordillera. Geol. Surv. Canad. Pap. 81-B, 249-254.
BUSTIN, R.M. 1983: Heating during thrust faulting in the Rocky Mountains: friction or fiction? Tectonophysics 95, 309-328..
BUSTIN, R.M., BARNES, M.A. & BARNES, W.C. 1985: Diagenesis 10. Quantification and modelling of organic diagenesis. Geoscience Canada 12, 4-21.
BUSTIN, R.M., CAMERON, A.R., GRIEVE, D.A. & KALKREUTH, W.D. 1983: Coal petrology - It's principles, methodes and applications. Geol. Assoc. of Canada, short course notes 3, Victoria, British Columbia.
BUTLER, R.W.H. 1991: Hydrocarbon maturation, migration and tectonic loading in the Western Alpine foreland thrust belt. In: England, W.A. & Fleet, A.J. (Eds.): Petroleum migration. Geol. Soc. Spec. Publ. 59 , 227-244.
CARON, C., HOMEWOOD, P. & WILDI, W. 1989: The Original Swiss Flysch: A Reappraisal of the Type Deposits in the Swiss Prealps. Earth Sci. Rev. 26, 1-45.
CATHLES, L.M. & SMITH, A.T. 1983: Thermal constraints on the formation of Mississippi Valley-type lead-zinc deposits and their implications for episodic basin dewatering and deposit genesis. Econ. Geol. 78, 233-249.
CERMÁK, V. 1979: Heat flow map of Europe. In: Cermák, V. & Rybach, L. (Eds.): Terrestrial heat flow in Europe. Springer Verlag, Heidelberg, Berlin, New York, 1-40.
— 1989: Crustal heat production and mantle heat flow in Central and Eastern Europe. Tectonophysics 159, 195-215.
CERMÁK, V. & RYBACH, L. 1989: Vertical distribution of heat production in the continental crust. Tectonophysics 159, 217-230.

CHAMLEY, H. 1989: Clay Sedimentology. Springer-Verlag, Berlin, Heidelberg, New York, London, Paris, Tokyo, Hong Kong.
CHANDRA, D. 1962: Reflectance and microstructures of weathered coals. Fuel (London) 41, 185-193.
CHANG, H.K., MACKENZIE, F.T. & SCHOONMAKER, J. 1986: Comparison between the diagenesis of dioctahedral and trioctahedral smectite, Brazilian offshore basins. Clays and Clay Min. 34, 407-423.
CHAPLET, M. 1992: Relations stratigraphiques et tectoniques entre nappe des Aravis et Bornes externes dans le synclinal de nappes de Thônes (Massif subalpin des Bornes - Haute-Savoie - France). Eclogae geol. Helv. 85, 23-43.
CHAROLLAIS, J. & AMBERGER, G. 1984: Savoie - Bassin molassique savoyard. In: Debrand-Passard, S., Courbouleix, S. & Lienhardt, M.-J. (Eds.): Synthèse géologique du Sud-Est de la France. Mém. du Bur. Rech. géol. min. 125 , 408-410.
CHAROLLAIS, J., BUSNARDO, R., CARDIN, M., CLAVEL, B., DECROUEZ, D., DELAMETTE, M., GORIN, G., LEPILLON, M., MONDAIN, P.H., ROSET, J. & VILLARS, F. 1988: Note explicative de la feuille Annecy-Bonneville 1/50'000. Bur. Rech. géol. min.,Orléans.
CHAROLLAIS, J., GINET, C., HUGUENEY, M. & MÜLLER, J.-P. 1981: Sur la présence de dents de mammifères à la base et dans la partie supérieure de la Molasse rouge du plateau des Bornes (Haute-Savoie, France). Eclogae geol. Helv. 85, 291-305.
CHAROLLAIS, J. & JAMET, M. 1990: Principaux résultats géologiques du forage Brizon 1 (BZN 1), Haute-Savoie, France. Mém. Soc. géol. France 156, 185-202.
CLENDENIN, C.W. & DUANE, M.J. 1990: Focused fluid flow and Ozark Mississippi Valley-type deposits. Geology 18, 116-119.
CONNAN, J. 1974: Time-temperature relation in oil genesis. Bull. amer. Assoc. Petroleum Geol. 58, 2516-2521.
CORREIA, M. 1969: Contribution à la recherche de zones favorables à la genèse du pétrole par l'observation microscopique de la matière organique figurée. Rev. Inst. franç. Pétrole 24, 1417-1454.
CRELLING, J.C., SCHRADER, R.H. & BENEDICT, L.G. 1979: Effects of weathered coal on coking properties and coke quality. Fuel 58, 542-546.
CRUMIÈRE, J.-P., PASCAL, F. & ESPITALIÉ, J. 1988: Evolutions diagénétiques comparées de la matière organique et des argiles. Influence de l'enfouissement normal et d'une anomalie thermique par surcharge des nappes alpines (Crétacé subalpin de Haute-Provence, France). C.R.Acad.Sci. Paris, t.306, Série II , 493-498.
DAMBERGER, H. 1968: Ein Nachweis der Abhängigkeit der Inkohlung von der Temperatur. Brennst.-Chemie 49, 73-77.
DAVIDSON, R.M. 1990: Natural oxidation of coal. IEA Coal Research 29.
DAVIS, A. 1978: The Reflectance of Coal. In: Karr, C. (Ed.): Analytical methods for coal and coal products. Academic Press, New York, 27-81.
DEBEGLIA, N. & GABLE, R. 1984: Socle, écorché anté-triasique. In: Debrand-Passard, J. & Courbouleix, S. (Eds.) Synthèse géologique du Sud-Est de la France, carte G3. Mém. Bur. Rech. géol. min. 126, vol. 2.
DECONINCK, J.-F. & CHAROLLAIS, J. 1986: Minéraux argileux des formations crétacées et tertiaires du domaine ultra-helvétique (unité de Nantbellet, Klippe de Sulens: Haute-Savoie): diagenèse et paléoenvironnement. Géologie Alpine 62, 11-30.
DECONINCK, J.-F. & DEBRABANT, P. 1985: Diagenèse des argiles dans le domaine subalpin: rôle respectifs de la lithologie, de l'enfouissement et de la surcharge tectonique. Rev. Géol. dyn. Géogr. phys. 26, 321-330.
DEICHMANN, N. 1990: Seismizität der Nordschweiz 1987-1989, und Auswertung der Edbebenserien von Günsberg, Läufelfingen und Zeglingen. Nagra techn. Ber. 90-46, Baden.
DEL REY, A.C. & HAMZA, V.M. 1989: Terrestrial Heat Flow Variations in the Northeastern Part of the State of Sao Paulo: A Case for Transport of Geothermal Heat by Interfracture Fluid Flows. In: A.E. Beck, G. Garven & L. Stegena (Eds): Hydrogeological Regimes and Their Subsurface Thermal Effects. Geophysical Monograph 47, IUGG Vol.2, Washington , 137-147.
DEMBICKI, H. 1984: An interlaboratoy comparison of source rock data. Geochimica et Cosmochimica Acta 48, 2641-2649.
DEMING, D. & NUNN, J.A. 1991: Numerical Simulations of Brine Migration by Topographically Driven Recharge. J. geophys. Res. 96, 2485-2499.
DEMING, D., NUNN, J.A. & EVANS, D.G. 1990: Thermal Effects of Compaction-Driven Groundwater Flow From Overthrust Belts. J. geophys. Res. 95, 6669-6683.
DEMING, D., SASS, J.H., LACHENBRUCH, A.H. & DE RITO, R.F. 1992: Heat flow and subsurface temperature as evidence for basin-scale ground-water flow, North Slope of Alaska. Bull. geol. Soc. Amer. 104, 528-542.
DIEBOLD, P., NAEF, H. & AMMANN, M. 1991: Zur Tektonik der zentralen Nordschweiz. Interpretation aufgrund regionaler Seimik, Oberflächengeologie und Tiefbohrungen. Nagra techn. Ber. 90-04, Wettingen.
DIEM, B. 1986: Die untere Meeresmolasse zwischen der Saane (Westschweiz) und der Ammer (Oberbayern). Eclogae geol. Helv. 79, 493-559.
DOEBL, F., HELING, D., HOMANN, W., KARWEIL, J., TEICHMÜLLER, M. & WELTE, D. 1974: Diagenesis of Tertiary clayey sediments and included dispersed organic matter in relationship to geothermics in the Upper Rhine Graben. In: Illies, J.H. & Fuchs, K. (Eds.): Approaches to taphrogenesis. Inter-Union Commission on Geodynamics, Scientific Report No.8, E.Schweizerbart'sche Verlagsbuchhandlung, Stuttgart, 192-207.

DONCIEUX, L. 1932: L'Oligocène de la vallée du Rhône et la région des Usses (Haute-Savoie). C.R. somm. Soc. Géol. France t.11, 22-23.
DONZÉ, P. & ENAY, R. 1972: Feuille XXXIII-30, Seyssel, et notice explicative. Carte géol. France 1:50000. Bur. Rech. géol. min., Orléans.
DOUXAMI, H. 1896: Étude sur les terrains tertiaires du Dauphiné, de la Savoie et de la Suisse occidentale. Ann. Univ. Lyon, Sér.I/27, 1-312.
DRURY, M.J. 1989: Fluid Flow in Crystalline Crust: Detecting Fractures by Temperature Logs. In: Beck, A.E., Garven, G. & Stegena, L. (Eds): Hydrogeological Regimes and Their Subsurface Thermal Effects. Geophysical Monograph 47, IUGG Vol.2, Washington, 129-135.
DUNOYER DE SEGONZAC, G. 1969: Les minéraux argileux dans la diagénèse. Passage au métamorphisme. Thèse Univ. Strasbourg, Mém. Serv. Carte Géol. Alsace-Lorraine 29, France.
— 1970: The transformation of clay minerals during diagenesis and low-grade metamorphism: a review. Sedimentology 15, 281-346.
DURAND, B. 1980: Kerogen - insoluble organic matter from sedimentary rocks. Editions Technip, Paris.
DURAND, B., ALPERN, B., PITTION, J.L. & PRADIER, B. 1986: Reflectance of vitrinite as a control of thermal history of sediments. In: Burrus, J. (Ed.): Thermal Modeling in Sedimentary Basins. 1st IFP Exploration Research Conference, Carcans, France, June 3-7 1985, Editions Technip, Paris, 441-474.
DURAND, B. & MONIN, J.C. 1980: Elemental analysis of kerogen (C, H, O, N, S, Fe). In: Durand, B. (Ed.): Kerogen - insoluble organic matter from sedimentary rocks. Editions Technip, Paris , 35-53.
EBERL, D.D. & HOWER, J. 1976: Kinetics of illite formation. Bull. geol. Soc. Amer. 87, 1326-1330.
ELLIOTT, W.C., ARONSON, J.L., MATISOFF, G. & GAUTIER, D.L. 1991: Kinetics of the Smectite to Illite Transformation in the Denver Basin: Clay Mineral, K-Ar Data, and Mathematical Model Results. Bull. amer. Assoc. Petroleum Geol. 75, 436-462.
ENGESSER, B., MAYO, N.A. & WEIDMANN, M. 1984: Nouveaux gisements de mammifères dans la Molasse subalpine vaudoise et fribourgeoise. Mém. suisses de Paléont. 107.
ESLINGER, E. & PEVEAR, D. 1988: Clay Minerals. SEPM Short Course 22.
ESPITALIÉ, J. 1986: Use of Tmax as a maturation index for different types of organic matter. Comparison with vitrinite reflectance. In: Burrus, J. (Ed.): Thermal Modeling in Sedimentary Basins. 1st IFP Exploration Research Conference, Carcans, France, June 3-7 1985, Editions Technip - Paris , 475-496.
ESPITALIÉ, J., DEROO, G. & MARQUIS, F. 1985a: La pyrolyse rock-eval et ses applications, première partie. Rev. Inst. franç. Pétrole 40, 563-579.
— 1985b: La Pyrolyse rock-eval et ses applications, deuxième partie. Rev. Inst. franç. Pétrole 40, 755-784.
— 1986: La pyrolyse rock-eval et ses applications, troisième partie. Rev. Inst. franç. Pétrole 41, 73-89.
FANG, H. & JIANYU, C. 1992: The cause and mechanism of vitrinite reflectance anomalies. J. Petrol. Geol. 15, 419-434.
FASEL, J.-M. 1986: Sédimentolgie de la Molasse d'Eau douce Subalpine entre le Léman et la Gruyère. Thèse Univ. Fribourg, Suisse, no.907.
FERMONT, W.J.J. 1988: Possible causes of abnormal vitrinite reflectance values in paralic deposits of the Carboniferous in the Achterhoek area, The Netherlands. Org. Geochem. 12, 401-411.
FERRERO, J. 1966: Nouvelle méthode empirique pour le dosage des minéraux par diffraction R.X. Rapport C.F.P. (Bordeaux), unpubl..
FOSCOLOS, A.E. & STOTT, D.F. 1975: Degree of diagenesis, stratigraphic correlations and potential sediment sources of Lower Cretaceous shale of Northeastern British Columbia Bull. Geol. Surv. Canada 250, 1-46.
FRANCU, J., MÜLLER, P., SUCHA, V. & ZATKALÍKOVÁ, V. 1990: Organic matter and clay minerals as indicators of thermal history in the Transcarpathian Depression (East Slovakian Neogene Basin) and the Vienna Basin. Geol. Zbor. Geol. carpath. (Bratislava) 41, 535-546.
FREI, H.-P. 1979: Stratigraphische Untersuchungen in der subalpinen Molasse der Nordost-Schweiz, zwischen Wägitaler AA und Urnäsch. Mitt. geol. Inst. ETH u. Univ. Zürich (N.F.) 233.
FREY, M. 1986: Very low-grade metamorphism of the Alps - an introduction. Schweiz. mineral. petrograph. Mitt. 66, 13-27.
— 1987: Low temperature metamorphism. Blackie, Glasgow, London.
FREY, M., HUNZIKER, J.C., ROGGWILER, P. & SCHINDLER, C. 1973: Progressive niedriggradige Metamorphose glaukonitführender Horizonte in den helvetischen Alpen der Ostschweiz. Contr. Mineral. and Petrol. 39, 185-218.
FREY, M. , TEICHMÜLLER, M., TEICHMÜLLER, R., MULLIS, J., KÜNZI, B., BREITSCHMID, A., GRUNER, U. & SCHWIZER, B. 1980: Very low-grade metamorphism in external parts of the Central Alps: Illite crystallinity, coal rank and fluid inclusion data. Eclogae geol. Helv. 73, 173-203.
FRIEDMAN, G.M. & SANDERS, J.E. 1978: Principles of sedimentology. Wiley, New York.
FÜCHTBAUER, H. 1964: Sedimentpetrographische Untersuchungen in der älteren Molasse nördlich der Alpen. Eclogae geol. Helv. 57, 157-298.
— 1967: Die Sandsteine in der Molasse nördlich der Alpen. Geol. Rdsch. 56, 266-300.
FÜCHTBAUER, H. & GOLDSCHMIDT, H. 1963: Beobachtungen zur Tonmineral-Diagenese. Proc. Inter. Clay Conf., 1st, Stockholm , 99-111.

FUNK, H.-P. 1985: Mesozoische Subsidenzgeschichte im Helvetischen Schelf der Ostschweiz. Eclogae geol. Helv. 78, 249-272.
GARVEN, G. & FREEZE, R.A. 1984: Theoretical analysis of the role of groundwater flow in the genesis of stratabound ore deposits: 1. Mathematical and numerical model. 2.Quantitative results. American Journal of Science 284, 1085-1174.
GASSER, U. 1966: Sedimentologische Untersuchungen in der äusseren Zone der subalpinen Molasse des Entlebuchs (Kt. Luzern). Eclogae geol. Helv. 59, 723-772.
— 1968: Die innere Zone der subalpinen Molasse des Entlebuchs (Kt. Luzern): Geologie und Sedimentologie. Eclogae geol. Helv. 61, 229-319.
GIGNOUX, M. & MORET, L. 1939: L'Oligocène du bassin du Rhône entre Genève et Seyssel. Étud. Rhodaniennes 15, 139-144.
GIOT, D., FARJANEL, G., GONZALES, G., BARFETY, J.C. & APRAHAMIAN, J. 1987: Evolution thèrmique enregistrée par les sédiments de couverture des massifs cristallins externes (Alpes, Savoie-Isère, France). Relations avec la structuration tectonique. Documents du Bur. Rech. géol. min. 142, GPF3-Thème 5, Novembre 1987.
GLASMANN, J.R., LARTER, S., BRIEDIS, N.A. & LUNDEGARD, P.D. 1989: Shale Diagenesis in the Bergen High Area, North Sea Clays and Clay Minerals 37, 97-112.
GLEADOW, A.J.W., DUDDY, I.R. & LOVERING, J.F. 1983: Fission track analysis: A new tool for the evaluation of thermal histories and hydrocarbon potential. Austral. Petroleum Explor. Assoc. J. 23, 93-102.
GOLDSTEIN, R.H. 1986: Reequilibration of fluid inclusions in low-temperature calcium-carbonate cement. Geology 14, 792-795.
GOODARZI, F. 1985a: Organic petrology of Hat Creek coal deposit No. 1, British Columbia. Int. J. Coal Geol. 5, 377-396.
— 1985b: Optical properties of vitrinite carbonized at different pressures. Fuel 84, 156-162.
— 1987: Comparison of reflectance data from various macerals from sub-bituminous coals. J. of Petroleum Geology 10, 219-226.
GORIN, G.E. & MONTEIL, E. 1990: Preliminary note on the organic facies, thermal maturity and dinoflagellate cysts of the Upper Maastrichtian Wang Formation in the the northern subalpine massifs (Western Alps, France). Eclogae geol. Helv. 83, 265-285.
GORIN, G., GÜLAÇAR, F. & CORNIOLEY, Y. 1989: Organic geochemistry, maturity, palynofacies and palaeoenvironment of Upper Kimmeridgian and Lower Tertiary organic-rich samples in the southern Jura (Ain, France) and subalpine massifs (Haute-Savoie, France). Eclogae geol. Helv. 82, 491-515.
GORIN, G., SIGNER, C. & AMBERGER, G. 1993: Structural configuration of the western Swiss Molasse Basin derived from reflection seismic. Eclogae geol. Helv. 86/3 (in press).
GREEN, P.F., DUDDY, I.R., GLEADOW, A.J.W. & LOVERING, J.F. 1989: Apatite fission track analysis as a paleotemperature indicator for hydrocarbon exploration. In: Naeser, N. & McCulloh, T.H. (Eds.): Thermal history of sedimentary basins: Methods and case histories. Springer-Verlag, New York , 181-195.
GRIESSER, J.-C. & RYBACH, L. 1989: Numerical Thermohydraulic Modeling of Deep Groundwater Circulation in Crystalline Basement: An Example of Calibration. In: Beck, A.E., Garven, G. & Stegena, L. (Eds.): Hydrogeological Regimes and Their Subsurface Thermal Effects. Geophysical Monograph 47, IUGG Vol.2, Washington , 65-74.
GUBLER, T. 1987: Zur Geologie der Oberen Süsswassermolasse zwischen Zürich und Zug. Diplomarbeit, Abteilung für Erdwissenschaften, ETH Zürich, unpubl..
GUELLEC, S., MUGNIER, J.-L., TARDY, M. & ROURE, F. 1990: Neogene evolution of the western Alpine foreland in the light of ECORS data and balanced cross-section. Mém. Soc. géol. France 156, 165-184.
GUYONNET, D. 1988: La structure de la montagne du Grand Crédo (Ain, France). Arch. Sci. Genève 41, 393-408.
HABICHT, J.K.A. 1987: Lexique stratigraphique international. Europe: Plateau Suisse (Molasse). Comm. Géol. Suisse et Serv. Hydrol. et Géol. National 1.
HANTKE, R. 1967: Geologische Karte des Kantons Zürich und seiner Nachbargebiete. Vjschr. natf. Ges. Zürich 112, 91-122.
— 1980: Die Obere Süsswassermolasse der Schweiz, ihr Paläorelief und ihre stratigraphische Fortsetzung in die Vogesenschüttung. Vjschr. naturf. Gesellsch. Zürich 125, 365-374.
HARRISON, T.M. & BÉ, K. 1983: 40Ar/39Ar age spectrum analysis of detrital microclines from southern San Joaquin Basin, California: An approach to determining the thermal evolution of sedimentary basins. Earth planet. Sci. Letters 64, 244-256.
HASZELDINE, R.S., SAMSON, I.M. & CORNFORD, C. 1984: Dating diagenesis in a petroleum basin, a new fluid inclusion method. Nature 307, 354-357.
HÉROUX, Y., CHAGNON, A. & BERTRAND, R. 1979: Compilation and correlation of major thermal maturation indicators. Bull. amer. Assoc. Petroleum Geol. 63, 2128-2144.
HITCHON, B. 1984: Geothermal gradients, hydrodynamics, and hydrocarbon occurrences, Alberta, Canada. Bull. amer. Assoc. Petroleum Geol. 68, 713-743.
HOCHULI, P.A. 1978: Palynologische Untersuchungen im Oligozän und Untermiozän der Zentralen und Westlichen Paratethys Beitr. Paläont. Oesterr. 4, 1-132.
HOFFERS, B. 1981: A model for hydrothermal convection in the Rhine Graben and its tectonic implications. Tectonophysics 73, 141-149.

HOFFMAN, J. & HOWER, J. 1979: Clay mineral assemblages as low grade metamorphic geothermometers: application to the thrust faulted disturbed belt of Montana, USA. SEPM Spec. Publ. 26, 55-79.
HOFMANN, F. 1951: Zur Stratigraphie und Tektonik des st. gallisch-thurgauischen Miozäns (Obere Süsswassermolasse) und zur Bodenseegeologie. Ber. st. gall. natw. Ges. 74, 3-87.
— 1960: Beitrag zur Kenntnis der Glimmersandsedimentation in der oberen Süsswassermolasse der Nord- und Nordostschweiz. Eclogae geol. Helv. 53, 1-25.
HOLLISTER, L.S. & CRAWFORD, M.L. 1981: Fluid inclusions: applications to petrology. Min. Assoc. Canada Short Course Handbook 6, .
HOMEWOOD, P. 1981: Faciès et environnements de dépôt de la Molasse de Fribourg. Eclogae geol. Helv. 74, 29-36.
HOMEWOOD, P., ALLEN P.A. & WILLIAMS, G.D. 1986: Dynamics of the Molasse Basin of western Switzerland. Spec. Publ. int. Ass. Sediment. 8, 199-217.
HOMEWOOD, P., ALLEN, P.A. & YANG, C.S. 1985: Palaeotidal range estimates from the Miocene Molasse. Abstr. 6th int. Ass. Sediment. Reg. Mtg. Lleida, 200-201.
HOMEWOOD, P., KELLER, B., SCHOEPFER, P. & YANG, C.S. 1989: Faciès, processus de sédimentation et reconstitution des conditions paléomarines dans la Molasse marine supérieure suisse. Bull. Soc. géol. France 8, 1015-1027.
HOMEWOOD, P., RIGASSI, D. & WEIDMANN, M. 1989: Le bassin molassique suisse. In: Purser, B.H. (Ed.), Dynamique et méthodes d'étude des bassins sédimentaires. Éditions Technip, Paris , 299-314.
HORVÁTH, Z.A. 1983: Study on maturation process of huminitic organic matter by means of high-pressure experiments. Acta geol. Hungarica 26, 137-148.
HOWER, J. 1981: Shale diagenesis. In: Longstaffe, F.J. (Ed): Clays and the Resource Geologist. Min. Assoc. of Canada, Short Course Handbook 7, 60-80.
HOWER, J., ESLINGER, E.V., HOWER, M.E. & PERRY, E.A. 1976: Mechanism of burial metamorphism of argillaceous sediment: 1.Mineralogical and chemical evidence. Bull. geol. Soc. Amer. 87, 725-737.
HUGGENBERGER, P. & WILDI, W. 1991: La tectonique du massif des Bornes (Chaînes Subalpines, Haute-Savoie, France). Eclogae geol. Helv. 84, 125-149.
HUTTON, A.C. & COOK, A.C. 1980: Influence of alginite on the reflectance of vitrinite from Joadja, NSW, and some other coals and oil shales containing alginite. Fuel 59, 711-714.
ILLIES, J.H. 1974: Intra-Plattentektonik in Mitteleuropa und der Rheintalgraben. Oberrhein. geol. Abhandl. 23, 1-24.
— 1975: Intraplate tectonics in stable Europe as related to plate tectonics in the Alpine system. Geol. Rdsch. 64, 677-699.
— 1977: Ancient and recent rifting in the Rhinegraben. Geol. Mijnbouw 56, 329-350.
INGRAM, G.R. & RIMSTIDT, J.D. 1984: Natural weathering of coal. Fuel 63, 292-296.
INOUE, A., BOUCHET, A., VELDE, B. & MEUNIER, A. 1989: Convenient Technique for Estimating Smectite Layer Percentage in Randomly Interstratified Illite/Smectite Minerals. Clays and Clay Minerals 37, 227-234.
INTERNATIONAL COMMITTEE FOR COAL PETROLOGY 1963: International handbook of coal petrography - 2nd edition. Centre National de la Recherche Scientifique, Paris, France.
— 1971: International handbook of coal petrography, 1st supplement to 2nd edition. Centre National de la Recherche Scientifique, Paris, France.
JACOB, H. & KUCKELKORN, K. 1977: Das Inkohlungsprofil der Bohrung Miesbach 1 und seine erdölgeologische Interpretation. Erdöl-Erdgas-Zeitschrift 93, 115-124.
JACOB, H., KUCKELKORN, K. & MÜLLER, M. 1982: Inkohlung und Tektonik im Bereich der gefalteten Molasse. Insbesondere am Beispiel der Bohrung Staffelsee 1. Erdöl und Kohle-Erdgas-Petrochemie vereinigt mit Brennstoffchemie 35, 510-518.
JOHNS, W.D. & KURZWEIL, H. 1979: Quantitative estimation of illite-smectite mixed phases formed during burial diagenesis. TMPM Tschermaks Min. Petr. Mitt. 26, 203-215.
JONES, J.M., MURCHISON, D.G. & SALEH, S.A. 1972: Variation of vitrinite reflectivity in relation to lithology. In: Van Gaertner, H.R. & Wehner, H. (Eds.): Advances in organic geochemistry. 1971, Pergamon Press, Oxford, 601-612.
JORDI, H.A. 1990: Tektonisch-strukturelle Uebersicht Westschweizerisches Molassebecken. Bull. Ver. Schweiz. Petroleum-Geol. u. -Ing. 56/130, 1-11.
JUNG, P. 1982: Nouveaux résultats biostratigraphiques dans le bassin molassique, depuis le Vorarlberg jusqu'en Haute-Savoie. Doc. Lab. Géol. Fac. Sci. Lyon, h.s. 7, 1-91.
KAEGI, D.D. 1985: On the identification and origin of pseudovitrinite. Int. J. Coal Geology 4, 309-319.
KÄLIN, B., RYBACH, L. & KEMPTER, E.H.K. 1992: Rates of Deposition, Uplift and Erosion in the Swiss Molasse Basin, Estimated from Sonic- and Density-Logs. Bull. Ver. schweiz. Petroleum-Geol. u. -Ing. 58/133, 9-22.
KALKREUTH, W.D. 1982: Rank and petrographic composition of selected Jurassic-Lower Cretaceous coals of British Columbia, Canada. Bull. Canad. Petrol. Geol. 30, 112-139.
KARNER, G.D. & DEWEY, J.F. 1986: Rifting: lithospheric versus crustal extension as applied to the Ridge Basin of southern California. In: Halbouty, M.T. (Ed.): Future petroleum provinces of the world. Mem. amer. Assoc. Petroleum Geol. 40, 317-337.
KARWEIL, J. 1956: Die Metamorphose der Kohlen vom Standpunkt der physikalischen Chemie Z. Dtsch. Geol. Ges. 107, 132-139.
KATZ, B.J. 1983: Limitations of "Rock-Eval" pyrolysis for typing organic matter. Org. Geochem. 4, 195-199.

KELLER, B. 1989: Fazies und Stratigraphie der Oberen Meeresmolasse (unteres Miozän) zwischen Napf und Bodenseegebiet. Thèse Univ. Bern, Schweiz.
— 1990: Wirkung von Wellen und Gezeiten bei der Ablagerung der Oberen Meeresmolasse. Mitt. natf. Ges. Luzern 31, 245-271.
— 1992: Hydrogeologie des schweizerischen Molasse-Beckens: Aktueller Wissensstand und weiterführende Betrachtungen. Eclogae geol. Helv. 85, 611-652.
KELLER, B., BLÄSI, H.-R., PLATT, N.H., MOZLEY, P.S. & MATTER, A. 1990: Sedimentäre Architektur der distalen Unteren Süsswassermolasse und ihre Beziehung zur Diagenese und den petrophysikalischen Eigenschaften am Beispiel der Bohrungen Langenthal. Nagra techn. Ber. 90-41, Baden.
KELLER, W.D., REYNOLDS, R.C. & INOUE, A. 1986: Morphology of clay minerals in the smectite-to-illite conversion series by scanning electron microscopy. Clays and Clay Min. 34, 187-197.
KEMPTER, E.H.K. 1987: Fossile Maturität, Paläothermogradienten und Schichtlücken in der Bohrung Weiach im Lichte von Modellberechnungen der thermischen Maturität. Eclogae geol. Helv. 80, 543-552.
KINDLER, P. 1986: Découverte du Paléocène supérieur-Eocène inférieur dans l'Ultrahelvétique savoyard (Préalpes chablaisiennes, France). Conséquences sédimentologiques et paléogéographiques. C.R. Ac. Sci. Paris t. 303, Série II, 1725-1730.
- 1988: Géologie des wildflyschs entre Arve et Giffre (Haute-Savoie, France). Publ. du Dép. de Géologie et de Paléontologie 6, Université de Genève, Suisse.
KISCH, H.J. 1980: Illite crystallinity and coal rank associated with lowest-grade metamorphism of the Taveyanne greywacke in the Helvetic zone of the Swiss Alps. Eclogae geol. Helv. 73, 753-777.
KISCH, H.J. 1983: Mineralogy and petrology of burial diagenesis (burial metamorphism) and incipient metamorphism in clastic rocks. In: Larsen, G. & Chilingar, G.V. (Eds.): Diagenesis in Sediments and Sedimentary Rocks (2). Dev. in Sedimentology 25B, Elsevier, Amsterdam, Oxford, New York, 289-493.
- 1987: Correlation between indicators of very low-grade metamorphism. In: Frey, M. (Ed.): Low temperature metamorphism. Blackie, Glasgow, London , 227-300.
KISSLING, D. 1974: L'Oligocène de l'extrémité occidentale du bassin molassique suisse. Stratigraphie et aperçu molassique. Thèse Univ. Genève, Suisse, No. 1648.
KOJIMA, K. & OGOSHI, H. 1973: Petrographic consideration of weathered coal. J. Fuel Soc. Jpn. 52, 885-895.
KRUMM, H., PETSCHICK, R. & WOLF, M. 1988: From diagenesis to anchimetamorphism, upper Austroalpine sedimentary cover in Bavaria and Tyrol. Geodinamica Acta 2, 33-47.
KÜBLER, B. 1964: Les argiles indicateurs de metamorphisme. Rev. Inst. franç. Pétrole 19, 1093-1112.
— 1968: Evaluation quantitative du métamorphisme par la cristallinité de l'illite. Bull. Cent. Rech. Pau-SNPA 2, 385-397.
— 1970: La composition des fractions fines et la distinction flysch-molasse dans le domaine alpin et périalpin. Bull. Soc. géol. France 7, 599-602.
— 1973: La corrensite, indicateur possible de milieux de sédimentation et du degré de transformation d'un sédiment. Bull. Cent. Rech.-Expl. Elf-Aquitaine Pau-SNPA 7, 543-556.
— 1983: Dosage quantitatif des minéraux majeurs des roches sédimentaires par diffraction X. Cah. Inst. Géol. Neuchâtel, Série AX N°1.1 & 1.2.
— 1984: Les indicateurs des transformation physiques et chimiques dans la diagenese: température et calorimétrie. In: Lagache, M. (Ed.): Thermométrie et barométrie géologiques. Soc. Franç. Min. et Crist., Paris 2, 489-596.
— 1987: Cristallinité de l'illite: méthodes normalisées de préparation, méthode normalisée de mesure, méthode automatique normalisée de mesure. Cah. Inst. Géol. Neuchâtel, A.D.X. série No. 2 (43).
— 1990: "Cristallinité" de l'illite et mixed-layers: brève révision. Schweiz. Mineral. Petrogr. Mitt. 70, 89-93.
KÜBLER, B., MARTINI, J. & VUAGNAT, M. 1974: Very low grade metamorphism in the Western Alps. Schweiz. mineral. petrogr. Mitt. 54, 461-469.
KÜBLER, B., PITTION, J.-L., HÉROUX, Y., CHAROLLAIS, J & WEIDMANN, M. 1979: Sur le pouvoir réflecteur dela vitrinite dans quelques roches du Jura, de la Molasse et des Nappes préalpines, helvétiques et penniques (Suisse occidentale et Haute-Savoie). Eclogae geol. Helv. 72, 347-373.
KUCKELKORN, K., HILTMANN, W. & SCHWERD, K. 1990: Zur Maturität und Erdölbildung in den Allgäuer Alpen (1). Erdöl Erdgas Kohle 106, 7-11.
LACOMBE, O., ANGELIER, J., BERGERAT, F. & LAURANT, PH. 1990: Tectoniques superposées et perturbations de contrainte dans la zone transformante Rhin-Saône: apport de l'analyse des failles et des macles de la calcite. Bull. Soc. géol. France 8, 853-863.
LAM, H.L., JONES, F.W. & LAMBERT, C. 1982: Geothermal gradients in the Hinton area of west-central Alberta. Can. J. Earth Sci. 19, 755-766.
LANDAIS, P., MONTHIOUX, M. & MEUNIER, J.-D. 1984: Importance of the oxidation/maturation pair in the evolution of humic coals. Org. Geochem. 7, 249-260.
LANSON, B. & CHAMPION, D. 1991: The I/S-to-illite reaction in the late stage of diagenesis. Amer. J. Sci. 291, 473-506.
LANSON, B. & VELDE, B. 1992: Decomposition of X-ray diffraction patterns: a convenient way to describe complex I/S diagenetic evolution. Clays and Clay Min. 40, 629-643.
LARTER, S. 1989: Chemical models of vitrinite reflectance evolution. Geol. Rdsch. 78, 349-359.

LATELTIN, O. 1988: Les dépôts turbiditiques oligocènes d'avant-pays entre Annecy (Haute-Savoie) et le Sanetsch (Suisse). Thèse Univ. Fribourg, Suisse, No.949.
LAUBSCHER, H.P. 1974: Basement uplift and decollement in the Molasse Basin. Eclogae geol. Helv. 67, 531-537.
— 1982: Die Südostecke des Rheintalgrabens - ein kinematisches und dynamisches Problem. Eclogae geol. Helv. 75, 101-116.
— 1986: The eastern Jura: Relation between thin-skinned and basement tectonics, local and regional. Geol. Rdsch. 75, 535-553.
— 1987: Die tektonische Entwicklung der Nordschweiz. Eclogae geol. Helv. 80, 287-303.
— 1992: Jura kinetics and the Molasse Basin. Eclogae geol. Helv. 85, 653-675.
LEJAY, A. 1991: Stratigraphie haute-résolution des dépôts de marées du bassin molassique suisse. Thèse Univ. Louis Pasteur Strasbourg, France, (unpubl.).
LEMCKE, K. 1959: Das Profil der Bohrung Chapelle 1. Bull. Ver. schweiz. Petroleum-Geol. u. -Ing. 26/70, 25-29.
— 1963: Die Ergebnisse der Bohrung Savigny1 bei Lausanne. Bull. Ver. schweiz. Petroleum-Geol. u. -Ing. 30/78, 4-11.
— 1972: Die Lagerung der jüngsten Molasse im nördlichen Alpenvorland. Bull. Ver. schweiz. Petroleum-Geol. u. -Ing. 39/95, 29-41.
— 1973: Zur nachpermischen Geschichte des nördlichen Alpenvorlandes. Geologica bavar. 69, 5-48.
— 1974: Vertikalbewegungen des vormesozoischen Sockels im nördlichen Alpenvorland vom Perm bis zur Gegenwart. Eclogae geol. Helv. 67, 121-133.
— 1988: Geologie von Bayern. I. Das bayerische Alpenvorland vor der Eiszeit. Erdgeschichte-Bau-Bodenschätze. E. Schweizerbart'sche Verlagsbuchhandlung (Nägele u. Obermiller), Stuttgart.
LEMCKE, K., BÜCHI, U.P. & WIENER, G. 1968: Einige Ergebnisse der Erdölexploration auf die mittelländische Molasse der Zentralschweiz. Bull. Ver. schweiz. Petroleum-Geol. u. -Ing. 35/87, 15-34.
LEMCKE, K. & WAGNER, R. 1961: Zur Kenntnis des vortertiären Untergrundes im Bodenseegebiet. Bull. Ver. schweiz. Petroleum-Geol. u. -Ing. 27/73, 9-14.
LEWIS, T. 1990: Fluids and Heat Flow. In: Nesbitt, B.E. (Ed.): Short Course on Fluids in Tectonically Active Regimes of the Continental Crust. Min. Assoc. of Canad., Short Course Handbook 18, Vancouver, 49-74.
LINIGER, H. 1925: Geologie des Delsberger Beckens und der Umgebung von Monvelier. Matér. Carte géol. Suisse (n.s.) 55.
LIPPMANN, F. 1954: Über einen Keuperton von Zaiserweiher bei Maulbronn. Heidelb. Beitr. Mineral. Petrogr. 4, 130-134.
— 1956: Clay minerals from the Röt member of the Triassic near Göttingen, Germany. J. sedim. Petrol. 26, 125-139.
LIPPMANN, F. & ROTHFUSS, H. 1980: Tonminerale in Taveyannaz-Sandsteinen. Schweiz. mineral. petrogr. Mitt. 60, 1-29.
LOHR, J. 1967: Die seismischen Geschwindigkeiten in der Ostschweiz. Bull. Ver. schweiz. Petroleum-Geol. u. -Ing. 34, 29-38.
LOPATIN, N.V. 1971: Temperature and geologic time as factors in coalification Akad. Nauk. SSSR, ser. geol. Izvestiya 3, 95-106.
LOUP, B. 1992a: Evolution de la partie septentrionale du domaine helvétique en Suisse occidentale au Trias et au Lias: contrôle par subsidence thermique et variations du niveau marin. Publications du Département de Géologie et de Paléontologie 12, Université de Genève, Suisse.
— 1992b: Mesozoic subsidence and stretching models of the lithosphere in Switzerland (Jura, Swiss Plateau and Helvetic realm). Eclogae geol. Helv. 85, 541-572.
MAJOROWICZ, J.A., JONES, F.W., LAM, H.L. & JESSOP, A.M. 1984: The variability of heat flow both regional and with depth in Southern Alberta, Canada: effect of groundwater flow? Tectonics 106, 1-29.
MARCHIONI, D.L. 1983: The detection of weathering in coal by petrographic, rheologic and chemical methods. Int. J. Coal Geol. 2, 231-259.
MATHIEU, Y. & VELDE, B. 1989: Identification of thermal anomalies using clay mineral composition. Clay Minerals 24, 591-602.
MATTER, A., HOMEWOOD, P., CARON, C., VANSTUIJVENBERG, J., WEIDMANN, M. & WINKLER, W. 1980: Flysch and Molasse of Western and Central Switzerland. In: Trümpy, R. (Ed.): Geology of Switzerland: A Guide Book. Part B: Geological Excursions, Schweiz. Geol. Komm., Wepf & Co. Publishers, Basel, New York, 261-293.
MATTER, A., PETERS, T., BLÄSI, H.-R., MEYER, J., ISCHI, H. & MEYER, C. 1988a: Sondierbohrung Weiach - Geologie, Textband. Nagra techn. Ber. NTB 86-01, Nagra, Baden.
MATTER, A., PETERS, T., BLÄSI, H.-R., SCHENKER, F. & WEISS, H.-P. 1988b: Sondierbohrung Schafisheim - Geologie, Textband. Nagra techn. Ber., NTB 86-03, Nagra, Baden.
MATTER, A., PETERS, T., ISENSCHMID, C., BLÄSI, H.-R. & ZIEGLER, H.-J. 1987: Sondierbohrung Riniken - Geologie, Textband. Nagra techn. Ber., NTP 86-02, Nagra, Baden.
MATTER, A. & WEIDMANN, M. 1992: Tertiary sedimentation in the Swiss Molasse: an overview. Eclogae geol. Helv. 85, 776-777.
MAURER, H., GERBER, M.E., & NABHOLZ, W. 1982: Sedimentpetrographie und Lithostratigraphie der Molasse im Einzugsgebiet der Langete. Eclogae geol. Helv. 75, 381-413.

MCCARTNEY, J.T. & TEICHMÜLLER, M. 1972: Classification of coals according to degree of coalification by reflectance of the vitrinite component. Fuel 51, 64-68.
MCCARTY, D.K. & THOMPSON, G.R. 1991: Burial Diagenesis in Two Montana Tertiary Basins. Clays and Clay Min. 39, 293-305.
MCCULLOH, T.H. & NAESER, N.D. 1989: Thermal History of Sedimentary Basins: Introduction and Overview. In: Naeser, N.D. & McCulloh, T.H. (Eds.): Thermal History of Sedimentary Basins: Methods and Case Histories. Springer-Verlag, New-York, Berlin, London, Paris, Tokyo, 1-11.
MCDONALD, D.A & SURDAM, R.C. 1984: Clastic Diagenesis. Mem. amer. Assoc. Petroleum Geol. 37.
MEIER, R., HURTIG, E. & LUDWIG, A. 1979: Fault Tectonics and Heat Flow in Europe. In: Cermak, V. & Rybach, L. (Eds.): Terrestrial heat flow in Europe. Springer Verlag, Heidelberg, Berlin, New York , 112-118.
MEUNIER, J.D. 1989: Assessment of low-temperature fluid inclusions in calcite using microthermometry. Economic Geology 84, 167-170.
MICHEL, P. & CAILLON, G. 1957: Quelques résultats des sondages exécutés en Savoie par la Régie Autonome des Pétroles. Bull. Soc. géol. France 6, 995-1008.
— 1960: Quelque précisions apportées par les récents travaux de la Régie autonome des pétroles en Savoie. C.R. Soc. géol. France 3, 53-54.
MILLOT, G. 1963: Géologie des argiles. Masson, Paris.
MILLOT, G. 1970: Geology of clays. Springer-Verlag, New York.
MONNIER, F. 1979: Corrélations minéralogiques et diagenèse dans le bassin molassique suisse. Thèse Univ. Neuchâtel, Suisse.
— 1982: Thermal diagenesis in the Swiss molasse basin: implications for oil generation. Can. J. Earth Sci. 19, 328-342.
MOORE, D.M. & REYNOLDS, R.C. 1989: X-ray diffraction and the identification and analysis of clay minerals. Oxford University Press, Oxford, New York.
MORET, L. 1934: Géologie du massif des Bornes et des klippes préalpines des Annes et de Sulens (Haute-Savoie). Mém. Soc. géol. France, n.s. 22.
MORGAN, P. 1982: Heat flow in rift zones. In: Palmason, G. (Ed.): Continental and oceanic rifts. American Geophysical Union, Geodynamic Series 8, 107-122.
MORNOD, L. 1949: Géologie de la région de Bulle (Basse-Gruyère). Molasse et bord alpin. Matér. Carte géol. Suisse (n.s.) 91.
MORRISON, S.J. & PARRY, W.T. 1986: Dioctahedral corrensite from Permian Red Beds, Lisbon Valley, Utah. Clays and Clay Min. 34, 613-624.
MOSAR, J. 1988: Métamorphisme transporté dans les Préalpes Schweiz. Mineral. Petrogr. Mitt. 68, 77-94.
MOSS, S.J. 1992a: Burial diagenesis, organic maturation and tectonic loading in the French Subalpine chains, S.E. France. Thesis University of Durham, GB, (unpubl.).
— 1992b: Organic maturation in the French Subalpine Chains: regional differences in burial history and the size of tectonic loads. J. geol. Soc. London 149, 503-515.
MUGNIER, J.-L. & MENARD, G. 1986: Le développement du bassin molassique suisse et l'évolution des Alpes externes: un modèle cinématique. Bull. Cent. Rech. Explor.-Prod. Elf-Aquitaine 10, 167-180.
MÜLLER, W.H., HUBER, M., ISLER, A. & KLEBOTH, P. 1984: Erläuterungen zur geologischen Karte der zentralen Nordostschweiz 1:100'000. Nagra techn. Ber. 84-25, Baden.
MULLIS, J. 1987a: Fluid inclusion studies during very low-grade metamorphism. In: M.Frey (ed.): Low temperature metamorphism. Blackie, Glasgow-London , 162-199.
— 1987b: Fluideinschluss-Untersuchung in den Nagra-Bohrungen der Nordschweiz. Eclogae geol. Helv. 80, 553-568.
MURCHISON, D.G., PEARSON, J. & RAYMOND, A.C. 1991: Anomalies in vitrinite reflectance gradients. Bull. Soc. géol. France 162, 183-191.
NAEF, H., DIEBOLD, P. & SCHLANKE, S. 1985: Sedimentation und Tektonik im Tertiär der Nordschweiz. Nagra techn. Ber. 85-14, Baden.
NAESER, C.W. 1979: Thermal history of sedimentary basins: fission-track dating of subsurface rocks. SEPM Spec. Publ. 26, 109-112.
— 1981: The fading of fission tracks in the geologic environment: Data from deep drill holes. Nuclear Tracks 5, 248-250.
NAGRA 1988: Sedimentstudie -Zwischenbericht 1988. Möglichkeiten zur Endlagerung langlebiger radioaktiver Abfälle in den Sedimenten der Schweiz. Nagra techn. Ber., 88-25.
NESBITT, B.E. 1990: Short Course on Fluids in Tectonically Active Regimes of the Continental Crust. Min. Assoc. of Canad., Short Course Handbook 18, Vancouver.
NEWMAN, J. & NEWMAN, N.A. 1982: Reflectance anomalies in Pike River coals: evidence of variability in vitrinite type, with implications for maturation studies and "Suggate rank". New Zealand J. Geol. Geophys. 25, 233-243.
OLIVER, J. 1986: Fluids expelled tectonically from orogenic belts: Their role in hydrocarbon migration and other geologic phenomena. Geology 14, 99-102.
OTTENJANN, K., TEICHMÜLLER, M. & WOLF, M. 1974: Spektrale Fluoreszenz-Messungen an Sporiniten mit Auflicht-Anregung, eine mikroskopische Methode zur Bestimmung des Inkohlungsgrades gering inkohlter Kohlen. Fortschr. Geol. Rheinld. u. Westf. 24, 1-36.

OXBURGH, E.R. & TURCOTTE, D.L. 1974: Thermal gradients and regional metamorphism in overthrust terrains with special reference to the eastern Alps. Schweiz. mineral. petrogr. Mitt. 54, 641-662.
PAVONI, N. 1955: Molassetektonik, Terrassen und Schotter zwischen Glattal, Oberem Zürichsee und Sihltal. Eclogae geol. Helv. 48, 360-363.
— 1956: Zürcher Molasse und Obere Süsswassermolasse der Ostschweiz, ein stratigraphischer Vergleich. Bull. Ver. schweiz. Petroleum-Geol. u. -Ing. 23/63, 25-32.
— 1957: Geologie der Zürcher Molasse zwischen Albis und Pfannenstil. Vjschr. naturf. Gesellsch. Zürich 102, 117-315.
— 1987: Die Seismotektonik der Nordschweiz. Eclogae geol. Helv. 80, 461-472.
PEARSON, D.E. & KWONG, H. 1979: Mineral matter as a measure of oxidation of a coking coal. Fuel 58, 63-66.
PEARSON, J. & MURCHISON, D.G. 1989: Influence of a sandstone washout on the properties of an underlying coal seam. Fuel 69, 251-253.
PEARSON, M.J. & SMALL, J.S. 1988: Illite-smectite diagenesis and palaeotemperatures in northern North Sea Quaternary to Mesozoic shale sequences. Clay Minerals 23, 109-132.
PERRY, E. & HOWER, J. 1970: Burial diagenesis in Gulf Coast pelitic sediments. Clays and Clay Min. 18, 165-177.
PERSON, M. & GARVEN, G. 1992: Hydrologic constraints on petroleum generation within continental rift basins: Theory and application to the Rhine Graben. Bull. amer. Assoc. Petroleum Geol. 76, 468-488.
PERSOZ, F. 1969: Fidélité de l'analyse quantitative des poudres de roches par diffraction X. Bull. Cent. Rech. Pau-SNPA 3, 329-355.
PETERS, K.E. 1986: Guidelines for Evaluating Petroleum Source Rock Using Programmed Pyrolysis. Bull. amer. Assoc. Petroleum Geol. 70, 318-329.
PETSCHICK, R. & FERREIRO MÄHLMANN, R. 1992: Paleogeothermal history of the Northern Calcareous Alps (western section) - geodynamic consequences. Terra Nova Abstract Supplement 2, ALCAPA meeting, Graz, Austria , 52-53.
PETTIJOHN, F.J., POTTER, P.E. & SIEVER, R. 1987: Sand and sandstones. Second edition. Springer Verlag, New York, Berlin, Heidelberg, London, Paris, Tokyo.
PFIFFNER, A.O. 1986: Evolution of the north Alpine foreland basin in the Central Alps. Spec. Publs. int. Ass. Sediment. 8, 219-228.
PITTMAN, E.D. 1979: Recent advances in sandstone diagenesis. Ann. Rev. Earth planet. Sci. 7, 39-62.
PLATT, N.H. 1992: Fresh-water carbonates from the Lower Freshwater Molasse (Oligocene, western Switzerland): sedimentology and stable isotopes. Sediment. Geol. 78, 81-99.
POLLASTRO, R.M. 1985: Mineralogical and morphological evidence for the formation of illite at the expense of illite/smectite. Clays and Clay Min. 33, 265-274.
POLLASTRO, R.M. & BARKER, C.E. 1986: Application of clay-mineral, vitrinite reflectance, and fluid inclusion studies to the thermal and burial history of the Pinedale anticline, Green River Basin, Wyoming. SEPM Spec. Publ. 38, 73-83.
POTTER, R.W. 1977: Pressure corrections for fluid inclusion homogenization temperatures based on volumetric properties of the system NaCl-H2O. J. Res. U.S. Geol. Survey 5, 603-607.
POTTER, R.W., CLYNNE, M.A. & BROWN, D.L. 1978: Freezing point depression of aqueous sodium chloride solutions. Economic Geol. 73, 284-285.
POWERS, M.C. 1959: Adjustement of clays to chemical changes and the concept of equivalue level. Clays and Clay Min. 6, 309-326.
PREZBINDOWSKI, D.R. & LARESE, R.E. 1987: Experimental stretching of fluid inclusions in calcite- Implications for diagenetic studies. Geology 15, 333-336.
PRICE, L.C. 1983: Geologic time as a parameter in organic metamorphism and vitrinite reflectance as an absolute paleogeothermometer. J. of Petroleum Geology 6, 5-38.
PRICE, L.C. & BARKER, C.E. 1985: Suppression of vitrinite reflectance in amorphous rich kerogen - a major unrecognized problem. J. Petrol. Geol. 8, 59-84.
PYTTE, A.M. & REYNOLDS, R.C. 1989: The Thermal Transformation of Smectite to Illite. In: Naeser, N.D. & McCulloh, T.H. (Eds.): Thermal History of Sedimentary Basins: Methods and Case Histories. Springer-Verlag, New-York, Berlin, London, Paris, Tokyo, 133-140.
QUIGLEY, T.M., MACKENZIE, A.S. & GRAY, J.R. 1987: Kinetic theory of petroleum generation. In: Doligez, B. (Ed.): Migration of hydrocarbons in sedimentary basins. Editions Technip, Paris , 649-665.
RAMSEYER, K. 1987: Diagenese des Buntsandsteins und ihre Beziehung zur tektonischen Entwicklung der Nordschweiz. Eclogae geol. Helv. 80, 383-395.
RAMSEYER, K. & BOLES, J.R. 1986: Mixed-Layer Illite/Smectite Minerals in Tertiary Sandstones and Shales, San Joaquin Basin, California Clays and Clay Min. 34, 115-124.
REGGIANI, L. 1989: Faciès lacustres et dynamique sédimentaire dans la Molasse d'eau douce inférieure Oligocène (USM) de Savoie. Eclogae geol. Helv. 82, 325-350.
RETTKE, R.C. 1981: Probable Burial Diagenetic and Provenance Effects on Dakota Group Clay Mineralogy, Denver Basin. Jour. Sed. Petrology 51, 541-551.
REY, J.-PH. & KÜBLER, B. 1983: Identification des micas des séries sedimentaires par diffraction X à partir de la série harmonique (00l) des préparations orientées Schweiz. mineral. petrogr. Mitt. 63, 13-36.

REYNOLDS, R.C. & HOWER, J. 1970: The Nature of Interlayering in Mixed-Layer Illite-Montmorillonites. Clays and Clay Minerals 18, 25-36.
REYNOLDS, R.C.JR. 1988: Mixed layer chlorite minerals. In: Bailey, S.W. (Ed.): Hydrous phyllosilicates (exclusive of micas). Min. Soc. Amer., Reviews in Mineralogy 19, 601-630.
RHOADES, A.H., BARBARINO, O.C. & GRAY, R.J. 1975: Coal rank parameters related to depth of burial for West Virginia high volatile coal. Abstr. Prog. Geol. Soc. Amer. 7, 1243.
RIGASSI, D.A. 1957: Le Tertiaire de la région Genevoise et Savoisienne. Bull. Ver. Schw. Petr.-Geol. u. Ing. 24/66, 19-34.
— 1977: Subdivision et datation de la Molasse "d'Eau Douce Inférieure" du Plateau Suisse. Paleolab News 1, 1-42.
ROBERSON, H.E. & LAHANN, R.W. 1981: Smectite to illite conversion rates: effect of solution chemistry. Clays and Clay Min. 29, 129-135.
ROBERT, P. 1985: Histoire géothermique et diagenèse organique. Bull. Cent. Rech. Expl.-Prod. Elf-Aquitaine, Mém.8, Pau.
ROBERTS, G. 1990: Structural controls on fluid migration in foreland thrust belts. In: Letouzey, J. (Ed.): Petroleum and tectonic in mobile belts. Editions Technip, Paris , 193-210.
— 1991: Structural controls on fluid migration through the Rencurel thrust zone, Vercors, French Sub-Alpine chains. In: England, W.A. & Fleet, A.J. (Eds.), Petroleum migration. Geol. Soc. Spec. Publ. 59 , 245-262.
ROEDDER, E. 1981: Origin of fluid inclusions and changes that occur after trapping. In: Hollister, L.S. & Crawford, M.L. (Eds.): Fluid inclusions: application to petrology. Min. Assoc. Canada, Short Course 6, 101-137.
— 1984: Fluid inclusions. Min. Soc. Amer., Reviews in Mineralogy 12, .
ROEDDER, E. & BODNAR, R.J. 1980: Geologic pressure determinations from fluid inclusion studies. Ann. Rev. Earth planet. Sci. 8, 263-301.
ROLLI, M. 1992: A basic computer program for the semi-quantitative analysis of mineral abundances in bulk rocks by X-ray powder diffraction. Lab. Minér., Pétrogr. & Géochim., Inst. Géol. Neuchâtel, Switzerland, (unpubl.).
ROSSET, J., CHAROLLAIS, J., TOUMARKINE, M., MANIVIT, H., CHATEAUNEUF, J.-J. & SCHAUB, H. 1976: Présentation des différentes unités du synclinal de Thônes (Haute-Savoie, France). Eclogae geol. Helv. 69, 359-402.
RUCHAT, C. 1977: Carte tectonique de la région du Genevois (1/50000). Serv. Cantonal de Géol., Genève, réf. 100.77.2, Suisse.
RYBACH, L. 1984: The paleogeothermal conditions of the Swiss molasse basin: implication for hydrocarbon potential. Rev. Inst. franç. Pétrole 39, 143-146.
RYBACH, L. & BODMER, P. 1980: Die geothermischen Verhältnisse der Schweizer Geotraverse im Abschnitt Basel-Luzern Eclogae geol. Helv. 73, 501-512.
RYBACH, L., EUGSTER, W. & GRIESSER, J.-C. 1987: Die geothermischen Verhältnisse in der Nordschweiz. Eclogae geol. Helv. 80, 521-534.
SAVIN, S.M. & LEE, M. 1984: Estimation of subsurface temperatures from oxygen isotope ratios of minerals. In: Durand, B. (Ed.): Thermal phenomena in sedimentary basins. Editions Technip, Paris, 65-70.
SAWATZKI, G. 1975: Etude géologique et minéralogique des flyschs à grauwackes volcaniques du synclinal de Thônes (Haute-Savoie, France). Arch. Sci. (Genève) 28, 265-368.
SCHAAD, W., KELLER, B. & MATTER, A. 1992: Die Obere Meeresmolasse (OMM) am Pfänder: Beispiel eines Gilbert-Deltakomplexes. Eclogae geol. Helv. 85, 145-168.
SCHAER, J.-P. 1992: Tectonic evolution and vertical movement in Western Switzerland. Eclogae geol. Helv. 85, 695-699.
SCHEGG, R. 1992: Coalification, shale diagenesis and thermal modelling in the Alpine Foreland basin: the Western Molasse basin (Switzerland/France) Org. Geochemistry 18, 289-300.
— 1992: Thermal maturity of the Swiss Molasse Basin: Indications for paleogeothermal anomalies? Eclogae geol. Helv. 85, 745-764.
SCHEGG, R. & MORITZ, R. 1993: Indications for paleogeothermal anomalies in the Molasse Basin (Switzerland & France). In: Parnell, J., Ruffell, A.H. & Moles, N.R. (Eds.): Geofluids '93, Contributions to an International Conference on fluid evolution, migration and interaction in rocks. Torquay, England, May 4-7, 1993 , 96-99.
SCHERER, F. 1966: Geologisch-palaeontologische Untersuchungen im Flysch und in der Molasse zwischen Thunersee und Eriz (Kt. Bern). Matér. Carte géol. Suisse (n.s.) 127.
SCHLANKE, S., HAUBER, L. & BÜCHI, U.P. 1978: Lithostratigraphie und Sedimentpetrographie der Molasse in den Bohrungen Tschugg 1 und Ruppoldsried 1. Eclogae geol. Helv. 71, 409-425.
SCHLUNEGGER, F. 1991: Stratigraphie, Sedimentologie und Tektonik der Unteren Süsswassermolasse östlich von Thun. Diplomarbeit, Geologisches Institut, Universität Bern, Suisse, (unpubl.).
SCHOEPFER, P. 1989: Sédimentologie et stratigraphie de la Molasse marine supérieure entre le Gibloux et l'Aar. Thèse Univ. Fribourg, Suisse, No. 965, (unpubl.).
SCHRADER, F. 1988: Das regionale Gefüge der Drucklösungsdeformation an Geröllen im westlichen Molassebecken. Geol. Rdsch. 77, 347-369.
SCHWEIZERISCHE GEOPHYSIKALISCHE KOMMISSION 1983: Geothermische Karte der Schweiz 1:500'000. Bundesamt für Landestopographie, Wabern, Karte 10.
SCOTCHMAN, I.C. 1987: Clay diagenesis in the Kimmeridge Clay Formation, onshore UK, and its relation to organic maturation. Mineralogical Magazine 51, 535-551.

SHEPHERD, T.J., RANKIN, A.H. & ALDERTON, D.H.M. 1985: A practical guide to fluid inclusion studies. Blackie, London.
SIBSON, R.H. 1987: Earthquake rupturing as a mineralizing agent in hydrothermal systems. Geology 15, 701-704.
— 1990: Faulting and Fluid Flow. In: Nesbitt, B.E. (Ed.): Short Course on Fluids in Tectonically Active Regimes of the Continental Crust. Min. Assoc. of Canad., Short Course Handbook 18, Vancouver, 93-132.
SIBSON, R.H., ROBERT, F. & POULSEN, K.H. 1988: High-angle reverse faults, fluid-pressure cycling, and mesothermal gold-quartz deposits. Geology 16, 551-555.
SIEGENTHALER, C. 1974: Die Nordhelvetische Flysch-Gruppe im Sernftal (Kt. Glarus). Thèse Univ. Zürich, Suisse.
SIGNER, C. 1992: Interprétation sismique structurale et sismostratigraphique entre Jura et front alpin dans la région genevoise. Diplôme, Dép. de Géolgie et Paléontologie, Université de Genève, (unpubl.).
SINCLAIR, H.D. & ALLEN, P.A. 1992: Vertical versus horizontal motions in the Alpine orogenic wedge: startigraphic response in the foreland basin. Basin Research 4, 215-232.
SINCLAIR, H.D., COAKLEY, B.J., ALLEN, P.A. & WATTS, A.B. 1991: Simulation of Foreland Basin Stratigraphy Using a Diffusion Model of Mountain Belt Uplift and Erosion: An Example from the Central Alps, Switzerland. Tectonics 10, 599-620.
SINGER, A. & MÜLLER, G. 1983: Diagenesis in argillaceous sediments. In: Larsen, G. & Chilingar, G.V. (Eds.): Diagenesis in Sediments and Sedimentary Rocks (2). Dev. in Sedimentology 25B, Elsevier, Amsterdam, Oxford, New York, 115-212.
SITTLER, C. 1965: Le paléogène des fossées rhénan et rhodanien. Etudes sédimentologiques et paléoclimatiques. Thèse Sci. nat. Univ. Strasbourg, France.
SITTLER, J.A. 1979: Effects of source material on vitrinite reflectance. Master's thesis, West Virginia University, Morgantown, Virginia.
SLEEP, N.H. 1971: Thermal effects of the formation of Atlantic continental margins by continental breakup. Geophys. J. royal astr. Soc. 24, 325-350.
SMALL, J.S., HAMILTON, D.L. & HABESCH, S. 1992a: Experimental simulation of clay precipitation within reservoir sandstones 1: Techniques and examples. J. sedim. Petrol. 62, 508-519.
— 1992b: Experimental simulation of clay precipitation within reservoir sandstones 2: Mechanism of illite formation and controls on morphology. J. sedim. Petrol. 62, 520-529.
SMART, G. & CLAYTON, T. 1985: The progressive illitization of interstratified illite-smectite from Carboniferous sediments of northern England and its relationship to organic maturity indicators. Clay Minerals 20, 455-466.
SOFIYEV, I.S., GERLENKE, I.A. & SEMASHEVA, I.N. 1962: On the effect of the environment of coal formation on the properties of the organic components of coal. Geochem. Doklady. Adkad. Nauk. SSSR 152, 181.
SPRECHER, C. & MÜLLER, W.H. 1986: Geophysikalisches Untersuchungsprogramm Nordschweiz: Reflexionsseismische Messungen 82. Nagra techn. Ber. 84-15, Baden.
SRODON, J. 1980: Precise identification of illite/smectite interstratifications by X-ray powder diffraction. Clays and Clay Min. 28, 401-410.
— 1984: X-ray powder diffraction identification of illitic materials. Clays and Clay Minerals 32, 337-349.
SRODON, J. & EBERL, D.D. 1984: Illite. In: Bailey, S.W. (Ed.): Micas. Min. Soc. Amer., Reviews in Mineralogy 13, 495-544.
STACH, E., MACKOWSKY, M.-TH., TEICHMÜLLER, M.& R., TAYLOR, G.H. & CHANDRA, D. 1982: Stach's textbook of coal petrology. 3. ed, Gebrüder Bornträger Berlin-Stuttgart.
STALDER, P.J. 1979: Organic and inorganic metamorphism in the Taveyannaz sandstone of the Swiss Alps and equivalent sandstones in France and Italy. J. sedim. Petrol. 49, 463-482.
STAPLIN, F.L. 1969: Sedimentary organic matter, organic metamorphism and oil and gas occurrence. Bull. Canad. Petrol. Geol. 17, 47-66.
STÄUBLE, M. & PFIFFNER, A. 1991: Processing, interpretation and modelling of seismic reflection data in the Molasse Basin of eastern Switzerland. Eclogae geol. Helv. 84, 151-175.
STECKLER, M.S. & WATTS, A.B. 1978: Subsidence of the Atlantic-type continental margin off New York. Earth planet. Sci. Letters 41, 1-13.
STERNER, S.M. & BODNAR, R.J. 1984: Synthetic fluid inclusions in natural quartz. 1. Compositional types synthesized and applications to experimental geochemistry. Geochim. cosmochim. Acta 48, 2659-2668.
SUTER, M. 1978: Geologische Interpretation eines reflexionsseismischen W-E-Profils durch das Delsberger Becken (Faltenjura). Eclogae geol. Helv. 71, 267-275.
SWEENEY, J.J. 1990: BASINMAT: Fortran Program Calculates Oil and Gas Generation Using a Distribution of Discrete Activation Energies Geobyte 5, 37-43.
SWEENEY, J.J. & BURNHAM, A.K. 1990: Evaluation of a Simple Model of Vitrinite Reflectance Based on Chemical Kinetics. Bull. amer. Assoc. Petroleum Geol. 74, 1559-1570.
TANNER, H. 1944: Beitrag zur Geologie der Molasse zwischen Ricken und Hörnli. Mitt. thurg. naturf. Gesellsch. 33, 1-108.
TEICHMÜLLER, M. 1979: Die Diagenese der kohligen Substanzen in den Gesteinen des Tertiärs und Mesozoikums des mittleren Oberrhein-Grabens. Fortschr. Geol. Rheinld. u. Westf. 27, 19-49.
TEICHMÜLLER, M. & DURAND, B. 1983: Fluorescence microscopical rank studies on liptinites and vitrinites in peat and coals, and comparison with results of the rock-eval pyrolysis. Int. J. Coal Geol. 2, 197-230.

TEICHMÜLLER, M. & TEICHMÜLLER, R. 1968: Geological aspects of coal metamorphism. In: Murchison, D.G. & Westoll, T.S. (Eds.): Coal and coal bearing strata. Oliver and Boyd, Edinburgh , 233-267.
— 1975: Inkohlungsuntersuchungen in der Molasse des Alpenvorlands. Geologica bavar. 73, 123-142.
— 1978: Coalification studies in the Alps. In: Clos, H. Roder, D. & Schmidt, K. (Eds.): Alps, Apennines, Hellenides. Scient. Report 38, 49-55.
— 1979: Zur geothermischen Geschichte des Oberrheingrabens. Zusammenfassung und Auswertung eines Symposiums. Fortschr. Geol. Rheinld. u. Westf. 27, 109-120.
— 1981: The significance of coalification studies to geology - a review. Bull. Cent. Rech. Explor.-Prod. Elf-Aquitaine 5, 491-534.
TEICHMÜLLER, R. & TEICHMÜLLER, M. 1986: Relations between coalification and palaeogeothermics in Variscan and Alpidic foredeeps of western Europe. In: Buntebarth, G. & Stegena, L. (Eds.): Lecture Notes in Earth Sciences 5: Paleogeothermics. Springer-Verlag, Berlin, Heidelberg, New-York, London, Paris, Tokyo, 53-78.
TING, F.T.C. 1978: Petrographic techniques in coal analysis. In: Karr, C. (Ed.): Analytical methods for coal and coal products. Academic Press, New York, 3-26.
TISSOT, B.P., PELET, R. & UNGERER, PH. 1987: Thermal history of sedimentary basins, maturation indices and kinetics of oil and gas generation. Bull. amer. Assoc. Petroleum Geol. 71, 1445-1466.
TISSOT, B.P. & WELTE, D.H. 1984: Petroleum formation and occurrence. 2. ed., 699 p., Springer-Verlag, Berlin-Heidelberg-New York-Tokyo.
TODOROV, I., SCHEGG, R. & CHOCHOV, S. 1992: Maturity studies in the Carboniferous Dobroudja coal basin (northeastern Bulgaria) - coalification, clay diagenesis and thermal modelling. Int. J. Coal Geol. 21, 161-185.
TODOROV, I., SCHEGG, R. & WILDI, W. 1993: Thermal maturity of Mesozoic and Cenozoic sediments in the south of the Rhine Graben and the Eastern Jura (Switzerland). Eclogae geol. Helv. 86/3 (in press).
TRÜMPY, R. 1980: Geology of Switzerland: a Guide Book. Part A: an Outline of the Geology of Switzerland. Schweiz. Geol. Komm., Wepf & Co. Publishers, Basel, New York.
TRÜMPY, R. & BERSIER, A. 1954: Les éléments des conglomérats oligocènes du Mont-Pèlerin. Eclogae geol. Helv. 47, 119-166.
UJETZ, B. & KINDLER, P. 1993: New foraminiferal evidence for the paleoecology and age of the Val d'Illiez Formation, Haute-Savoie, France. Abstr. First Meeting of Swiss Sedimentologists, January 30, 1993, Fribourg, 29.
UNGERER, PH. 1990: State of the art of research in kinetic modelling of oil formation and expulsion. Org. Geochem. 16, 1-25.
UNGERER, PH. & PELET, R. 1987: Extrapolation of oil and gas formation kinetics from laboratory experiments to sedimentary basins. Nature 327, 52-54.
VAN HINTE, J.E. 1978: Geohistory analysis - application of micropaleontology in exploration geology. Bull. amer. Assoc. Petroleum Geol. 62, 201-222.
VELDE, B. 1979: Clays and clay minerals in nature and synthetic systems. Elsevier, New York.
VELDE, B., SUZUKI, T. & NICOT, E. 1986: Pressure-Temperature-Composition of Illite/Smectite Mixed-Layer Minerals: Niger Delta Mudstones and Other Examples Clays and Clay Min. 34, 435-441.
VELDE, B. & VASSEUR, G. 1992: Estimation of the diagenetic smectite to illite transformation in time-temperature space. Amer. Mineralogist 77, 967-976.
VOLLMAYR, T. & WENDT, A. 1987: Die Erdgasbohrung Entlebuch 1, ein Tiefenaufschluss am Alpennordrand. Bull. Ver. schweiz. Petroleum-Geol. u. -Ing. 53, 67-79.
VROLIJK, P., MYERS, G. & MOORE, J.C. 1988: Warm fluid migration along tectonic melanges in the Kodiak accretionary complex, Alaska. J. geophys. Res. 93, 10313-10324.
VUITEL, J.-M. 1987: Application de la méthode de Srodon pour la détermination d'interstratifiés "illite-smectite" à partir de diagrammes R-X sur des préparations de routine glycolées de fraction granulométriques inférieures à 2 µm. Cah. Inst. Géol. Neuchâtel, série A.X. No. 13 (44).
WAGNER, A. & WELLHÄUSER, F. 1966: Corrélations pétrographiques et stratigraphiques de l'Oligocène dans l'est du bassin de Bellegarde-Seyssel (Haute-Savoie, France). C.R. SPHN Genève IV-VI.
WAPLES, D.W. 1980: Time and temperature in petroleum formation: application of Lopatin's method to petroleum exploration. Bull. amer. Assoc. Petroleum Geol. 64, 916-926.
WAPLES, D.W., KAMATA, H. & SUIZU, M. 1992a: The art of maturity modeling. Part 1: Finding a satisfactory geologic model. Bull. amer. Assoc. Petroleum Geol. 76, 31-46.
— 1992b: The art of maturity modeling. Part 2: Alternative models and sensivity analysis. Bull. amer. Assoc. Petroleum Geol. 76, 47-66.
WATTS, A.B. & RYAN, W.B.F. 1976: Flexure of the lithosphere and continental margin basins. Tectonophysics 36, 25-44.
WEAVER, C.E. 1956: The distribution and identification of mixed-layer clays in sedimentary rocks. Am. Miner. 41, 202-221.
— 1960: Possible use of clay minerals in serach for oil. Bull. amer. Assoc. Petroleum Geol. 44, 1505-1518.
— 1979: Geothermal alteration of clay minerals and shales: diagenesis. Office of Nuclear Waste Isolation Technical Report 21, 176.
— 1989: Clays, muds, and shales. Developments in Sedimentology, 44, Elsevier, Amsterdam, Oxford, New-York, Tokyo.

WEI, Z.P., HERMANRUD, C. & LERCHE, I. 1990: Numerical basin modelling of the Sleipner field, North Sea Terra Nova 2, 31-42.
WEIDMANN, M. 1982: Situation et description des coupes visitées en 1978. Doc. Lab. Géol. Fac. Sci. Lyon H.S. 7, 11-24.
— 1988: Feuille 1243 Lausanne, Atlas géologique de la Suisse au 1:25'000, avec notice explicative. Service hydrol.-géol. national, Berne-Bâle, Suisse.
— (in press): Notice explicative de la feuille 1204 Romont de l'Atlas géologique de la Suisse 1:25'000. Service hydrol.-géol. national, Berne-Bâle, Suisse.
WEIDMANN, M., HOMEWOOD, P. & FASEL, J.-M. 1982: Sur les terrains subalpins et le Wildflysch entre Bulle et Montreux. Bull. Soc. vaud. Sci. nat. 76, 151-183.
WEIR, A.H., ORMEROD, E.G. & EL MANSEY, I.M.I. 1975: Clay mineralogy of sediments of the western Nile Delta. Clay Miner. 10, 369-386.
WELTE, D.H. & YALCIN, M.N. 1988: Basin modelling - A new comprehensive method in petroleum geology. Org. Geochem. 13, 141-151.
WENGER, L.M. & BAKER, D.R. 1987: Variations in vitrinite reflectance with organic facies - examples from Pennsylvanian cyclothems of the midcontinent, U.S.A. Org. Geochem. 11, 411-416.
WILDI, W., BLONDEL, T., CHAROLLAIS, J., JAQUET, J.-M., WERNLI, R. 1991: Tectonique en rampe latérale à la terminaison occidentale de la Haute-Chaîne du Jura. Eclogae geol. Helv. 84, 265-277.
WILDI, W., FUNK, H., LOUP, B., AMATO, E. & HUGGENBERGER, P. 1989: Mesozoic subsidence history of the European marginal shelves of the alpine Tethys (Helvetic realm, Swiss Plateau and Jura) Eclogae geol. Helv. 82, 817-840.
WILDI, W. & HUGGENBERGER, P. 1993: Reconstitution de la plate-forme européenne anté-orogénique de la Bresse aux Chaînes subalpines; éléments de cinématique alpine (France et Suisse occidentale). Eclogae geol. Helv. 86, 47-64.
WILSON, M.D. & PITTMAN, E.D. 1977: Authigenic clays in sandstones: recognition and influence on reservoir properties and paleoenvironmental analysis. J. sedim. Petrol. 47, 3-31.
WOLF, M. 1961: Sporenstratigraphische Untersuchungen in der gefalteten Molasse der Murnauer Mulde (Oberbayern). Geologica bavar. 46, 53-92.
WOLF, M. & HAGEMANN, H.W. 1987: Inkohlung und Geothermik in meso- und paläozoischen Sedimenten der Nordschweiz und Vergleich zu Inkohlungsdaten aus Süddeutschland. Eclogae geol. Helv. 80, 535-542.
WOOD, D.A. 1988: Relationship between thermal maturity indices calculated using Arrhenius equation and Lopatin method: implications for petroleum exploration. Bull. amer. Assoc. Petroleum Geol. 72, 115-134.
WOODS, T.L., BETHKE, P.M., BODNAR, R.J. & WERRE, R.W.JR. 1981: Supplementary components and operation of the U.S. Geological Survey gas-flow heating/freezing stage. U.S. Geol. Surv. Open File Rep. 81-954.
ZHANG, E. & DAVIS, A. 1993: Coalification patterns of the Pennsylvanian coal measures in the Appalachian foreland basin, western and south-central Pennsylvania. Bull. geol. Soc. Amer. 105, 162-174.
ZIEGLER, P.A. 1987: Late Cretaceous and Cenozoic intra-plate compressional deformations in the Alpine foreland - a geodynamic model. Tectonophysics 137, 389-420.
— 1988: Evolution of the Arctic-North Atlantic and the Western Tethys. Mem. amer. Assoc. Petroleum Geol. 43.
— 1992: European Cenozoic rift system. Tectonophysics 208, 91-111.
ZIMMERMANN, M.A., KÜBLER, B., OERTLI, H.J., FRAUTSCHI, J.-M., MONNIER, F., DERES, F. & MONBARON, M. 1976: Molasse d'eau douce inférieure du plateau suisse. Subdivision par l'indice de détritisme. Essai de datation par nannofossiles. Bull. Cent. Rech. Pau-SNPA 10, 585-625.

TABLES

Table A1
Vitrinite reflectance data for the Molasse Basin.

No = sample number
X-Coord. & Y-Coord. = Swiss coordinates
Rr = mean vitrinite reflectance, values in italic are not used for the interpretation of results -> reworked material (see chapter 3.3)
s = standard deviation
n = number of measurements

A= Alteration:
0 = fresh
1 = slightly altered
2 = moderately altered
3 = strongly altered
4 = completely altered

MA: qualitative maceral analysis:
V : Vitrinite > 95%
C : Vitrinite + Liptinite > 95%
D : Vitrinite > Liptinite and Inertinite
VI: Vitrinite + Inertinite > 95%

	No	Location	X-coord.	Y-Coord.	Altitude	Rr	s	n	A	MA
HAUTE-SAVOIE and GENEVA BASIN										
Plateau Molasse										
OMM	RS16	La Maladière	476600	106900	400	0.40	0.07	99	2	V
	RS36	Le Fornant	484550	97400	340	0.35	0.08	100	2	V
	RS37	Le Fornant	484550	97400	340	0.45	0.04	50	0	V
	RS39	Le Fornant	484600	97400	340	0.37	0.04	51	2	V
	RS40	Le Fornant	484600	97400	340	0.28	0.07	100	3	V
	RS41	Le Fornant	484650	97400	340	0.39	0.04	49	2	V
	RS65	Franclens	475100	99600	420	0.43	0.03	50	0	C
	RS66	Bassy	476100	93100		0.43	0.03	49	1	V
	RS67	Seyssel	476200	89600	260	0.37	0.06	60	2	V
	RS68	St.André	480850	87700	350	0.41	0.04	50	2	V
	RS69	St.André	480850	87700	350	0.42	0.03	50	1	V
	RS71	Chez les Gay	482350	78400	390	0.32	0.05	50	1	V
USM	RS3	Peissy (Forage)	489970	119055	282	0.48	0.05	50	1	V
	RS6	Peissy (Forage)	489970	119055	275	0.47	0.05	37	3	V
	RS206	Vernier	497750	118800	392	0.48	0.03	50	0	V
Subalpine Molasse ("Molasse du Plateau de Bornes")										
USM	RS1	Lucinges	514200	115800	800	0.57	0.02	50	0	V
	Weid93	Mornex/Esserts	506000	112000	600	0.53	0.04	51	1	C
	RS81	Cran-Gevriér	495900	84700	420	0.51	0.05	100	1	V
	RS82	Cruseilles	496600	98200	760	0.47	0.03	50	0	V
	RS83	Pont de la Caille	497800	96650	605	0.52	0.04	50	0	V
	RS89	Le Vernay	498950	102050	870	0.51	0.04	51	0	V
	RS91	La Mouille	500000	103250	860	0.54	0.06	50	2	V
	RS92	La Mouille	500200	103450	860	0.50	0.08	100	1	V
	RS93	Clarnant	500750	104000	850	0.48	0.04	50	1	V
	RS94	Cornillon	501550	103600	760	0.50	0.04	50	1	V
	RS96	Les Chavannes	502850	103400	810	0.79	0.07	53	2	VI
	RS102	Le Reposoir	500250	93920	640	1.41	0.13	50	3	V
	RS128	Daudens	506600	97900	670	1.25	0.07	50	1	V
	RS137	Viaison	507425	113250	460	0.55	0.04	21	1	V
	RS139	Viaison	507425	112950	420	0.71	0.05	50	2	V
	RS140	Esserts-Salève	505950	112150	590	1.01	0.07	24	3	V
	RS228	Mont Gosse	506975	113500	605	0.60	0.10	29	3	V
	RS229	Mornex	507125	113200	510	0.51	0.05	30	2	V
	RS234	Césarge	506650	112575	460	0.54	0.05	50	1	V
	RS235	Césarge	506650	112575	465	0.54	0.03	52	2	V
	RS236	Césarge	506650	112250	480	0.62	0.04	52	2	V
UMM	RS109	Le Chêne	504750	91400	680	0.56	0.09	101	2	V
	RS112	Le Chêne	504950	91600	700	0.53	0.06	50	1	V
	RS129	Le Clos	510300	98850	820	0.50	0.04	50	0	V
	RS131	Le Clos	510250	98750	830	0.45	0.05	101	0	C
	RS133	Cady	512650	99900	740	0.64	0.05	50	0	V
	RS144	St.Maurice	516050	100700	580	0.80	0.07	50	0	C
	Wi2065	Roche sur Foron, "Pont Lavillat"	511200	101000	700	0.57	0.06	62	0	V
Subalpine Chains ("Massif des Bornes", "Massif des Bauges", "Massif de Platé")										
UMM	RS12	Ht-Rumilly	517800	100000	680	0.78	0.08	92	0	C
	RS13	Plan Bois	509800	92200	780	0.58	0.05	50	3	V
	RS114	Chez Gerlier	505150	89620	910	0.55	0.08	100	1	C
	RS115	Naves	503000	88080	600	0.61	0.06	50	2	V
	RS119	Nanoir	504250	86150	600	0.65	0.09	100	1	V

	No	Location	X-coord.	Y-Coord.	Altitude	Rr	s	n	A	MA
	RS120	Nanoir	504250	86150	600	0.56	0.04	50	1	V
	RS122	Combadieu	503350	86620	540	0.53	0.04	50	1	V
	RS124	Combadieu	503400	86700	570	0.55	0.05	50	1	V
	RS134	Montisel	515020	98050	1060	0.66	0.06	100	0	C
	RS136	Montisel	515020	98050	1060	0.57	0.04	50	3	V
	RS147	St.Laurent	516550	99030	840	0.64	0.06	50	0	V
	RS151	Delairaz	518950	99250	880	0.60	0.04	101	0	C
	RS156	La Grange	522400	101050	720	0.66	0.04	100	2	C
	RS168	La Villaz	517100	85000	850	0.81	0.09	50	2	C
	RS186	Les Volées	524600	100250	900	0.65	0.05	108	0	C
	RS188	Les Volées	524600	100250	900	0.62	0.04	50	2	C
	RS191	Cenise	523980	96600	1640	0.75	0.04	50	1	V
	RS196	Plan Bois	509800	92200	750	0.57	0.04	96	1	C
Eocene Fm.	RS203	Entrevernes ("Couches Diablerets")	502650	69300	980	0.49	0.05	50	1	D
	RS204	Entrevernes ("Couches Diablerets")	502650	69300	980	0.51	0.05	50	1	V
	Wi2052	Les Carroz	538400	97700	1170	1.61	0.12	51	1	V
	Wi2056	Les Carroz	538400	97700	1170	1.55	0.10	100	3	V
	Wi2053	Les Carroz	538400	97700	1170	1.53	0.18	50	1	V
WESTERN SWITZERLAND										
Plateau Molasse										
OMM	RS325	Flon de Carrouge	550120	164970	580	0.51	0.04	50	0	V
	RS326	Broye	551680	165870	535	0.46	0.02	50	0	V
	RS351	La Neirigue	562450	167450		0.37	0.03	50	2	C
	Weid4	Ruisseau de Manloud	538960	156410	707	0.34	0.05	73	1	V
	Weid6	Flon Morand	542180	155635	775	0.45	0.04	99	0	V
	Weid7	Le Flon	540180	156220	680	0.36	0.03	100	1	V
	Weid13	Ruisseau des Losiardes (Lausanne)	542890	155210	760	0.44	0.02	49	0	V
	Weid14	Riau Gresin, pt. 605	551290	170420	605	0.42	0.04	99	0	V
	Weid15	Ruisseau de Lavaux-Morattel, pt564	560500	177950	564	0.43	0.05	100	1	C
	Weid16	Ruisseau de Planche-Roguin	561800	181440	540	0.43	0.05	69	1	C
	Weid17	La Neirigue	563565	170940	710	0.53	0.06	99	1	V
	Weid18	La Glâne, sur Châtel	566350	175760	650	0.49	0.07	70	2	V
	Weid19	Ruisseau de Seigneux, près 13 Cantons	556830	175050	550	0.55	0.05	100	1	V
	Weid20	Ruisseau de Colans	555400	171950	590	0.39	0.03	103	1	V
	Weid21	La Glâne, Moulin de Chénens	566280	176010	650	0.48	0.06	104	1	V
	Weid22	Ruisseau de Trey	560290	179780	520	0.55	0.04	50	2	V
	Weid23	Ruisseau des Vaux	555380	170810	610	0.48	0.05	100	0	V
	Weid24	La Trémeule	558210	176340	550	0.58	0.08	101	0	D
	Weid26	Chemin Seigneux - Les Granges	557060	174990	530	0.56	0.07	101	0	V
	Weid27	La Cerjaule, sous "Onze Malles"	551360	171770	620	0.48	0.06	50	2	V
	Weid28	La Cerjaule, Chêne brûlé	552680	173240	550	0.41	0.05	50	1	V
	Weid29	La Cerjaule, sous les Envers	553035	173670	540	0.46	0.02	50	0	V
	Weid30	Le Recoulet, pt 631 Pissevache	552660	174560	630	0.39	0.03	50	0	C
	Weid31	Le Recoulet, pt 531	553340	173910	530	0.45	0.04	50	1	V
	Weid33	Ruiss. de la Chasse, Lucens	554950	174720	605	0.41	0.03	50	0	V
	Weid35	Ruiss. de Villeneuve	556260	177390	490	0.52	0.06	50	2	V
	Weid51	Grand Mont	538350	157150		0.53	0.05	50	1	V
	Weid53	Montenailles	539150	155600		0.51	0.03	30	1	V
	Weid82	Scierie de Croisettes	540800	155700		0.56	0.07	50	0	V
	Weid87	Le Flon, près Epalinges	540180	156240		0.48	0.06	50	1	V
	Weid105	Le Flon	552380	178160	620	0.43	0.03	50	0	C
	Weid106	La Glâne	564810	175940	660	*1.07*	0.11	50	3	V
	Weid107	Ruiss. de Villardin	552000	165720	580	*1.22*	0.12	30	3	V
	Weid111	Le Flon	552360	178440	630	0.38	0.04	50	3	V
	Weid123	Centrale, Lucens	553130	171520	530	0.47	0.03	50	0	V
	Weid127	Le Flonzel, Tour de St. Martin	547780	180810	510	0.41	0.04	50	0	C
	Weid126	Le Mausson, Grangettes	563600	169450	775	0.37	0.04	54	0	V
	Weid125	Le Flonzel, La Scie	547630	180060	560	0.40	0.02	50	0	V
	Weid124	Tour de la Molière	552910	183140	672	0.28	0.04	28	3	C
	Weid129	Carrière du Dézaley (Seiry)	554060	185270	600	0.41	0.05	50	0	C
	Weid131	Sarine, Illens	574800	176600	595	0.44	0.03	48	1	V
	Weid134	Matran	573550	181370	595	0.26	0.05	20	4	V
	Weid135	La Glâne, Sous Gerby	573000	179760	585	0.43	0.03	50	1	V
	Weid136	Villars-s.-Glâne	575620	181930	630	0.30	0.06	30	4	V
	Weid137	La Glâne, Les Esserts	571220	178500	605	0.45	0.05	50	2	V
	Weid138	La Mérine, Chalet Coucou	549420	168710	710	0.31	0.06	41	2	V
	Weid139	Cottens	570650	178130	620	0.96	0.07	50	4	V
	Weid140	La Glâne, Les Epites	570330	176000	635	0.42	0.06	50	1	V
	Weid141	Sarine, Prés d'en Bas, Posieux	575050	178440	580	0.25	0.03	50	4	V
	Weid142	Sarine, La Souche	575840	178960	580	0.41	0.05	50	2	V
	Weid143	Sarine, au-dessous de Monténan	575720	179430	575	0.41	0.04	50	1	V
	Weid144	Sarine, au-dessous de Monténan	575720	179430	575	0.44	0.03	40	1	V
	Weid145	Sarine, usine d'Hauterive	576320	179800	610	0.42	0.03	50	1	V
	Weid146	Ruisseau d'Arconciel	575630	177360	695	0.41	0.07	21	3	V
	Weid147	Sarine, l'Augette	575120	177360	593	0.44	0.03	50	0	V
	Weid148	Sarine, W de la Gottala	575020	176870	595	0.38	0.07	50	1	V
	Weid149	Praz Sasson	575410	176290	635	0.40	0.08	50	2	V

	No	Location	X-coord.	Y-Coord.	Altitude	Rr	s	n	A	MA
	Weid150	Sarine, sous le château d'Illens	574990	176560	600	0.49	0.04	50	0	V
	Weid151	Sarine, captage 1901	575345	175320	630	0.41	0.04	50	0	V
	Weid152	Rio des Arbagny	575300	175820	640	0.38	0.03	50	1	V
	Weid153	Route barrage-Treyvaux	575400	174200	710	0.36	0.05	50	1	V
	Weid154	Sarine, S de l'Auge	574870	174780	605	0.41	0.06	50	1	V
	Weid156	Lac de la Gruyère	574020	173430	675	0.54	0.05	50	1	V
	Weid158	Riau du Glèbe	568840	174430	678	0.40	0.04	50	0	V
	Weid161	Fallenbach, Fromenacker	576510	172220	602	0.42	0.06	51	1	V
USM	Weid1	Flon Morand	541870	155245	750	0.50	0.03	69	0	V
	Weid3	Talent 8	534620	168290	630	0.51	0.04	98	0	V
	Weid5	Talent 16	534810	168000	650	0.46	0.06	93	0	VI
	Weid8	Talent 2	534880	170210	500	0.45	0.06	100	1	V
	Weid25	Ruiss. de Villarzel, Moulin des Anes	559640	178010	510	0.53	0.05	100	0	V
	Weid54	Sauvabelin	538850	153950		0.47	0.04	50	0	C
	Weid55	Prilly	536000	154000		0.47	0.04	50	2	V
	Weid56	Bois Mermet	537950	154200		0.57	0.05	50	0	V
	Weid57	Malley	536000	152900		0.45	0.05	50	3	V
	Weid58	Renens	535650	153775	435	0.46	0.02	50	0	V
	Weid59	Place du Tunnel à Lausanne	538400	153000		0.53	0.04	50	0	V
	Weid60	Place Chaudron à Lausanne	537600	152800		0.60	0.04	50	0	V
	Weid61	Place Chaudron à Lausanne	537600	152750		0.46	0.03	50	3	V
	Weid62	La Borde	538200	153300		0.54	0.04	50	1	C
	Weid63	Roveréaz	540900	153850		0.47	0.04	50	0	V
	Weid76	Venne, AR	539600	154800		0.49	0.04	50	0	V
	Weid85	Arrissoules	549280	183700	530	0.64	0.05	50	2	C
	Weid86	Ruiss. de la Croix	549700	183600	560	0.54	0.04	50	2	V
	Weid88	Bottens	540000	163000		0.51	0.04	50	1	V
	Weid89	Cuarny	542900	180100	570	0.52	0.04	50	2	V
	Weid91	La Mentue	543000	169000	610	0.43	0.02	50	0	V
	Weid92	Bavois, AR N1	533600	169600	570	0.40	0.02	50	0	V
	Weid95	Bavois	533200	170800	450	0.47	0.03	50	0	V
	Weid114	Talent 2	534880	170210	500	0.55	0.02	50	0	V
	Weid128	Chandelar-Flon Morand	540940	153830		0.46	0.03	49	0	V
	Weid130	Anboranges	551410	159200		*1.16*	0.09	16	1	V
Subalpine Molasse										
USM	RS280	Oron le Châtel	557230	158350		0.59	0.04	50	0	C
	RS281	Les Barattes	561640	162880		0.45	0.06	67	1	C
	RS283	Progens	559050	159090		0.37	0.04	50	1	V
	RS284	Bois du Riez	557520	161800		0.50	0.04	50	0	C
	RS324	Ecotaux	555850	154125	650	*1.14*	0.19	50	2	V
	RS353	Forêt de la Joux	560960	163780	900	0.47	0.05	50	1	C
	Weid10	Au Laviau / Jongny	554400	147900	630	0.76	0.07	100	1	V
	Weid12	La Gisetta	562800	161460	850	0.44	0.04	50	0	C
	Weid100	Ruiss. de St.Amour	546700	154800		0.54	0.07	45	0	C
	Weid101	Crêt Rouge	546640	155360		0.59	0.07	70	0	D
	Weid102	Les Charbonnières	548700	156100		0.58	0.05	50	0	D
	Weid104	Parimbot	551900	161650		0.47	0.07	60	0	C
	Wi2036	Oron (VD)	552200	156400	625	0.63	0.08	73	0	D
	Wi2037	Oron	552200	156400	625	0.46	0.05	50	0	D
	Wi2038	Oron	552300	156450	625	0.43	0.05	50	0	D
	Wi2039	Les Thioleyres	552300	154675	660	0.39	0.03	50	0	D
LAKE THUN AREA										
Subalpine Molasse										
USM	RS354	Losenegg	622075	181250	750	0.65	0.06	50	0	V
	RS355	Gitzischöpf	624050	178275	1160	0.48	0.03	50	0	V
	RS356	Teuffenthal	621150	181150	915	0.50	0.05	52	0	V
	RS357	Schlötteren	624575	184750	945	0.60	0.03	50	0	V
	RS358	Homberg	617750	181400	680	0.54	0.03	50	0	V
	RS359	Losenegg	621750	181425	740	0.46	0.04	50	0	V
	RS360	Gärbi	621450	181700	730	0.68	0.04	50	0	V
	RS361	Losenegg	621825	181450	750	0.49	0.06	38	2	V
	RS362	Homberg	617800	181300	710	0.50	0.02	50	0	V
	RS363	Reust	622250	180875	800	0.50	0.04	50	1	C
EASTERN SWITZERLAND										
Plateau Molasse										
OSM	RS213	Ober Tägernau	708850	233350	470	0.44	0.02	50	0	C
	RS214	Bruederwald	715850	249600	710	0.35	0.03	50	0	V
	RS215	Bärtobel	712200	247500	740	0.38	0.05	50	1	V
	RS216	Bärtobel	712900	247800	800	0.25	0.04	40	1	C
	RS217	Leiachertobel	714150	246700	810	0.27	0.02	50	0	V
	RS218	Leiachertobel	713750	246550	845	0.36	0.04	50	1	V

	No	Location	X-coord.	Y-Coord.	Altitude	Rr	s	n	A	MA
	RS219	Chlihörnli	713440	248380	930	0.21	0.02	50	0	V
	RS220	Chlihörnli	713530	248300	1000	0.31	0.04	50	1	V
	RS222	Fischbach	721600	277700	605	0.42	0.03	50	1	V
	RS238	Brunnentobel	682700	236150	730	0.37	0.03	50	1	V
	RS240	Kyburg	698000	256750	560	0.29	0.04	50	2	V
	RS241	Neuheim	687350	229575	555	0.36	0.02	50	1	V
	RS242a	Aeugst a. Albis	678800	237850	620	0.43	0.04	50	1	C
	RS242b	Aeugst a. Albis	678800	237850	620	0.47	0.08	50	0	D
	RS243	Schwizertobel	681700	238200	635	0.59	0.05	50	0	C
	RS244	Käpfnach (Stolleneingang)	688750	234550	420	0.48	0.02	50	0	V
	RS245	Käpfnach	688750	234550	420	0.54	0.05	50	1	D
	RS246	Brütten	693400	257950	432	0.48	0.04	50	0	V
	RS247	Baar	683675	227480	475	0.37	0.03	50	0	C
	RS248a	Pfefferberg	686600	232575	650	0.41	0.05	50	1	D
	RS248b	Pfefferberg	686600	232575	650	0.46	0.02	50	0	V
OMM	RS211	Echeltsschwil	715250	234750	630	0.44	0.04	50	0	D
	RS212	Curtiberg	708850	232850	460	0.42	0.04	50	2	V
	RS226	Mägenwil	660550	251075	500	0.44	0.04	50	1	V
	RS237	Ränggloch	660850	210100	520	0.50	0.03	60	0	V
	RS297	Hanenberg	661300	251150	490	0.40	0.05	50	3	V
	RS300	Mägenwil	659950	251050	520	0.52	0.04	50	0	V
	RS311	Würenlos	669650	255700	420	0.44	0.03	50	0	C
USM	RS209	Uznaberg	715150	232600	490	0.54	0.03	50	0	V
	RS210	Neuhüsler Tobel	714550	233800	490	0.47	0.03	50	1	V
	RS249	Zug	682100	223252	535	0.45	0.04	50	0	V
Subalpine Molasse										
USM	RS239	Mühlebachtobel (Greit)	691250	223750	980	0.58	0.05	50	1	C
	Weid52	Teufen	747000	251000		0.53	0.03	50	0	V
	Weid78	Bräun-Wanne	728935	229410		0.50	0.04	50	3	V
NORTHERN SWITZERLAND										
Miocene Fm.	RS224	Bois de Raube ("Vogesenschotter")	585100	246450	565	0.24	0.02	50	2	V
	Weid96	Tramelan (OSM)	230000	580000		0.28	0.04	50	0	C
Oligocene Fm.	RS223	Brocheni Fluh (USM)	621900	247550	880	0.30	0.02	50	0	V
	Weid2	Dornachbrugg 2 ("Molasse alsacienne")	612660	259840		0.41	0.03	97	0	V
	Weid97	Délemont ("Molasse alsacienne")	600140	243090		0.50	0.04	50	2	V
	Weid112	Moûtier ("Molasse alsacienne")	594290	235600		0.55	0.07	50	1	C
	Weid119	Sondage Delémont 1 ("Molasse alsacienne")	592880	244510	400	0.41	0.05	50	1	V
	Weid120	Sondage Delémont 1 (UMM s.l.)	592880	244510	370	0.49	0.04	68	1	V

Table A2:

Comparison of vitrinite reflectance data
1) between published and own data from Western Switzerland
2) with the Geological Survey of Canada in Calagary
(on same samples from Haute-Savoie)

① **this study** — **Kübler et al. (1979)**

No	%Rr	No	%Rr	Δ %Rr
Weid44	0.43	8144	0.37	0.06
Weid65	0.75	8152	0.65	0.10
Weid67	0.81	8150	0.88	0.07
Weid68	0.56	8147	0.45	0.11
Weid72	0.59	8143	0.59	0.00
Weid98	0.46	8146	0.38	0.08
Weid76	0.49	8139	0.39	0.10
Weid85	0.64	8137	0.43	0.21
			average	***0.09***

②

	Geneva	**Calgary**	
No	**%Rr**	**%Rr**	**Δ %Rr**
RS12	0.78	0.75	0.03
RS16	0.4	0.35	0.05
RS36	0.35	0.3	0.05
RS40	0.28	0.25	0.03
RS81	0.51	0.47	0.04
RS131	0.45	0.45	0.00
RS134	0.66	0.64	0.02
RS151	0.6	0.58	0.02
RS156	0.66	0.64	0.02
RS186	0.65	0.64	0.01
		average	***0.03***

Legend:
No=sample number
Rr=mean average vitrinite reflectance
Δ %Rr=difference in vitrinite reflectance values

Table A3
Vitrinite reflectance data of Mesozoic sediments in Northern Switzerland (modified from Todorov, Schegg & Wildi 1993)

X-Coord. & Y-Coord. = Swiss coordinates
%Rr = mean vitrinite reflectance, values in brackets should be treated with care as the standard deviation are to high
S = standard deviation
N = number of measurements

Sample,№	Location	X-Coord.	Y-Coord.	Age	Stratigraphy	%Rr	S	N
LATE JURASSIC								
IT3	Oberehrendingen	668500	261000	Oxfordian	Effinger Schichten	0.49	0.09	58
MIDDLE JURASSIC								
IT10	Asperchlus	647400	252800	Bathonian	Hauptrogenstein	0.40	0.04	72
IT13	Meltingen	612000	248300	Aalenian	Opalinus Ton	0.55	0.06	52
IT58	Muttenz	616912	264108	Aalenian	Opalinus Ton	0.55	0.06	50
IT65	Muttenz	617802	262950	Aalenian	Opalinus Ton	[0.69]	0.13	40
EARLY JURASSIC								
IT7	Staffelegg	647000	254000	Toarcian	Jurensis Mergel	0.58	0.07	46
IT8	Staffelegg	647000	254000	Toarcian	Jurensis Mergel	[0.44]	0.11	26
IT30	Delémont	581430	245223	Toarcian	Jurensis Mergel	0.62	0.09	15
IT66	Muttenz	617802	262950	Toarcian	Jurensis Mergel	0.52	0.06	50
IT67	Muttenz	617802	262950	Toarcian	Jurensis Mergel	0.69	0.08	13
IT1	Schämbelen	659000	257000	Toarcian	Posidonia Schiefer	0.49	0.09	52
IT20	Delémont	581430	245223	Toarcian	Posidonia Schiefer	0.54	0.09	60
IT21	Delémont	581430	245223	Toarcian	Posidonia Schiefer	0.48	0.09	36
IT22	Delémont	578875	248683	Toarcian	Posidonia Schiefer	0.45	0.07	46
IT23	Delémont	578875	248683	Toarcian	Posidonia Schiefer	0.53	0.09	58
IT24	Delémont	578875	248683	Toarcian	Posidonia Schiefer	0.53	0.10	46
IT25	Delémont	579180	248070	Toarcian	Posidonia Schiefer	0.48	0.06	44
IT26	Delémont	579180	248070	Toarcian	Posidonia Schiefer	0.54	0.08	29
IT28	Delémont	581430	245223	Toarcian	Posidonia Schiefer	0.50	0.10	55
IT29	Delémont	581430	245223	Toarcian	Posidonia Schiefer	0.51	0.09	50
IT62	Muttenz	616811	264222	Sinemurian	Obtusus Ton	[0.63]	0.14	25
IT68	Muttenz	617802	262950	Sinemurian	Obtusus Ton	0.61	0.06	45
IT52	Frick	642000	262000	Hettangian	Insektenmergel	[0.66]	0.11	30
IT53	Frick	642000	262000	Hettangian	Insektenmergel	0.54	0.08	36
IT63	Muttenz	616811	264222	Hettangian	Insektenmergel	0.70	0.09	44
LATE TRIASSIC								
IT14	Grindel	605000	247500	Rhaetian	Rhät	0.80	0.06	70
IT31	Delémont	579180	248070	Rhaetian	Rhät	0.56	0.10	22
IT49	Balmberg	608300	234800	Rhaetian	Rhät	0.55	0.09	53
IT50	Delémont	578875	248683	Rhaetian	Rhät	0.61	0.10	76
IT51	Delémont	578875	248683	Rhaetian	Rhät	[0.65]	0.12	25
IT64	Muttenz	616811	264222	Rhaetian	Rhät	0.66	0.09	50
IT68a	Muttenz	617802	262950	Rhaetian	Rhät	0.49	0.08	20
IT37	Trimbach	633500	247000	Middle Keuper	Gipskeuper	[0.66]	0.13	55
IT38	Trimbach	633500	247000	Middle Keuper	Gipskeuper	[0.78]	0.15	74
IT39	Belchenflue	628200	246300	Middle Keuper	Gipskeuper	[0.75]	0.11	65
IT59	Muttenz	616673	264299	Middle Keuper	Gipskeuper	[0.64]	0.12	32
IT69	Muttenz	617994	262765	Middle Keuper	Gipskeuper	0.64	0.09	30
IT70	Muttenz	617994	262765	Middle Keuper	Gipskeuper			
IT60	Muttenz	616673	264299	Early Keuper	Letten Kohle	0.69	0.08	50
IT61	Muttenz	616673	264299	Early Keuper	Letten Kohle	[0.70]	0.13	52
MIDDLE TRIASSIC								
IT71	Muttenz	617060	263832	Late Muschelkalk	Trigonodus Dolomit	0.76	0.09	33

Table B1
Rock-Eval pyrolysis results for samples from the OMM, USM, UMM and Eocene Fm. in the Haute-Savoie and Geneva Basin.

No = sample number
X-Coord. & Y-Coord. = Swiss coordinates
S1, S2, S3, Tmax, TOC=primary Rock-Eval parameters (see chapter 2.2.3.4)
OI = Oxygen Index (S3/TOC)
HI = Hydrogen Index (S2/TOC)
PI = Production Index (S1/S1+S2)
Rr = mean vitrinite reflectance

OMM											
No	X-Coord.	Y-Coord.	S1	S2	S3	TOC	Tmax	OI	HI	PI	Rr
			mg HC/g rock	mg HC/g rock	mg CO2/g rock	wt. %	°C	mg CO2/TOC	mg HC/g TOC		%
RS16	476600	106900	0.21	1.27	36.17	28.4	474	127	4	0.14	0.40
RS36	484550	97400	0.20	1.34	7.93	10.7	413	74	13	0.13	0.35
RS37	484550	97400	0.49	8.89	37.91	59.9	436	63	15	0.05	0.45
RS41	484650	97400	3.01	7.05	8.39	10.3	421	81	68	0.30	0.39
RS65	475100	99600	5.70	42.97	55.90	49.5	387	113	87	0.12	0.43
RS66	476100	93100	8.17	11.79	71.58	52.5	380	136	22	0.41	0.43
RS67	476200	89600	1.67	3.19	31.32	14.9	432	211	21	0.34	0.37
RS68	480850	87700	1.79	7.65	47.91	42.1	459	114	18	0.19	0.41
RS71	482350	78400	0.06	0.71	11.19	5.6	459	199	13	0.08	0.32
S2>0.2 TOC>0.5	Minimum		0.06	0.71	7.93	5.6	380	63	4	0.05	0.32
	Maximum		8.16	42.97	71.57	59.9	474	211	87	0.41	0.45
	Mean		**2.37**	**9.43**	**34.25**	**30.4**	**429**	**124**	**29**	**0.20**	**0.39**
	Standard Deviation		2.83	13.17	22.27	20.9	32	52	28	0.13	0.04
	Count	9									
S1>0.2 S2>0.2 TOC>0.5	Minimum		0.21	1.27	8.39	10.3	380	63	4	0.05	0.37
	Maximum		8.16	42.97	71.57	59.9	474	211	87	0.41	0.45
	Mean		**3.00**	**11.83**	**41.31**	**36.8**	**427**	**121**	**34**	**0.22**	**0.41**
	Standard Deviation		2.92	14.17	19.98	19.2	35	47	31	0.13	0.03
	Count	7									
USM											
RS1	514200	115800	2.23	113.68	11.51	75.1	431	15	151	0.02	0.57
RS3	489970	119055	0.71	8.88	8.76	12.1	425	72	73	0.07	0.48
RS6	489970	119055	0.06	0.66	3.28	2.1	440	158	32	0.08	0.47
RS54	487950	100050	0.01	0.27	0.46	0.3	419	136	79	0.04	n.d.
RS81	495900	84700	0.10	10.95	48.74	61.3	496	80	18	0.01	0.51
RS82	496600	98200	0.87	72.61	22.67	71.6	424	32	101	0.01	0.47
RS83	497800	96650	0.88	37.80	22.40	68.7	442	33	55	0.02	0.52
RS88	499450	100800	35.54	132.60	0.99	87.8	442	1	151	0.21	n.d.
RS89	498950	102050	0.28	20.84	31.13	74.7	458	42	28	0.01	0.51
RS91	500000	103250	0.06	1.52	8.53	3.2	571	269	48	0.04	0.54
RS92	500200	103450	0.55	7.07	47.26	45.5	447	104	16	0.07	0.50
RS93	500750	104000	0.09	8.80	41.84	49.2	485	85	18	0.01	0.48
RS94	501550	103600	1.27	23.89	43.94	54.3	432	81	44	0.05	0.50
RS96	502850	103400	0.02	1.18	2.28	1.9	437	122	63	0.02	0.79
RS102	500250	93920	0.19	1.86	10.98	50.6	517	22	4	0.09	1.41
RS128	506600	97900	0.07	0.16	1.94	1.9	445	104	9	0.30	1.25
RS139	507425	112950	0.05	0.38	0.72	1.4	438	53	27	0.12	0.71
RS140	505950	112150	0.15	2.08	0.50	2.4	459	21	87	0.07	1.06
RS206	497750	118800	0.17	14.21	26.31	64.5	438	41	22	0.01	0.48
RS229	507125	113200	0.01	0.27	5.19	3.0	493	171	9	0.04	0.51
RS234	506650	112575	0.19	19.71	30.47	61.1	482	50	32	0.01	0.54
RS235	506650	112575	0.09	15.04	31.71	57.8	482	55	26	0.01	0.54
RS236	506650	112250	0.10	6.06	31.70	51.5	516	62	12	0.02	0.62
RS352	490000	130000	0.19	4.67	2.23	6.1	433	37	77	0.04	0.47
Weid93	506000	112000	0.62	280.45	25.01	68.6	429	36	409	0.00	0.53
S2>0.2 TOC>0.5	Minimum		0.01	0.26	0.46	0.3	419	1	4	0.00	0.47
	Maximum		35.54	280.45	48.74	87.8	571	269	409	0.21	1.41
	Mean		**1.85**	**32.73**	**19.11**	**40.6**	**460**	**74**	**66**	**0.04**	**0.60**
	Standard Deviation:		7.19	63.37	16.45	30.8	38	61	84	0.05	0.23
	Count	25									
S1>0.2 S2>0.2 TOC>0.5	Minimum		0.28	7.07	0.99	12.1	424	1	16	0.00	0.47
	Maximum		35.54	280.45	47.26	87.8	458	104	409	0.21	0.57
	Mean		**4.77**	**77.53**	**23.74**	**62.1**	**437**	**46**	**114**	**0.05**	**0.51**
	Standard Deviation		11.55	88.66	15.46	22.4	11	33	121	0.07	0.03

No	X-Coord.	Y-Coord.	S1	S2	S3	TOC	Tmax	OI	HI	PI	Rr
			mg HC/g rock	mg HC/g rock	mg CO2/g rock	wt. %	°C	mg CO2/TOC	mg HC/g TOC		%
UMM											
RS12	517800	100000	0.51	16.74	0.91	10.2	441	9	164	0.03	0.78
RS13	509800	92200	0.12	4.08	0.25	2.2	435	11	183	0.03	0.58
RS109	504750	91400	0.14	0.58	0.37	1.0	439	37	57	0.19	0.56
RS114	505150	89620	4.39	102.84	11.76	67.9	428	17	151	0.04	0.55
RS115	503000	88080	0.56	33.83	14.99	59.2	445	25	57	0.02	0.61
RS120	504250	86150	0.02	0.57	1.26	1.2	441	108	49	0.03	0.56
RS124	503400	86700	0.46	48.31	20.34	68.3	447	30	71	0.01	0.55
RS129	510300	98850	1.07	109.78	10.59	73.4	414	14	150	0.01	0.50
RS131	510250	98750	0.75	88.79	11.98	63.6	424	19	140	0.01	0.45
RS136	515020	98050	0.23	8.76	1.05	6.5	433	16	135	0.03	0.57
RS144	516050	100700	0.15	3.03	4.23	7.4	460	57	41	0.05	0.80
RS151	518950	99250	8.48	142.89	13.85	70.2	434	20	203	0.06	0.60
RS156	522400	101050	1.07	45.61	9.29	35.8	443	26	127	0.02	0.66
RS168	517100	85000	0.06	0.75	0.70	1.4	450	49	52	0.07	0.81
RS186	524600	100250	30.30	261.05	3.61	78.7	441	5	332	0.10	0.65
RS191	523980	96600	20.03	244.88	5.08	78.5	443	6	312	0.08	0.75
RS196	509800	92200	6.08	205.75	5.10	71.7	419	7	287	0.03	0.57
Wi2065	511200	101000	2.78	122.64	22.16	67.0	431	33	183	0.02	0.57
S2>0.2 TOC>0.5	Minimum		0.02	0.57	0.25	1.0	414	5	41	0.01	0.45
	Maximum		30.30	261.05	22.16	78.7	460	108	332	0.19	0.81
	Mean		**4.29**	**80.05**	**7.64**	**42.5**	**437**	**27**	**150**	**0.05**	**0.62**
	Standard Deviation		8.15	86.44	7.02	32.7	11	25	91	0.04	0.10
	Count	18									
S1>0.2 S2>0.2 TOC>0.5	Minimum		0.23	8.76	0.91	6.5	414	5	57	0.01	0.45
	Maximum		30.30	261.05	22.16	78.7	447	33	332	0.10	0.78
	Mean		**5.90**	**110.14**	**10.05**	**57.8**	**434**	**17**	**178**	**0.04**	**0.60**
	Standard Deviation		9.16	83.97	6.80	24.4	9	9	86	0.03	0.09
	Count	13									
Eocän											
Wi2053	538400	97700	0.00	1.24	0.23	7.5	569	3	17	0.00	1.53

Table C1
A: Bulk rock mineralogy of shale samples from the Haute-Savoie and Geneva Basin
B: Bulk rock mineralogy of sandstones samples from the Haute-Savoie and Geneva Basin

No = sample number
X-Coord. & Y-Coord. = Swiss coordinates
Altitude = meters over sea-level
Qz = Quartz (in %)
Fsp = K-Feldspars (in %)
Plag = Na-Feldspars (in %)
Cc = Calcite (in %)
Dol = Dolomite (in %)
Py = Pyrite (in %)
ID = non-identified components (in %)

Calculated parameters (Zimmermann et al. 1976)
C = Carbonate indices = dolomite / (dolomite + calcite)
S = Silicate indices = quartz / (quartz + feldspars)
D = Detrtitism index = S-C

	No	Location	X-coord.	Y-Coord.	Altitude	Qz	Fsp	Plag	Cc	Dol	Py	ID	C	S	D
HAUTE-SAVOIE and GENEVA BASIN															
A: Shale															
Plateau Molasse															
OMM	RS31	Beauchâtel	478500	104800	380	22	5	6	18	2	0	47	0.1	0.7	0.6
	RS64	Franclens	474900	99500	400	36	2	0	5	0	0	57	0	0.9	0.9
	RS75	Hauteville sur Fier	485000	84900	350	24	3	13	14	16	0	30	0.5	0.6	0.1
	RS76	Hauteville sur Fier	485150	84800	340	19	7	6	24	8	0	36	0.3	0.6	0.3
	RS78	Belleville	490400	82700	400	34	0	11	15	4	1	35	0.2	0.8	0.5
USM	RS5	Peissy (Forage)	489970	119055	281	34	5	14	16	5	0	26	0.2	0.6	0.4
	RS8	Peissy (Forage)	489970	119055	211	32	3	0	23	5	0	37	0.2	0.9	0.7
	RS42	Le Fornant	484800	97500	345	32	5	17	30	5	0	11	0.1	0.6	0.4
	RS43	Le Fornant	484900	97600	345	42	7	16	0	20	0	15	1	0.6	-0.4
	RS44	Le Fornant	485100	97800	345	11	0	7	16	5	0	61	0.2	0.6	0.4
	RS45	Le Fornant	485250	98000	345	22	0	0	40	0	0	38	0	1	1
	RS48	Serrasson	485200	95600	380	32	5	15	19	4	0	25	0.2	0.6	0.4
	RS49	Serrasson	484800	95500	380	31	5	19	19	8	0	18	0.3	0.6	0.3
	RS51	Le Pont Rouge	478700	97600	320	28	7	16	16	2	0	31	0.1	0.5	0.4
	RS52	Mons	479990	98400	300	14	0	0	54	0	0	32	0	1	1
	RS53	Ruiss. de Coquetière	487950	100050	540	12	0	3	0	53	0	32	1	0.8	-0.2
	RS56	Ruiss. de la Findreuze	477600	94400	280	26	5	13	0	26	0	30	1	0.6	-0.4
	RS80	Pont Verre	491850	83650	380	22	0	0	16	3	0	59	0.2	1	0.8
	RS329	Genève	499550	117820	360	3	0	3	16	5	0	73	0.2	0.5	0.3
	RS330	Onex	496000	115000	430	20	3	9	19	3	2	44	0.1	0.6	0.5
	RS331	Avanchet	496200	119000	380	18	0	6	24	3	0	49	0.1	0.8	0.6
	RS345	Chatillon	492350	99100	400	36	6	10	31	3	0	14	0.1	0.7	0.6
Subalpine Molasse ("Molasse du Plateau de Bornes")															
USM	RS84	Picaillon	499000	96650	620	36	3	5	20	4	0	32	0.2	0.8	0.7
	RS86	Deyrier	499990	97500	610	39	4	11	1	0	0	45	0	0.7	0.7
	RS87	Ruiss. des Follats	499100	98900	750	20	0	0	40	0	0	40	0	1	1
	RS90	La Mouille	500000	103250	860	36	4	6	25	4	0	25	0.1	0.8	0.6
	RS95	Les Chavannes	502850	103400	810	28	0	13	26	3	0	30	0.1	0.7	0.6
	RS97	La Nérulaz	503600	98250	780	28	3	12	10	1	0	46	0.1	0.7	0.6
	RS98	La Nérulaz	503550	97950	740	39	11	17	3	1	0	29	0.3	0.6	0.3
	RS99	Le Chênay	503450	96850	640	20	4	12	17	3	0	44	0.2	0.6	0.4
	RS100	Le Reposoir	500050	93900	660	31	3	13	12	4	0	37	0.3	0.7	0.4
	RS101	Le Reposoir	500050	93900	660	24	0	7	21	3	0	45	0.1	0.8	0.6
	RS103	Les Tavernettes	501600	93050	510	23	0	8	30	6	0	33	0.2	0.7	0.6
	RS104a	Le Chênet	502150	91600	570	15	3	4	15	1	0	62	0.1	0.7	0.6
	RS125	Les Jouvenons	500400	89950	590	18	4	7	15	1	1	54	0.1	0.6	0.6
	RS126	Daudens	506500	97750	670	27	0	8	23	8	0	34	0.3	0.8	0.5
	RS127	Daudens	506500	97880	670	16	0	7	17	4	1	55	0.2	0.7	0.5
	RS138	Viaison	507425	112950	420	29	0	11	29	5	0	26	0.1	0.7	0.6
	RS141	Perraz	515600	108950	520	31	4	19	17	3	0	26	0.2	0.6	0.4
	RS142	Coudray	510450	102150	720	33	0	9	21	9	0	28	0.3	0.8	0.5
	RS143	Les Crues	509950	101250	820	29	0	14	28	3	0	26	0.1	0.7	0.6
UMM	RS108	Crêt Lambert	505580	93600	680	31	5	8	24	4	0	28	0.1	0.7	0.6
	RS109	Le Chêne	504750	91400	680	41	15	20	16	3	0	5	0.2	0.5	0.4

	No	Location	X-coord.	Y-Coord.	Altitude	Qz	Fsp	Plag	Cc	Dol	Py	ID	C	S	D
UMM	RS110	Le Chêne	504750	91400	680	23	0	5	25	3	0	44	0.1	0.8	0.7
	RS130	Le Clos	510300	98850	820	28	0	8	22	4	0	38	0.2	0.8	0.6
	RS132	Cady	512600	99700	760	19	0	4	25	1	0	51	0	0.8	0.8
	RS145	St.Maurice	516050	100700	580	26	4	6	24	3	0	38	0.1	0.7	0.6
Subalpine Chains ("Massif des Bornes", "Massif des Bauges")															
UMM	RS105	Pte de Puvat	514800	89990	1580	51	0	0	22	6	1	20	0.2	1	0.8
	RS106	Pte de Puvat	515300	89750	1680	16	0	16	50	0	1	17	0	0.5	0.5
	RS107	Montagne des Auges	515450	90050	1770	16	0	4	60	0	0	20	0	0.8	0.8
	RS113	Chez Gerlier	505150	89620	910	27	5	14	10	4	2	38	0.3	0.6	0.3
	RS116	Naves	503000	88080	600	21	0	4	22	1	0	52	0	0.8	0.8
	RS117	Sur les Bois	502820	86050	570	14	0	0	51	1	2	32	0	1	1
	RS118	Sur les Bois	502800	86150	530	18	3	6	2	0	0	71	0	0.7	0.7
	RS121	Nanoir	504250	86150	600	29	5	19	0	0	0	47	?	0.5	0.5
	RS123	Combadieu	503350	86620	540	24	4	12	12	2	0	46	0.1	0.6	0.5
	RS135	Montisel	515020	98050	1060	22	8	9	20	3	0	38	0.1	0.6	0.4
	RS146	St.Laurent	516450	99000	840	34	4	13	18	3	0	28	0.1	0.7	0.5
	RS148	Declairaz	518550	99050	800	20	0	0	67	0	0	13	0	1	1
	RS153	Sur les Saix	519600	100050	1120	36	3	17	8	1	0	35	0.1	0.6	0.5
	RS155	La Grange	522400	101050	720	30	0	17	25	0	0	28	0	0.6	0.6
	RS157	Pont de Lessy	521250	94750	1130	12	0	0	72	2	0	14	0	1	1
	RS158	Montagne des Arjules	521320	94200	1280	26	0	17	23	0	0	34	0	0.6	0.6
	RS160	Paradis	520700	93400	1620	14	0	6	58	0	0	22	0	0.7	0.7
	RS167	La Villaz	517200	85050	850	37	5	29	27	0	0	2	0	0.5	0.5
	RS173	Les Eculés	519700	86900	880	26	0	10	29	0	0	35	0	0.7	0.7
	RS176	Grand Bornand	521370	88800	1040	30	0	19	24	2	0	25	0.1	0.6	0.5
	RS181	Le Chimaillon	524200	92250	1330	17	0	10	50	2	3	18	0	0.6	0.6
	RS187	Les Volées	524600	100250	900	18	0	9	45	2	2	24	0	0.7	0.6
	RS190	Cenise	524350	97080	1630	13	0	8	11	1	0	67	0.1	0.6	0.5
	RS197	Plan Bois	509800	92200	750	24	3	13	9	3	0	48	0.3	0.6	0.4
Eocene	RS165	Mont Durand	520800	85250	1110	52	0	0	21	5	1	21	0.2	1	0.8
Fm.	RS205	Entrevernes	502650	69300	980	25	0	0	50	0	3	22	0	1	1
B: Sandstone															
Plateau Molasse															
OMM	RS35	Le Fornant	484400	97300	335	30	11	27	24	3	0	5	0.1	0.4	0.3
	RS38	Le Fornant	484550	97400	340	37	11	24	19	4	0	5	0.2	0.5	0.3
	RS72	Chez les Gay	482350	78400	390	42	10	19	8	8	0	13	0.5	0.6	0.1
	RS73	La Poterie	481400	77850	410	40	6	15	37	1	0	1	0	0.7	0.6
	RS77	Biolley	487650	83900	320	42	9	18	20	6	1	4	0.2	0.6	0.4
	RS340	Frangy	484400	97300	335	38	6	22	31	3	0	0	0.1	0.6	0.5
USM	RS2	Peissy (Forage)	489970	119055	337	35	10	39	1	1	1	13	0.5	0.4	-0.1
	RS327	Avully (forage)	489000	114100	340	28	7	29	10	2	0	24	0.2	0.4	0.3
	RS328	Genève	499400	119600	400	34	5	25	23	4	0	9	0.1	0.5	0.4
	RS332	Genève	499000	117375	369	33	5	12	37	0	0	13	0	0.7	0.7
	RS343	Chatillon	492350	99100	400	29	0	7	52	1	0	11	0	0.8	0.8
Subalpine Molasse ("Molasse du Plateau de Bornes")															
USM	RS83	Pont de la Caille	497800	96650	605	47	13	30	6	2	1	1	0.3	0.5	0.3
	RS137	Viaison	507425	113250	460	24	9	45	16	0	0	6	0	0.3	0.3
	RS227	Mont Gosse	506900	113500	625	31	13	20	30	1	0	5	0	0.5	0.5
	RS228	Mont Gosse	506975	113500	605	33	37	25	0	0	0	5	?	0.3	0.3
	RS232	Césarge	506850	112725	440	28	22	25	17	2	0	6	0.1	0.4	0.3
	RS250	Rossat	511325	114020	450	39	11	30	18	1	0	1	0.1	0.5	0.4
	RS350	Cruseilles	496600	98200	760	27	18	25	25	4	0	1	0.1	0.4	0.2
UMM	RS112	Le Chêne	504950	91600	700	37	19	19	22	2	0	1	0.1	0.5	0.4
	RS133	Cady	512650	99900	740	34	9	28	21	2	0	6	0.1	0.5	0.4
	RS252	Lucinge	514400	116950	980	34	11	28	17	0	0	10	0	0.5	0.5
Subalpine Chains ("Massif des Bornes", "Massif des Bauges")															
UMM	RS119	Nanoir	504250	86150	600	37	15	39	7	1	0	1	0.1	0.4	0.3
	RS147	St.Laurent	516550	99030	840	40	11	31	11	2	0	5	0.2	0.5	0.3
	RS150	Declairaz	518900	99150	850	36	4	19	15	0	0	26	0	0.6	0.6
	RS154	Sur les Saix	519600	100050	1120	45	6	12	16	1	0	20	0.1	0.7	0.7
	RS163	St.Jean de Sixt	520800	86000	1040	37	19	38	5	0	0	1	0	0.4	0.4
	RS166	La Villaz	517200	85050	830	41	8	48	0	0	0	3	?	0.4	0.4
	RS172	Forgeassoud	519300	86100	950	35	28	36	0	0	0	1	?	0.4	0.4
	RS191	Cenise	523980	96600	1640	35	4	24	14	1	1	21	0.1	0.6	0.5

Table C2

A: Relative content of phyllosilicates in the <2µm fraction of shale samples from the Haute-Savoie and Geneva Basin

B: Relative content of phyllosilicates in the <2µm fraction of sandstone samples from the Haute-Savoie and Geneva Basin

No = sample number
X-Coord. & Y-Coord. = Swiss coordinates
Altitude = meters over sea-level
M = Mica (in %)
C = Chlorite (in %)
I/S = Mixed-layer illite/smectite (in %)
K = Kaolinite (in %)
Co = Corrensite (in %)
Se = Serpentinite (in %)

	No	Location	X-coord.	Y-Coord.	Altitude	M	C	I/S	K	Co	Se
HAUTE-SAVOIE and GENEVA BASIN											
A: Shale											
Plateau Molasse											
OMM	RS31	Beauchâtel	478500	104800	380	51	23	26	0	0	0
	RS64	Franclens	474900	99500	400	32	4	60	4	0	0
	RS75	Hauteville sur Fier	485000	84900	350	46	36	18	0	0	0
	RS76	Hauteville sur Fier	485150	84800	340	53	32	15	0	0	0
	RS78	Belleville	490400	82700	400	30	40	30	0	0	0
USM	RS5	Peissy (Forage)	489970	119055	281	40	46	14	0	0	0
	RS8	Peissy (Forage)	489970	119055	211	36	41	22	0	0	0
	RS42	Le Fornant	484800	97500	345	52	40	8	0	0	0
	RS43	Le Fornant	484900	97600	345	32	26	42	0	0	0
	RS44	Le Fornant	485100	97800	345	49	40	11	0	0	0
	RS45	Le Fornant	485250	98000	345	50	29	21	0	0	0
	RS48	Serrasson	485200	95600	380	46	52	2	0	0	0
	RS49	Serrasson	484800	95500	380	50	38	12	0	0	0
	RS51	Le Pont Rouge	478700	97600	320	35	31	34	0	0	0
	RS52	Mons	479990	98400	300	50	20	25	5	0	0
	RS53	Ruiss. de Coquetière	487950	100050	540	49	36	15	0	0	0
	RS56	Ruiss. de la Findreuze	477600	94400	280	45	34	21	0	0	0
	RS80	Pont Verre	491850	83650	380	41	27	32	0	0	0
	RS329	Genève	499550	117820	360	49	39	12	0	0	0
	RS330	Onex	496000	115000	430	39	30	31	0	0	0
	RS331	Avanchet	496200	119000	380	45	34	21	0	0	0
	RS345	Chatillon	492350	99100	400	27	24	49	0	0	0
Subalpine Molasse ("Molasse du Plateau de Bornes")											
USM	RS84	Picaillon	499000	96650	620	40	24	36	0	0	0
	RS86	Deyrier	499990	97500	610	52	40	8	0	0	0
	RS87	Ruiss. des Follats	499100	98900	750	38	47	15	0	0	0
	RS90	La Mouille	500000	103250	860	60	18	22	0	0	0
	RS95	Les Chavannes	502850	103400	810	67	28	5	0	0	0
	RS97	La Nérulaz	503600	98250	780	58	34	8	0	0	0
	RS98	La Nérulaz	503550	97950	740	38	29	33	0	0	0
	RS99	Le Chênay	503450	96850	640	60	33	2	5	0	0
	RS100	Le Reposoir	500050	93900	660	62	31	7	0	0	0
	RS101	Le Reposoir	500050	93900	660	36	28	34	0	0	0
	RS103	Les Tavernettes	501600	93050	510	59	38	3	0	0	0
	RS104a	Le Chênet	502150	91600	570	72	22	6	0	0	0
	RS125	Les Jouvenons	500400	89950	590	67	19	14	0	0	0

	No	Location	X-coord.	Y-Coord.	Altitude	M	C	I/S	K	Co	Se
	RS126	Daudens	506500	97750	670	57	35	8	0	0	0
	RS127	Daudens	506500	97880	670	56	32	12	0	0	0
	RS138	Viaison	507425	112950	420	56	32	12	0	0	0
	RS141	Perraz	515600	108950	520	52	19	20	9	0	0
	RS142	Coudray	510450	102150	720	35	25	10	30	0	0
	RS143	Les Crues	509950	101250	820	40	46	14	0	0	0
UMM	RS108	Crêt Lambert	505580	93600	680	49	16	16	19	0	0
	RS109	Le Chêne	504750	91400	680	55	17	8	20	0	0
	RS110	Le Chêne	504750	91400	680	45	21	15	19	0	0
	RS130	Le Clos	510300	98850	820	43	24	18	15	0	0
	RS132	Cady	512600	99700	760	44	16	26	15	0	0
	RS145	St.Maurice	516050	100700	580	51	25	24	0	0	0
Subalpine Chains ("Massif des Bornes", "Massif des Bauges")											
UMM	RS105	Pte de Puvat	514800	89990	1580	76	11	13	0	0	0
	RS106	Pte de Puvat	515300	89750	1680	53	17	18	12	0	0
	RS107	Montagne des Auges	515450	90050	1770	47	18	21	14	0	0
	RS113	Chez Gerlier	505150	89620	910	52	18	16	14	0	0
	RS116	Naves	503000	88080	600	68	10	11	11	0	0
	RS117	Sur les Bois	502820	86050	570	61	10	11	18	0	0
	RS118	Sur les Bois	502800	86150	530	51	17	6	26	0	0
	RS121	Nanoir	504250	86150	600	60	10	30	0	0	0
	RS123	Combadieu	503350	86620	540	47	30	23	0	0	0
	RS135	Montisel	515020	98050	1060	60	26	14	0	0	0
	RS146	St.Laurent	516450	99000	840	56	13	26	5	0	0
	RS148	Declairaz	518550	99050	800	38	10	33	19	0	0
	RS153	Sur les Saix	519600	100050	1120	52	22	18	8	0	0
	RS155	La Grange	522400	101050	720	39	29	32	0	0	0
	RS157	Pont de Lessy	521250	94750	1130	42	22	26	10	0	0
	RS158	Montagne des Arjules	521320	94200	1280	73	23	4	0	0	0
	RS160	Paradis	520700	93400	1620	47	13	21	19	0	0
	RS167	La Villaz	517200	85050	850	57	15	19	9	0	0
	RS173	Les Eculés	519700	86900	880	48	20	32	0	0	0
	RS176	Grand Bornand	521370	88800	1040	52	22	20	6	0	0
	RS181	Le Chimaillon	524200	92250	1330	46	29	16	9	0	0
	RS187	Les Volées	524600	100250	900	47	17	28	8	0	0
	RS190	Cenise	524350	97080	1630	42	28	30	0	0	0
	RS197	Plan Bois	509800	92200	750	57	15	20	8	0	0
Eocene	RS165	Mont Durand	520800	85250	1110	52	16	27	5	0	0
Fm.	RS205	Entrevernes	502650	69300	980	33	8	16	43	0	0

B: Sandstone

Plateau Molasse

OMM	RS35	Le Fornant	484400	97300	335	46	33	21	0	0	0
	RS38	Le Fornant	484550	97400	340	49	36	15	0	0	0
	RS72	Chez les Gay	482350	78400	390	39	27	34	0	0	0
	RS73	La Poterie	481400	77850	410	32	43	16	9	0	0
	RS77	Biolley	487650	83900	320	44	31	24	0	0	0
	RS340	Frangy	484400	97300	335	29	23	42	0	0	6
USM	RS2	Peissy (Forage)	489970	119055	337	41	24	20	4	0	11
	RS327	Avully (forage)	489000	114100	340	21	19	50	0	0	10
	RS328	Genève	499400	119600	400	37	28	27	0	0	8
	RS332	Genève	499000	117375	369	31	29	40	0	0	0
	RS343	Chatillon	492350	99100	400	34	27	39	0	0	0

	No	Location	X-coord.	Y-Coord.	Altitude	M	C	I/S	K	Co	Se
Subalpine Molasse ("Molasse du Plateau de Bornes")											
USM	RS137	Viaison	507425	113250	460	22	18	0	5	43	12
	RS227	Mont Gosse	506900	113500	625	19	26	3	0	28	24
	RS228	Mont Gosse	506975	113500	605	7	5	1	2	66	19
	RS232	Césarge	506850	112725	440	4	5	0	0	80	11
	RS250	Rossat	511325	114020	450	10	12	0	0	78	0
	RS350	Cruseilles	496600	98200	760	12	13	1	0	51	23
UMM	RS112	Le Chêne	504950	91600	700	23	23	33	21	0	0
	RS133	Cady	512650	99900	740	27	30	14	29	0	0
	RS252	Lucinge	514400	116950	980	29	15	1	0	55	0
Subalpine Chains ("Massif des Bornes", "Massif des Bauges")											
UMM	RS119	Nanoir	504250	86150	600	60	21	19	0	0	0
	RS147	St.Laurent	516550	99030	840	63	31	6	0	0	0
	RS150	Declairaz	518900	99150	850	63	25	12	0	0	0
	RS154	Sur les Saix	519600	100050	1120	51	28	21	0	0	0
	RS163	St.Jean de Sixt	520800	86000	1040	51	19	16	8	0	6
	RS166	La Villaz	517200	85050	830	35	47	17	0	0	0
	RS172	Forgeassoud	519300	86100	950	52	28	20	0	0	0
	RS191	Cenise	523980	96600	1640	55	39	6	0	0	0

Table C3
Absolute intensities (in CPM = counts per minute) of main peaks of phyllosilicates in the <2m fraction of samples from the Haute-Savoie and Geneva Basin.

No = sample number
Strat. = Lithostratigraphic group
M1 = Mica (001)
M2 = Mica (002)
M5 = Mica (005)
C1 = Chlorite (001)
C2 = Chlorite (002)
C3 = Chlorite (003)
C4 = Chlorite (004)
C5 = Chlorite (005)
I/S = Mixed-layer illite/smectite (001/001)
K1 = Kaolinite (001)
Co2 = Corrensite (002)
Se1 = Serpentinite (001)

No	Strat.	M1	M2	M5	C1	C2	C3	C4	C5	I/S	K1	Co2	Se1
RS2	USM	13383	4689	1433	6020	7499	1859	3983	1076	7129	1362	-	4155
RS5	USM	55393	24005	12673	28223	66876	16451	38684	5471	42723	-	-	-
RS8	USM	27086	11453	7280	16799	32629	11613	20265	3541	12840	-	-	-
RS31	OMM	34133	14264	7695	12690	15355	4810	12552	1885	26343	-	-	-
RS35	OMM	26888	9085	7493	12174	19512	4513	20638	1291	15569	-	-	-
RS38	OMM	29215	10170	5100	10713	23478	5624	10952	1834	14067	-	-	-
RS42	USM	52694	20894	10619	20689	42232	13560	20954	3309	14121		-	-
RS43	USM	10732	3073	1810	9482	7860	2153	3868	1368	39892		-	-
RS44	USM	56712	25297	13931	27055	49625	14310	28330	4215	15191		-	-
RS45	USM	40963	16679	9823	14610	23948	7929	13859	2182	20482		-	-
RS48	USM	39325	13911	6415	14473	42530	9610	18797	3165	3533		-	-
RS49	USM	43641	15567	8351	19242	36014	9106	17325	3085	23910		-	-
RS51	USM	54547	21046	9470	21551	47948	14529	22990	3462	51410		-	-
RS52	USM	25214	7903	4587	12228	11799	3869	6740	1244	28948	2359	-	-
RS53	USM	31535	15997	7739	12557	26517	7416	15398	2399	5523		-	-
RS56	USM	14295	5143	2690	5480	10713	3512	5952	1261	6546		-	-
RS58	USM	11091	4064	3449	-	5233	2894	4556	1256	35215	3400	-	-
RS64	OMM	12220	3990	1740	-	1484	-	1946	-	23371	1500	-	-
RS70	OMM	20118	6594	3569	15562	17281	4138	7362	1059	10278	-	-	-
RS72	OMM	25046	9200	5027	16440	18201	4636	9028	1854	20000	-	-	-
RS73	OMM	8795	3011	1661	4178	13961	3629	7239	1188	4408	2718	-	-
RS75	OMM	37274	13754	7996	11338	30859	7803	15437	2772	36546	-	-	-
RS76	OMM	32617	10667	5396	6521	19308	4389	8718	1128	9112	-	-	-
RS77	OMM	11976	4227	2733	3191	8424	2270	4366	1428	6612	-	-	-
RS78	OMM	14314	5474	3219	21667	21855	5853	10488	1673	17547	-	-	-
RS80	USM	15880	4532	2683	6754	10577	2277	4508	1257	12538	-	-	-
RS83	USM	4267	1300	1502	1536	14625	-	10550	5298	-	-	-	-
RS84	USM	28903	10562	5789	-	17485	4409	9329	-	26210	-	-	-
RS86	USM	70814	32522	16374	24120	53670	18006	30523	3812	10800	-	-	-
RS87	USM	24411	10522	6030	10739	30782	8249	14809	2177	4827	-	-	-
RS90	USM	14266	4894	3805	6141	3666	-	3414	-	8016	-	-	-
RS95	USM	30416	13957	9557	6201	15071	3096	6442	1175	2193	-	-	-
RS97	USM	36500	17409	10671	8654	23258	5633	10642	1590	2358	-	-	-
RS98	USM	37109	16954	9147	11568	27873	7598	14329	2285	32296	-	-	-
RS99	USM	47490	19327	11825	10856	29247	6417	12906	2026	2710	3800	-	-
RS100	USM	42886	19503	11743	8383	23171	5764	11106	1847	10780	-	-	-
RS101	USM	39411	20702	11877	14385	30915	10196	19375	3770	38444	-	-	-
RS103	USM	27857	11951	7812	6205	17576	4396	7319	1320	1554	-	-	-
RS104a	USM	17438	3807	4405	1919	5082	1478	2961	-	1325	1000	-	-
RS105	UMM	17567	7409	5537	1038	2726	-	1257	-	2101	-	-	-
RS106	UMM	11609	3943	2190	1824	6571	1004	2139	-	2577	3200	-	-
RS107	UMM	11569	5103	2864	2086	8665	1234	3002	-	3357	3000	-	-
RS108	UMM	16623	7141	5235	3544	11707	1103	3810	-	5855	6000	-	-
RS109	UMM	22446	9098	5330	4420	15864	2041	5731	967	1500	8000	-	-
RS110	UMM	17427	7912	5444	4019	14902	1477	5479	1443	2128	7600	-	-
RS112	UMM	15646	5449	3007	8266	15741	3012	12407	1518	22075	14300	-	-
RS113	UMM	24236	10218	6728	4926	13415	2804	5962	1001	2834	6000	-	-
RS116	UMM	23775	10366	7178	1787	3602	-	2885	-	2832	4300	-	-
RS117	UMM	17494	6313	3499	1768	3078	1016	2617	968	2640	5600	-	-
RS118	UMM	30573	12780	6748	6702	25770	3513	8952	1306	3000	15600	-	-
RS119	UMM	21877	8630	4748	4560	8365	1621	3789		6240		-	-

No	Strat.	M1	M2	M5	C1	C2	C3	C4	C5	I/S	K1	Co2	Se1
RS121	UMM	30098	13406	6357	-	4038	2774	4334	-	8072	-	-	-
RS123	UMM	34018	13881	8092	-	21688	4039	11441	1827	15960	-	-	-
RS125	USM	71168	33318	21014	12561	22712	7723	16332	2517	3505	-	-	-
RS126	USM	27872	11924	7354	7635	19126	4890	8770	1693	3048	-	-	-
RS127	USM	74937	31197	16900	18673	42592	11702	20901	2805	15776	-	-	-
RS130	UMM	13373	4269	2057	5230	7832	2021	4860	961	3435	-	-	-
RS132	UMM	22438	7493	4021	5561	8329	1323	6354	1252	12255	8000	-	-
RS133	UMM	22459	9130	4374	11989	25055	5663	19539	1757	11260	25000	-	-
RS135	UMM	23992	10534	6556	3923	10827	2022	4311	1015	6840	-	-	-
RS137	USM	11042	4497	2179	4500	8727	2794	5853	1204	-	2400	21360	6036
RS138	USM	17424	7749	4676	4995	10453	2346	4490	1029	2281	-	-	-
RS141	USM	18353	8570	4610	2700	6052	1712	3813	1137	7500	-	-	-
RS142	USM	27976	13235	7606	14133	20073	14179	21538	4817	7456	23000	-	-
RS143	USM	25799	11551	5371	13989	25505	7498	12381	2352	5579	-	-	-
RS145	UMM	15437	6879	3860	2949	6659	1463	2902	1336	4380	-	-	-
RS146	UMM	13303	4968	2937	1652	3366	1108	2666		3780	1000	-	-
RS147	UMM	22217	8078	4121	4045	10981	2039	7278	1756	1997	-	-	-
RS148	UMM	6285	1767	1060	-	1098	-	1210	-	3420	2700	-	-
RS150	UMM	20200	9497	4945	2445	7883	2239	5575	-	4080	-	-	-
RS153	UMM	10230	3939	1595	1803	4083	1160	2905	900	3420	1500	-	-
RS154	UMM	19051	6887	3619	3641	10367	2210	4715	-	7620	-	-	-
RS155	UMM	16254	6143	3488	2912	8302	1498	3680	-	4320	-	-	-
RS157	UMM	8341	3547	1370	1399	5665	1463	3735	-	4165	3300	-	-
RS158	UMM	22047	8831	5182	2078	6978	1564	4245	-	1200	-	-	-
RS160	UMM	9370	2878	1966	1684	3447	1013	2182	845	2640	2500	-	-
RS163	UMM	12167	4224	2387	4916	4216	1150	3143	1000	3540	1800	-	1300
RS165	Eocene Fm.	16335	7704	4887	-	4150	-	2628	875	7354	1500	-	-
RS166	UMM	10462	4055	2002	-	13906	5227	10024	1133	5160	-	-	-
RS167	UMM	10309	3350	2192	1836	2500	-	2483	-	3180	1200	-	-
RS172	UMM	19276	7331	4057	13020	10236	2365	6343	1191	7680	-	-	-
RS173	UMM	16325	7032	3914	1616	6256	1304	3624	-	7260	-	-	-
RS176	UMM	20287	7867	4432	2245	9355	1524	3744	1070	3420	1800	-	-
RS181	UMM	14102	5516	2292	2962	6107	2129	3909	945	2760	2200	-	-
RS187	UMM	15132	5859	2697	1596	5008	1312	3347	1081	4500	2500	-	-
RS190	UMM	20807	8352	4904	2258	12953	2274	5159	1366	7020	-	-	-
RS191	UMM	24152	8426	4467	4973	17283	3018	7116	1823	2700	-	-	-
RS197	UMM	20305	9278	5125	2656	5063	1374	2905	-	4221	2600	-	-
RS205	Eocene Fm.	10817	3090	1096	-	2784	-	2185	-	-	-	-	-
RS227	USM	6775	2952	1614	2880	7882	1536	3431	1178	1500	-	10140	8674
RS228	USM	5631	3520	1955	-	4014	-	4355	1518	500	1400	56321	16412
RS232	USM	6322	3394	1640	-	5411	1633	5969	3877	-	-	155881	20604
RS250	USM	34723	16082	6527	-	39524	9835	20098	8084	-	-	260488	-
RS252	UMM	21539	9849	1997	-	11212	2430	5496	1653	800	-	41450	-
RS327	USM	67328	30011	3188	-	60213	14222	32947	7228	157423	-	-	27401
RS328	USM	70582	27794	13775	18552	53817	13591	28891	3939	52621	-	-	16317
RS329	USM	37468	16290	8298	13997	29673	7089	15849	2199	9743	-	-	-
RS330	USM	40617	14877	7508	14061	31557	7875	18247	2944	32445	-	-	-
RS331	USM	17821	6335	3363	5847	13497	2885	7030		8600	-	-	-
RS332	USM	55496	21023	10755	19025	53210	10643	25178	3434	71931	-	-	-
RS340	OMM	28391	8274	3324	8862	22669	5253	9585	2750	40894	-	-	-
RS343	USM	35915	14878	7671	13292	29207	8092	16393	2920	41222	-	-	-
RS345	USM	19563	7362	4432	7156	17320	3382	8042	1499	34403	-	-	-
RS350	USM	12215	5049	2047	-	13094	2512	7877	2209	-	-	50740	21412

Table C4
Absolute intensities (in CPM = counts per minute) of associated minerals in the <2µm and the 2-16µm fraction.
No = sample number
Strat. = lithostratigraphic group
Qz (<2) = Quartz (100), <2µm fraction
Kfsp (<2) = K-feldspar at about 3.25 Å, <2µm fraction
Plag (<2) = Plagioclase at about 3.19 Å, <2µm fraction
Qz (2-16) = Quartz (100), 2-16µm fraction
Kfsp (2-16) = K-feldspar at about 3.25 Å, 2-16µm fraction
Plag (2-16) = Plagioclase at about 3.19 Å, 2-16µm fraction
Qz 100/101 (BR) = relation between the intensities of the (100) and (101) peak of quartz from the bulk rock analysis

No	Strat.	Qz (<2)	Kfsp (<2)	Plag (<2)	Qz (2-16)	Kfsp (2-16)	Plag (2-16)	Qz 100/101 (BR)
RS2	USM	7786	-	980	7974	10104	2148	0.18
RS5	USM	54239	8384	3820	21762	16863	5284	0.18
RS8	USM	40272	6580	-	21104	1678	6407	0.17
RS31	OMM	28537	3998	2279	13926	5775	4128	0.18
RS35	OMM	17407	3203	3221	27824	12314	20188	0.18
RS38	OMM	17783	1820	4085	11085	50305	9386	0.18
RS42	USM	38304	4674	3402	18794	24147	7350	0.2
RS43	USM	17791	1551	1953	29338	60647	21196	0.2
RS44	USM	52656	9401	8168	18725	24139	5070	0.16
RS45	USM	37463	8096	4468	16550	6413	6137	0.17
RS48	USM	25097	3849	5536	14941	28550	8501	0.17
RS49	USM	33411	5254	5160	23670	24867	8723	0.18
RS51	USM	34140	5939	2843	17009	10968	7604	0.19
RS52	USM	18226	4014	1754	14548	24468	14832	0.19
RS53	USM	36595	3761	1918	18771	11379	3637	0.18
RS56	USM	12232	1639	1329	14682	22211	10488	0.16
RS58	USM	35532	3960	1799	16100	5187	9672	-
RS64	OMM	173337	1605	-	19184	1433	4161	0.17
RS70	OMM	12943	2662	954	18707	75798	18130	0.17
RS72	OMM	17943	2041	1335	12491	94438	9869	0.2
RS73	OMM	7363	1278	1755	6215	17433	3213	0.19
RS75	OMM	33500	4826	2625	18368	82895	15187	0.18
RS76	OMM	19550	2185	2486	14896	8863	7070	0.17
RS77	OMM	8453	1556	1567	21132	22361	6106	0.15
RS78	OMM	22277	2649	1393	21831	12090	3410	0.18
RS80	USM	12261	1745	-	22689	2232	5778	0.17
RS83	USM	12626	1124	2259	12876	35751	17547	0.19
RS84	USM	22192	3231	1643	30512	2560	3417	0.18
RS86	USM	58904	8060	5236	31382	25540	8934	0.16
RS87	USM	23250	3806	1878	11924	2634	2700	0.16
RS90	USM	14878	1473	2694	-	-	-	0.19
RS95	USM	26198	1872	3149	14595	26585	6884	0.17
RS97	USM	29882	2447	3979	12848	14696	4133	0.18
RS98	USM	29374	5281	4245	17014	14677	4477	0.16
RS99	USM	34900	2722	3247	16833	20901	3279	0.16
RS100	USM	32489	2563	3690	14921	15953	3945	0.16
RS101	USM	47958	6693	3651	24064	9148	4699	0.17
RS103	USM	23470	2222	3028	16610	15025	2960	0.17
RS104a	USM	12737	1297	1426	5353	5939	2766	0.17
RS105	UMM	20915	1773	-	14982	-	2058	0.17
RS106	UMM	8821	2357	2405	10443	6594	1272	0.17
RS107	UMM	18583	1503	4079	16515	9531	2163	0.18
RS108	UMM	17530	1364	1433	15512	11206	4004	0.2
RS109	UMM	22611	1232	1521	15414	11508	3773	0.2
RS110	UMM	22613	2072	2069	16574	8232	1918	0.18
RS112	UMM	45137	2116	4116	31556	27482	19362	0.19
RS113	UMM	21445	2143	4872	17078	23133	6479	0.2
RS116	UMM	22553	1971	1405	13551	6892	4948	0.18
RS117	UMM	12999	1040	2792	9967	12492	3475	0.18
RS118	UMM	33112	3436	4598	17027	15252	7116	0.17
RS119	UMM	15650	1233	1762	6525	10786	-	0.16
RS121	UMM	25602	-	2694	14409	22900	4647	0.2
RS123	UMM	41540	5881	3889	22608	9257	3952	0.16
RS125	USM	59326	9479	5271	15757	8734	4281	0.17
RS126	USM	21038	2827	2442	18961	17539	3570	0.18
RS127	USM	55033	5505	6170	20759	14654	6971	0.18
RS130	UMM	13519	1498	1096	21111	10130	3031	0.18
RS132	UMM	23037	2521	1188	20858	3957	3401	0.16
RS133	UMM	48449	4654	4154	29666	16128	10985	0.19
RS135	UMM	19442	1518	3121	13252	11684	3503	0.16

No	Strat.	Qz (<2)	Kfsp (<2)	Plag (<2)	Qz (2-16)	Kfsp (2-16)	Plag (2-16)	Qz 100/101 (BR)
RS137	USM	9052	1037	1440	19530	20841	6060	0.19
RS138	USM	14721	1139	1844	16497	19217	7635	0.18
RS141	USM	16778	2124	8400	10038	14185	4802	0.19
RS142	USM	46956	-	3543	27936	5485	1686	0.18
RS143	USM	20783	3627	2993	19000	31009	4651	0.19
RS145	UMM	11543	1887	1613	16192	12452	6898	0.18
RS146	UMM	11650	1289	1386	14082	15960	3310	0.17
RS147	UMM	17709	2094	5170	16108	26001	5926	0.18
RS148	UMM	11460	1486	1163	9496	3592	2811	0.16
RS150	UMM	31849	2854	3377	18450	15169	3303	0.19
RS153	UMM	7125	1062	1016	2741	1871	990	0.18
RS154	UMM	12012	1289	2007	5945	11886	3407	0.15
RS155	UMM	12426	1495	1658	11063	14238	1379	0.19
RS157	UMM	10412	2409	1810	7456	4281	1035	0.17
RS158	UMM	17146	2029	4382	12289	18045	1728	0.18
RS160	UMM	3.34	1245	1385	8096	9120	1389	0.16
RS163	UMM	8204	-	-	4486	7872	1735	0.19
RS165	Eocene Fm.	25928	1947	-	18371	1223	1611	0.19
RS166	UMM	34134	1770	6758	26190	64522	14215	0.16
RS167	UMM	7864	1285	1909	5738	14765	1944	0.18
RS172	UMM	24853	2080	4539	21669	19409	4597	0.17
RS173	UMM	15951	1617	3943	5674	7519	-	0.18
RS176	UMM	15325	1550	1640	11120	11046	1147	0.16
RS181	UMM	11562	1269	3256	8739	8838	-	0.16
RS187	UMM	12404	1972	4973	6172	17579	1032	0.16
RS190	UMM	17267	-	4750	15077	10657	1013	0.18
RS191	UMM	19641	2372	4743	11307	21649	4609	0.16
RS197	UMM	18638	1756	2594	10457	11197	3624	0.16
RS205	Eocene Fm.	7836	2322	1175	8224	-	1346	0.2
RS227	USM	31550	2785	4478	14397	29359	14753	0.18
RS228	USM	21869	1441	2261	16453	12961	7396	0.19
RS232	USM	17337	1826	4132	18304	24769	10656	0.18
RS250	USM	30222	3526	2844	21945	16655	7072	0.14
RS252	UMM	53067	3208	7396	26476	31607	8862	0.22
RS327	USM	60279	8860	6403	29176	20882	6557	0.16
RS328	USM	50375	8053	10236	26476	26591	9302	0.2
RS329	USM	28425	3283	4503	13158	28594	9403	-
RS330	USM	43484	6696	3318	32372	27511	10543	0.18
RS331	USM	11904	1842	-	13422	4637	-	0.17
RS332	USM	31066	3889	3102	30442	12522	5887	0.17
RS340	OMM	29439	3384	10333	33480	55834	10382	0.2
RS343	USM	33949	2869	3615	18405	18464	10396	0.2
RS345	USM	22600	3011	1541	31288	13680	8031	0.18
RS350	USM	26255	1473	6012	30250	49707	17727	0.15

Table C5

A: Estimation of the percentage of smectite layers in mixed-layer illite/smectite in shale samples from the Haute-Savoie and Geneva Basin

B: Estimation of the percentage of smectite layers in mixed-layer illite/smectite inf sandstones samples from the Haute-Savoie and Geneva Basin

No = sample number
X-Coord. & Y-Coord. = Swiss coordinates
Altitude = meters above sea-level

IS1 (Å) = 001/001 peakof I/S in Å
IS1 = 001/001 peak of I/S in °2θ
IS2 = 001/002 peakof I/S in °2θ
IS3 = 002/003 peak of I/S in °2θ
peak position

Δ1 = angular difference of the 001/002 and the 002/003 peak of I/S in °2θ
Δ2 = angular difference of the 001/001 and the 001/002 peak of I/S in °2θ
S (IS1) = estimation of the % smectite layers in I/S using the position of 001/001 peak (Weaver 1956)
S (IS2) = estimation of the % smectite layers in I/S using the position of 001/002 peak (Moore & Reynolds 1989)
S (IS3) = estimation of the % smectite layers in I/S using the position of 002/003 peak (Moore & Reynolds 1989)
S (Δ1a) = estimation of the % smectite layers in I/S using the angular difference Δ1 (Moore & Reynolds 1989)
S (Δ1b) = estimation of the % smectite layers in I/S using the angular difference Δ1 (Vuitel 1987, Srodon 1984)
S (Δ1/Δ2) = estimation of the % smectite layers in I/S using the angular differences Δ1 and Δ2 (Vuitel 1987, Srodon 1984)
IC = illite cristallinity in °2θ

	No	Location	X-coord.	Y-Coord.	Altitude	IS1 (Å)	IS1	IS2	IS3	Δ1	Δ2	S (IS1)	S (IS2)	S (IS3)	S (Δ1a)	S (Δ1b)	S (Δ1/Δ2)	IC
HAUTE-SAVOIE and GENEVA BASIN																		
A: Shale																		
Plateau Molasse																		
OMM	RS31	Beauchâtel	478500	104800	380	16.52	5.34	9.67	16.00	6.33	4.33	73	44	71	53	59	52	0.34
	RS64	Franclens	474900	99500	400	16.57	5.33	9.47	16.12	6.65	4.14	75	34	62	44	49	60	0.70
	RS75	Hauteville sur Fier	485000	84900	350	16.99	5.20	-	15.84	-	-	98	-	85	-	-	-	0.27
	RS76	Hauteville sur Fier	485150	84800	340	17.49	5.05	10.25	15.74	5.49	5.20	100	84	96	100	94	94	0.19
	RS78	Belleville	490400	82700	400	15.38	5.74	10.00	-	-	4.26	46	64	-	-	-	-	0.44
USM	RS5	Peissy (Forage)	489970	119055	281	16.25	5.40	10.20	15.80	5.60	4.80	63	80	89	83	89	87	0.40
	RS8	Peissy (Forage)	489970	119055	211	16.55	5.34	10.10	16.20	6.10	4.76	74	71	56	61	68	61	0.63
	RS42	Le Fornant	484800	97500	345	16.43	5.37	10.21	15.90	5.69	4.84	69	81	79	78	85	81	0.28
	RS43	Le Fornant	484900	97600	345	16.61	5.31	10.28	15.87	5.59	4.97	77	87	82	83	90	89	0.34
	RS44	Le Fornant	485100	97800	345	15.97	5.53	10.00	16.30	6.30	4.47	56	64	51	54	60	54	0.36
	RS45	Le Fornant	485250	98000	345	16.37	5.40	9.82	15.98	6.16	4.42	67	52	72	59	66	58	0.41
	RS48	Serrasson	485200	95600	380	13.01	6.79	-	-	-	-	30	-	-	-	-	-	0.23
	RS49	Serrasson	484800	95500	380	16.17	5.46	-	-	-	-	61	-	-	-	-	-	0.35
	RS51	Le Pont Rouge	478700	97600	320	17.04	5.18	10.45	15.91	5.46	5.27	100	100	78	100	95	95	0.29
	RS52	Mons	479990	98400	300	16.43	5.37	10.03	15.85	5.82	4.66	69	66	84	72	80	74	0.38

	No	Location	X-coord.	Y-Coord.	Altitude	IS1 (Å)	IS1	IS2	IS3	Δ1	Δ2	S (IS1)	S (IS2)	S (IS3)	S (Δ1a)	S (Δ1b)	S (Δ1/Δ2)	IC
USM	RS53	Ruiss. de Coquetière	487950	100050	540	15.84	5.57	-	-	-	-	53	-	-	-	-	-	0.38
	RS56	Ruiss. de la Findreuze	477600	94400	280	17.56	5.02	-	-	-	-	100	-	-	-	-	-	0.22
	RS80	Pont Verre	491850	83650	380	17.18	5.13	10.20	16.04	5.84	5.07	100	80	67	71	79	77	0.28
	RS329	Genève	499550	117820	360	16.89	5.23	-	-	-	-	92	-	-	-	-	-	0.17
	RS330	Onex	496000	115000	430	17.33	5.10	9.23	15.65	6.42	4.13	100	22	100	50	56	59	0.33
	RS331	Avanchet	496200	119000	380	17.06	5.17	-	-	-	-	100	-	-	-	-	-	0.24
	RS345	Chatillon	492350	99100	400	17.69	4.99	10.15	15.76	5.61	5.16	100	75	93	82	89	90	-
Subalpine Molasse ("Molasse du Plateau de Bornes")																		
USM	RS84	Picaillon	499000	96650	620	16.55	5.33	-	16.00	-	-	74	-	71	-	-	-	0.36
	RS86	Deyrier	499990	97500	610	15.19	5.82	-	-	-	-	44	-	-	-	-	-	0.36
	RS87	Ruiss. des Follats	499100	98900	750	15.24	5.80	-	-	-	-	44	-	-	-	-	-	0.36
	RS90	La Mouille	500000	103250	860	16.67	5.31	-	-	-	-	79	-	-	-	-	-	0.30
	RS95	Les Chavannes	502850	103400	810	14.77	5.98	-	-	-	-	40	-	-	-	-	-	0.17
	RS97	La Nérulaz	503600	98250	780	14.46	6.11	-	-	-	-	38	-	-	-	-	-	0.17
	RS98	La Nérulaz	503550	97950	740	16.91	5.22	10.53	15.99	5.46	5.31	93	100	71	100	95	95	0.26
	RS99	Le Chênay	503450	96850	640	13.30	6.64	-	-	-	-	31	-	-	-	-	-	0.19
	RS100	Le Reposoir	500050	93900	660	16.47	5.36	-	-	-	-	71	-	-	-	-	-	0.24
	RS101	Le Reposoir	500050	93900	660	16.99	5.19	10.09	15.95	5.86	4.90	98	70	75	70	78	70	0.38
	RS103	Les Tavernettes	501600	93050	510	13.01	6.79	-	-	-	-	30	-	-	-	-	-	0.19
	RS104a	Le Chênet	502150	91600	570	10.66	8.29	-	-	-	-	17	-	-	-	-	-	0.18
	RS125	Les Jouvenons	500400	89950	590	13.17	6.71	-	-	-	-	31	-	-	-	-	-	0.39
	RS126	Daudens	506500	97750	670	14.10	6.98	-	-	-	-	36	-	-	-	-	-	0.25
	RS127	Daudens	506500	97880	670	16.47	5.36	10.00	16.00	6.00	4.64	71	64	71	65	72	66	0.31
	RS138	Viaison	507425	112950	420	12.38	7.13	-	16.50	-	-	26	-	41	-	-	-	0.21
	RS141	Perraz	515600	108950	520	14.30	6.17	-	-	-	-	37	-	-	-	-	-	0.28
	RS142	Coudray	510450	102150	720	15.87	5.56	9.05	16.95	7.90	3.49	53	13	25	11	21	32	0.31
	RS143	Les Crues	509950	101250	820	15.67	5.64	-	-	-	-	50	-	-	-	-	-	0.26
UMM	RS108	Crêt Lambert	505580	93600	680	15.92	5.55	9.30	-	-	3.75	54	26	-	-	-	-	0.22
	RS109	Le Chêne	504750	91400	680	15.67	5.64	9.20	-	-	3.56	50	21	-	-	-	-	0.16
	RS110	Le Chêne	504750	91400	680	10.20	8.67	-	-	-	-	11	-	-	-	-	-	0.27
	RS130	Le Clos	510300	98850	820	13.04	6.78	-	-	-	-	30	-	-	-	-	-	0.43
	RS132	Cady	512600	99700	760	17.04	5.18	9.62	16.60	6.98	4.44	100	41	37	35	41	42	0.24
	RS145	St.Maurice	516050	100700	580	10.03	8.84	-	17.50	-	-	7	-	4	-	-	-	0.23
Subalpine Chains ("Massif des Bornes", "Massif des Bauges")																		
UMM	RS105	Pte de Puvat	514800	89990	1580	10.46	8.45	-	-	-	-	15	-	-	-	-	-	0.17
	RS106	Pte de Puvat	515300	89750	1680	10.09	8.77	-	-	-	-	8	-	-	-	-	-	0.25
	RS107	Montagne des Auges	515450	90050	1770	10.39	8.50	-	-	-	-	14	-	-	-	-	-	0.27
	RS113	Chez Gerlier	505150	89620	910	10.14	8.73	-	-	-	-	9	-	-	-	-	-	0.22
	RS116	Naves	503000	88080	600	10.23	8.64	-	-	-	-	11	-	-	-	-	-	0.17

	No	Location	X-coord.	Y-Coord.	Altitude	IS1 (Å)	IS1	IS2	IS3	Δ1	Δ2	S (IS1)	S (IS2)	S (IS3)	S (Δ1a)	S (Δ1b)	S (Δ1/Δ2)	IC
UMM	RS117	Sur les Bois	502820	86050	570	10.34	8.55	-	-	-	-	13	-	-	-	-	-	0.15
	RS118	Sur les Bois	502800	86150	530	15.78	5.60	9.74	16.21	6.47	4.14	52	48	56	49	55	48	0.39
	RS121	Nanoir	504250	86150	600	10.40	8.51	-	-	-	-	14	-	-	-	-	-	0.82
	RS123	Combadieu	503350	86620	540	16.90	5.23	10.09	15.96	5.87	4.86	92	70	74	70	78	73	0.19
	RS135	Montisel	515020	98050	1060	10.45	8.45	-	17.00	-	-	14	-	24	-	-	-	0.21
	RS146	St.Laurent	516450	99000	840	10.40	8.50	-	-	-	-	14	-	-	-	-	-	0.34
	RS148	Declairaz	518550	99050	800	10.26	8.62	-	-	-	-	12	-	-	-	-	-	0.76
	RS153	Sur les Saix	519600	100050	1120	10.73	8.24	-	-	-	-	17	-	-	-	-	-	0.35
	RS155	La Grange	522400	101050	720	10.16	8.70	-	17.50	-	-	10	-	4	-	-	-	0.30
	RS157	Pont de Lessy	521250	94750	1130	10.55	8.37	-	17.50	-	-	16	-	4	-	-	-	0.77
	RS158	Montagne des Arjules	521320	94200	1280	10.45	8.46	-	-	-	-	14	-	-	-	-	-	0.22
	RS160	Paradis	520700	93400	1620	10.32	8.56	-	-	-	-	13	-	-	-	-	-	0.20
	RS167	La Villaz	517200	85050	850	10.08	8.77	-	-	-	-	8	-	-	-	-	-	0.27
	RS173	Les Eculés	519700	86900	880	10.60	8.35	-	-	-	-	16	-	-	-	-	-	0.57
	RS176	Grand Bornand	521370	88800	1040	10.43	8.48	-	17.50	-	-	14	-	4	-	-	-	0.22
	RS181	Le Chimaillon	524200	92250	1330	10.12	8.74	-	17.50	-	-	9	-	4	-	-	-	0.21
	RS187	Les Volées	524600	100250	900	10.12	8.74	-	-	-	-	9	-	-	-	-	-	0.33
	RS190	Cenise	524350	97080	1630	10.60	8.34	-	17.20	-	-	16	-	17	-	-	-	0.53
	RS197	Plan Bois	509800	92200	750	10.22	8.65	-	-	-	-	11	-	-	-	-	-	0.25
Eocene	RS165	Mont Durand	520800	85250	1110	10.31	8.58	-	17.50	-	-	12	-	4	-	-	-	0.23
Fm.	RS205	Entrevernes	502650	69300	980	11.10	7.96	-	-	-	-	20	-	-	-	-	-	1.22
B: Sandstone																		
Plateau Molasse																		
OMM	RS35	Le Fornant	484400	97300	335	16.05	5.50	9.76	15.90	6.14	4.26	57	49	79	59	66	58	0.25
	RS38	Le Fornant	484550	97400	340	16.28	5.42	-	-	-	-	64	-	-	-	-	-	0.18
	RS72	Chez les Gay	482350	78400	390	13.04	6.78	-	-	-	-	30	-	-	-	-	-	0.19
	RS73	La Poterie	481400	77850	410	16.66	5.30	-	-	-	-	79	-	-	-	-	-	0.15
	RS77	Biolley	487650	83900	320	17.12	5.15	-	-	-	-	100	-	-	-	-	-	0.19
	RS340	Frangy	484400	97300	335	16.66	6.03	-	-	-	-	79	-	-	-	-	-	0.26
USM	RS2	Peissy (Forage)	489970	119055	337	12.98	6.80	-	-	-	-	30	-	-	-	-	-	0.33
	RS327	Avully (forage)	489000	114100	340	16.69	5.29	10.67	15.79	5.12	5.38	80	100	90	100	99	100	0.34
	RS328	Genève	499400	119600	400	16.94	5.21	10.30	16.00	5.70	5.09	95	89	71	78	85	84	0.25
	RS332	Genève	499000	117375	369	17.13	5.16	10.02	15.86	5.84	4.86	100	65	83	71	79	75	0.29
	RS343	Chatillon	492350	99100	400	17.47	5.05	10.07	15.68	5.61	5.02	100	69	100	82	89	91	0.26
Subalpine Molasse ("Molasse du Plateau de Bornes")																		
USM	RS137	Viaison	507425	113250	460	10.40	8.50	9.35	17.40	8.05	0.85	14	28	9	7	18	15	0.23
	RS227	Mont Gosse	506900	113500	625	10.78	8.20	-	-	-	-	18	-	-	-	-	-	0.18
	RS228	Mont Gosse	506975	113500	605	10.65	8.30	-	-	-	-	17	-	-	-	-	-	0.17

	No	Location	X-coord.	Y-Coord.	Altitude	IS1 (Å)	IS1	IS2	IS3	Δ1	Δ2	S (IS1)	S (IS2)	S (IS3)	S (Δ1a)	S (Δ1b)	S (Δ1/Δ2)	IC
USM	RS232	Césarge	506850	112725	440	10.53	8.40	-	-	-	-	15	-	-	-	-	-	0.28
	RS250	Rossat	511325	114020	450	10.40	8.50	-	-	-	-	14	-	-	-	-	-	0.26
	RS350	Cruseilles	496600	98200	760	10.78	8.20	-	-	-	-	18	-	-	-	-	-	-
UMM	RS112	Le Chêne	504950	91600	700	17.09	5.16	9.57	15.80	6.23	4.41	100	39	89	56	63	71	0.33
	RS133	Cady	512650	99900	740	16.84	5.24	-	15.84	-	-	89	-	85	-	-	-	0.16
	RS252	Lucinge	514400	116950	980	10.92	8.10	9.20	17.10	7.90	1.10	19	21	20	11	21	22	0.26
Subalpine Chains ("Massif des Bornes", "Massif des Bauges")																		
UMM	RS119	Nanoir	504250	86150	600	13.43	6.58	9.93	-	-	3.35	32	59	-	-	-	-	0.19
	RS147	St.Laurent	516550	99030	840	13.12	6.73	9.11	16.75	7.64	2.38	30	16	32	18	27	28	0.19
	RS150	Declairaz	518900	99150	850	10.64	8.31	9.10	17.00	7.90	0.79	17	15	24	11	21	21	0.18
	RS154	Sur les Saix	519600	100050	1120	10.45	8.46	9.10	17.20	8.10	0.64	14	15	17	6	17	16	0.12
	RS163	St.Jean de Sixt	520800	86000	1040	10.26	8.62	-	-	-	-	12	-	-	-	-	-	0.31
	RS166	La Villaz	517200	85050	830	13.87	6.37	-	-	-	-	35	-	-	-	-	-	0.26
	RS172	Forgeassoud	519300	86100	950	10.63	8.32	-	-	-	-	16	-	-	-	-	-	0.25
	RS191	Cenise	523980	96600	1640	10.60	8.34	-	-	-	-	16	-	-	-	-	-	0.22

Table C6
Positions and intensities of basal reflections of corrensite and calculated d-spacing.

No = sample number
(00l) = peak identification
2θ air dried = position of peak in °2θ, air dried preparation
Abs. Int. CPM = absolute intensities in CPM (counts per minute)
Norm. Int. % = normalised intensities, in % of the (002) reflection
d-spacing air dried = d-spacing calculated according to Bragg's law, air dried preparation
2θ glycolated = position of peak in °2θ, glycolated preparation
Abs. Int. CPM = absolute intensities in CPM (counts per minute)
Norm. Int. % = normalised intensities, in % of the (002) reflection
d-spacing glycolated = d-spacing calculated according to Bragg's law, glycolated preparation

No.	(00l)	2θ air dried	2θ glycolated	Abs. Int. CPM	Norm. Int. %	d-spacing air dried	d-spacing glycolated
RS232	1	-	-	-	-	-	-
	2	6.26	5.6	97158	100	28.22	31.54
	3	9.75	13	12900	13	27.19	-
	4	-	-	-	-	-	-
	5	15.79	11.33	1459	2	28.04	-
	6	18.46	17.09	4992	5	28.81	31.11
	7	-	19.94	-	-	-	31.14
	8	24.64	22.98	5881	6	28.88	30.94
	9	-	25.81	-	-	-	31.04
	10	-	-	-	-	-	-
	11	-	31.76	-	-	-	30.97
RS250	1	-	-	-	-	-	-
	2	6.2	5.61	176576	100	28.49	31.48
	3	9.49	11.35	13473	8	27.94	-
	4	-	-	-	-	-	-
	5	15.86	17.12	2491	1	27.92	-
	6	18.68	19.99	20524	12	28.48	31.07
	7	-	-	-	-	-	-
	8	25.07	22.94	28190	16	28.39	30.99
	9	-	25.85	-	-	-	30.99
	10	-	-	-	-	-	-
	11	-	31.77	-	-	-	30.96
				8817	3		

Table D1
Thermal modelling of 8 sections in Northern Switzerland (modified from Todorov, Schegg & Wildi 1993)

%Rr = mean random vitrinite reflectance, values in brackets should be treated with care as the standard deviations are too high
Tmax = calculated maximum paleotemperature for each modelled formation
PGG = calculated paleogeothermal gradients during Late Paleogene and Early Neogene
*, **, *** = vitrinite reflectance values from Matter et al. (1988a), (1988b) and (1987) respectively
(f) = vitrinite reflectance values marked by (f) are based on spectral fluorescence measurements

Thermal Modelling

Modelled Profile	Location	Formation	Age	%Rr - measured	%Rr- calculated	Tmax (°C)	PGG (°C/km)
DELEMONT	Delémont	Rhät	Late Triassic	0.56-[0.65]	0.59	97	
	Delémont	Jurensis Mergel	Early Jurassic	0.62	0.58	96	
	Delémont	Posidonia Schiefer	Early Jurassic	0.45-0.54	0.58	96	
	Delémont	UMM s.l.	Oligocene	0.49	0.29	37	80
	Delémont	Molasse alsacienne	Oligocene	0.41	0.28	36	
	Tramelan	OSM	Miocene	0.28	0.26	26	
	Bois de Raube	Vogesenschotter	Miocene	0.24	0.26	26	
MUTTENZ	Muttenz	Trigonodus Dolomit	Middle Triassic	0.76	0.71	123	
	Muttenz	Letten Kohle	Late Triassic	0.69-[0.70]	0.68	119	
	Muttenz	Gipskeuper	Late Triassic	[0.64]	0.66	117	
	Muttenz	Rhät	Late Triassic	0.49-0.66	0.62	108	100
	Muttenz	Insektenmergel	Early Jurassic	0.70	0.60	106	
	Muttenz	Obtusus Ton	Early Jurassic	0.61-[0.63]	0.59	104	
	Muttenz	Jurensis Mergel	Early Jurassic	0.52-0.69	0.57	102	
	Muttenz	Opalinus Ton	Middle Jurassic	0.55-[0.69]	0.56	101	
TRIMBACH	Belchenflue and Trimbach	Gipskeuper	Late Triassic	[0.66-0.78]	0.67	111	50
	Brocheni Flue	USM	Oligocene	0.30	0.41	70	
PASS-WANG	Balmberg and Grindel	Rhät	Late Triassic	0.55-0.80	0.57	94	
	Meltingen	Opalinus Ton	Middle Jurassic	0.55	0.55	92	70
	Brocheni Flue	USM	Oligocene	0.30	0.32	45	
STAFFEL-EGG	Frick	Insektenmergel	Early Jurassic	0.54-[0.66]	0.51	88	
	Staffelegg	Jurensis Mergel	Early Jurassic	[0.44]-0.58	0.50	85	
	Schämbelen	Posidonia Schiefer	Early Jurassic	0.49	0.50	85	85
	Asperchlus	Hauptrogenstein	Middle Jurassic	0.40	0.42	71	
WEIACH	Well Weiach	Wellen Mergel	Middle Triassic	0.70*	0.75	127	
		Orbicularis Mergel	Middle Triassic	0.62*	0.74	125	
		Letten Kohle	Late Triassic	0.62*	0.67	116	75
		Opalinus Ton	Middle Jurassic	0.60*	0.60	104	
		Würtenbergia Schichten	Middle Jurassic	0.55*	0.52	93	
		Küssaburg Schichten	Late Jurassic	0.46*	0.45	83	
SCHAFIS-HEIM	Well Schafisheim	Orbicularis Mergel	Middle Triassic	0.47 / 0.90-0.92 (f)**	0.55	95	
		Estherien Schiefer	Late Triassic	0.60 (f)**	0.51	88	
		Insektenmergel	Early Jurassic	0.46**	0.48	83	
		Opalinus Ton	Middle Jurassic	0.50 (f)**	0.47	82	40
		Blagdeni Schichten	Middle Jurassic	0.45**	0.45	78	
		Effinger Schichten	Late Jurassic	0.39**	0.42	72	
	Mägenwil	OMM	Miocene	0.48	0.29	36	
	Hanenberg	OMM	Miocene	0.40	0.29	36	
RINIKEN	Well Riniken	Orbicularis Mergel	Middle Triassic	0.41 / 0.80-1.05 (f)***	0.47	82	
		Dolomitmergel	Middle Triassic	0.44 / 0.45-0.50 (f)***	0.47	81	
		Trigonodus Dolomit	Middle Triassic	0.55-0.65 (f)***	0.44	77	60
		Posidonia Schiefer	Early Jurassic	0.43 / 0.30-0.40 (f)***	0.39	65	
		Opalinus Ton	Middle Jurassic	0.35-0.60 (f)***	0.38	63	
		Hauptrogenstein	Middle Jurassic	0.40 / 0.40 (f)***	0.34	53	

PLATES

PLATE 1

Microscopic pictures of coals in reflected white light.

A) Sample RS242b: Desmocollinite (DC) associated with macerals of the liptinite and inertinite group. cutinite (C), inertodetrinite (I), telocollinite (T), fusinite (F), pyrite (P).

B) Sample RS242b: fusinite (F), semifusinite (SF), telocollinite (T), desmocollinite (DC), liptinite (L).

C) Sample RS65: Telocollinite associated with the liptinite maceral resocollinite (R).

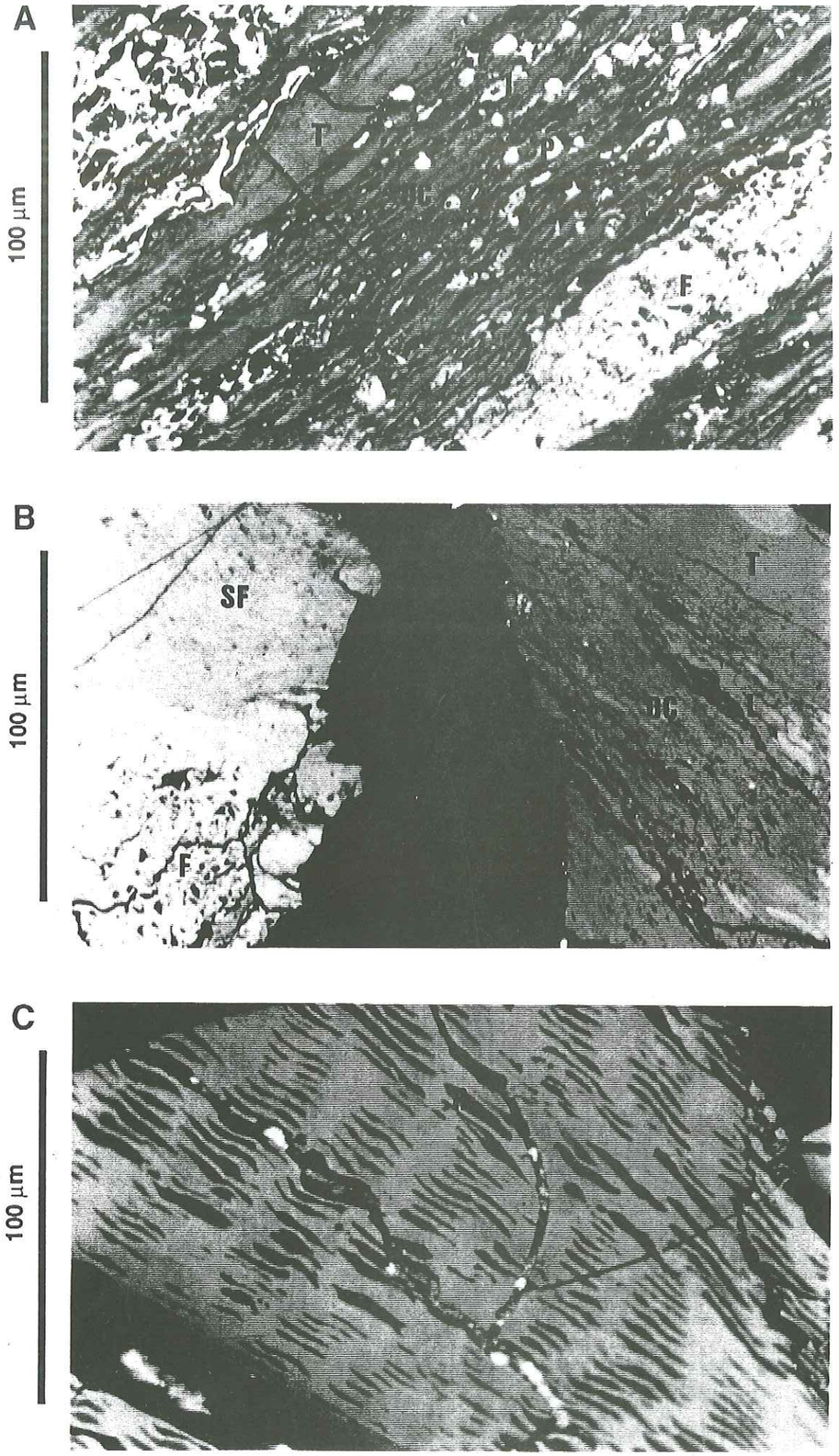

PLATE 2

Microscopic pictures of coals in reflected white light showing different levels of alteration.

A) Sample Weid12: Fresh telocollinite.

B) Sample RS65: Slightly altered telocollinite.

C) Sample RS71: Moderately altered telocollinite.

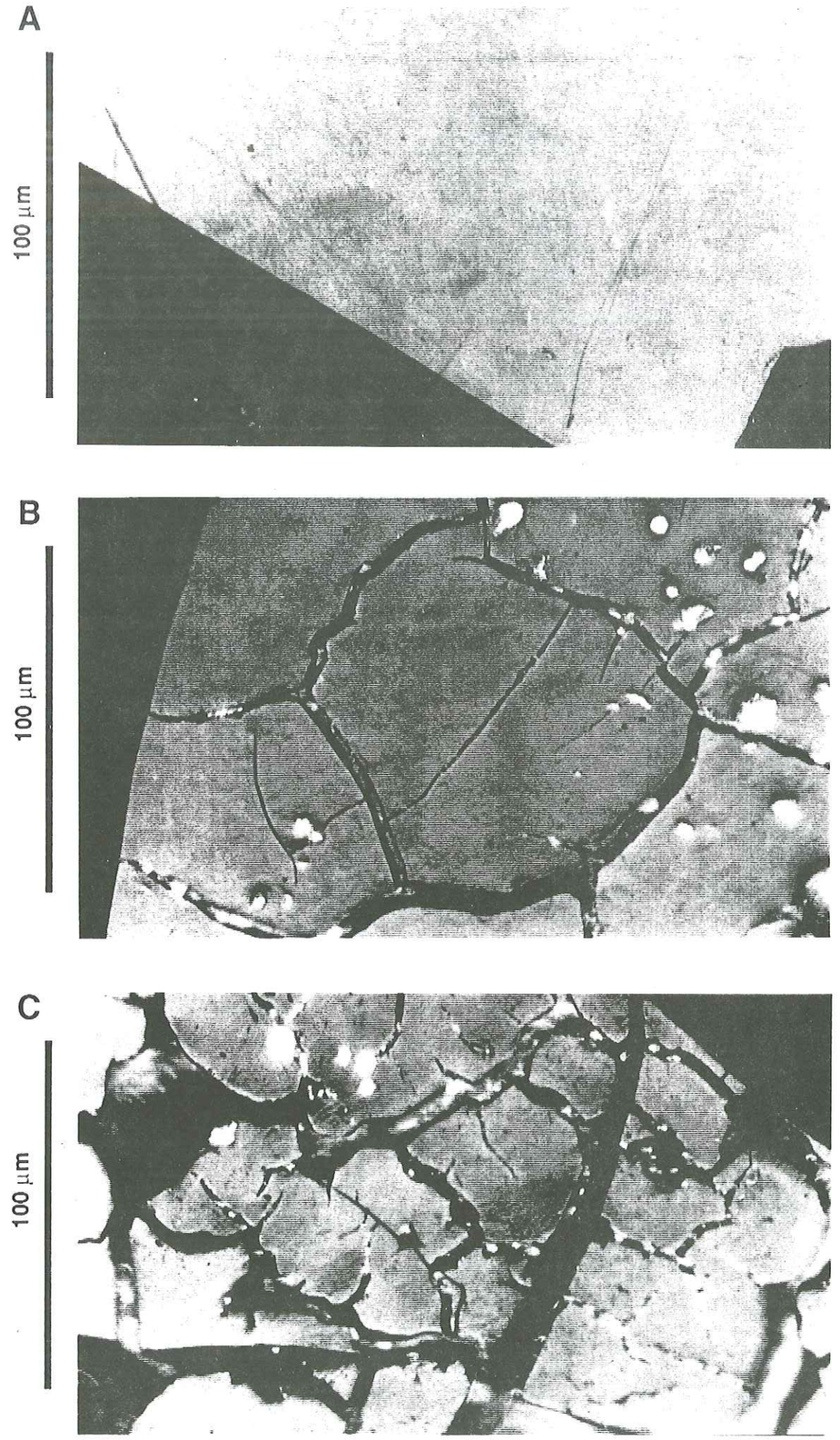

PLATE 3

Microscopic pictures of coals in reflected white light showing different levels of alteration.

A) Sample Weid17: Moderately altered telocollinite.

B) Sample RS91: Strongly altered telocollinite.

C) Sample RS6: Completely altered telocollinite.

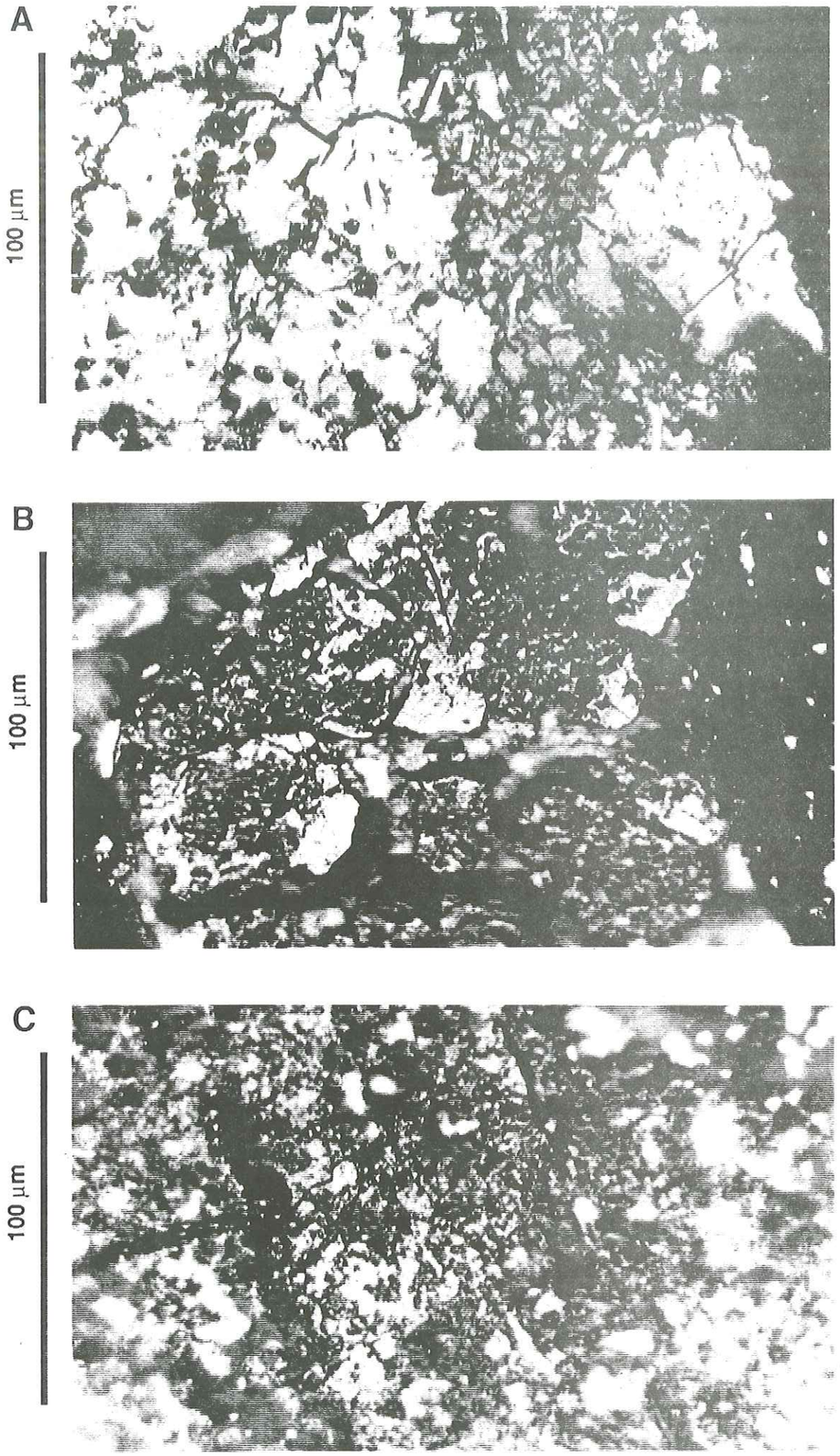

ANNEXES

Caption for annex 1: Reflectance histograms

RS2 = sample number
Rr = mean random reflectance (in %)
s = standard deviation
n = number of measurements

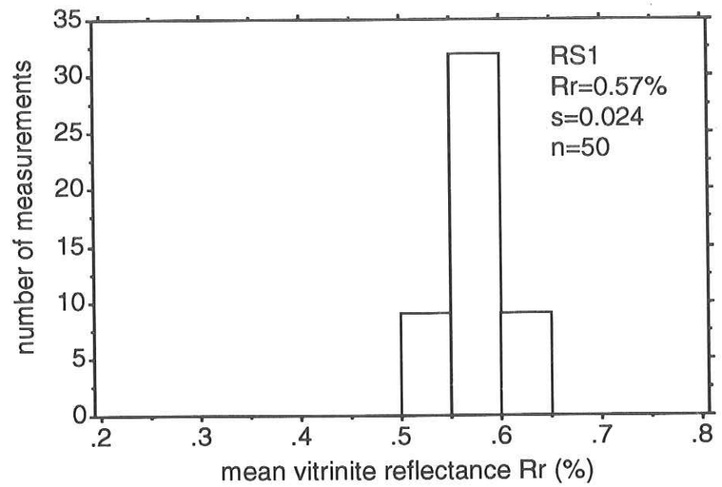

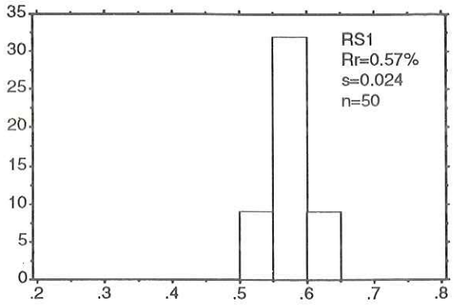
RS1
Rr=0.57%
s=0.024
n=50

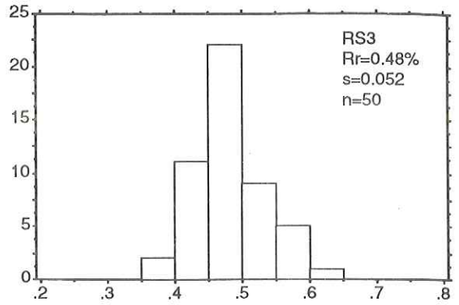
RS3
Rr=0.48%
s=0.052
n=50

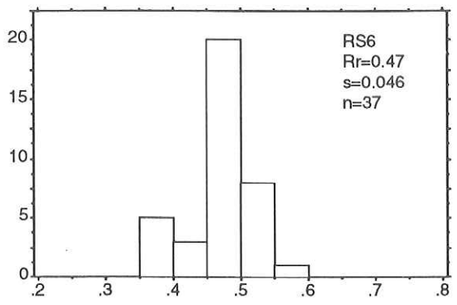
RS6
Rr=0.47
s=0.046
n=37

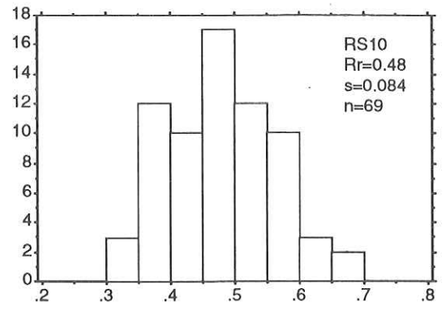
RS10
Rr=0.48
s=0.084
n=69

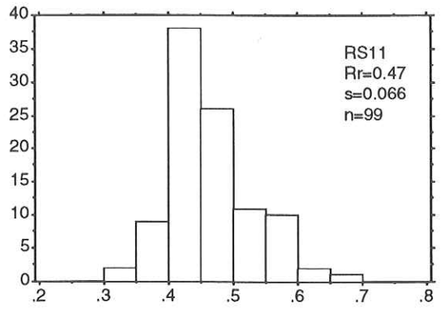
RS11
Rr=0.47
s=0.066
n=99

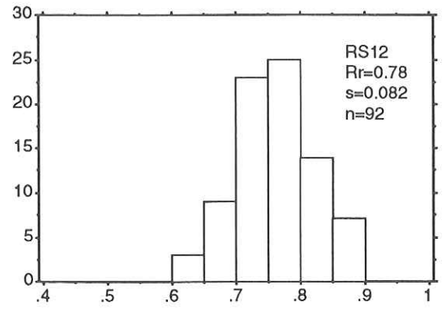
RS12
Rr=0.78
s=0.082
n=92

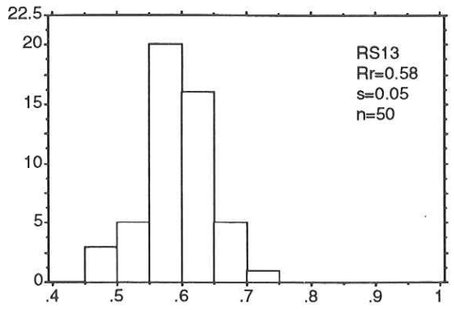
RS13
Rr=0.58
s=0.05
n=50

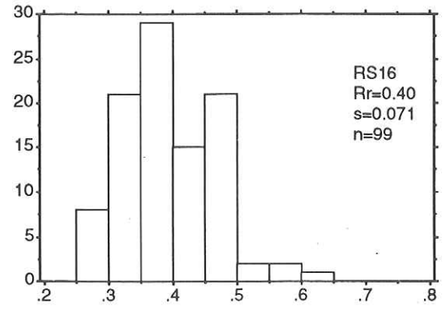
RS16
Rr=0.40
s=0.071
n=99

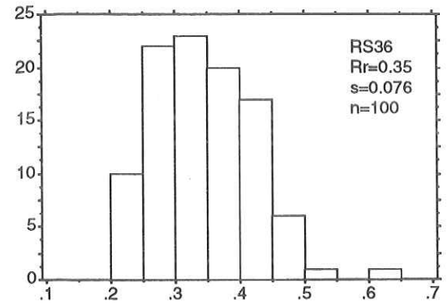
RS36
Rr=0.35
s=0.076
n=100

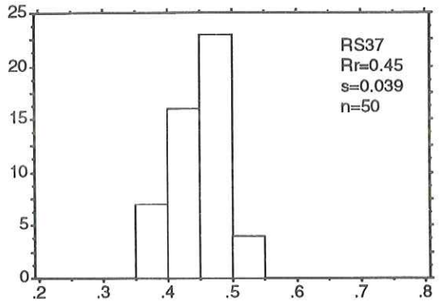
RS37
Rr=0.45
s=0.039
n=50

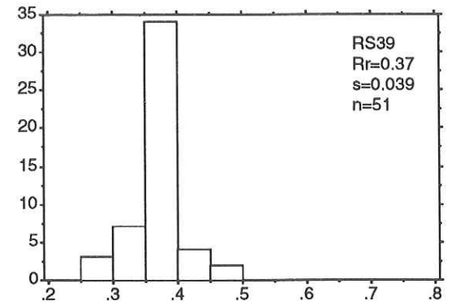
RS39
Rr=0.37
s=0.039
n=51

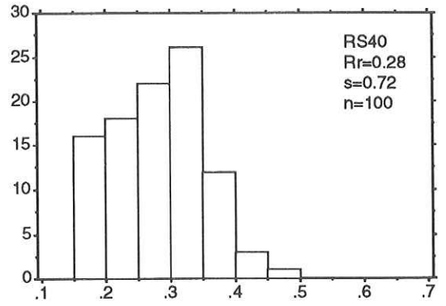
RS40
Rr=0.28
s=0.72
n=100

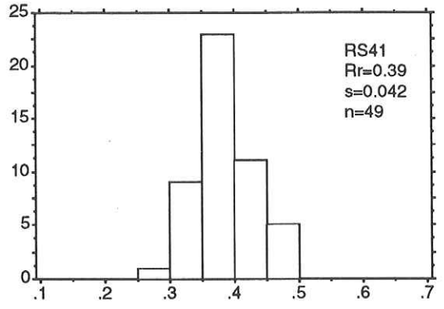
RS41
Rr=0.39
s=0.042
n=49

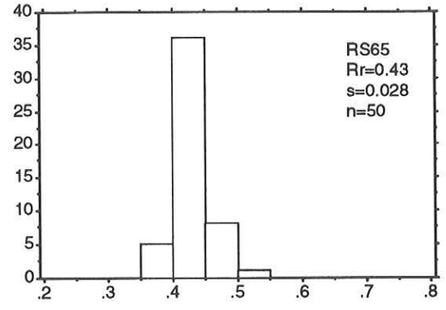
RS65
Rr=0.43
s=0.028
n=50

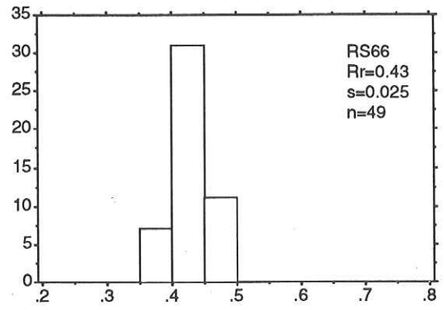
RS66
Rr=0.43
s=0.025
n=49

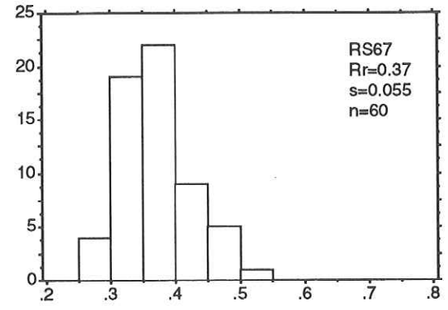
RS67
Rr=0.37
s=0.055
n=60

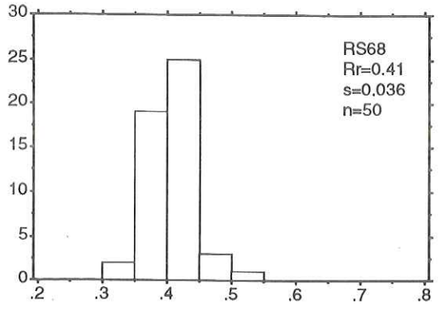
RS68
Rr=0.41
s=0.036
n=50

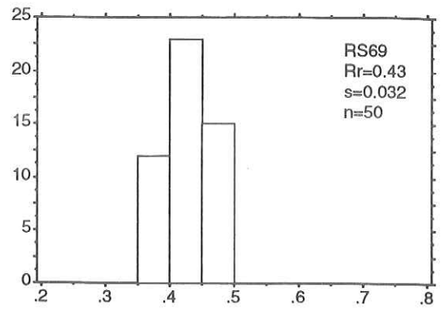
RS69
Rr=0.43
s=0.032
n=50

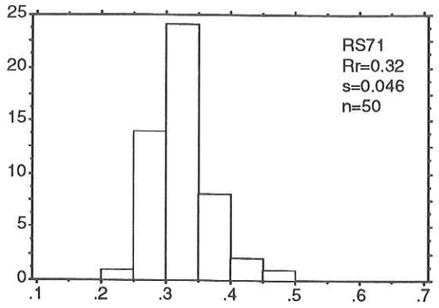
RS71
Rr=0.32
s=0.046
n=50

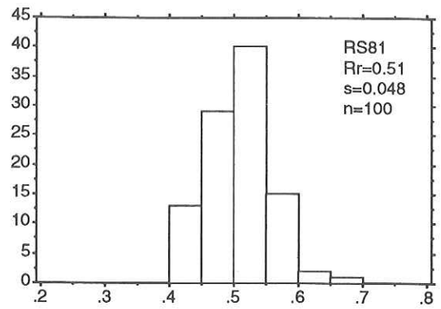
RS81
Rr=0.51
s=0.048
n=100

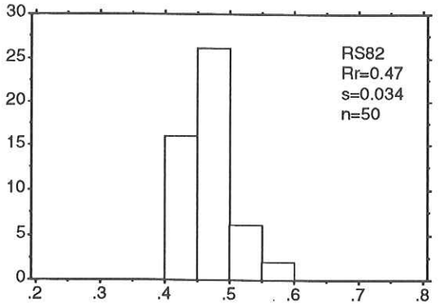
RS82
Rr=0.47
s=0.034
n=50

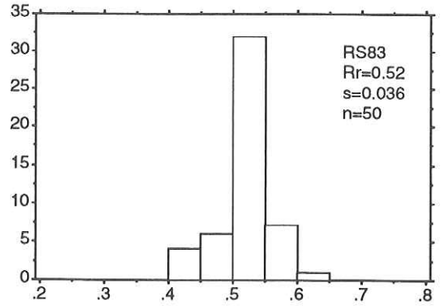
RS83
Rr=0.52
s=0.036
n=50

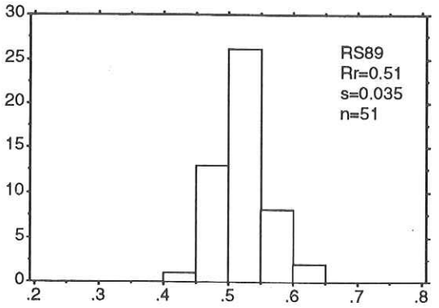
RS89
Rr=0.51
s=0.035
n=51

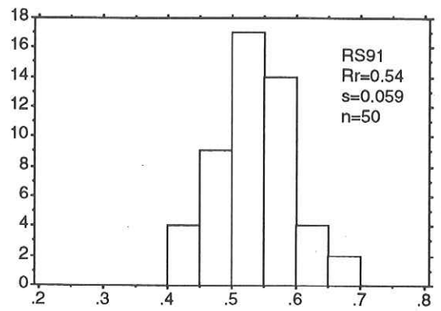
RS91
Rr=0.54
s=0.059
n=50

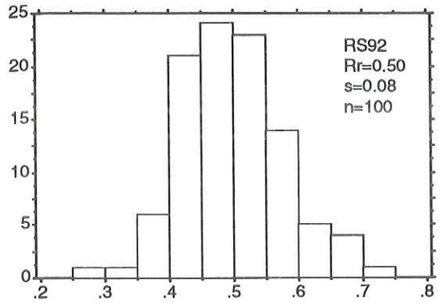
RS92
Rr=0.50
s=0.08
n=100

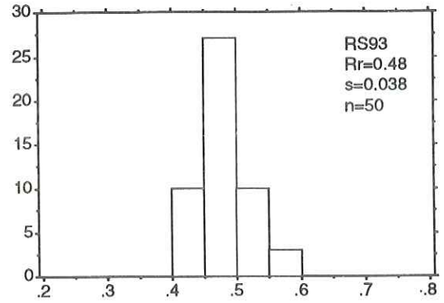
RS93
Rr=0.48
s=0.038
n=50

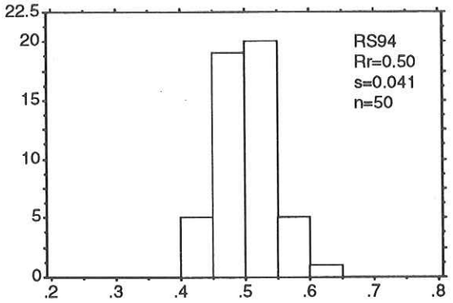
RS94
Rr=0.50
s=0.041
n=50

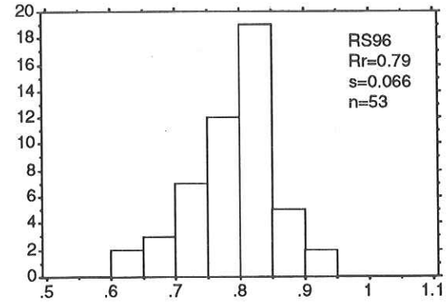
RS96
Rr=0.79
s=0.066
n=53

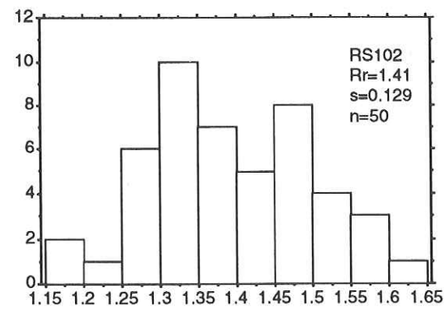
RS102
Rr=1.41
s=0.129
n=50

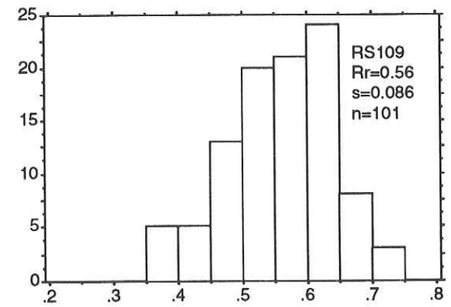
RS109
Rr=0.56
s=0.086
n=101

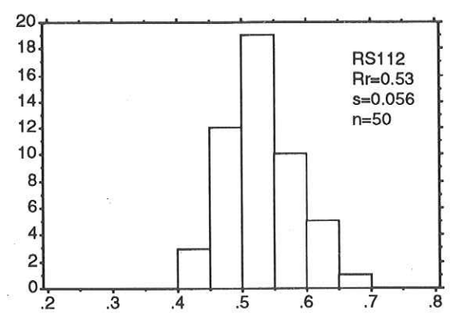
RS112
Rr=0.53
s=0.056
n=50

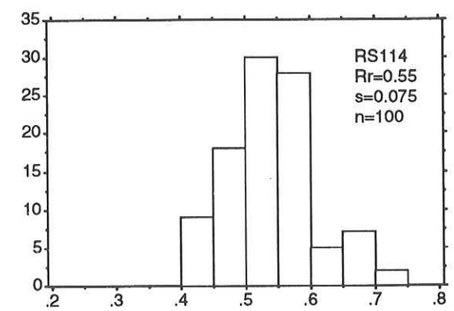
RS114
Rr=0.55
s=0.075
n=100

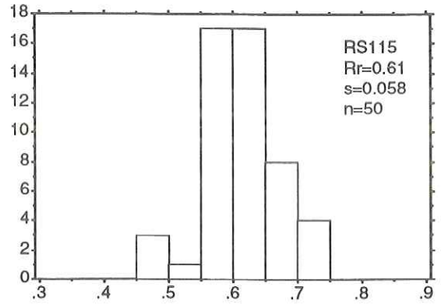
RS115
Rr=0.61
s=0.058
n=50

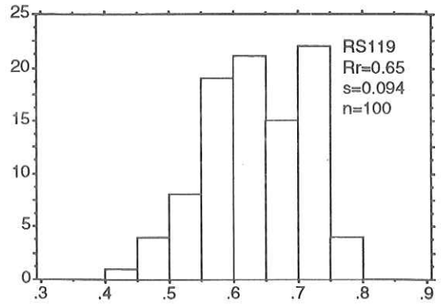
RS119
Rr=0.65
s=0.094
n=100

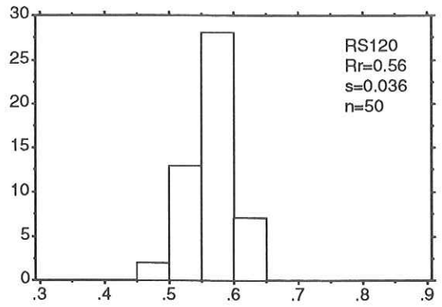
RS120
Rr=0.56
s=0.036
n=50

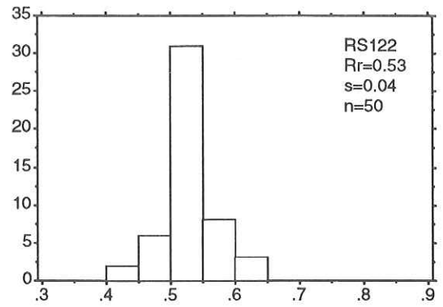
RS122
Rr=0.53
s=0.04
n=50

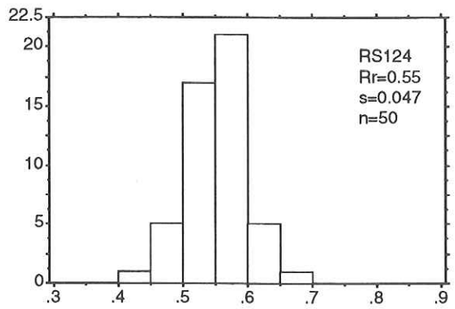
RS124
Rr=0.55
s=0.047
n=50

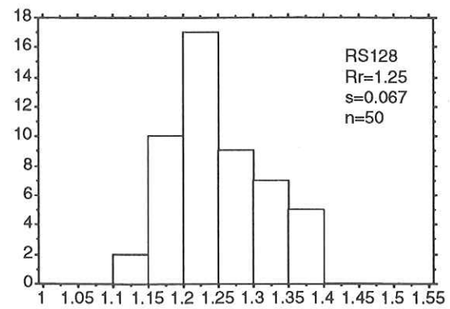
RS128
Rr=1.25
s=0.067
n=50

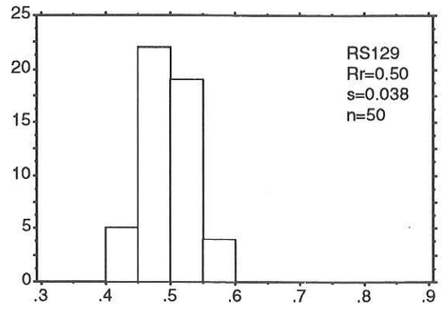
RS129
Rr=0.50
s=0.038
n=50

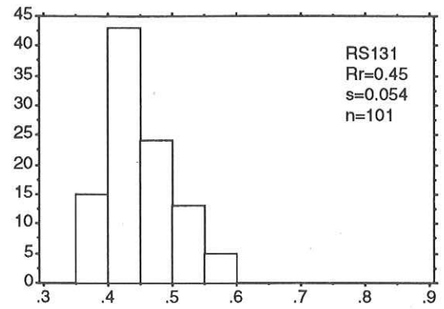
RS131
Rr=0.45
s=0.054
n=101

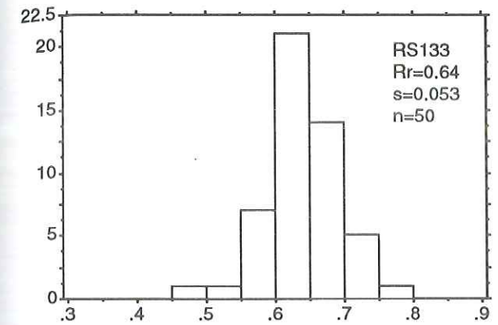
RS133
Rr=0.64
s=0.053
n=50

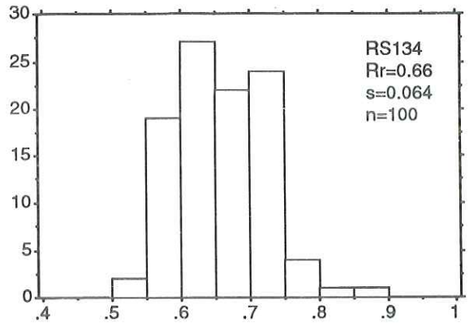
RS134
Rr=0.66
s=0.064
n=100

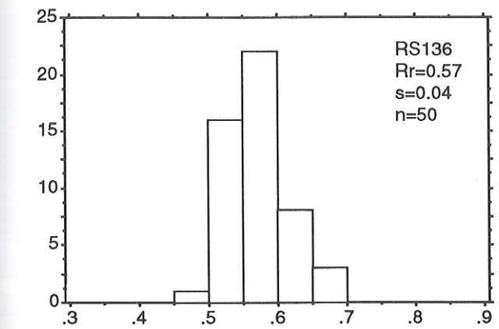
RS136
Rr=0.57
s=0.04
n=50

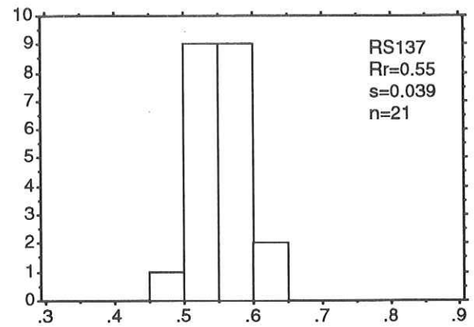
RS137
Rr=0.55
s=0.039
n=21

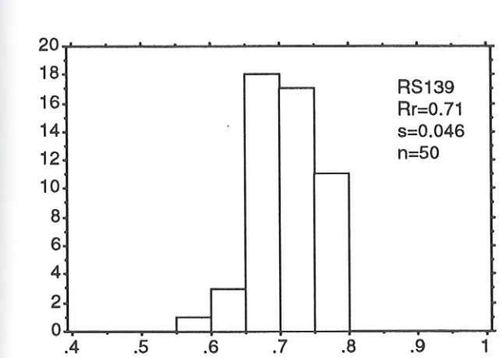
RS139
Rr=0.71
s=0.046
n=50

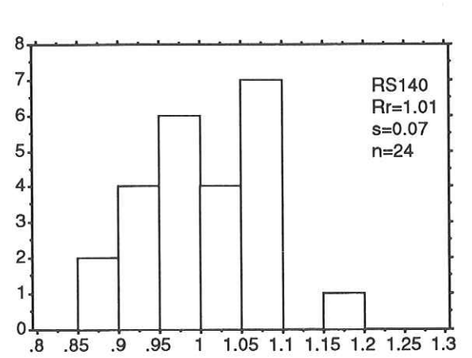
RS140
Rr=1.01
s=0.07
n=24

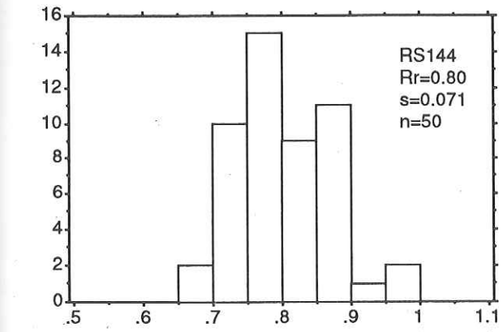
RS144
Rr=0.80
s=0.071
n=50

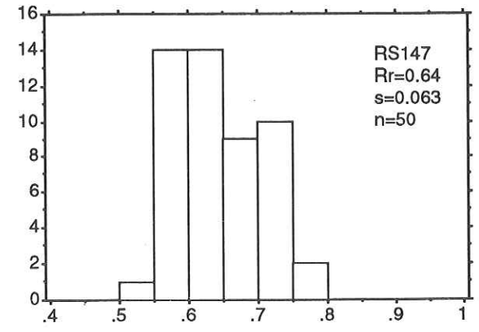
RS147
Rr=0.64
s=0.063
n=50

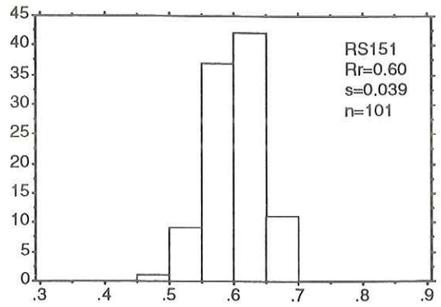
RS151
Rr=0.60
s=0.039
n=101

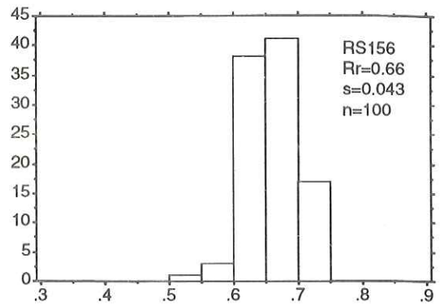
RS156
Rr=0.66
s=0.043
n=100

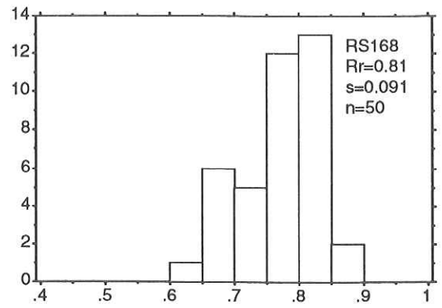
RS168
Rr=0.81
s=0.091
n=50

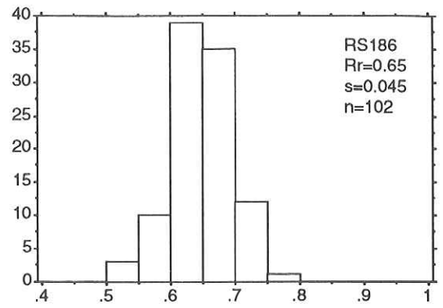
RS186
Rr=0.65
s=0.045
n=102

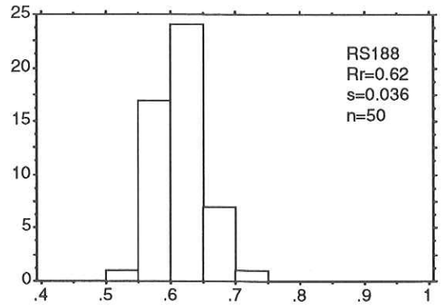
RS188
Rr=0.62
s=0.036
n=50

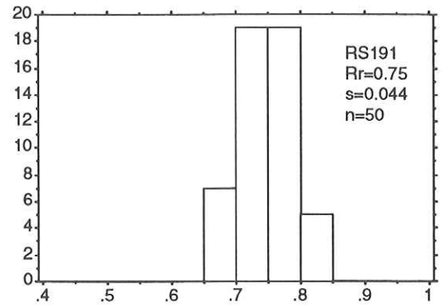
RS191
Rr=0.75
s=0.044
n=50

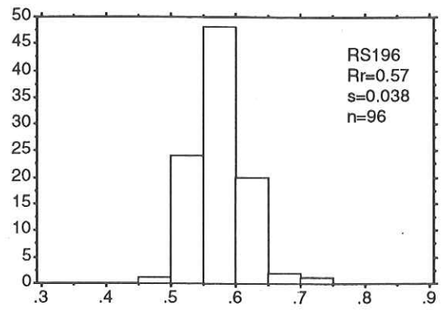
RS196
Rr=0.57
s=0.038
n=96

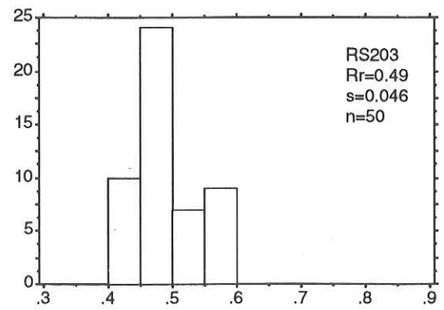
RS203
Rr=0.49
s=0.046
n=50

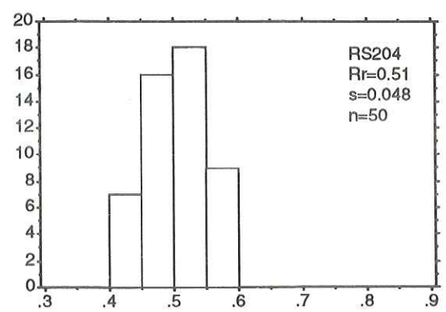
RS204
Rr=0.51
s=0.048
n=50

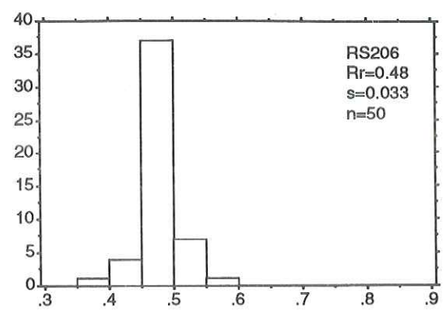
RS206
Rr=0.48
s=0.033
n=50

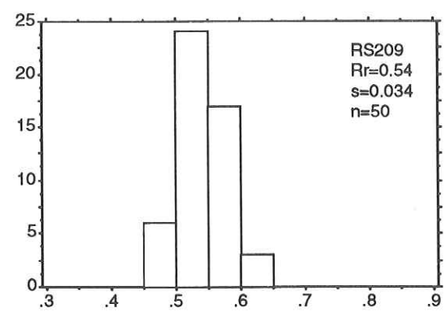
RS209
Rr=0.54
s=0.034
n=50

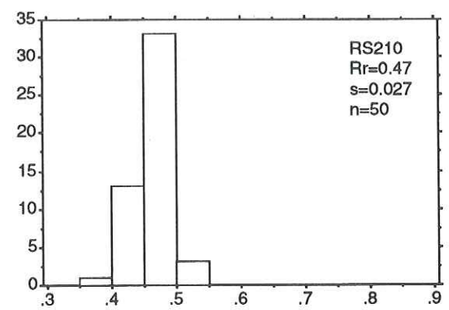
RS210
Rr=0.47
s=0.027
n=50

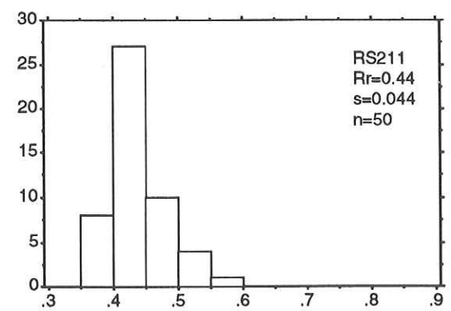
RS211
Rr=0.44
s=0.044
n=50

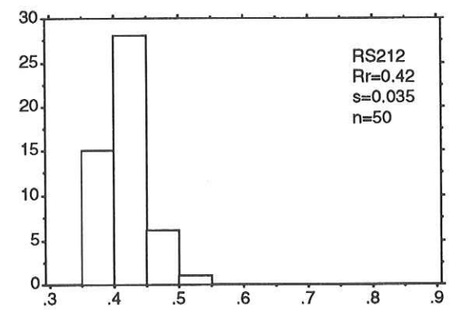
RS212
Rr=0.42
s=0.035
n=50

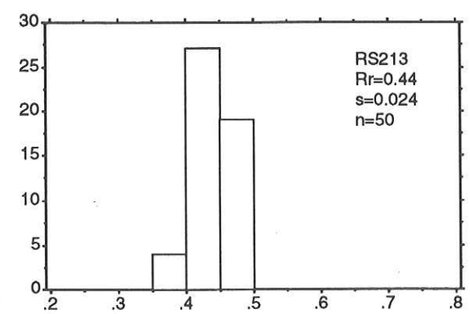
RS213
Rr=0.44
s=0.024
n=50

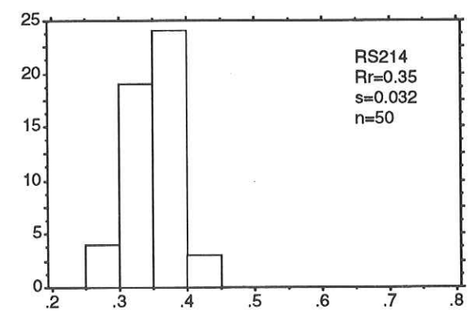
RS214
Rr=0.35
s=0.032
n=50

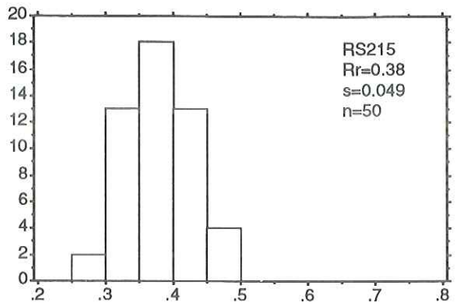
RS215
Rr=0.38
s=0.049
n=50

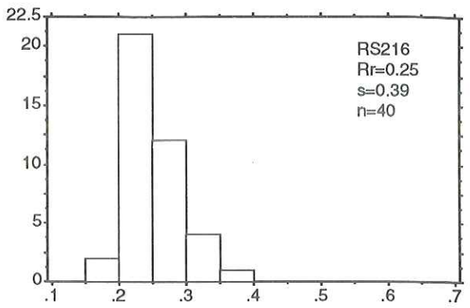
RS216
Rr=0.25
s=0.39
n=40

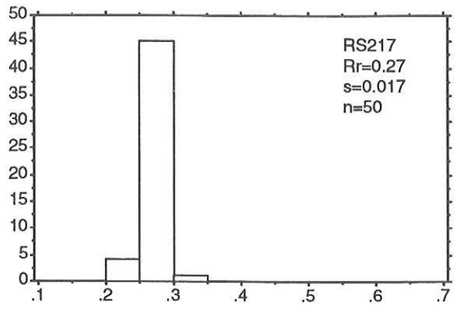
RS217
Rr=0.27
s=0.017
n=50

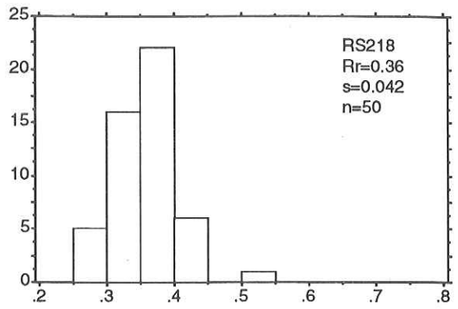
RS218
Rr=0.36
s=0.042
n=50

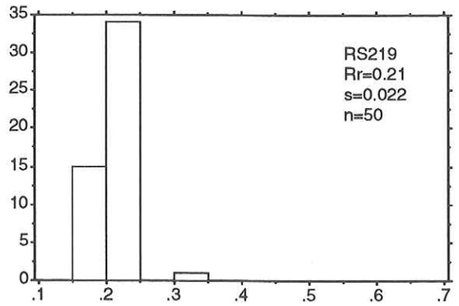
RS219
Rr=0.21
s=0.022
n=50

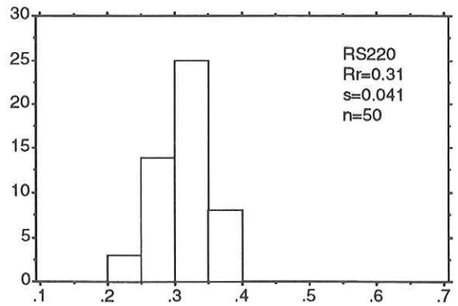
RS220
Rr=0.31
s=0.041
n=50

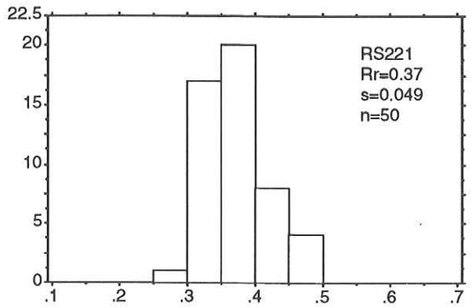
RS221
Rr=0.37
s=0.049
n=50

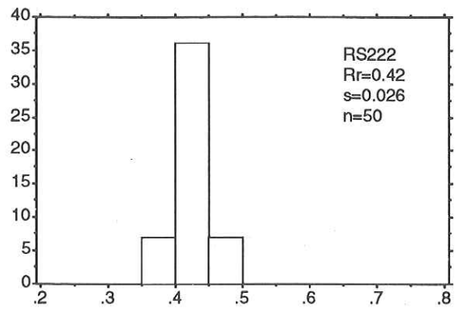
RS222
Rr=0.42
s=0.026
n=50

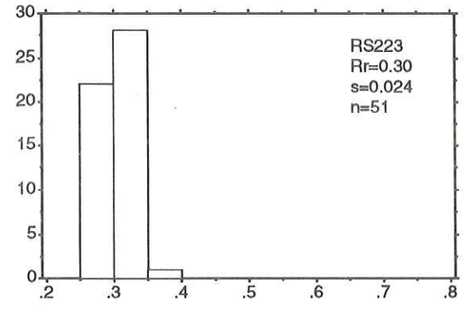
RS223
Rr=0.30
s=0.024
n=51

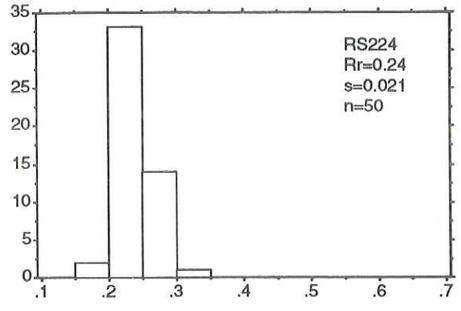
RS224
Rr=0.24
s=0.021
n=50

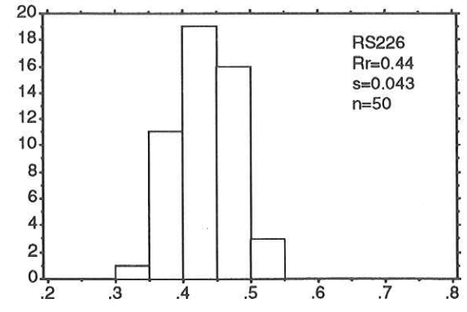
RS226
Rr=0.44
s=0.043
n=50

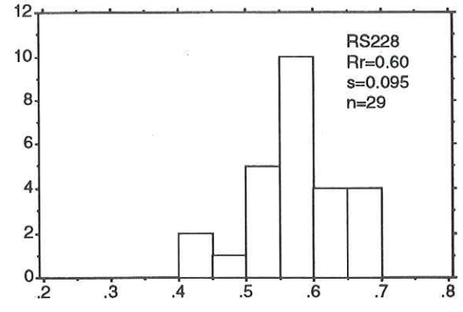
RS228
Rr=0.60
s=0.095
n=29

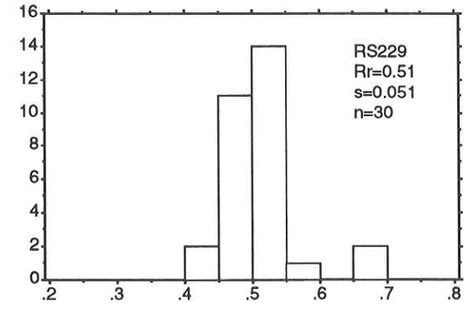
RS229
Rr=0.51
s=0.051
n=30

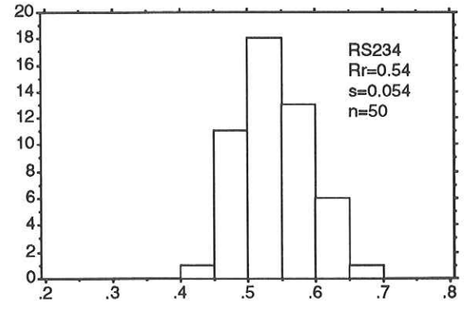
RS234
Rr=0.54
s=0.054
n=50

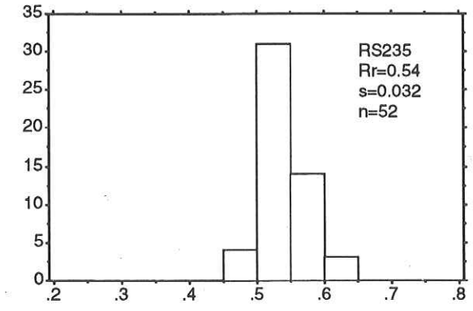
RS235
Rr=0.54
s=0.032
n=52

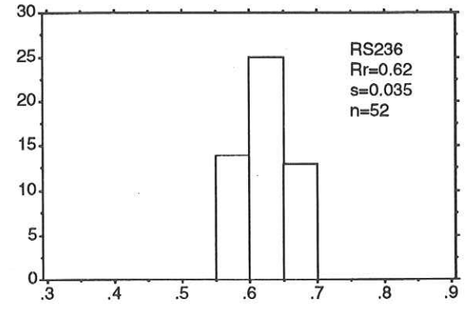
RS236
Rr=0.62
s=0.035
n=52

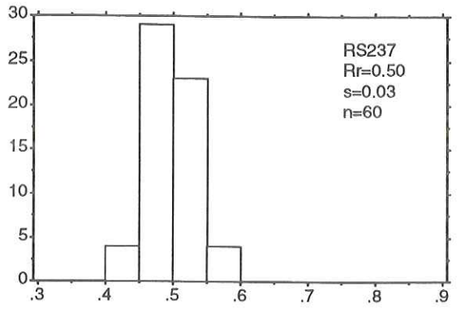
RS237
Rr=0.50
s=0.03
n=60

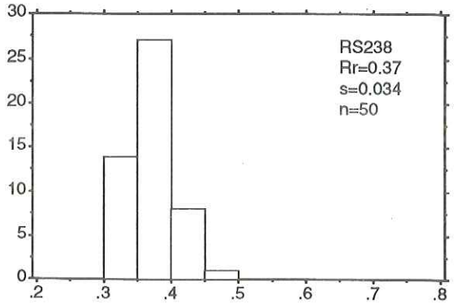
RS238
Rr=0.37
s=0.034
n=50

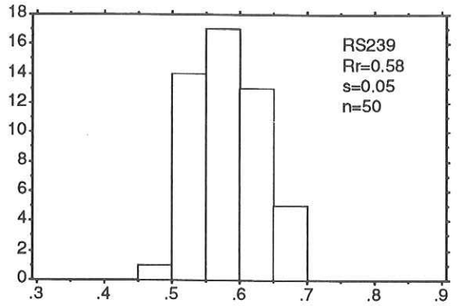
RS239
Rr=0.58
s=0.05
n=50

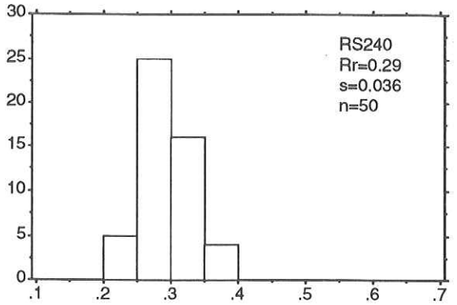
RS240
Rr=0.29
s=0.036
n=50

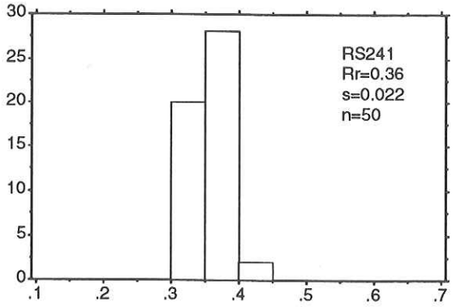
RS241
Rr=0.36
s=0.022
n=50

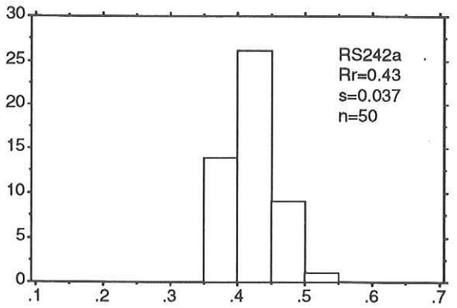
RS242a
Rr=0.43
s=0.037
n=50

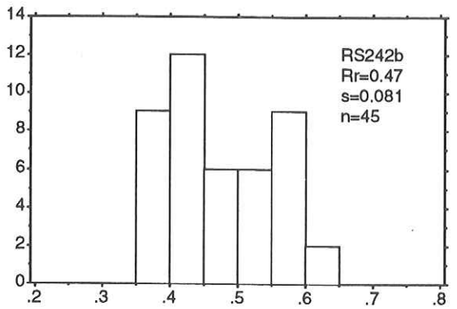
RS242b
Rr=0.47
s=0.081
n=45

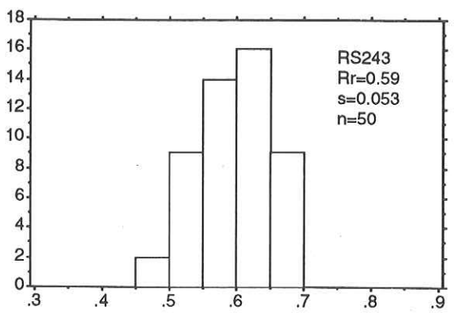
RS243
Rr=0.59
s=0.053
n=50

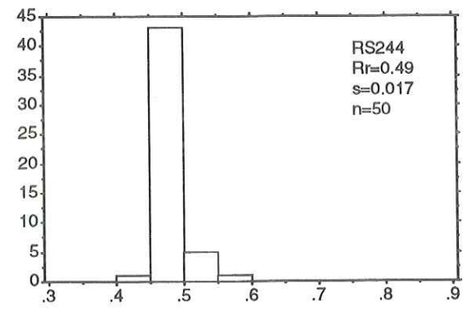
RS244
Rr=0.49
s=0.017
n=50

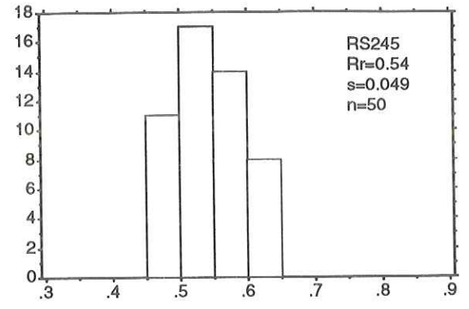
RS245
Rr=0.54
s=0.049
n=50

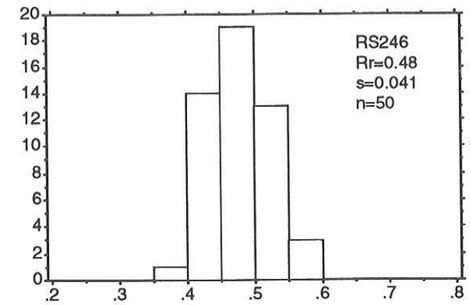
RS246
Rr=0.48
s=0.041
n=50

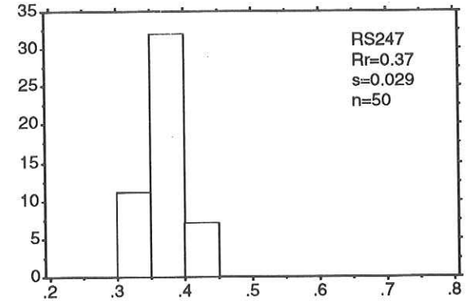
RS247
Rr=0.37
s=0.029
n=50

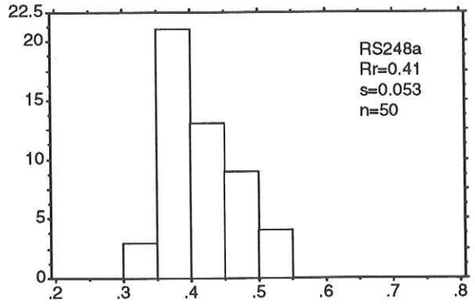
RS248a
Rr=0.41
s=0.053
n=50

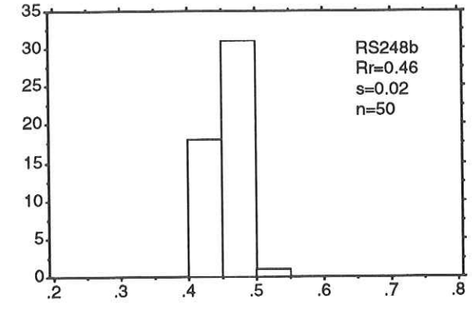
RS248b
Rr=0.46
s=0.02
n=50

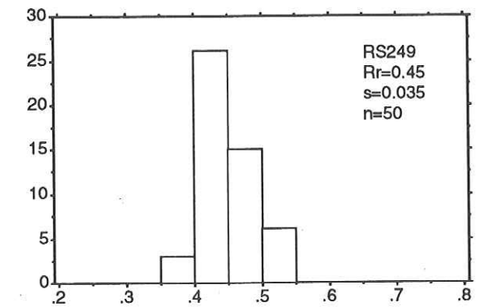
RS249
Rr=0.45
s=0.035
n=50

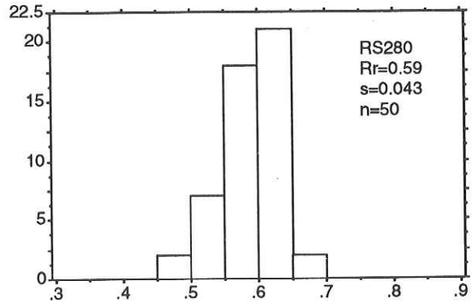
RS280
Rr=0.59
s=0.043
n=50

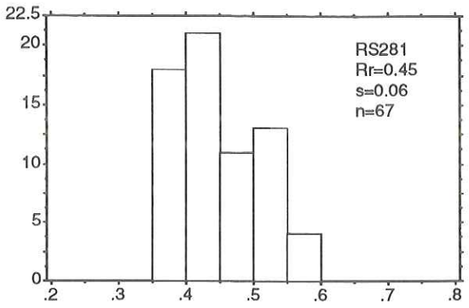
RS281
Rr=0.45
s=0.06
n=67

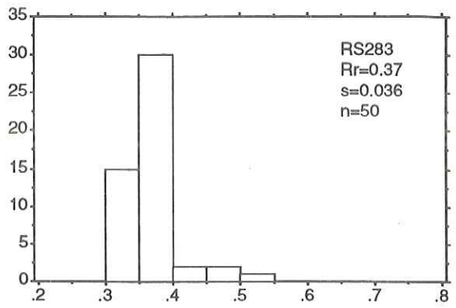
RS283
Rr=0.37
s=0.036
n=50

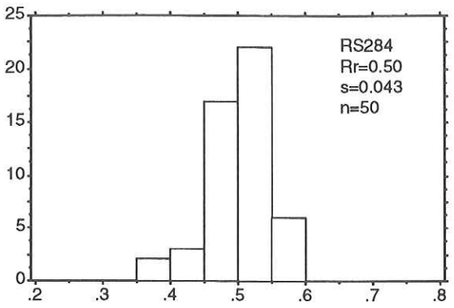
RS284
Rr=0.50
s=0.043
n=50

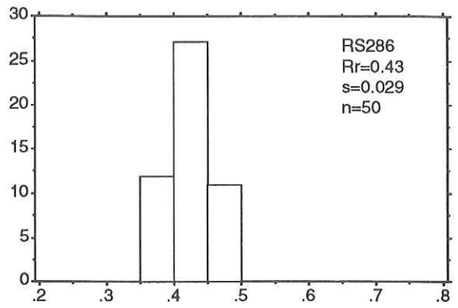
RS286
Rr=0.43
s=0.029
n=50

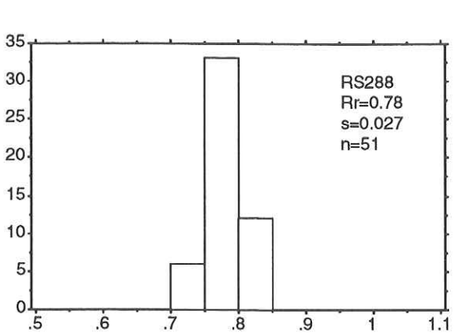
RS288
Rr=0.78
s=0.027
n=51

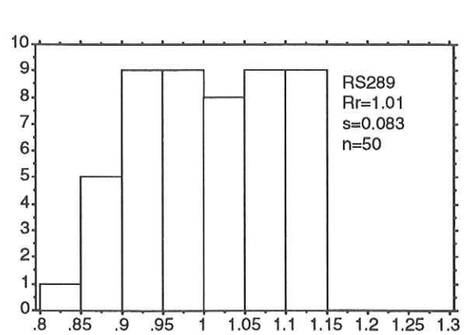
RS289
Rr=1.01
s=0.083
n=50

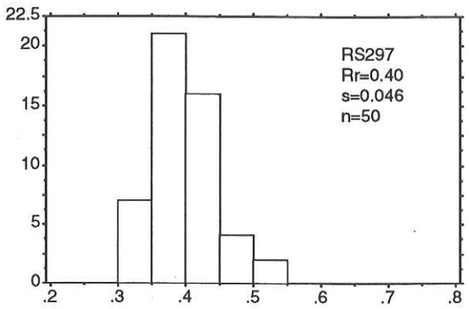
RS297
Rr=0.40
s=0.046
n=50

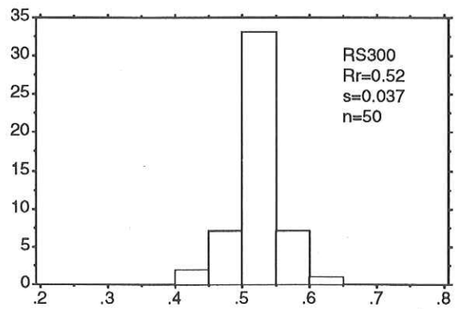
RS300
Rr=0.52
s=0.037
n=50

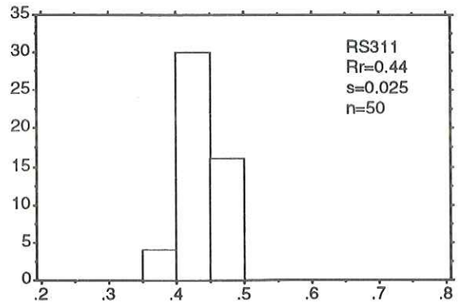
RS311
Rr=0.44
s=0.025
n=50

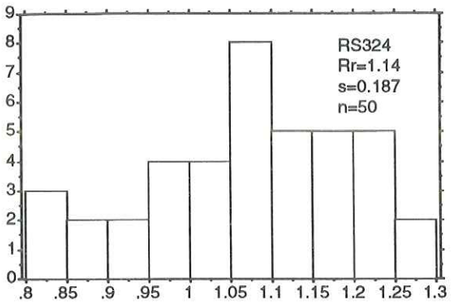
RS324
Rr=1.14
s=0.187
n=50

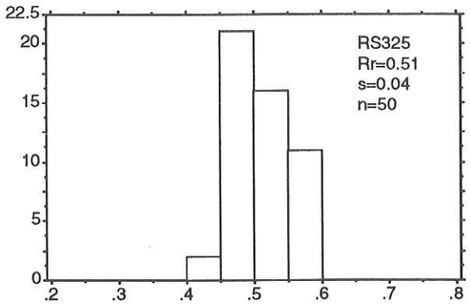
RS325
Rr=0.51
s=0.04
n=50

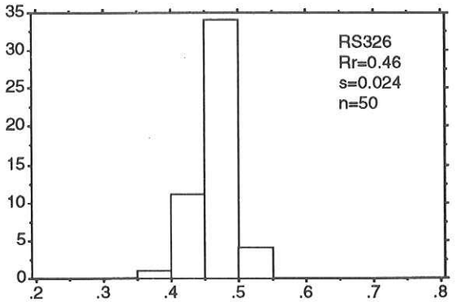
RS326
Rr=0.46
s=0.024
n=50

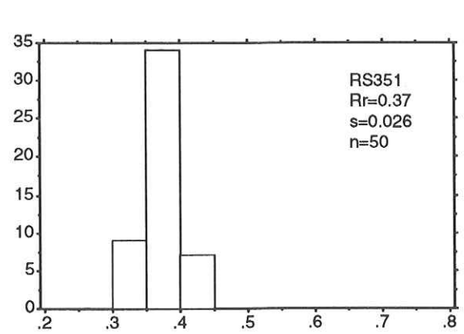
RS351
Rr=0.37
s=0.026
n=50

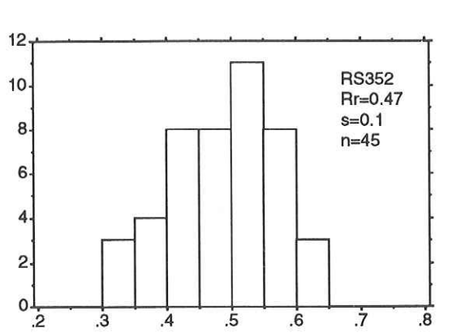
RS352
Rr=0.47
s=0.1
n=45

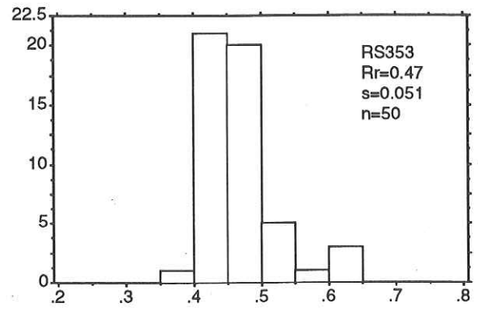
RS353
Rr=0.47
s=0.051
n=50

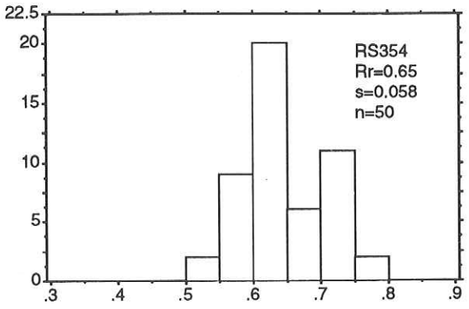
RS354
Rr=0.65
s=0.058
n=50

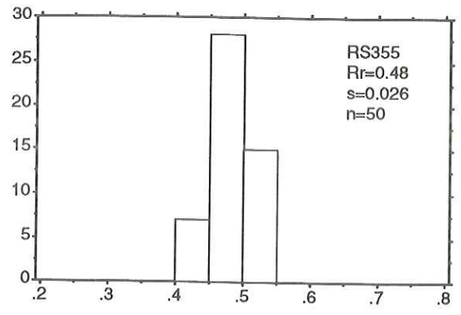
RS355
Rr=0.48
s=0.026
n=50

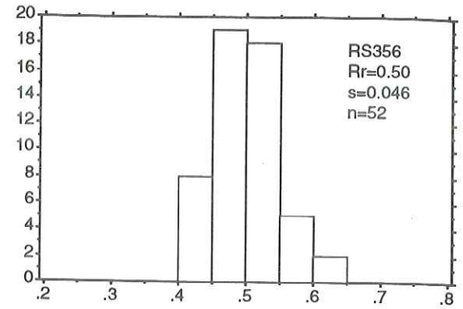
RS356
Rr=0.50
s=0.046
n=52

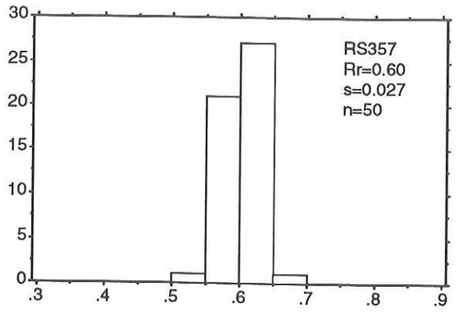
RS357
Rr=0.60
s=0.027
n=50

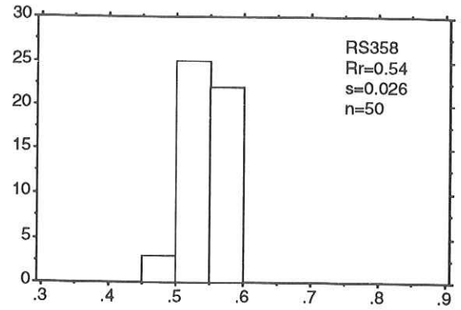
RS358
Rr=0.54
s=0.026
n=50

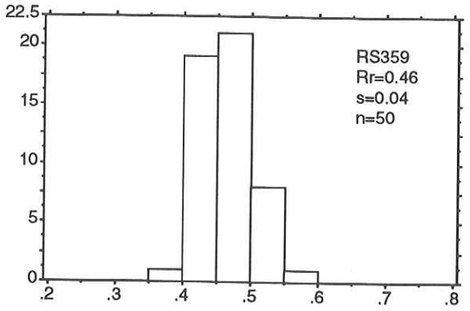
RS359
Rr=0.46
s=0.04
n=50

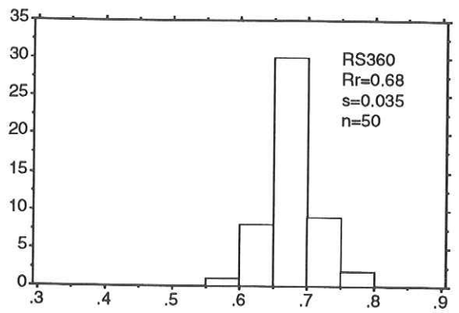
RS360
Rr=0.68
s=0.035
n=50

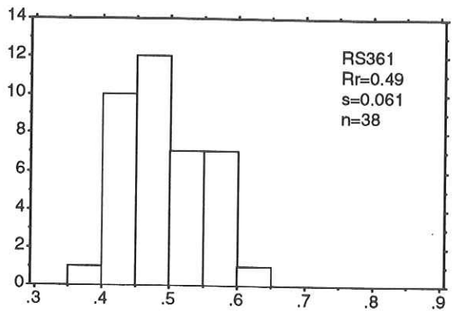
RS361
Rr=0.49
s=0.061
n=38

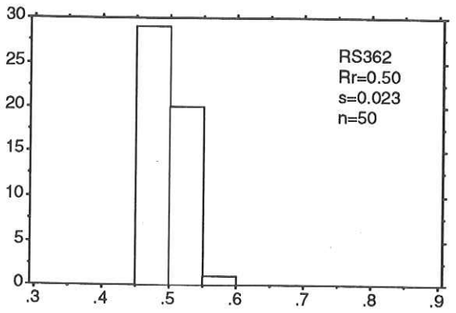
RS362
Rr=0.50
s=0.023
n=50

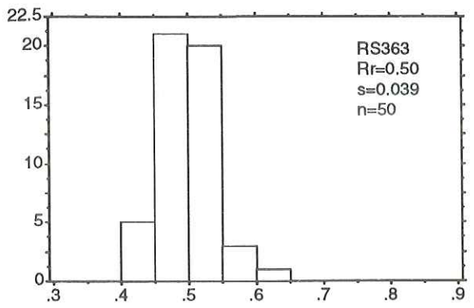
RS363
Rr=0.50
s=0.039
n=50

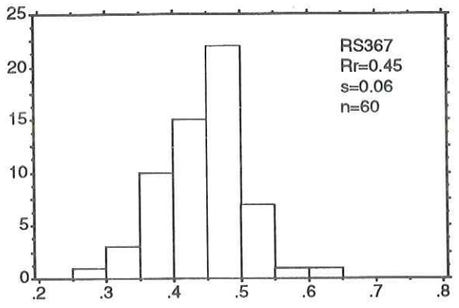
RS367
Rr=0.45
s=0.06
n=60

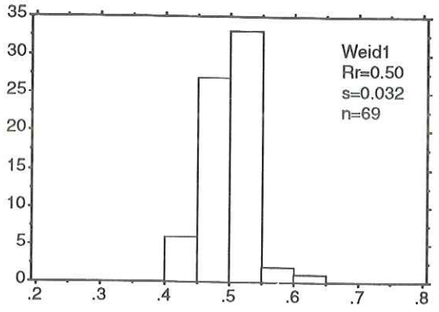
Weid1
Rr=0.50
s=0.032
n=69

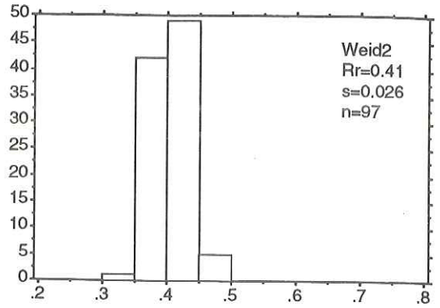
Weid2
Rr=0.41
s=0.026
n=97

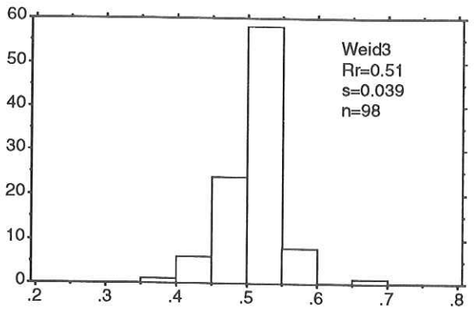
Weid3
Rr=0.51
s=0.039
n=98

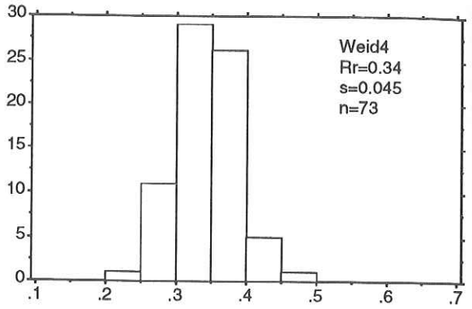
Weid4
Rr=0.34
s=0.045
n=73

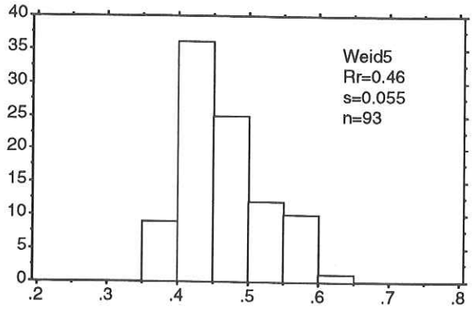
Weid5
Rr=0.46
s=0.055
n=93

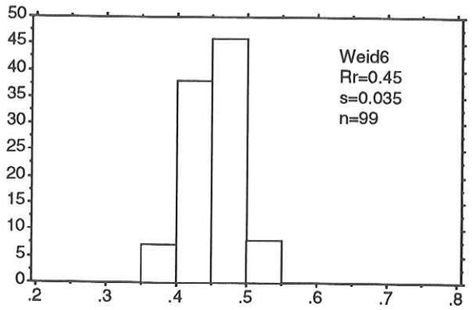
Weid6
Rr=0.45
s=0.035
n=99

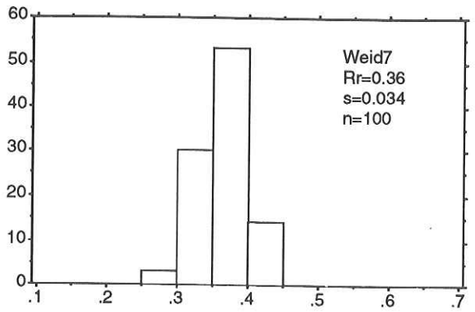
Weid7
Rr=0.36
s=0.034
n=100

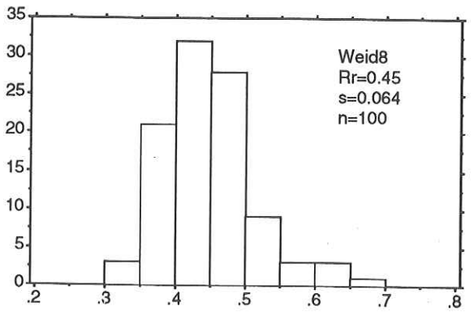
Weid8
Rr=0.45
s=0.064
n=100

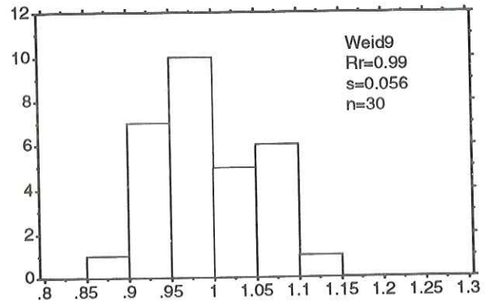
Weid9
Rr=0.99
s=0.056
n=30

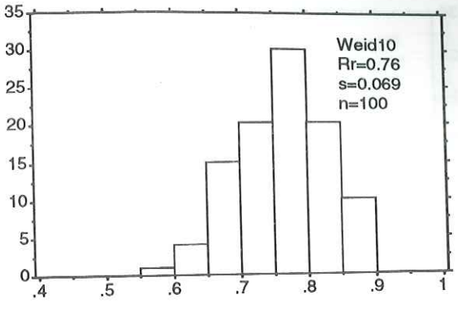
Weid10
Rr=0.76
s=0.069
n=100

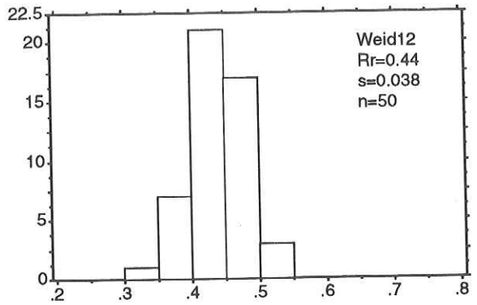
Weid12
Rr=0.44
s=0.038
n=50

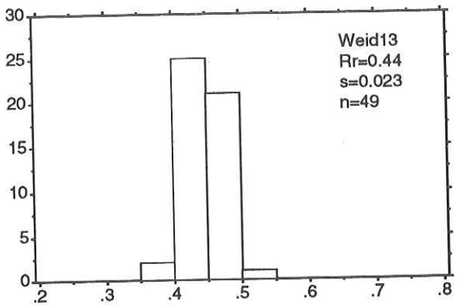
Weid13
Rr=0.44
s=0.023
n=49

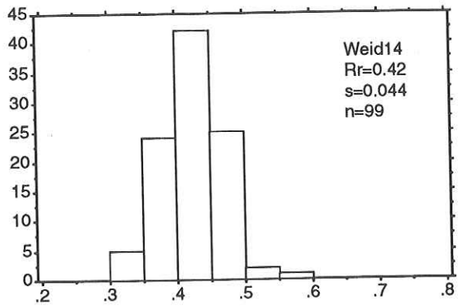
Weid14
Rr=0.42
s=0.044
n=99

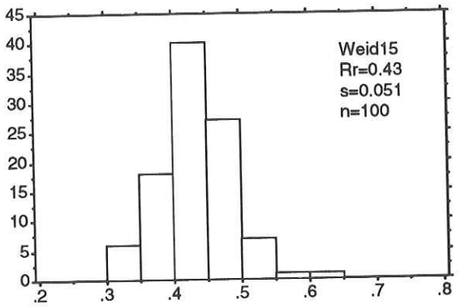
Weid15
Rr=0.43
s=0.051
n=100

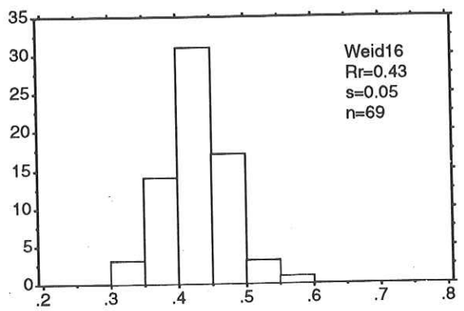
Weid16
Rr=0.43
s=0.05
n=69

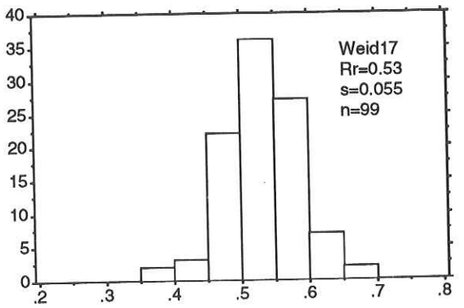
Weid17
Rr=0.53
s=0.055
n=99

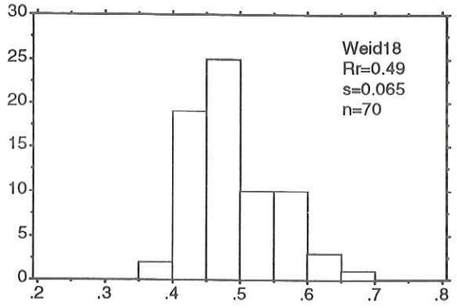
Weid18
Rr=0.49
s=0.065
n=70

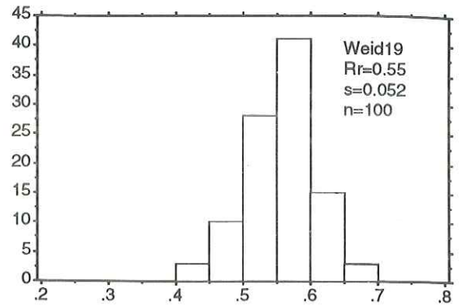
Weid19
Rr=0.55
s=0.052
n=100

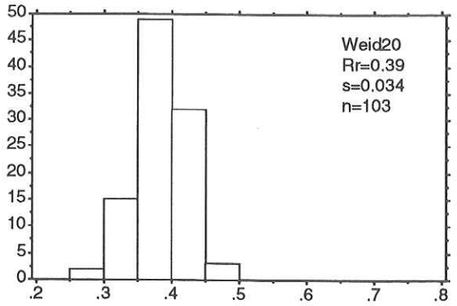
Weid20
Rr=0.39
s=0.034
n=103

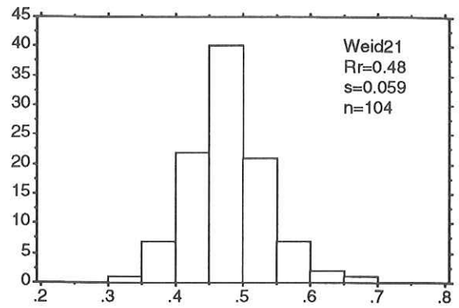
Weid21
Rr=0.48
s=0.059
n=104

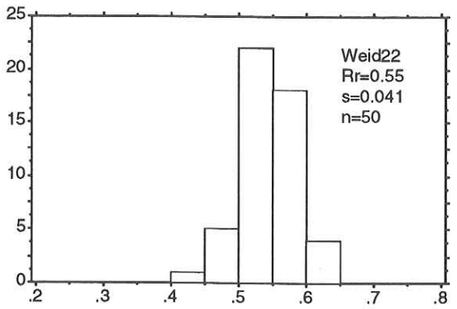
Weid22
Rr=0.55
s=0.041
n=50

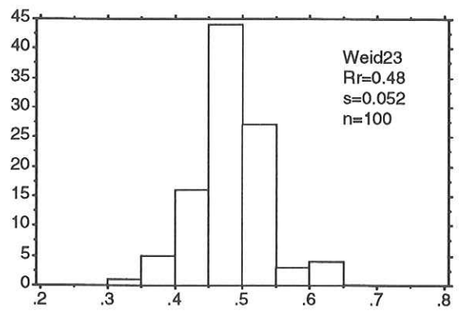
Weid23
Rr=0.48
s=0.052
n=100

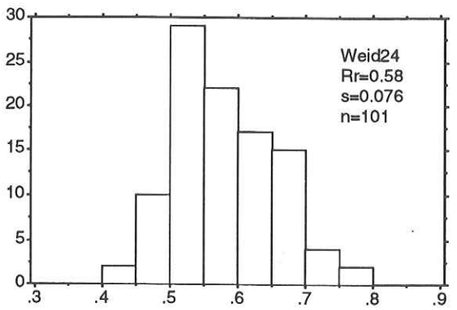
Weid24
Rr=0.58
s=0.076
n=101

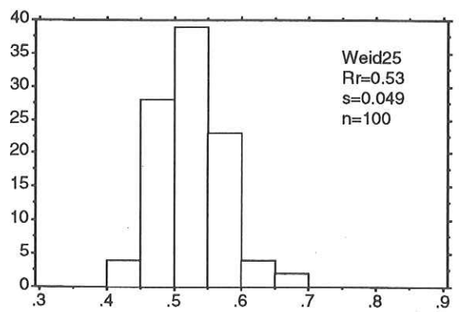
Weid25
Rr=0.53
s=0.049
n=100

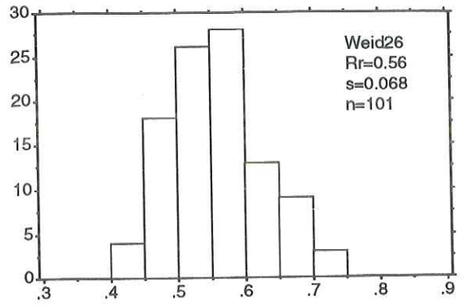
Weid26
Rr=0.56
s=0.068
n=101

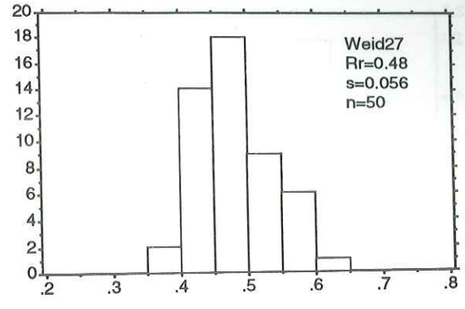
Weid27
Rr=0.48
s=0.056
n=50

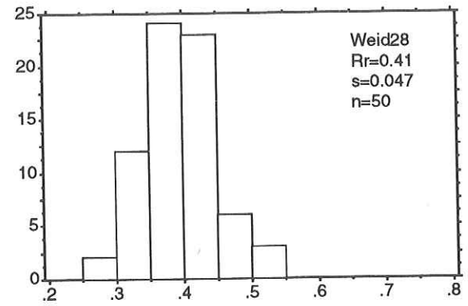
Weid28
Rr=0.41
s=0.047
n=50

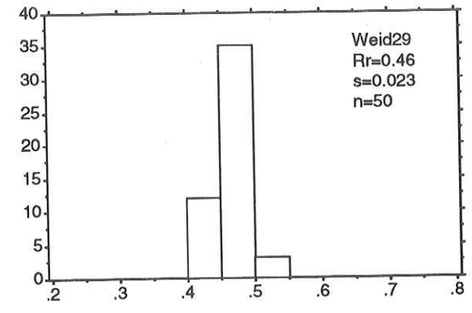
Weid29
Rr=0.46
s=0.023
n=50

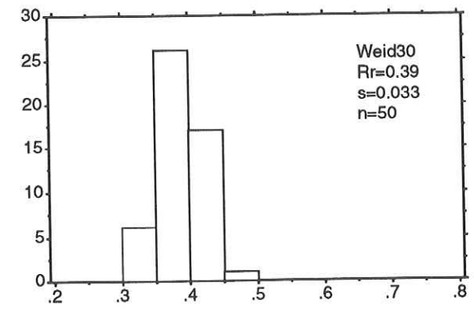
Weid30
Rr=0.39
s=0.033
n=50

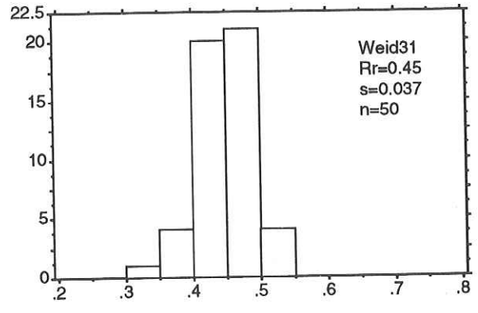
Weid31
Rr=0.45
s=0.037
n=50

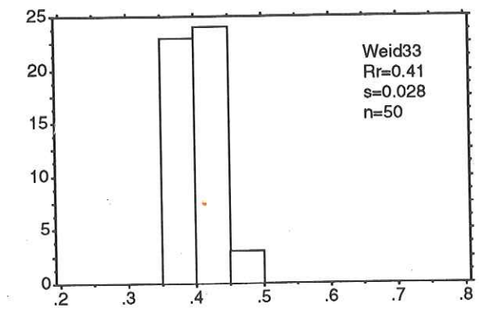
Weid33
Rr=0.41
s=0.028
n=50

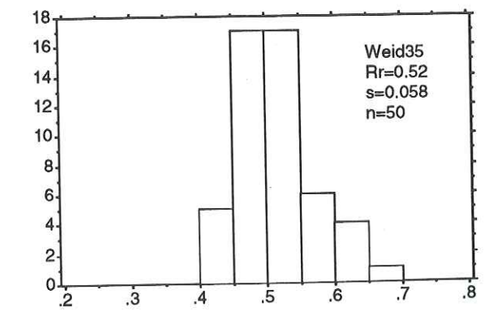
Weid35
Rr=0.52
s=0.058
n=50

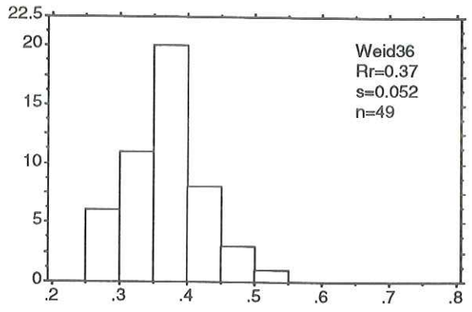
Weid36
Rr=0.37
s=0.052
n=49

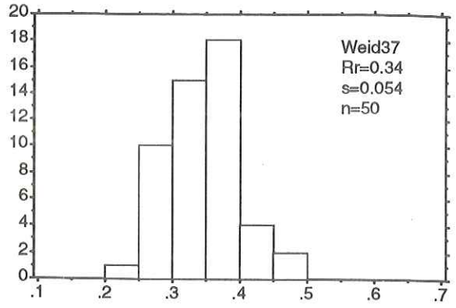
Weid37
Rr=0.34
s=0.054
n=50

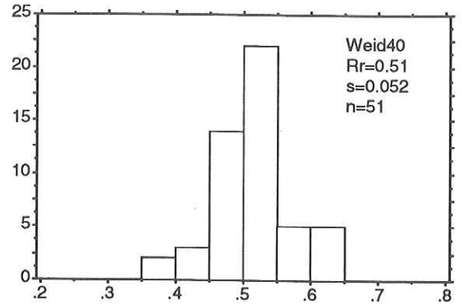
Weid40
Rr=0.51
s=0.052
n=51

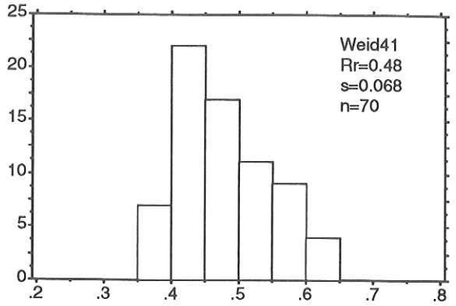
Weid41
Rr=0.48
s=0.068
n=70

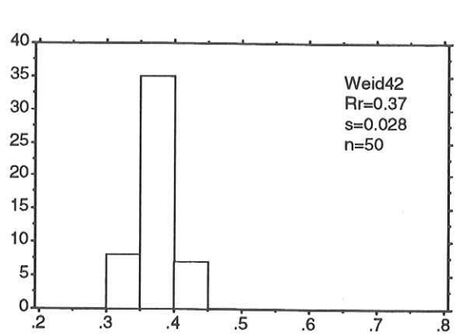
Weid42
Rr=0.37
s=0.028
n=50

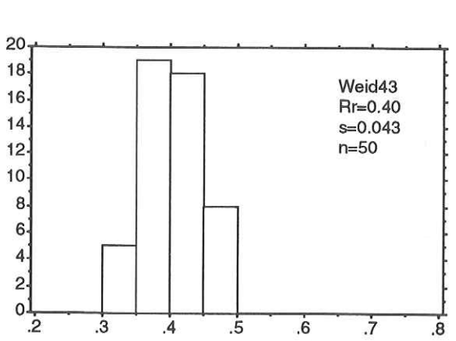
Weid43
Rr=0.40
s=0.043
n=50

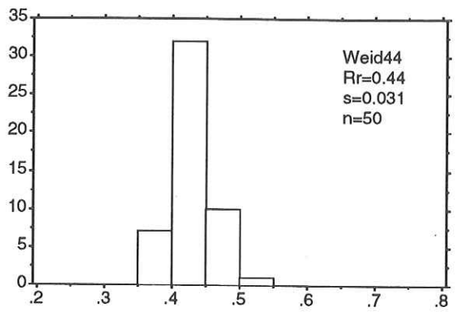
Weid44
Rr=0.44
s=0.031
n=50

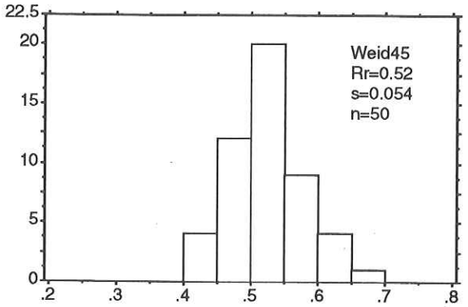
Weid45
Rr=0.52
s=0.054
n=50

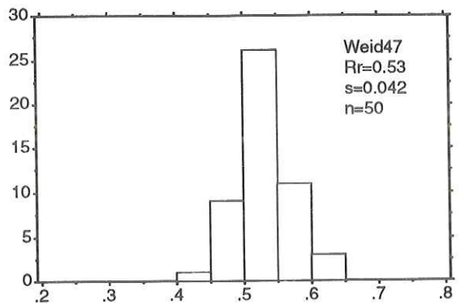
Weid47
Rr=0.53
s=0.042
n=50

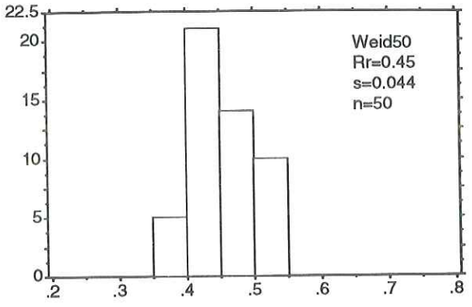
Weid50
Rr=0.45
s=0.044
n=50

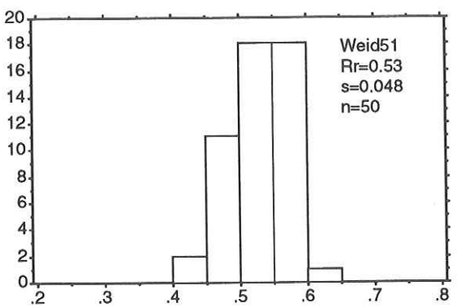
Weid51
Rr=0.53
s=0.048
n=50

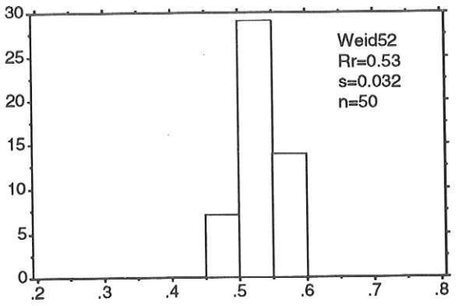
Weid52
Rr=0.53
s=0.032
n=50

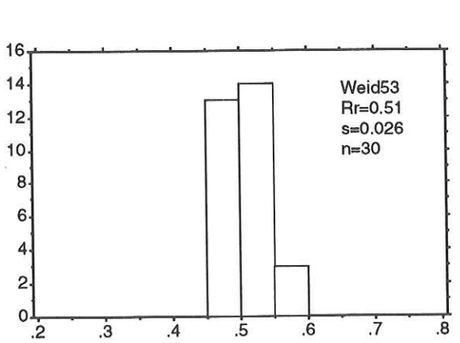
Weid53
Rr=0.51
s=0.026
n=30

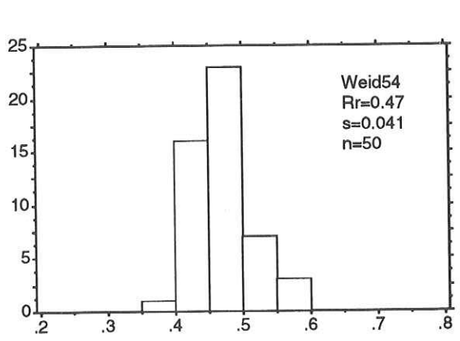
Weid54
Rr=0.47
s=0.041
n=50

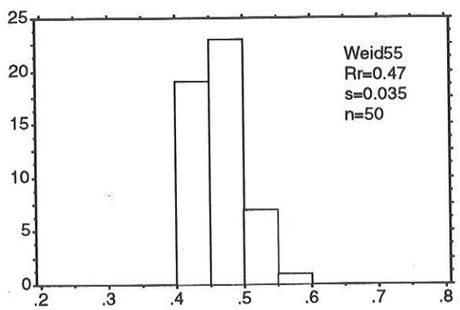
Weid55
Rr=0.47
s=0.035
n=50

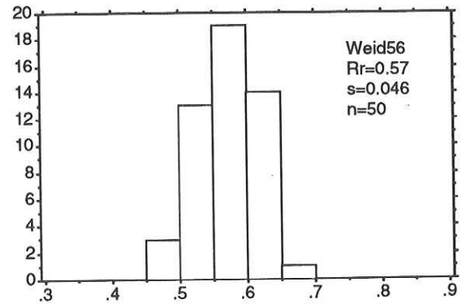
Weid56
Rr=0.57
s=0.046
n=50

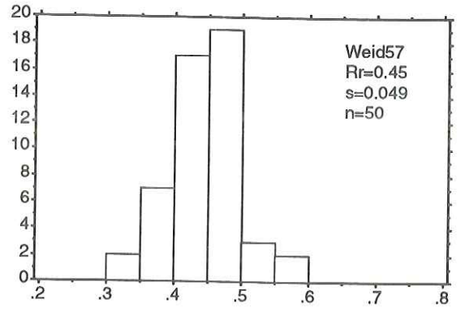
Weid57
Rr=0.45
s=0.049
n=50

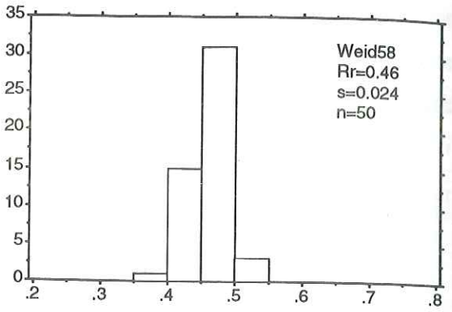
Weid58
Rr=0.46
s=0.024
n=50

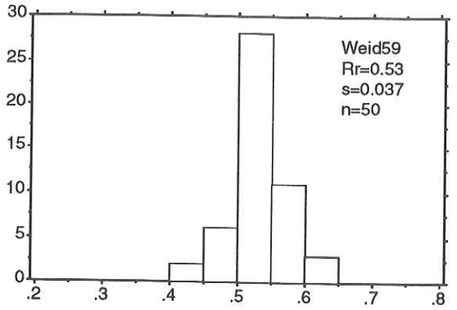
Weid59
Rr=0.53
s=0.037
n=50

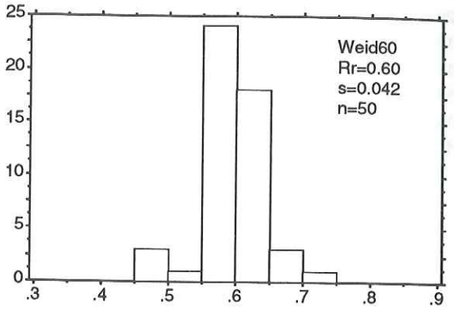
Weid60
Rr=0.60
s=0.042
n=50

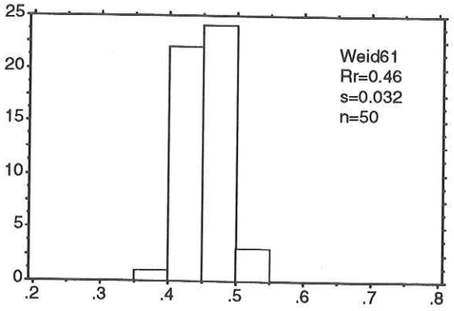
Weid61
Rr=0.46
s=0.032
n=50

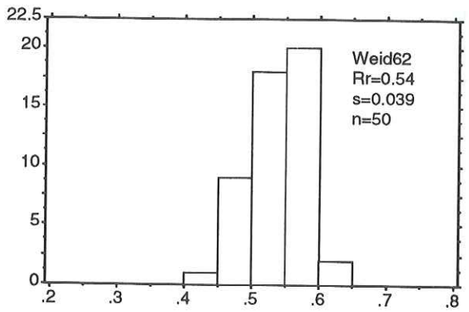
Weid62
Rr=0.54
s=0.039
n=50

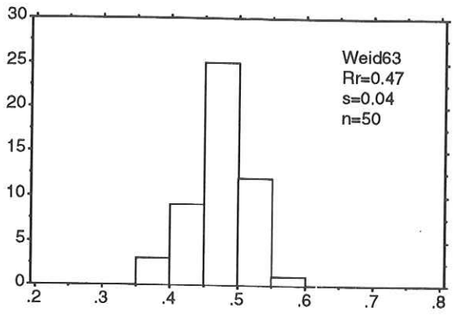
Weid63
Rr=0.47
s=0.04
n=50

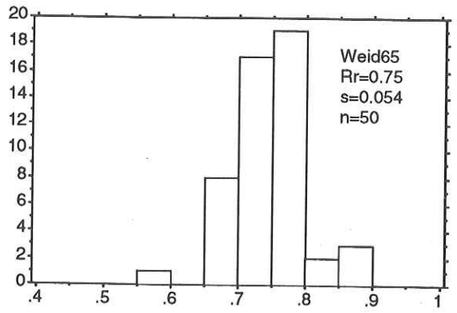
Weid65
Rr=0.75
s=0.054
n=50

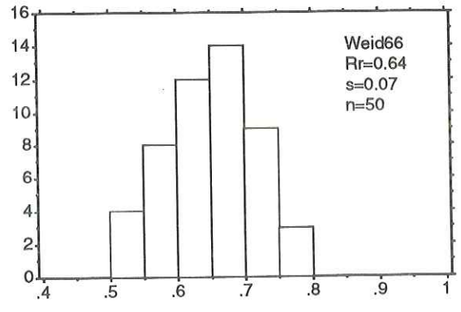
Weid66
Rr=0.64
s=0.07
n=50

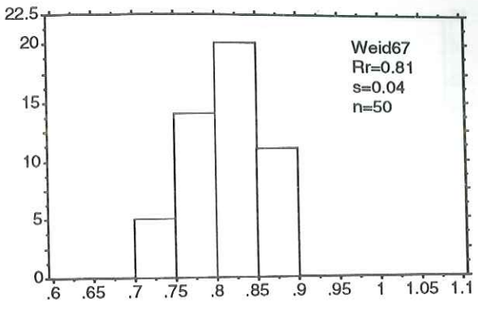
Weid67
Rr=0.81
s=0.04
n=50

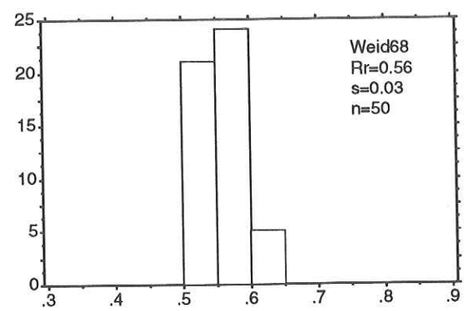
Weid68
Rr=0.56
s=0.03
n=50

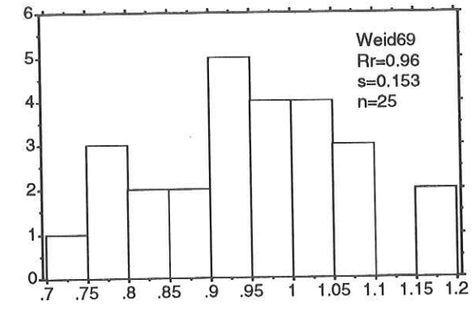
Weid69
Rr=0.96
s=0.153
n=25

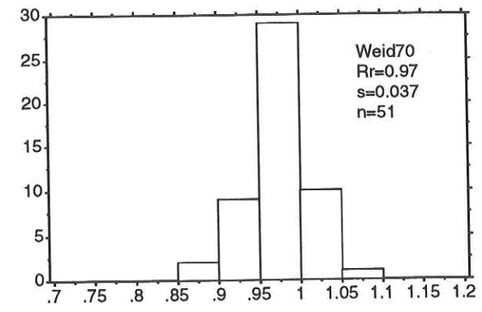
Weid70
Rr=0.97
s=0.037
n=51

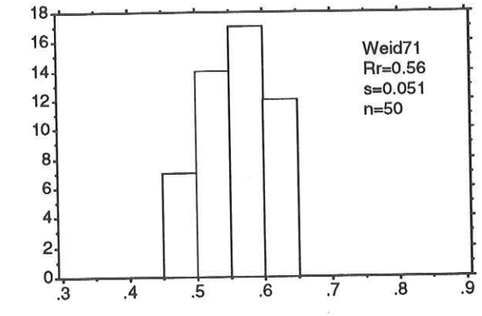
Weid71
Rr=0.56
s=0.051
n=50

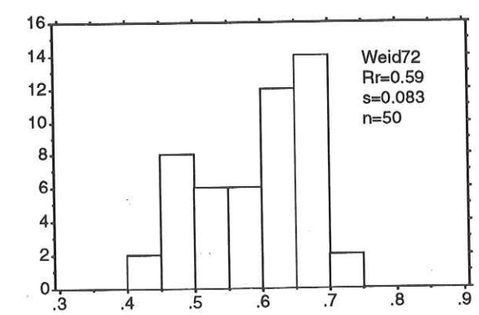
Weid72
Rr=0.59
s=0.083
n=50

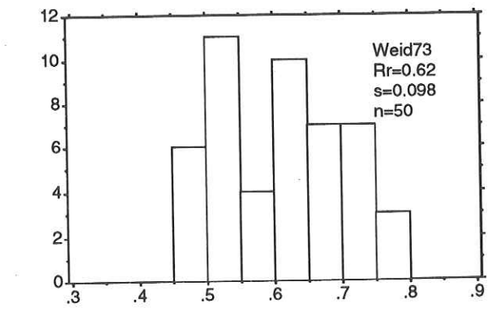
Weid73
Rr=0.62
s=0.098
n=50

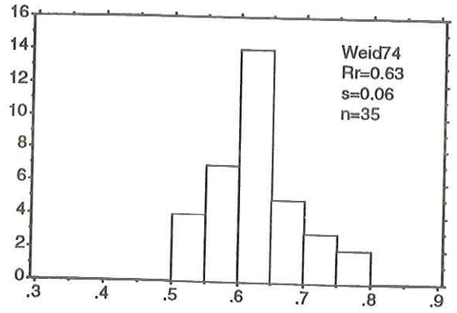
Weid74
Rr=0.63
s=0.06
n=35

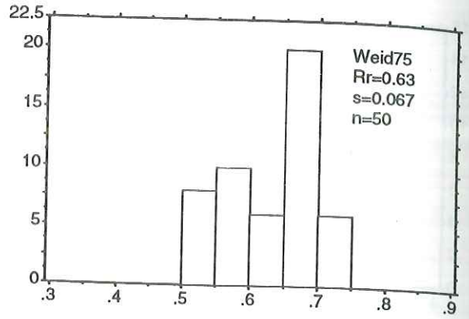
Weid75
Rr=0.63
s=0.067
n=50

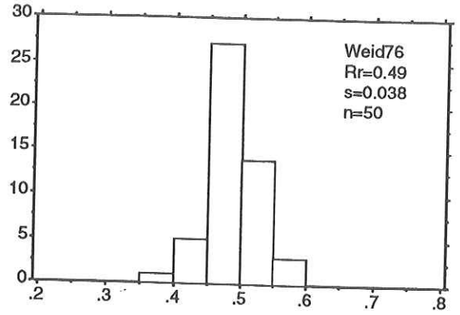
Weid76
Rr=0.49
s=0.038
n=50

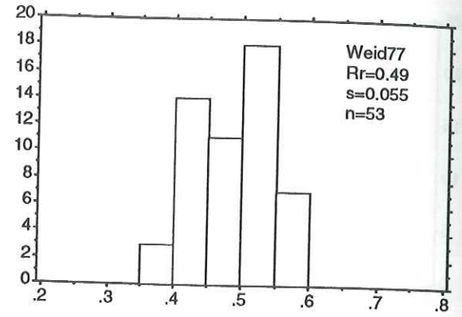
Weid77
Rr=0.49
s=0.055
n=53

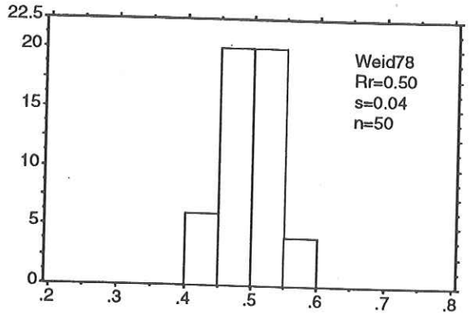
Weid78
Rr=0.50
s=0.04
n=50

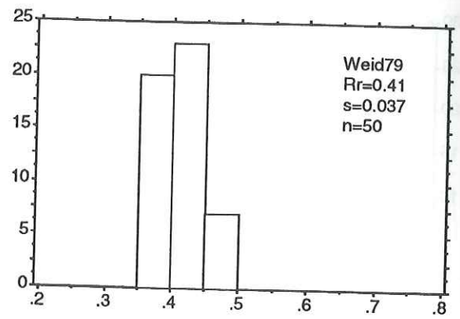
Weid79
Rr=0.41
s=0.037
n=50

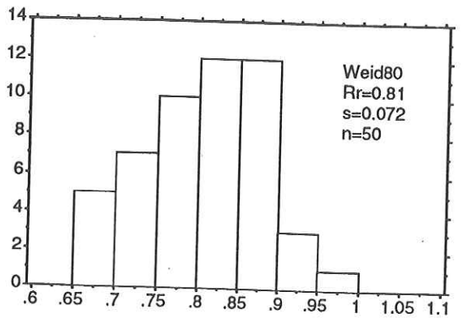
Weid80
Rr=0.81
s=0.072
n=50

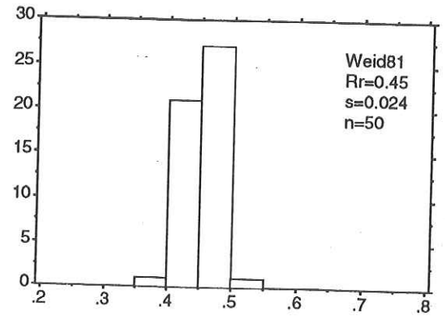
Weid81
Rr=0.45
s=0.024
n=50

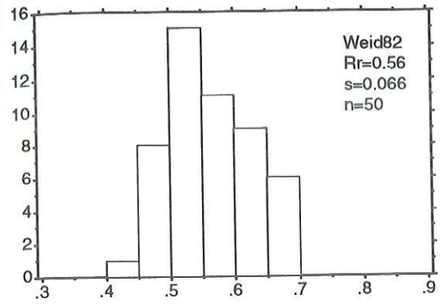
Weid82
Rr=0.56
s=0.066
n=50

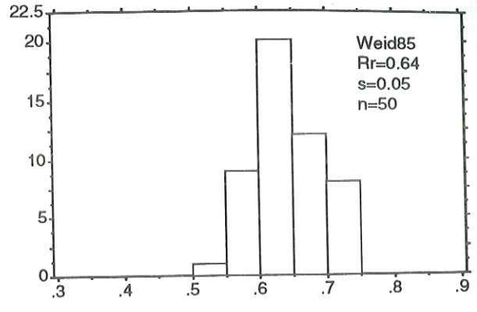
Weid85
Rr=0.64
s=0.05
n=50

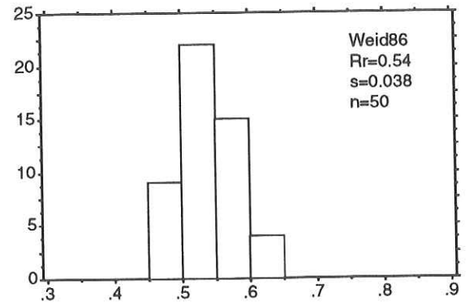
Weid86
Rr=0.54
s=0.038
n=50

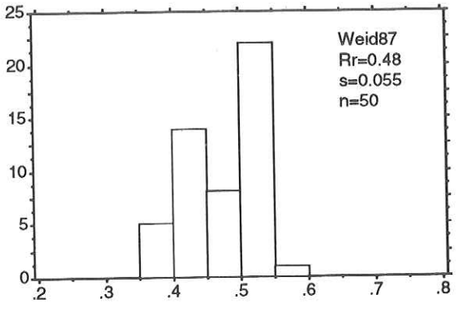
Weid87
Rr=0.48
s=0.055
n=50

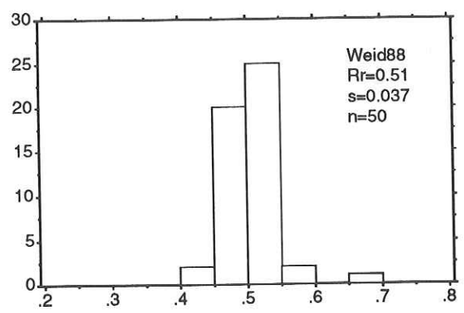
Weid88
Rr=0.51
s=0.037
n=50

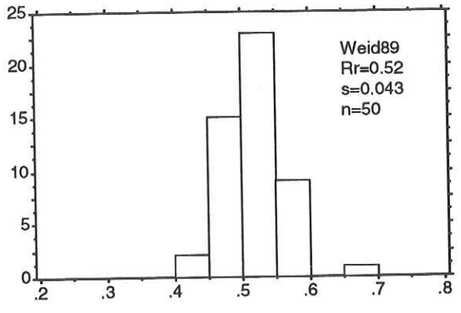
Weid89
Rr=0.52
s=0.043
n=50

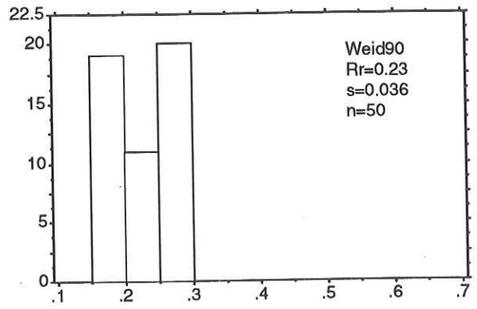
Weid90
Rr=0.23
s=0.036
n=50

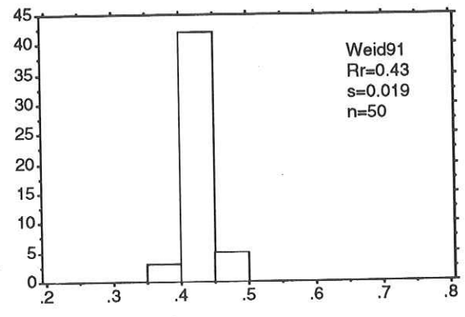
Weid91
Rr=0.43
s=0.019
n=50

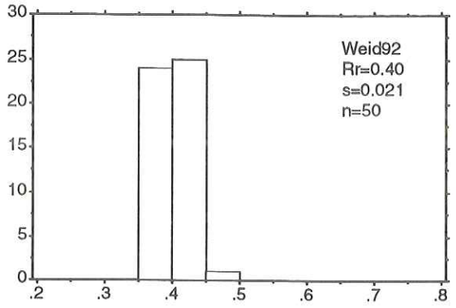
Weid92
Rr=0.40
s=0.021
n=50

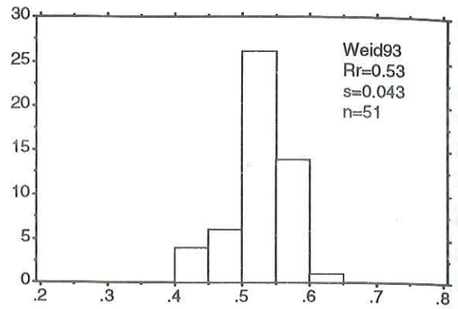
Weid93
Rr=0.53
s=0.043
n=51

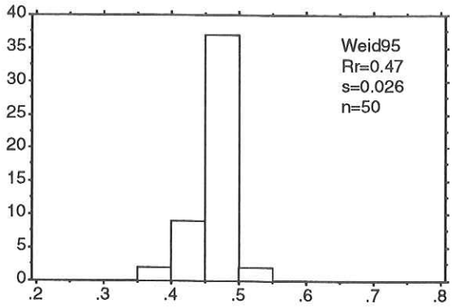
Weid95
Rr=0.47
s=0.026
n=50

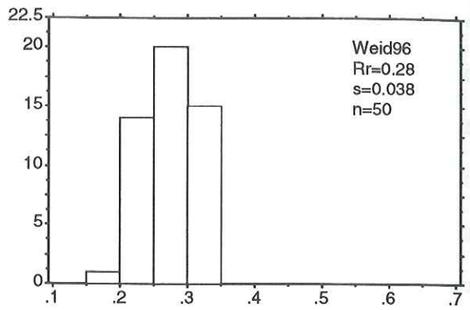
Weid96
Rr=0.28
s=0.038
n=50

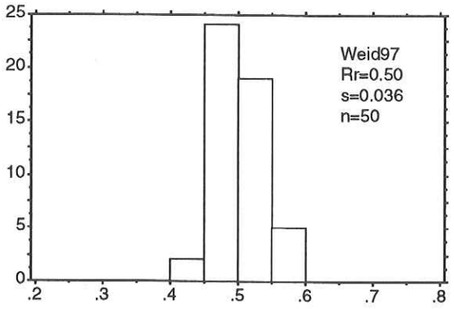
Weid97
Rr=0.50
s=0.036
n=50

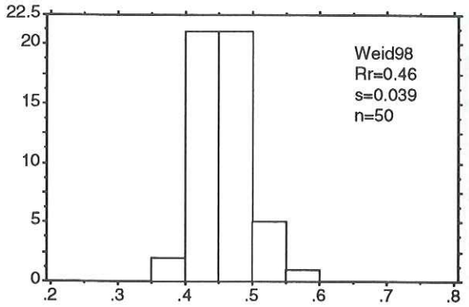
Weid98
Rr=0.46
s=0.039
n=50

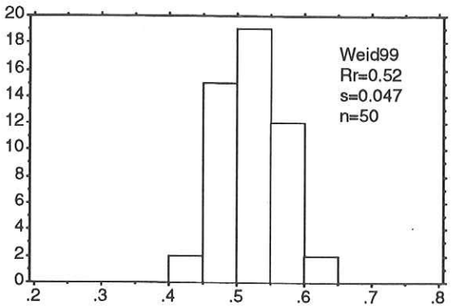
Weid99
Rr=0.52
s=0.047
n=50

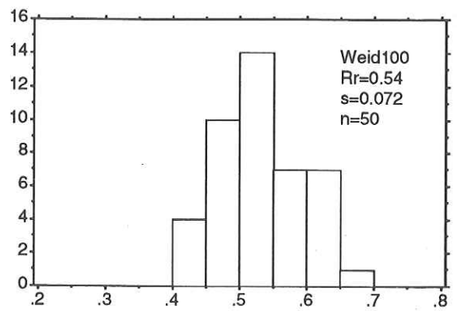
Weid100
Rr=0.54
s=0.072
n=50

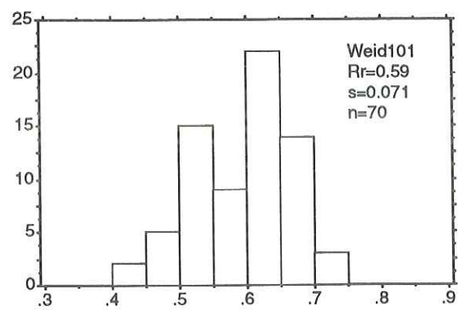
Weid101
Rr=0.59
s=0.071
n=70

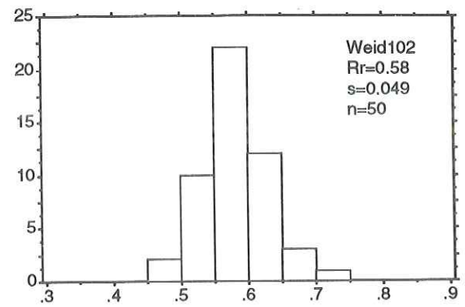
Weid102
Rr=0.58
s=0.049
n=50

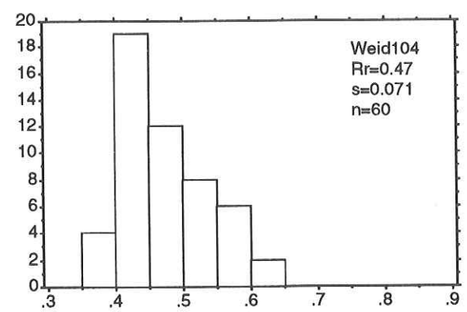
Weid104
Rr=0.47
s=0.071
n=60

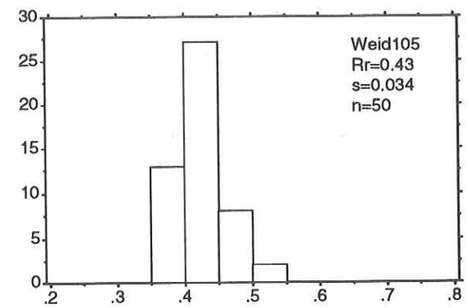
Weid105
Rr=0.43
s=0.034
n=50

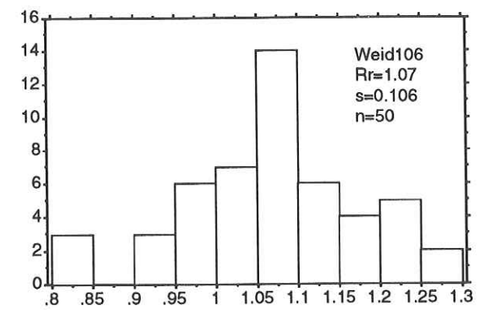
Weid106
Rr=1.07
s=0.106
n=50

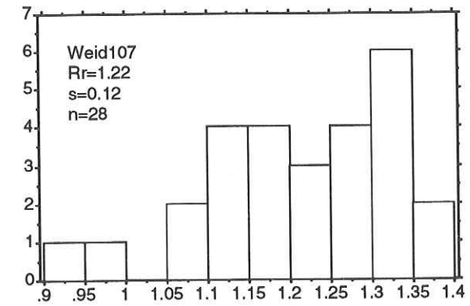
Weid107
Rr=1.22
s=0.12
n=28

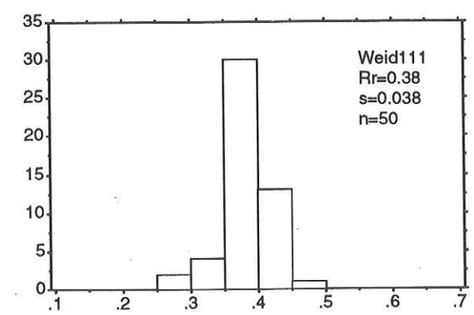
Weid111
Rr=0.38
s=0.038
n=50

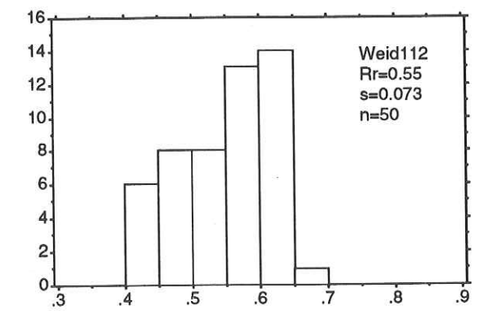
Weid112
Rr=0.55
s=0.073
n=50

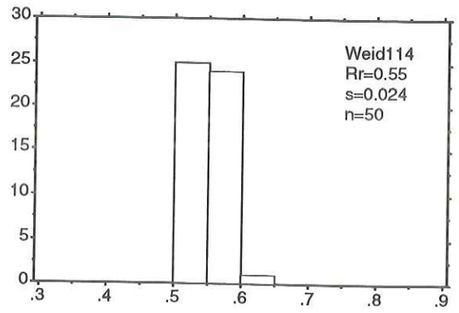
Weid114
Rr=0.55
s=0.024
n=50

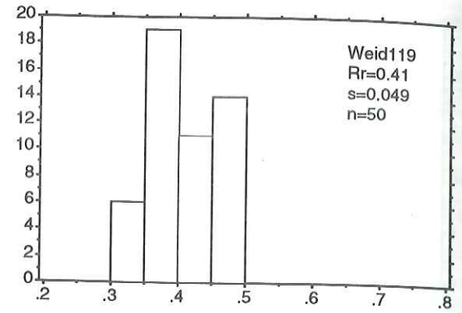
Weid119
Rr=0.41
s=0.049
n=50

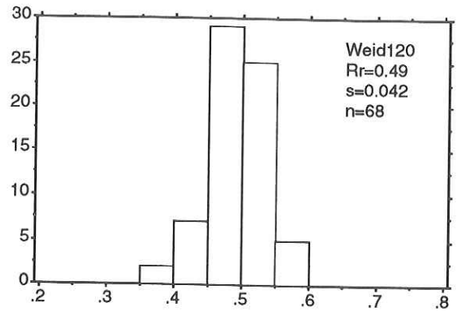
Weid120
Rr=0.49
s=0.042
n=68

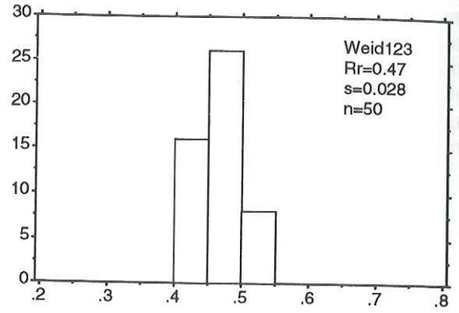
Weid123
Rr=0.47
s=0.028
n=50

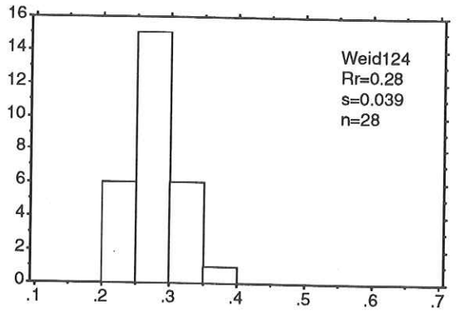
Weid124
Rr=0.28
s=0.039
n=28

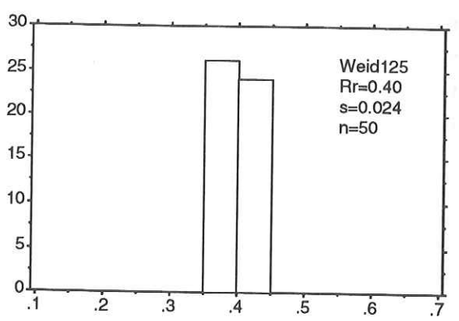
Weid125
Rr=0.40
s=0.024
n=50

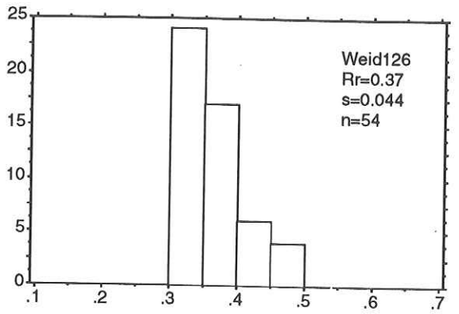
Weid126
Rr=0.37
s=0.044
n=54

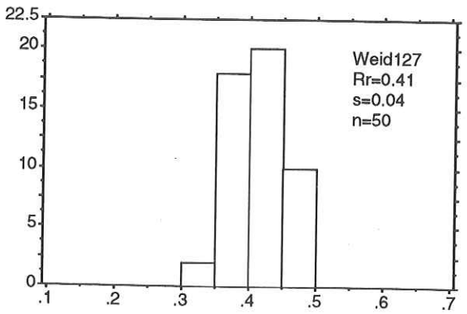
Weid127
Rr=0.41
s=0.04
n=50

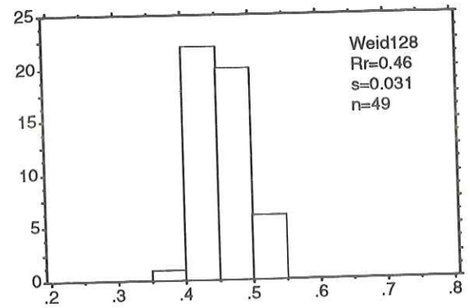
Weid128
Rr=0.46
s=0.031
n=49

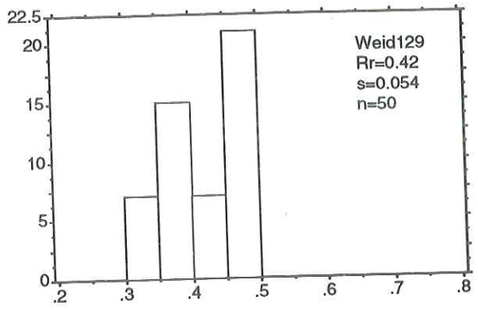
Weid129
Rr=0.42
s=0.054
n=50

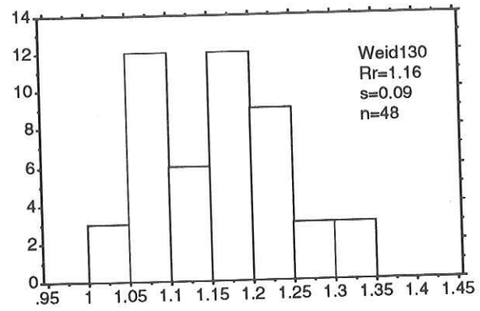
Weid130
Rr=1.16
s=0.09
n=48

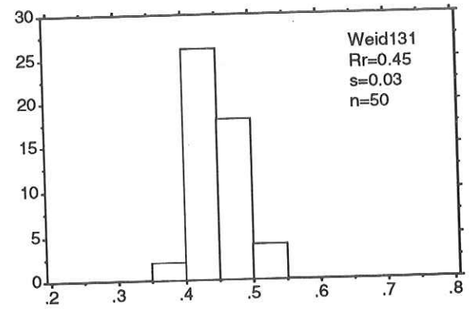
Weid131
Rr=0.45
s=0.03
n=50

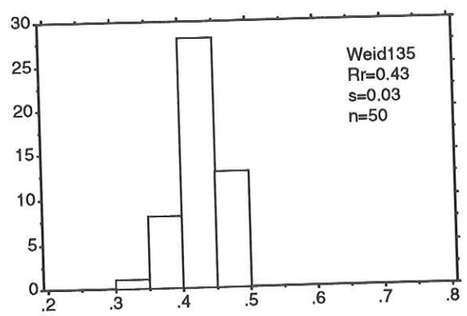
Weid135
Rr=0.43
s=0.03
n=50

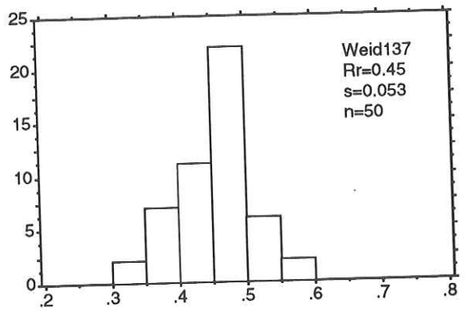
Weid137
Rr=0.45
s=0.053
n=50

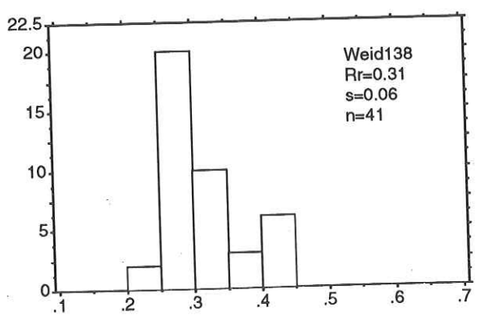
Weid138
Rr=0.31
s=0.06
n=41

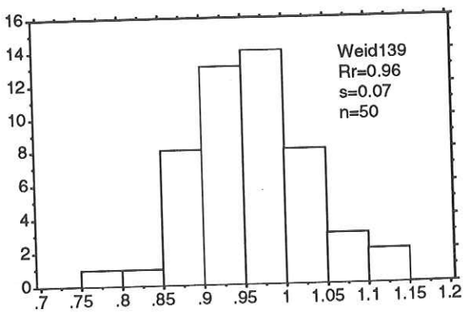
Weid139
Rr=0.96
s=0.07
n=50

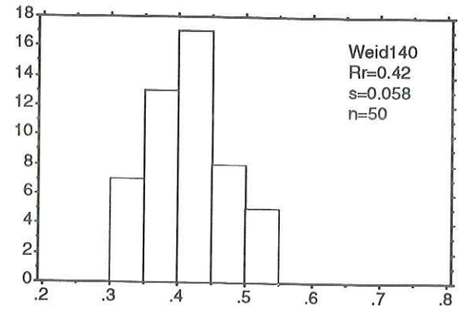
Weid140
Rr=0.42
s=0.058
n=50

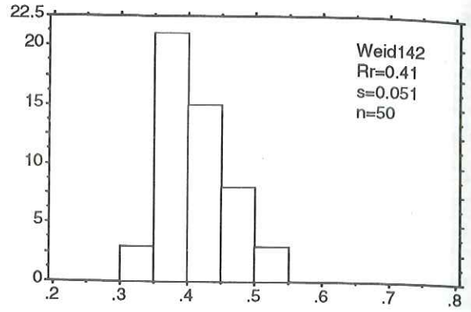
Weid142
Rr=0.41
s=0.051
n=50

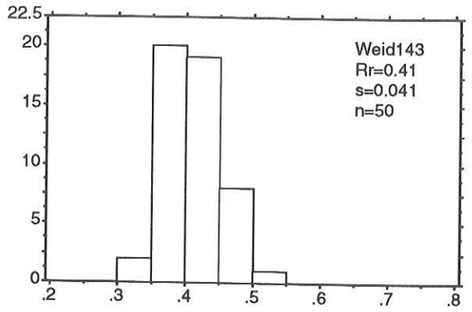
Weid143
Rr=0.41
s=0.041
n=50

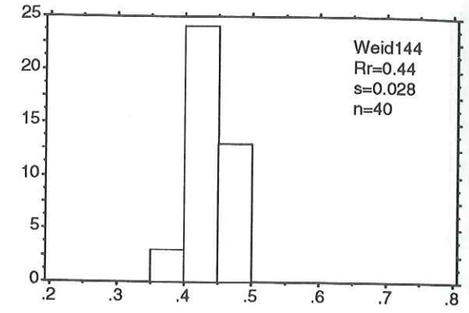
Weid144
Rr=0.44
s=0.028
n=40

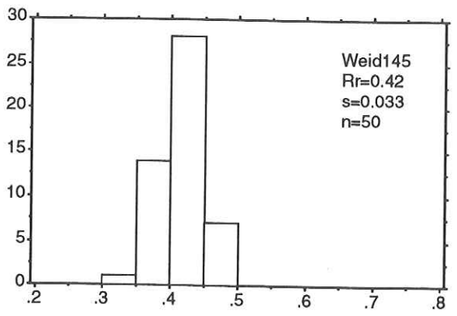
Weid145
Rr=0.42
s=0.033
n=50

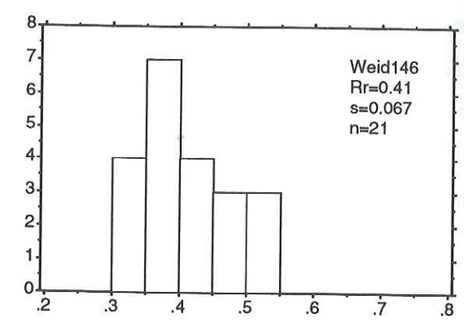
Weid146
Rr=0.41
s=0.067
n=21

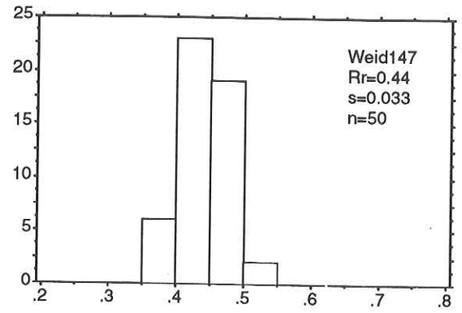
Weid147
Rr=0.44
s=0.033
n=50

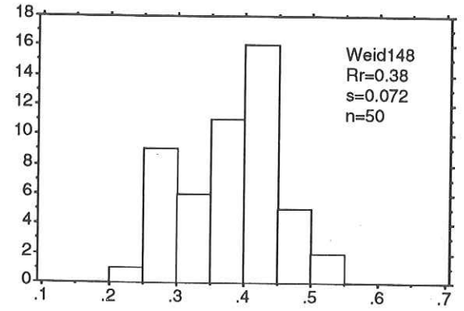
Weid148
Rr=0.38
s=0.072
n=50

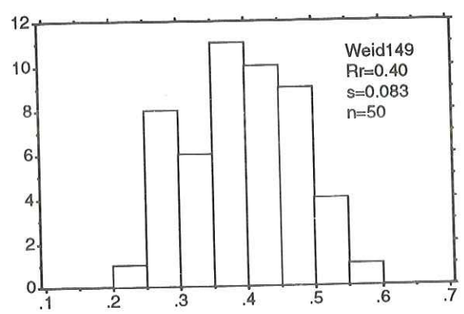
Weid149
Rr=0.40
s=0.083
n=50

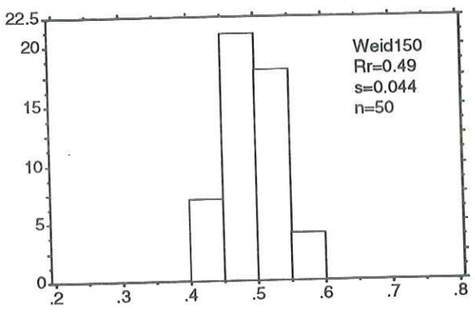
Weid150
Rr=0.49
s=0.044
n=50

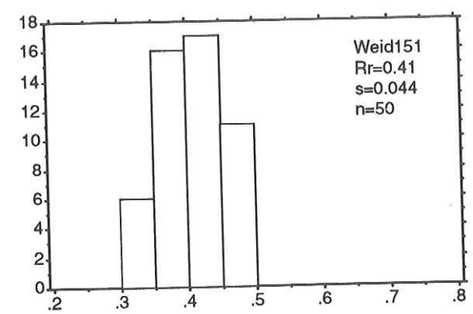
Weid151
Rr=0.41
s=0.044
n=50

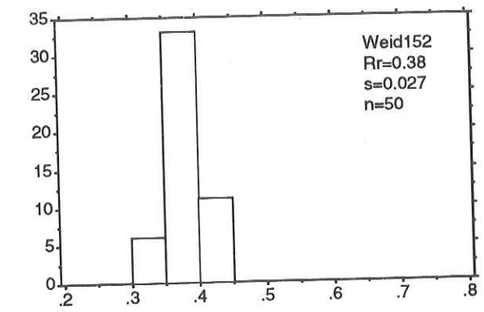
Weid152
Rr=0.38
s=0.027
n=50

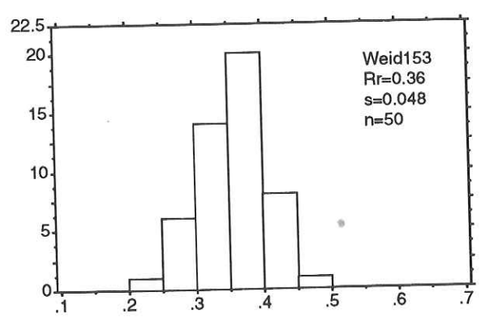
Weid153
Rr=0.36
s=0.048
n=50

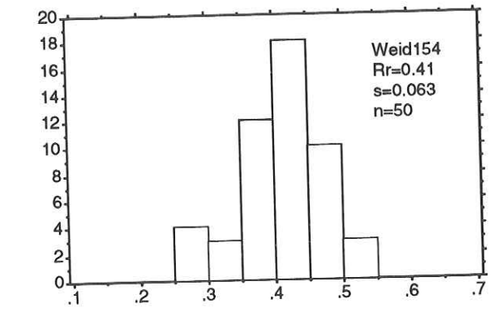
Weid154
Rr=0.41
s=0.063
n=50

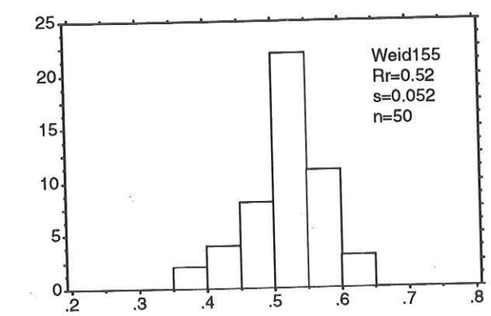
Weid155
Rr=0.52
s=0.052
n=50

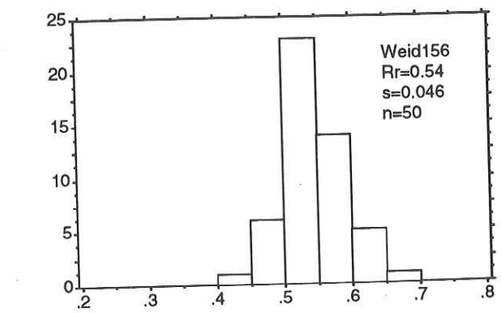
Weid156
Rr=0.54
s=0.046
n=50

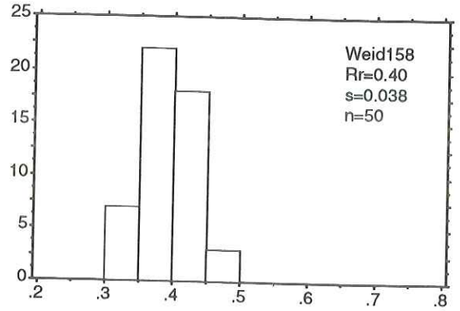
Weid158
Rr=0.40
s=0.038
n=50

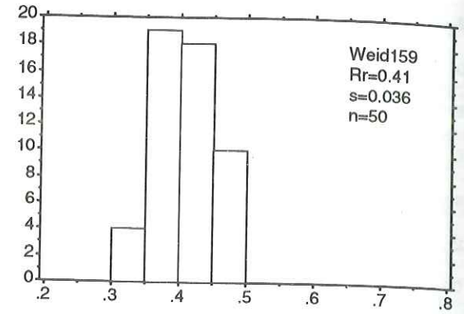
Weid159
Rr=0.41
s=0.036
n=50

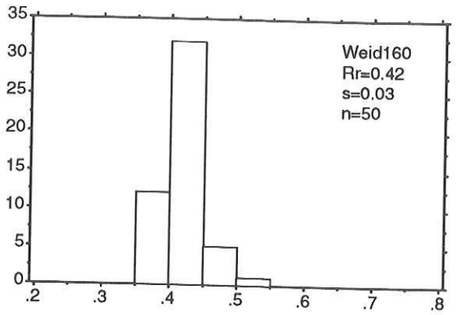
Weid160
Rr=0.42
s=0.03
n=50

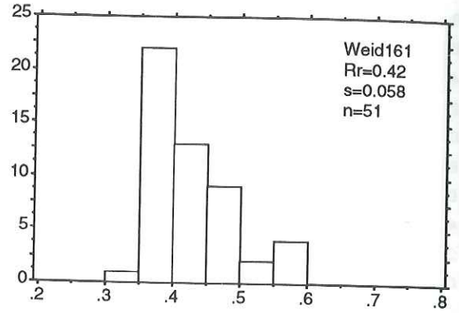
Weid161
Rr=0.42
s=0.058
n=51

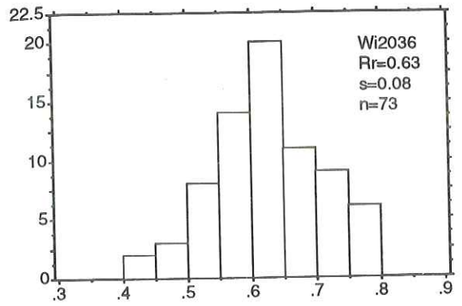
Wi2036
Rr=0.63
s=0.08
n=73

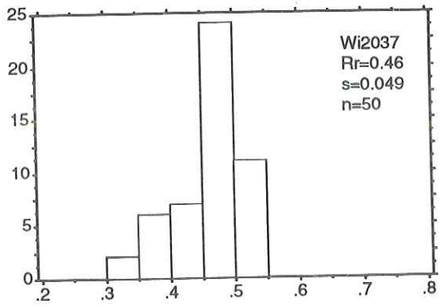
Wi2037
Rr=0.46
s=0.049
n=50

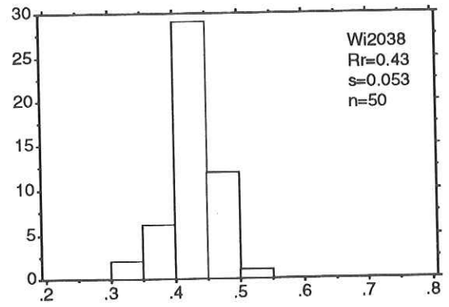
Wi2038
Rr=0.43
s=0.053
n=50

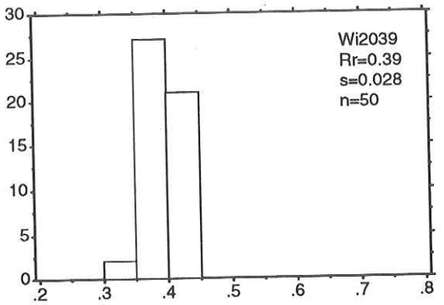
Wi2039
Rr=0.39
s=0.028
n=50

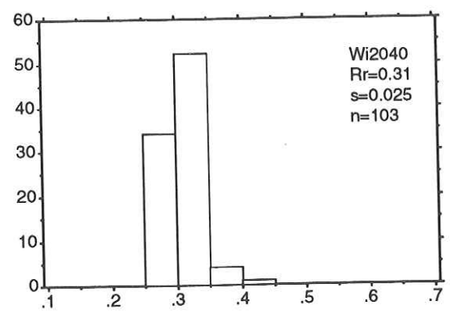
Wi2040
Rr=0.31
s=0.025
n=103

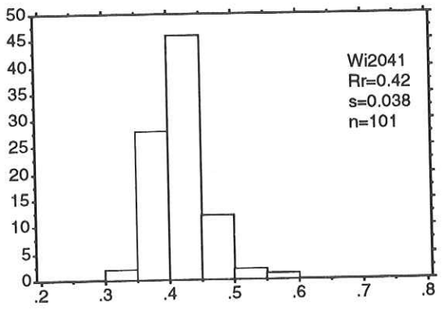
Wi2041
Rr=0.42
s=0.038
n=101

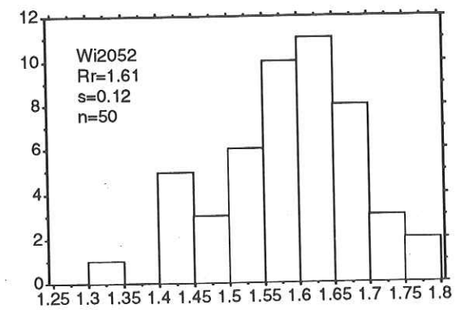
Wi2052
Rr=1.61
s=0.12
n=50

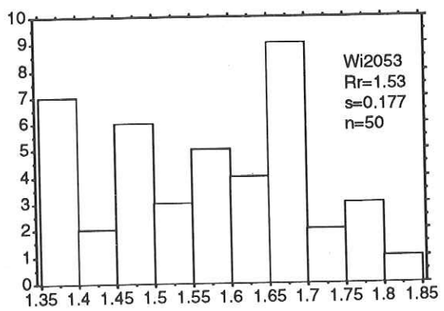
Wi2053
Rr=1.53
s=0.177
n=50

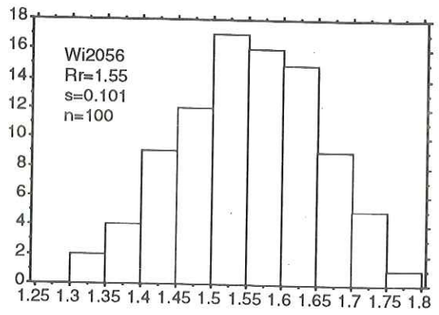

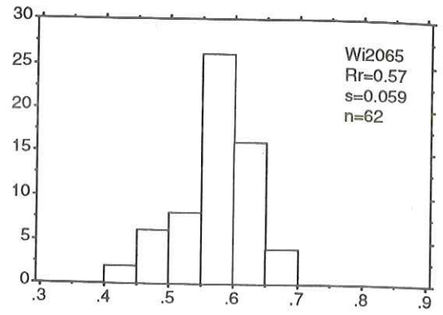

Caption for annex 2-4: X-ray diffraction patterns

M1 = Mica (001), M2 = Mica (002), ...
C1 = Chlorite (001), C2 = Chlorite (002), ...
K1 = Kaolinite (001), K2 = Kaolinite (002)
I/S1 = Mixed-layer illite smectite (001/001)
I/S2 = Mixed-layer illite smectite (001/002)
I/S3 = Mixed-layer illite smectite (002/003)
Se = Serpentine
Co1 = Corrensite (001), Co2 = Corrensite (002), ...
Qz = Quartz
Kfsp = K-feldspar
Plag = Plagioclase

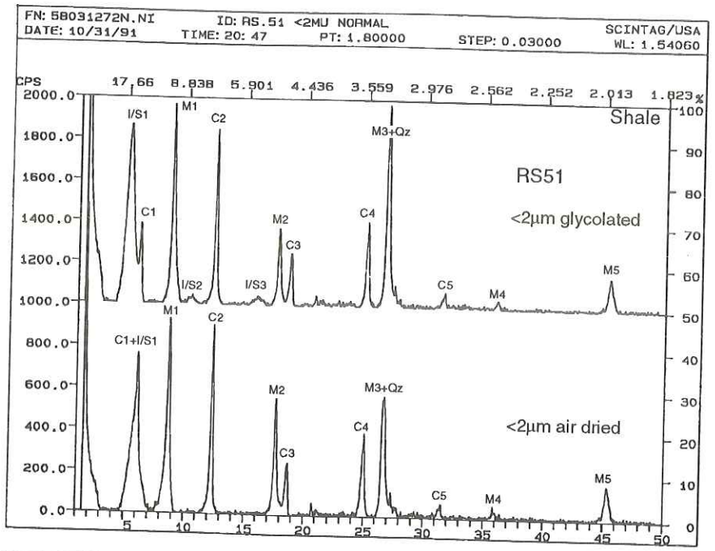

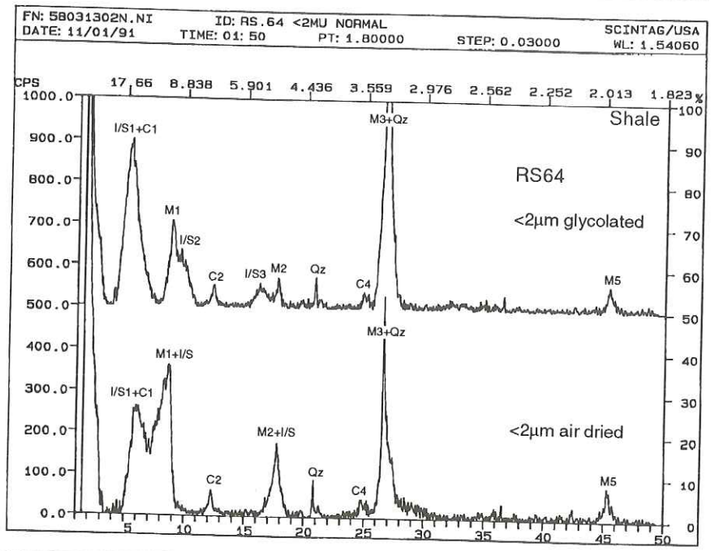

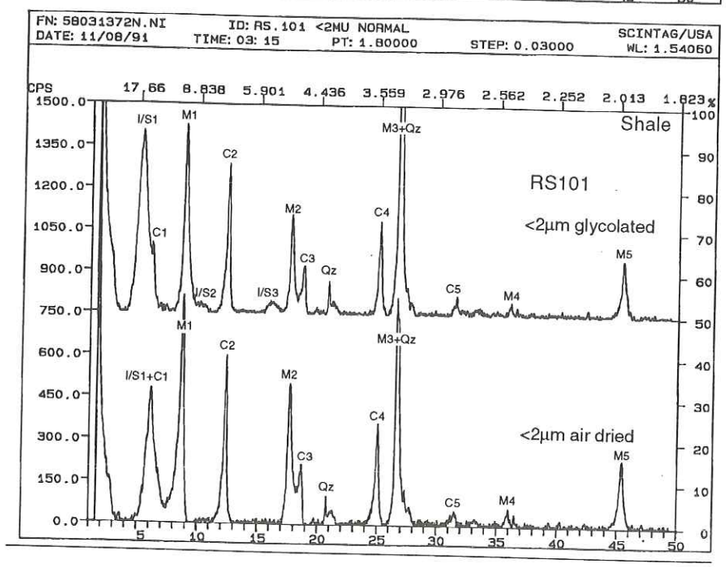

Annex 2

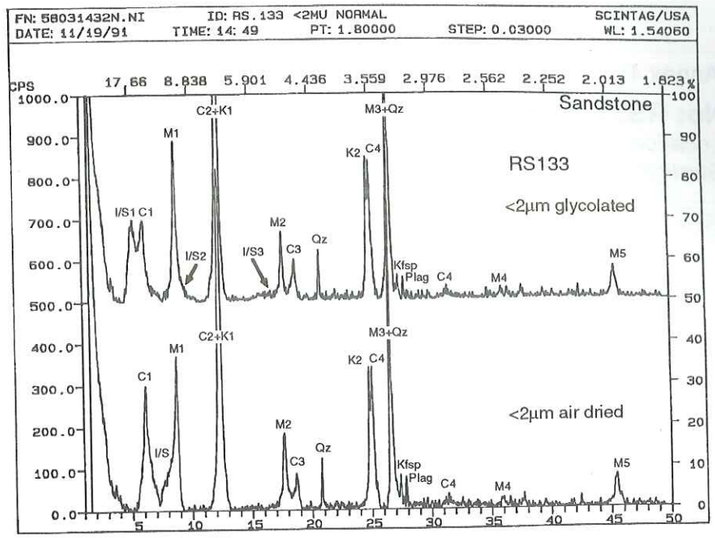

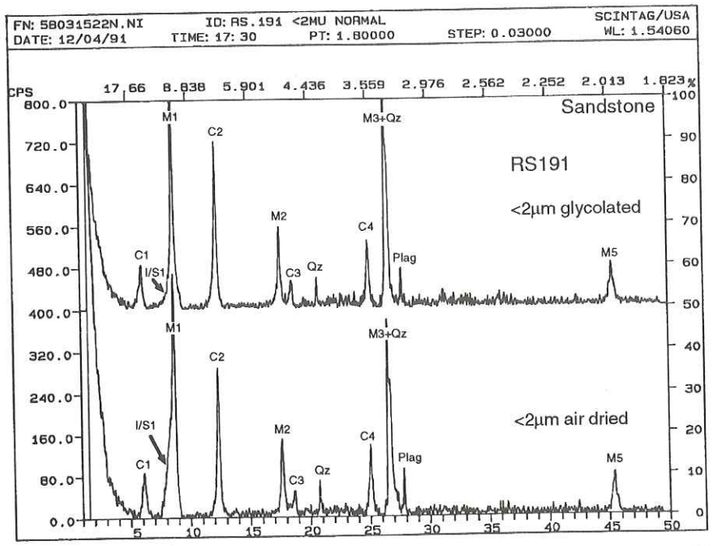

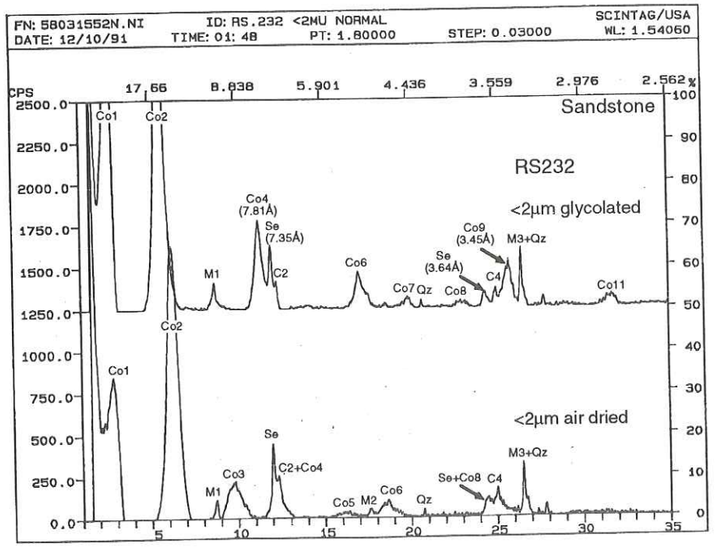

Annex 3

Annex 4

No: RS322

Location : Linn *X/Y-coordinates* : 650850/257850
Stratigraphy : OSM *Lithology* : Sandstone

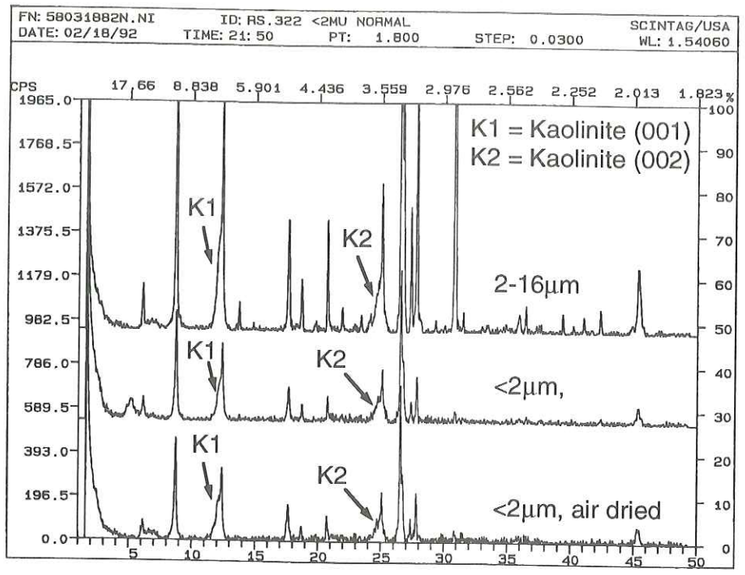

No: RS323

Location : Kirchberg *X/Y-coordinates* : 647200/251300
Stratigraphy : USM *Lithology* : Shale